SYNTHESIS AND EVALUATION OF ENZYME-ACTIVATED NITROXYL (HNO) GENERATORS

A THESIS

SUBMITTED IN PARTIAL FULFILLMENT OF THE

REQUIREMENTS

OF THE DEGREE OF

DOCTOR OF PHILOSOPHY

BY

LAXMAN R. SAWASE

20163424

INDIAN INSTITUTE OF SCIENCE EDUCATION

AND RESEARCH (IISER), PUNE – 411 008

2023

Dedicated to……

My Family

भारतीय विज्ञान शिक्षा एवं अनुसंधान संस्थान पुणे
INDIAN INSTITUTE OF SCIENCE EDUCATION AND RESEARCH PUNE
डॉ. होमी भाभा मार्ग, पुणे 411008, महाराष्ट्र, भारत | Dr. Homi Bhabha Road, Pune 411008, Maharashtra, India
T +91 20 2590 8001 W www.iiserpune.ac.in

IISER PUNE

CERTIFICATE

Certified that the work incorporated in the thesis entitled, " ***Synthesis and Evaluation of Enzyme Activated Nitroxyl (HNO) Generators***" submitted by ***LAXMAN R. SAWASE*** was carried out by the candidate, under my supervision. The work presented here or any part of it has not been included in any other thesis submitted previously for the award of any degree or diploma from any other University or institution.

Date: 16th March, 2023

Pune (MH), India

C. Harinath

Prof. Harinath Chakrapani

डॉ. हरिनाथ चक्रपाणी / Dr. Harinath Chakrapani
प्रोफेसर/Professor
रसायन विज्ञान विभाग /Department of Chemistry
भारतीय विज्ञान शिक्षा एवं अनुसंधान संस्थान
Indian Institute of Science Education & Research
पुणे / Pune- 411 008, भारत/India

भारतीय विज्ञान शिक्षा एवं अनुसंधान संस्थान पुणे
INDIAN INSTITUTE OF SCIENCE EDUCATION AND RESEARCH PUNE
डॉ. होमी भाभा मार्ग, पुणे 411008, महाराष्ट्र, भारत | Dr. Homi Bhabha Road, Pune 411008, Maharashtra, India
T +91 20 2590 8001 W www.iiserpune.ac.in

IISER PUNE

DECLARATION

I declare that this written submission represents my ideas in my own words and where others' ideas have been included, I have adequately cited and referenced the original sources. I also declare that I have adhered to all principles of academic honesty and integrity and have not misrepresented or fabricated or falsified any idea/data/fact/source in my submission. I understand that violation of the above will be cause for disciplinary action by the Institute and can also evoke penal action from the sources which have thus not been properly cited or from whom proper permission has not been taken when needed.

Date: 16th March, 2023
Pune (MH), India

Laxman R. Sawase
20163424

Table of contents

Table of Contents I

General Remarks VI

List of Abbreviations VIII

Acknowledgments XII

Abstract XIV

Chapter 1. Introduction

1.1. Nitric Oxide (NO) 1

1.2. Nitroxyl (HNO/NO^-) 1

1.3. Biosynthesis of HNO 2

1.4. Reactivity of HNO 3

1.4.1. Reaction of HNO with H_2S, persulfide and thiols 3

1.4.2. Reaction with metalloproteins 5

1.4.3. Reactivity of molecular oxygen 6

1.4.4. Reaction with NO 7

1.5. Therapeutic application of HNO 7

1.5.1. HNO in the treatment of alcoholism 7

1.5.2. HNO in the cardiovascular system 8

1.5.3. HNO in ischemia-reperfusion injury 9

1.5.4. HNO in vasodilation 9

1.5.5. HNO in cancer 10

1.5.6. HNO as antioxidant 11

1.6. HNO donors 11

1.6.1. HNO generation in aqueous condition 12

1.6.2. Light-triggered approach for HNO generation 13

1.6.3. Thiol and thermally-activated approach for HNO generation 14

1.6.4. Chemically and enzymatically triggered approach for HNO generation 15

1.6.5. Limitations with existing HNO donors 16
1.7. HNO detection 17
1.7.1. Phosphine-based HNO probes 17
1.7.2. Thiol-based HNO probes 20
1.7.3. Prefluorescent HNO probe 20
1.7.4. Copper (II) based probe for the HNO detection 21
1.7.5. Detection of N_2O (HNO dimer) by GC/MS 22
1.7.6. Limitations with the existing HNO probes 23
1.8. Aim 23
1.9. References 25

Chapter 2. Esterase-triggered Nitroxyl (HNO) Donors with a Fluorescence Reporter

2.1. Introduction 35
2.2. Result and discussion 36
2.2.1. Synthesis 36
2.2.2. HNO generation and fluorescence emission study 39
2.2.2.1. *In vitro* HNO generation 39
2.2.2.2. Time course of HNO generation 41
2.2.3. Photophysical properties 43
2.2.3.1. The measurement of UV absorbance 43
2.2.3.2. The measurement of fluorescence 44
2.2.3.3. Stability of fluorescence in different pH 44
2.2.3.4. Stability of fluorescence over time 45
2.2.3.5. Time-resolved photoluminescence (PL) measurements 46
2.2.4. HNO generation and release of **7** from **2h** and **3h** 47
2.2.4.1. HNO generation from **2h** and **3h** 47
2.2.4.2. Concentration-dependent release of **7** in buffer 49
2.2.4.3. Concomitant release of HNO and **7** 50
2.2.5. Nitric oxide (NO) generation 51
2.2.6. LC/MS analysis 54
2.2.6.1. Decomposition of **2h** 54

2.2.6.2. Stability of **3h** 56
2.2.6.3. Decomposition of **3h** 57
2.2.7. Mechanism 58
2.2.8. Polysulfide measurement by LCMS analysis 59
2.2.8.1. Mechanism of polysulfide generation and trapping of polysulfide 60
2.2.8.2. Structures of sulfur species trapped by HPE-IAM 61
2.2.8.3. Polysulfide formation from **4** 64
2.2.9. Concentration-dependent release of **7** in A549 cell lysate 65
2.2.10. MTT assay for cell viability 66
2.2.11. Intracellular generation of HNO and **7** in MCF-7 cells 68
2.3. Summary 70
2.4. Experimental protocols 71
2.4.1. Synthesis and characterization: 71
2.4.2. HNO detection by using **5** 77
2.4.3. Photophysical properties of **7** 78
2.4.3.1. Measurement of absorbance of **7** 78
2.4.3.1. Measurement of absorbance of **7** 78
2.4.3.3. Time-resolved photoluminescence (PL) measurements of **7** 79
2.4.4. Detection of **7** 79
2.4.5. Griess assay for nitrite detection 79
2.4.6. Decomposition of **2h** and **3h** using LC/MS 80
2.4.7. Polysulfide measurement using LC/MS 80
2.4.8. Detection of **7** releases in A549 cell lysate 81
2.4.9. Cell viability Assay 82
2.4.10. Detection of HNO and **7** in MCF-7 cells 82
2.5. NMR spectra 83
2.6. References 103

Chapter 3. β-glucosidase activated Nitroxyl (HNO) donors

3.1. Introduction 106
3.2. Result and discussion 108
3.2.1. Synthesis 108
3.2.2. HNO generation study 110
3.2.2.1. Evaluation of HNO generation using **5** 110
3.2.3. NO detection 111
3.2.4. HPLC study 112
3.2.5. Computational study 113
3.2.6. MTT assay for the cell viability 119
3.3. Summary 120
3.4. Experimental protocol 121
3.4.1. Synthesis and characterization 121
3.4.2. HNO detection by fluorescence study 127
3.4.3. Nitric oxide detection by Griess assay 127
3.4.4. Decomposition study by HPLC 127
3.4.5. Cell viability assay 128
3.5. NMR spectra 129
3.6. References 141

Chapter 4. β-galactosidase triggered Nitroxyl (HNO) donors

4.1. Introduction 143
4.2. Result and discussion 146
4.2.1. Synthesis 146
4.2.2. HNO generation study 147
4.2.2.1. Detection of HNO generation using **5** 147
4.2.2.2. Detection of N_2O by headspace GC analysis 148
4.2.2.3. Detection of HNO using *N*-acetyl tryptophan 149
4.2.3. Detection of Nitric oxide (NO) 150
4.2.4. HPLC study 151
4.2.4.1. Stability of compound **20a** in buffer (pH 7.4) 151
4.2.4.2. Decomposition of **20a** in the presence of β-galactosidase 152

4.2.4.3. Decomposition of **20b** in the presence of β-galactosidase 152
4.2.5. Computational studies 153
4.2.6. Polysulfide measurement by LC/MS analysis 157
4.2.7. Cell viability assay 161
4.2.8. ROS quenching by compound **20a** in senescent cells 162
4.3. Summary 163
4.4. Experimental protocol 164
4.4.1. Synthesis and characterization 164
4.4.2. HNO detection by using **5** 167
4.4.3. Analysis of Nitrous Oxide (N_2O) by Headspace Gas Chromatography 167
4.4.4. NAT-NO detection 168
4.4.5. Nitric oxide (NO) detection by Griess assay 168
4.4.6. Decomposition study by HPLC 168
4.4.7. Polysulfide measurement using LC/MS 169
4.4.8. Cell viability Assay 169
4.5. NMR spectra 170
4.6. References 175

Appendix-I: Synopsis 180
Appendix-II: List of Figures 203
Appendix-III: List of Schemes 213
Appendix-IV: List of Tables 215
Appendix-V: List of Publication 216

- Thin-layer chromatography (TLC) was performed using silica gel 60 GF254 precoated aluminium backed plates (0.25 mm thickness) and visualization was accomplished by irradiation with short and long UV light at 254 and 365 nm respectively or by staining with bromocresol green or phosphomolybdic acid (PMA) for the identification of carboxylic acid or alcohols respectively.
- ^{19}F spectra were recorded on a JEOL (376 MHz) using an external reference (α, α, α-trifluorotoluene, δF = -63.72 ppm).
- ^{1}H and ^{13}C spectra were recorded on JEOL or Bruker 400 MHz (or 100 MHz for ^{13}C) spectrometers using tetramethylsilane (TMS) as an internal standard.
- Chemical shifts (δ) are reported in ppm downfield from CDCl3 (δ = 7.26 and 77.2 ppm) or DMSO-*d6* (δ = 2.50 and 39.5 ppm) or CD3OD (δ = 3.31 and 49.0 ppm) for ^{1}H and ^{13}C-NMR respectively as an internal reference. The coupling constants (*J*) are given in Hz. Multiplicities are indicated using the following abbreviations: br (broad), m (multiplet), s (singlet), d (doublet), t (triplet), q (quartet), dd (doublet of doublet), dt (doublet of triplet).
- Column chromatography was performed using Rankem silica gel (60-120 mesh) eluting with petroleum ether and ethyl acetate (EtOAc).
- Preparative High Performance Liquid Chromatography (Prep HPLC) was carried out on a Combiflash EZ Prep UV equipped with a Kromasil®C-18 preparative column (21.5 mm x 250 mm, 10 μm) at a flow rate of 12 mL/min.
- High-resolution mass spectra were obtained from HRMS-ESI-QTOF (quadrupole time-of flight).
- FT-IR spectra were recorded using Bruker ALPHA FT-IR spectrometer and reported in cm^{-1}.
- LC/MS experiments were performed either on a Sciex X500R QTOF mass spectrometer fitted with an Exion UHPLC system or on a Bruker Daltonics ESI-QTOF (Maxis Impact) mass spectrometer connected to a Thermo Dionex (Ultimate 3000) micro-LC system in a positive ion mode using high resolution multiple reaction monitoring (MRM-HR) and information dependent acquisition (IDA) method.
- Absorbance measurement were carried out using SHIMADZU, UV-2600 UV-Vis spectrophotometer.

- Fluorescence measurements were carried out using a Horiba Jobin Yvon Fluorolog Fluorescence Spectrophotometer or an EnSight Multimode Plate Reader (PerkinElmer) in a 96-well plate format.
- Time-resolved PL studies were performed using Horiba Jobin Yvon Flurolog-3 spectrofluorometer (HORIBA Scientific) and Time-Correlated Single Photon Counting (TCSPC) system.

ACN = Acetonitrile

AHF = Acute heart failure

ALDH = Aldehyde dehydrogenase

AS = Angeli's salt

ASGPR = Asialoglycoprotein receptor

AUC = Area under the curve

α = Relative amplitude

β-Gal = β-galactosidase

β-Glu = β-glucosidase

BH_4 = Tetrahydrobiopterin

BOC = *t*-butoxy carbonyl

BODIPY = Boron dipyrromethene

cAMP = Cyclic adenosine monophosphate

cGMP = Cyclic guanosine monophosphate

CGRP = Calcitonin gene-related peptide

CHISQ = Chi-square

CN^- = Cyanide anion

$CuSO_4$ = Copper sulfate

Cyt c = Cytochrome c

DCC = Dicyclohexylcarbodiimide

DCM = Dichloromethane

DMAP = Dimethyl aminopyridine

DMSO = Dimethyl sulfoxide

eNOS = Endothelial nitric oxide synthases

ESIPT = Excited state intramolecular proton transfer

EDG = Electron donating group

EWG = Electron withdrawing group

EDC.HCl = 1-ethyl-3-(3-dimethylaminopropyl) carbodiimide hydrochloride

ES = Esterase

EtOAc = Ethyl acetate

E. Coli = Escherichia coli

FRET = Forster resonance energy transfer

FMN = Flavin mononucleotide

FAD = Flavin adenosine dinucleotide

GAPDH = Glyceraldehyde-3-phosphate dehydrogenase

GCMS = Gas chromatography-mass spectrometry

GSH = Glutathione

HABA = Hydroxylamino-barbituric acid

HIF-1α = Hypoxia-inducible factor-1α

HILIC = Hydrophilic interaction liquid chromatography

HNO = Nitroxyl

3,2-HNM = *O*-(3-hydroxy-2-naphthalenyl)-methyl

6,2-HNM = *O*-(6-hydroxy-2-naphthalenyl)-methyl

H_2N-CN = Cyanamide

H_2NOH = Hydroxylamine

HO-1 = Heme oxygenase-1

H_2O_2 = Hydrogen peroxide

HPLC = High-performance liquid chromatography

H_2S = Hydrogen sulfide

H_2S_2 = Hydrogen disulfide

H_2S_n = Polysulfide

HSNO = Thionitrous acid

ICT = Intramolecular charge transfer

IDA-HR = High-resolution information-dependent acquisition

iNOS = Inducible nitric oxide synthase

IPA/NO = Isopropylamino diazeniumdialate

IR = Ischemia reperfusion

LG = Leaving group

LTCC = L-type calcium channel

Lyso = Lysosome

MHC = Myosin heavy chain

Mito = Mitochondria

MLC = Myosin light chain

MRM-HR = Hogh-resolution-multiple reaction monitoring

MTT = 3-(4,5-dimethylthiazol-2-yl)-2,5-diphenyltetrazolium bromide

NAC = *N*-acetyl cysteine

NB = Nitrobenzene

$NaBH_4$ = Sodium borohydride

NADPH = Reduced form of Nicotinamide adenine dinucleotide phosphate (NADP)

NAT = *N*-acetyl tryptophan

NAT-NO = *N*-nitroso-*N*-acetyl tryptophan

NHPI = *N*-hydroxy phthalimide

nNOS = Neuronal nitric oxide synthases

NOHA = *N*-hydroxy-*L*-arginine

N_2O = Nitrous oxide

NO = Nitric oxide

NO^- = Nitroxyl anion

NO_2 = Nitrogen dioxide

NO_2^- = Nitrite

NO_3 = Nitrogen dioxide

NOS = Nitric oxide synthase

NTR = Nitroreductase

Na_2SO_4 = Sodium sulfate

ODQ = *1*H-[1,2,4]oxadiazolo-[4, 3-a]quinoxalin-1-one

$ONOO^-$ = Peroxinitrite

PARP = Poly ADP-ribose polymerase

PBS = Phosphate buffer saline

PET = Photoinduced electron transfer

PG = Protecting group

PI3K = Phosphatidylinositol 3-kinase

PLN = Phospholamban

PMSF = Phenylmethylsulfonyl chloride

QTOF = Quadrupole time-of-flight

RFI = Relative fluorescence intensity

RNS = Reactive nitrogen species

ROS = Reactive oxygen species

RSH = Thiol

RSSH = Persulfide

$RSO\text{-}NH_2$ = Sulfinamide

RS-SR = Disulfide

RyR2 = Ryanodine receptor

S_8 = Elemental sulfur

SARCA2A = Sarcoplasmic reticulum Ca^{2+} adenosine triphosphate

sGC = Soluble guanylyl cyclase

SOD = Superoxide dismutase

SR = Sarcoplasmic reticulum

TAC = Time to amplitude converter

TCSPC = Time-correlated single photon counting

TEMPO-9-AC = 4-((9-acridinecarbonyl)amino)-2,2,6,6-tetramethylpiperidin-1-oxyl

TFA = Trifluoroacetic acid

THF = Tetrahydrofuran

TLC = Thin layer chromatography

TRPL = Time resolved photoluminescence

τ = Excited state

VEGF = Vascular endothelial growth factor

w/o ES = Without esterase

First and foremost, I would like to express my deepest gratitude to my supervisor, Prof. Harinath Chakrapani for his invaluable guidance and constant support throughout my Ph.D. journey. He constantly kept me motivated and encouraged in my ups and downs in the Ph.D. as well as in my personal life. Without his support and guidance, it would have been impossible for me to reach this milestone. I feel fortunate to have him as my research supervisor.

I would like to thank the former director of IISER Pune Prof. K. N. Ganesh and the current director Prof. Jayant B. Udgaonkar for providing excellent infrastructure and facilities at IISER Pune. I would like to thank Prof. M. Jayakannan and Prof. H.N. Gopi (Former chair of the chemistry department) and Prof. Nirmalya Ballav (Current chair of the chemistry department) for providing world-class facilities. I gratefully acknowledge the funding agency CSIR for the fellowship.

I am extremely grateful to our collaborators Dr. Vinayak (Prof. J. Toscano, John Hopkins University, USA) and Dr. Meysam, Shreyas, Abraham and Kavya (Prof. Deepak Saini, IISc, Bangalore) for their continued support that has helped me to make significant progress in projects and complete my Ph.D. dissertation. I would like to thank our collaborator Dr. Sidharth Chopra (CDRI, Lukhnow) for his assistance in antibacterial studies.

I would like to sincerely thank my RAC members Dr. D. S. Reddy, Dr. Nithyanandhan (NCL Pune), and Prof. Srinivas Hotha for their important suggestions, ideas, and valuable feedback during RAC meetings. A special thanks to my former lab members: - Dr. Vinayak, Dr. Kundan, Dr. Ravikumar (Mentor and Friend), Dr. Ajay, Dr. Amogh, Dr. Minhaj, Dr. Amol, Dr. Preeti, Dr. Prerona, Dr. Pooja, Dr. Kavita, Jishnu, Saurabh, Harshit, Farhan, Gaurav, Aswin, MJ, Suraj, Manjima, Swetha, Sushma.

A sincere and special thanks to Anand (Andy) for being a friend, and mentor. I had never ever met such a nice person. Highly motivated towards science, super talented, but still down the earth (Rare combination). I am lucky enough to have a friend like you. Thanks to Suman for helping and keeping us updated and for endless discussions on any random topics. Keep your attitude towards life to keep challenging yourself to be better and better, will be happy to see you at high. Thanks to Bharat, Utsav, Simran, Pooja, Hariprasad, Abhishek, Arnab, Mahima, and Shayandeep for help and for maintaining a healthy lab environment.

I am grateful to Dr. Siddhesh Kamat and his group members (Arnab, Aakash) and Dr. Amrita Hazra and her group members.

A special thanks to Mayuresh, Mahesh, Yathish, Tushar, Sanjay, and Mrs. Sayalee for their administrative help throughout my doctoral study. Sandip (HRMS), Nitin and Sandip (NMR), Ganesh (IR). Thanks to Ramlal Sir and Irfana Kureshi for help, allowing me to stay with family in the hostel during the pandemic situation.

Thanks to Dr. Nagesh More, Dr. Manikandan, Dr. Trimbak Mete (Mentor and big brothers), Iranna, and Yogesh (Master) for being alongside me as best friends. Thanks to Vikas Khade, Sachin Nalawade, Utreshwar Gavhane, and their family members for the all love and support in my ups and downs.

Thanks to IISER friends- Prakash, Debasis, Aman, Pankaj, Puneet, and Prachi.

A heartfelt thanks to my childhood friend Om Shinde (from 8th std to yet), who always alongside me in every good and worst situation. I am fortunate enough to have him in my life as a friend. Thanks to all my friends - Pandurang, Mauli, Bhausaheb, Balu, Nitin, Baliram, Ramesh, Sandip, Ashitosh, Anurath, Bharat, Dnyaneshwar, Bhagwat, Sunil, Satish.

A special thanks to Helix and Resonance cricket team for giving me to play my favourite sports game, always giving me a chance as an opener batsman with jersey no. 7.

Finally, I would like to acknowledge the most important people in my life- my father-Rambhau Sawase, my mother-Laxmibai Sawase, grandmother-Rukmeen Dhanwade, uncle-Sakharam Sawase, my brother-Balu Sawase and my soulmate Mayuri Sawase, my little princess Mrunmayee for all their sacrifices, for all the love and for their continuous support in everything.

Abstract

Nitroxyl (HNO), which is a one electron reduced sibling of nitric oxide (NO), activates intracellular signalling pathways, and has vasodilatory and anti-oxidant properties. Recently, a small molecule that generates HNO has emerged as a safe and effective candidate in the treatment of acute heart failure (AHF). Spontaneous generation of HNO is required for cardiovascular applications. Given that HNO is a short-lived and reactive towards biomolecules, controlled and site-directed generation is a prerequisite for other potential therapeutic applications. HNO donors that can be activated by light, chemical or enzyme are reported but have limitations including uncontrolled HNO release, diminished HNO yields, the generation of toxic by-product(s), and concurrent NO release that may complicate mechanistic interpretations. To overcome these limitations, we designed and synthesized a focussed library of *N*,*N*,*O*-protected hydroxylamines that can be activated by enzymes to produce HNO. First, we synthesized compounds that are candidates for activation by esterase to generate HNO. Using a variety of assay, we demonstrate that this class of compounds produce HNO and the HNO generating profile can be modulated by structural modifications. Using these results as the foundation, we designed a donor that produces HNO as well as a fluorescent signal that can act as a reporter for HNO release. The release of HNO within cells was demonstrated using imaging studies. A nearly concomitant increase in fluorescence due to the reporter was also observed. Consistent with the intermediacy of HNO, these donors were also capable of enhancing sulfane sulfur pool in the presence of hydrogen sulfide suggesting possible antioxidant activity for this class of compounds. Next, to enhance the aqueous solubility of donors, we developed glucosidase and galactosidase-activated nitroxyl donors. Upon activation by β-glycosidase, controlled and nearly quantitative HNO release was observed. Lastly, the β-galactosidase-activated donor was found to mitigate reactive oxygen species in senescent cells, which are known to over-express β-galactosidase. Together, we have developed a series of triggerable and tuneable HNO donors that can permeate cells to enhance HNO, and the design allows for incorporating a fluorescence reporter.

CHAPTER 1: Introduction

1.1. Nitric Oxide (NO)

Several reactive nitrogen species, such as $ONOO^-$, NO_2, NO_3 and NO are present in the biological system. Nitric Oxide (NO) has been widely studied free radical reactive nitrogen species. It was named "Molecule of the Year" in 1992 by a science magazine.[1] It is endogenously produced by 5-electron oxidation of *L*-arginine to *L*-citrulline in the presence of NADPH and oxygen by the enzyme nitric oxide synthases (NOS).[2,3,4] Additional cofactors such as flavin mononucleotide (FMN), flavin adenine dinucleotide (FAD), heme, calmodulin and tetrahydrobiopterin (BH_4) are also essential to facilitate electron transfer during the production of NO. Three major distinct isoforms of NOS are present in mammalian cells, such as neuronal NOS (nNOS), inducible NOS (iNOS) and endothelial NOS (eNOS). NO is a significant gaseous signaling molecule that is involved in a variety of physiological processes, such as vasodilation,[2] neurotransmissions,[5] inhibition of platelet aggregation,[6] and host defense mechanisms[7] (Figure 1.1).

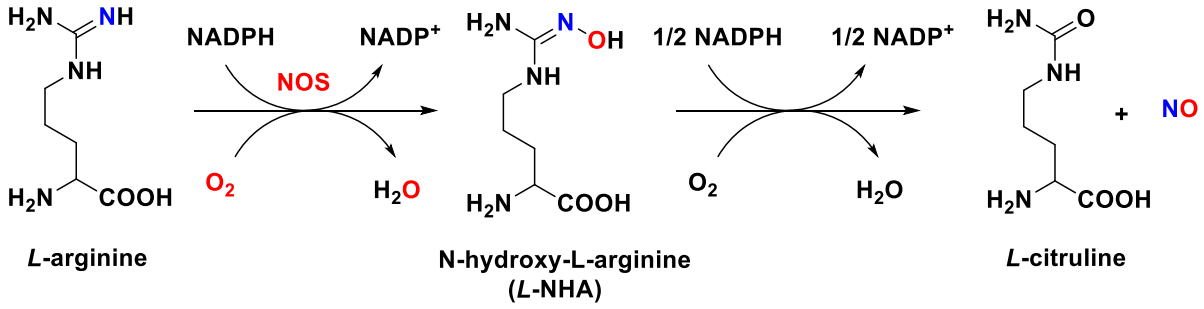

Figure 1.1. Biosynthetic pathway for NO production

1.2. Nitroxyl (HNO/NO^-)

Nitroxyl/nitroxyl anion (HNO/NO^-), also known as azanone, nitrosyl hydride, hydrogen oxonitrate and hydridooxidonitrogen, 1-electron-reduced and protonated form of nitric oxide.[8] Nitroxyl was first reported by Angeli *et al* in 1896.[9] It is a short-lived species that rapidly dimerizes with a second-order rate constant (k = 8 x 10^6 M^{-1} s^{-1}) to give hyponitrous acid in an aqueous solution. Hyponitrous acid forms nitrous oxide (N_2O) and water upon decomposition (Eq. 1)[10] (Scheme 1.1).

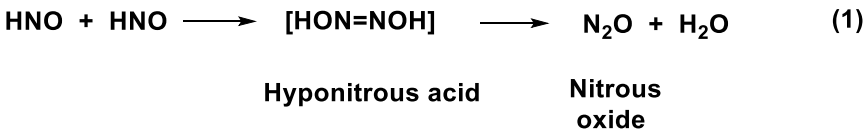

Scheme 1.1. The mechanism for the dimerization of HNO to form N_2O

Three geometrical parameters were used by Orgel to define the structure of the simple triatomic molecule HNO such as the N-O bond length (r_{N-O}), the N-H bond length (r_{N-H}), and the H-N-O angle (θ_{H-N-O}).[11] Next, Dalby has experimentally established the molecular geometry of HNO using the rotational analysis constants, r_{N-H} = 1.063 Å, r_{N-O} = 1.212 Å, and θ_{H-N-O} = 108.6 for the HNO singlet ground state.[12] The electronic ground state of HNO is singlet (^{1}HNO) and deprotonation of HNO generates nitroxyl anion ($^3NO^-$) termed oxonitrate (1^-) which is isoelectronic with dioxygen (O_2). Due to the different spin states of ^{1}HNO and $^3NO^-$, deprotonation of ^{1}HNO and the protonation of $^3NO^-$ in an aqueous solution, is spin forbidden and slow reactions.[13] The lifetime of HNO was estimated to be ~ 0.1 s by Dalby based on gas phase absorption spectra in the region of 6500-7000 Å.[12] The acid/base chemistry of HNO is one of its most distinctive and fascinating features. Due to its spontaneous dimerization into N_2O and water, direct experimental determination of the p*K*a of HNO by measuring equilibrium concentrations of HNO and/or NO^- is challenging. In 2002, Hauk K. N. and coworkers reported the theoretically calculated p*K*a value of 11.6 $\pm$ 3.4, but Shafirovich and Lymar later revised the p*K*a (^{1}HNO/^{3}NO) value to 11.4.[14,10] It suggested that HNO is a weak acid and exists solely at physiological pH.

1.3. Biosynthesis of HNO

Interestingly, HNO is believed to be endogenously synthesized by various biosynthetic pathways like its sibling, NO. Several plausible biosynthetic pathways for the endogenous generation of HNO have been proposed; (1) Oxidation of *L*-arginine by NOS in the absence of tetrahydrobiopterin (BH_4) cofactor;[15] (2) Interconversion between NO and HNO facilitated by superoxide dismutase;[16] (3) Reduction of NO to HNO by cytochrome *c*;[17] (4) Oxidation of hydroxylamine by heme protein;[18] (5) Reduction of nitrite by hydrogen sulphide (H_2S) in the presence of heme protein;[19] (6) the reaction of thionitrous acid (HSNO) with hydrogen sulfide (H_2S)[20] and (7) the reaction between NO and H_2S[21] (Figure 1.2). Together, these pathways may contribute to the endogenous generation of HNO.

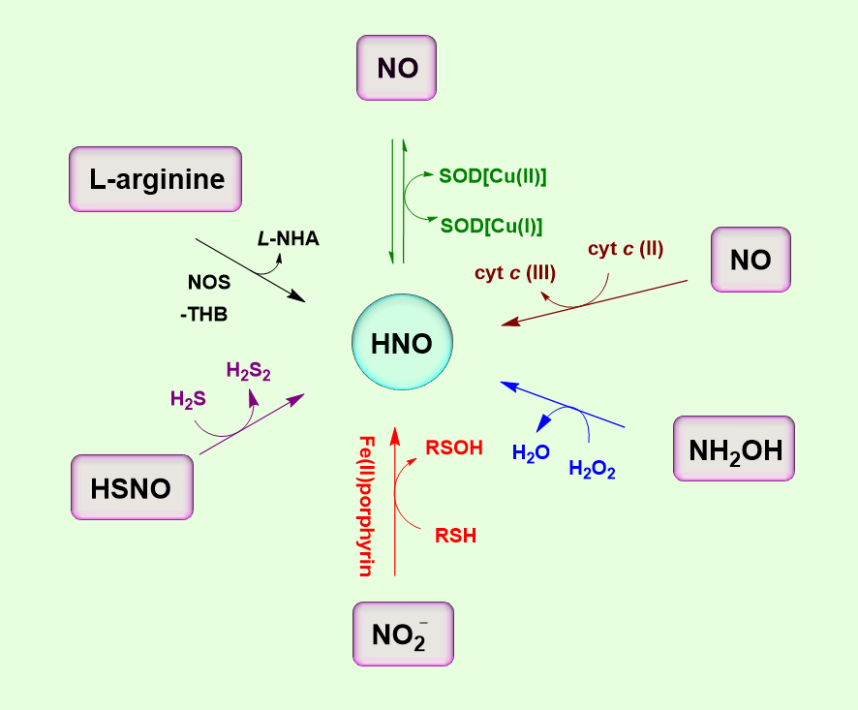

Figure 1.2. Biosynthesis of HNO generation. **NOS**: Nitric Oxide Synthase; **BH_4**: Tetrahydrobiopterin; ***L*-NHA**: *N*-hydroxy-*L*-arginine; **SOD**: Superoxide Dismutase

1.4. Reactivity of HNO

Interpretation of the reactivity of HNO is crucial given the interest in HNO prodrugs as potential therapeutics.

1.4.1. Reaction of HNO with H_2S, persulfides and thiols

A distinct feature of HNO from other nitrogen oxides is its high thiophilicity. Recently, Toscano and coworkers studied the reaction of HNO with hydrogen sulfide and persulfide. HNO reacts with the hydrogen sulfide to form an *N*-mercaptohydroxylamine intermediate which further reacts with hydrogen sulfide to produce polysulfides and elemental sulfur. Similarly, persulfide reacts with HNO to afford polysulfides following the same mechanism (Scheme 1.2) [22].

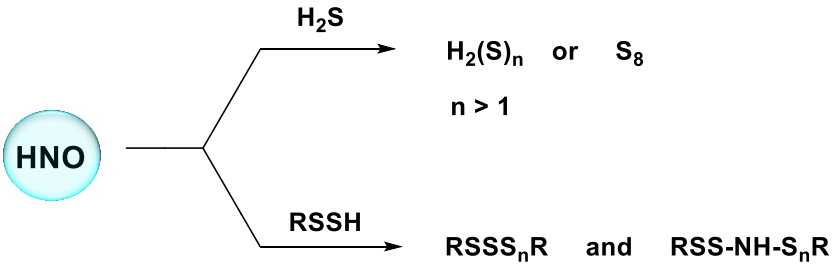

Scheme 1.2. The reaction of HNO with the hydrogen sulfide and persulfides

Owing to the thiophilic nature of HNO, it majorly targets the thiols and thiol-containing proteins. Thiol attacks the electrophilic nitrogen atom of HNO to generate an unstable intermediate *N*-hydroxy-sulfenamide, which is later rearranged to sulfinamide or disulfide depending on the physiological thiol concentration (Scheme 1.3).[23]

The rate constant for the reaction between HNO and glutathione (GSH) is 8 x 10^6 M^{-1} s^{-1}.[24] It has been demonstrated that HNO modifies the thiol residues of several proteins at physiological conditions, resulting in a potential protein function (Table 1.1). For example, HNO interacts with the thiol residues of glycolytic protein glyceraldehyde-3-phosphate dehydrogenase (GAPDH),[25,26] aldehyde dehydrogenase (ALDH),[27,28] soluble guanylyl cyclase (sGC),[29,30,31,32,33,34,35] DNA repair protein poly (ADP-ribose) polymerase (PARP),[36] the cysteine proteases papain[37] and cathepsin B.[38,39] HNO also regulates the vasorelaxation by interacting with the iron or thiol site.[32] HNO induces activation of myofilament proteins, which has potential in the treatment of congestive heart failure.[40,21]

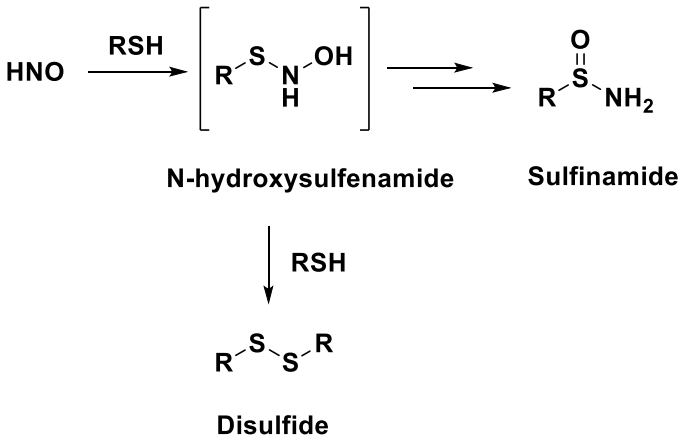

Scheme 1.3. The reaction of HNO with thiols

Table 1.1: Rate constant of HNO with biomolecules

Biomolecules	k (M^{-1} s^{-1})
Glutathione[24]	8 x 10^6
Papain[37]	2 x 10^7
N-acetyl-*L*-cysteine[24]	5 x 10^5
L-cysteine[24]	4.5 x 10^6
Oxygen[41]	3 x 10^3
NO[8]	5.8 x 10^6
Cu/Zn Superoxide Dismutase[24]	1 x 10^6
Mn Superoxide Dismutase[24]	7 x 10^5
Catalase[24]	3 x 10^5
Metmyoglobin[42]	8 x 10^5
Oxymyoglobin[42]	1 x 10^7
Horseradish Peroxidase[24]	2 x 10^6
Tempol[24]	8 x 10^4

1.4.2. Reaction with metalloproteins

In addition to thiols, HNO also interacts with the metalloproteins such as heme proteins and superoxide dismutase. Studies have shown that HNO can interact with metalloenzymes in either ferrous or ferric forms. The most commonly observed interactions between HNO and metalloproteins are redox and substitution reactions. Sadler and coworkers showcased that HNO reduces met (Fe^{III})-myoglobin to ferrous (Fe^{II})-NO myoglobin (Eq. 2).[43] A ferrous (Fe^{II}) heme protein either trap HNO directly to form a ferrous (Fe^{II})-HNO complex (Eq. 3) or reduction of Ferrous (Fe^{II})-NO Mb complex (Eq. 4). The oxymyoglobin and HNO react similarly to NO to form a corresponding ferric heme protein (Eq. 5) (Scheme 1.4).[42,44,45,46]

$$MbFe(III) + HNO \longrightarrow MbFe(II)\text{-}NO + H^+ \quad (2)$$

$$MbFe(II) + HNO \longrightarrow MbFe(II)\text{-}HNO \quad (3)$$

$$MbFe(II)\text{-}NO + e^- + H^+ \longrightarrow MbFe(II)\text{-}HNO \quad (4)$$

$$MbFe(II)O^2 + HNO \longrightarrow MbFe(III) + NO + HOO^- \quad (5)$$

Scheme 1.4. The reaction of HNO with the myoglobin

Furthermore, HNO interacts with aquacobalmin (H_2O-Cbl^+(III)) and forms nitroxyl cobalmin (NO^--Cbl(III)) (Eq. 6).[47] This interaction takes place in a stepwise manner; (i) Initially, HNO reduces Cbl(II)alamin to Cbl(I)alamin by the release of NO (Eq. 7); (ii) Oxidation of Cbl(I)alamin to Cbl(II)alamin by HNO (Eq. 8); (iii) Finally, Cbl(II)alamin reacts rapidly with NO to form nitroxylcobalmin (NO^--Cbl^-(III)) (Eq. 9) (Scheme 1.5).[48,49]

$$H_2O\text{-}Cbl^+(III) + HNO \longrightarrow NO^-\text{-}Cbl(III) + H_3O^+ \quad (6)$$

$$Cbl(II) + HNO \longrightarrow Cbl(I) + NO + H^+ \quad (7)$$

$$Cbl(I) + HNO + H^+ \longrightarrow Cbl(II) + 1/2\ N_2 + H_2O \quad (8)$$

$$Cbl(II) + NO \longrightarrow NO^-\text{-}Cbl(III) \quad (9)$$

Scheme 1.5. The reaction of HNO with the aquacobalmin

Additionally, the copper (II) center of superoxide dismutase was reduced by HNO to yield the copper(I) complex and release NO. Interestingly, Cu/Zn superoxide dismutase is catalyzed by the interconversion of HNO/NO (Eq. 10).[16] Nevertheless, metalloproteins (heme protein and superoxide dismutase) do not discriminate between HNO and NO due to reductive nitrosylation reaction. Marti and coworkers showed the Mn (III) and Co(III) porphyrins selectively react with HNO while the Mn(II) and Co(II) porphyrins react only with the NO (Scheme 1.6).[50]

$$HNO + SOD[Cu(II)] \rightleftharpoons NO + SOD[Cu(I)]\text{-}H^+ \quad (10)$$

Scheme 1.6. The reaction of HNO with the superoxide dismutase

1.4.3. Reactivity with molecular oxygen

Recently, Sikora and coworkers have reported the reaction of molecular oxygen and HNO under physiological conditions. Molecular oxygen has a triplet ground state and can therefore react with nitroxyl anion ($^3NO^-$) to form peroxynitrite ($ONOO^-$) with the rate constant of ~1.8 x 10^4 M^{-1} s^{-1} (Eq. 11). However, it reacts slowly with nitroxyl (^1HNO) (Eq. 12) due to a spin forbidden process. Furthermore, the peroxynitrite product has been detected and quantified peroxynitrite product using a fluorescent probe (Scheme 1.7).[41,51,16,52]

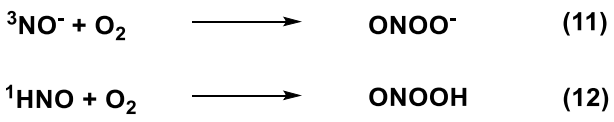

Scheme 1.7. The reaction of HNO with the oxygen

1.4.4. Reaction with NO

Both ^1HNO and $^3NO^-$ react with NO to afford the hyponitrite radical anion. Furthermore, it reacts with NO to generate $N_3O_3^-$ anion, that decomposes to N_2O and NO_2^- (Scheme 1.8).[8]

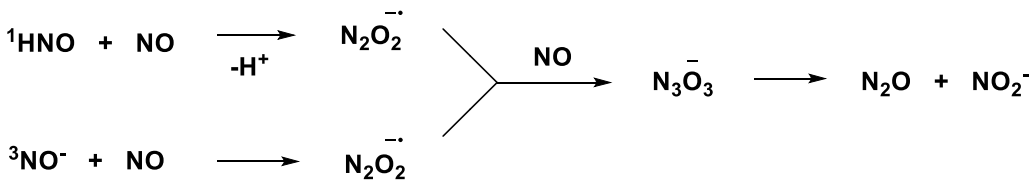

Scheme 1.8: The reactions of HNO and NO^- with the NO

1.5. Therapeutic application of HNO

The selectivity in the reaction of HNO with thiols and thiol proteins is the key aspect of the therapeutic activity of HNO.

1.5.1. HNO in the treatment of alcoholism

In the presence of catalase and hydrogen peroxide, cyanamide (H_2N-CN) acts as an HNO precursor. It forms the unstable *N*-hydroxycyanamide intermediate which releases HNO and cyanide anion. The enzyme alcohol dehydrogenase catalyzed the conversion of ethanol to acetaldehyde, which was then converted to acetic acid by aldehyde dehydrogenase. HNO acts

as a potent inhibitor of aldehyde dehydrogenase by modification of the thiol residues on aldehyde dehydrogenase to sulfinamide (Scheme 1.9)[27,28].

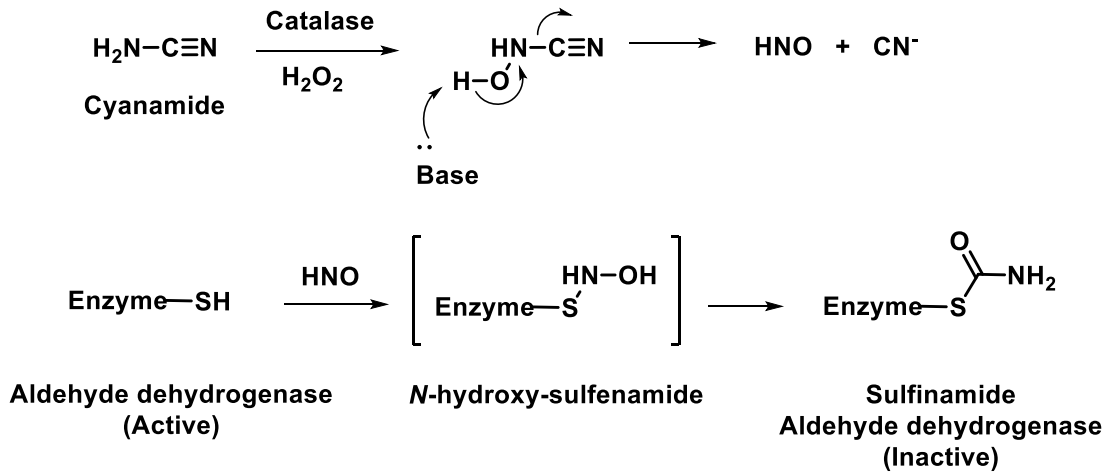

Scheme 1.9: Mechanism of generation of HNO from cyanamide and inactivation of aldehyde dehydrogenase by HNO

1.5.2. HNO in the cardiovascular system

Heart failure is characterized as a condition in which the left heart is unable to pump out sufficient oxygen-rich blood into circulation to meet the body's needs. The standard therapy for heart failure constitutes the use of vasodilators, inotropic agents, and loop diuretics (Figure 1.3). An increased arterial stiffening is associated with myocardial dysfunction in heart failure. Targeting vascular abnormalities, such as decreasing vascular stiffness, and lowering vascular resistance, may be pivotal avenues for the treatment of heart failure.

HNO has a unique and potentially important effect on the heart including vasorelaxation and enhanced cardiac contractility. Paolocci and coworkers reported that HNO has not only a positive inotropic (myocardial contractility) but also positive lusitropic (myocardial relaxation) effect on the heart. These effects were independent of β-adrenoceptor signaling, a potentially novel mechanism for modulating heart function.[53] Further, several research groups showed that HNO can increase myocyte Ca^{2+} cycling by activation of the SARCA2A (sarcoplasmic Ca^{2+} reuptake pump) via interacting with the phospholamban (SARCA2A regulating protein) and activation of ryanodine receptor-2 (RyR2). These characteristics have led to the current pharmaceutical development of HNO donors as heart failure therapies (Figure 1.3).[54,55,56,57]

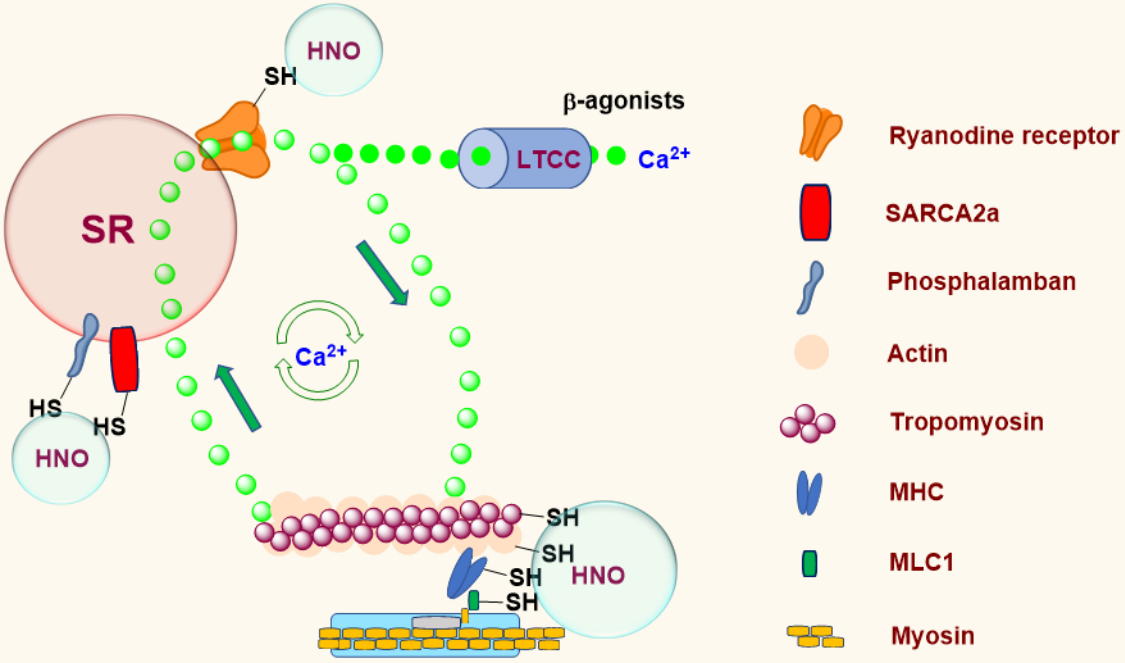

Figure 1.3: Role of HNO in the cardiovascular system.

1.5.3. HNO in ischemia-reperfusion injury

Wink, Feelisch and Paolocci's research groups studied the pharmacological effects of HNO on the ischemia-reperfusion injury model.[58] Before reperfusion, pretreatment of Angeli's salt to the isolated rat heart offered considerable protection against subsequent reperfusion injury, suggesting ischemic preconditioning. Ma and coworkers showed that in an ischemia/reperfusion (IR) injury model system, infusion of Angeli's salt during reperfusion induces an exacerbation of reperfusion damage in an ischemia/reperfusion (IR) injury model.[59] Despite this, it is still unclear how HNO causes ischemia-reperfusion damage.

1.5.4. HNO in vasodilation

By interacting with the regulatory ferrous heme on sGC, HNO can activate sGC and promote vasodilation. Several downstream pathways have been proposed for HNO-mediated vasodilation, including activation of voltage and calcium-dependent potassium channels, an increase in the level of CGRP (calcitonin gene-related peptide) and activation of cGMP/cAMP-dependent signaling.[29,30,31,32,33,34] Kass and coworkers studied sGC antagonist [*1*H-[1,2,4]oxadiazolo-[4, 3-a]quinoxalin-1-one] (ODQ) blocks HNO-vasodilation in vitro,

which indicates an sGC dependent mechanism using CXL-1020 (HNO donor).[35] Similarly, Fukuto and coworkers also studied HNO-mediated vasodilation using Angeli's salt and IPA/NO[60] (Figure 1.4).

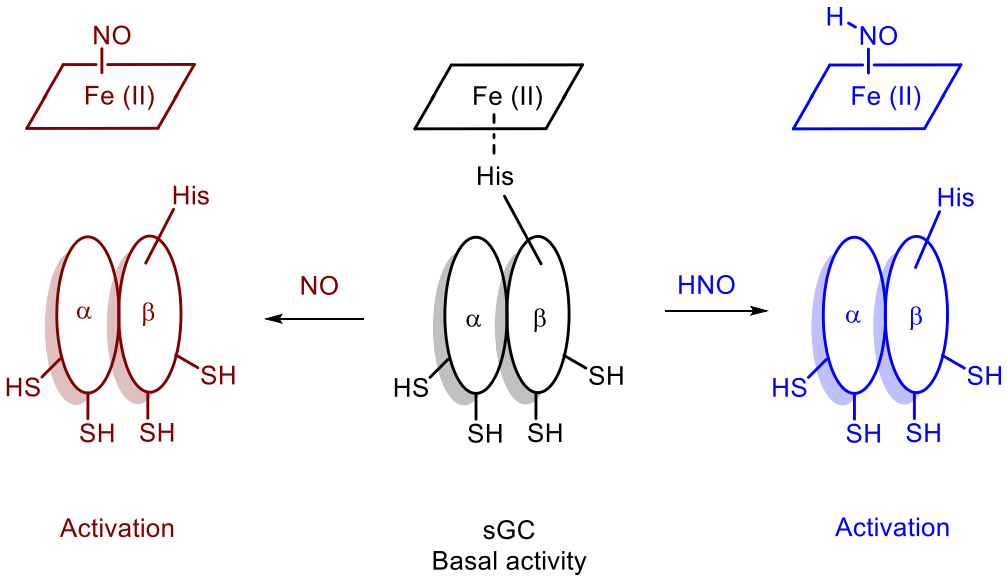

Figure 1.4: Proposed mechanism for the effect of HNO on the sGC activity

1.5.5. HNO in cancer

HNO has shown promising anti-cancer effects. It is well known that HNO can interact with the specific thiol proteins that are involved in the modulation of cellular functions.

The majority of solid tumors rely heavily on glycolysis as a significant energy source, GAPDH (Glyceraldehyde -3-phosphate dehydrogenase) is one of the key enzymes in the glycolytic process. GAPDH activity can be irreversibly inhibited by HNO.[25]

Treatment with HNO resulted in an inhibition of tumor angiogenesis and increased apoptosis in breast cancer xenografts.[26,43] In addition, HNO may also be a useful adjuvant to cancer chemotherapy. Inhibition of poly (ADP-ribose) polymerase (PARP) by Angeli's salt has also been demonstrated in a breast cancer cell line.[36] Given that, PARP is an important component of the DNA repair machinery, it may be a crucial target in cancer therapy. As several chemotherapies and radiation therapies rely on inducing DNA damage in cancer cells. The efficacy of these treatments could be improved by HNO donors by inhibiting PARP. These indicate the efficacy of HNO in cancer chemotherapy (Figure 1.5).

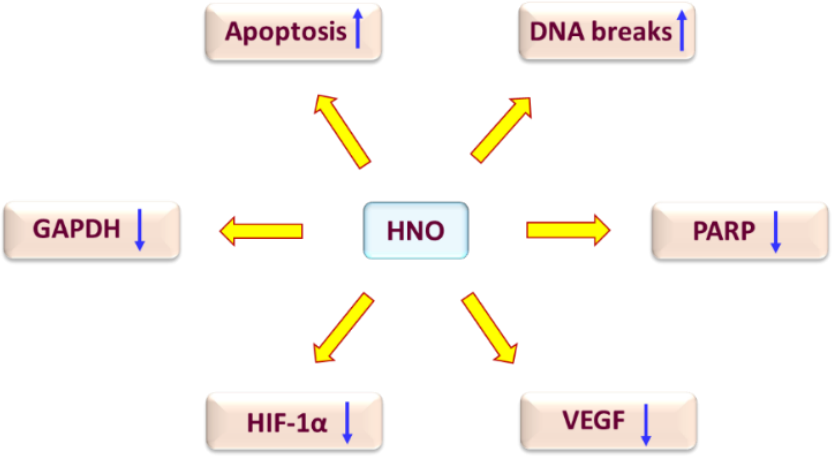

Figure 1.5: Role of HNO in the cancer therapy

1.5.6. HNO as antioxidant

Previous studies have shown that HNO has a pro-oxidant property, capable of inducing DNA breaks and intracellular thiol depletion.[61] In redox biology, the role of HNO has been studied and it can cause both pro-oxidant and antioxidant effects. Earlier studies demonstrated that HNO has a pro-oxidant property, capable of inducing DNA breaks and intracellular thiol depletion. HNO was also found to induce heme oxygenase-1 (HO-1, an anti-oxidant enzyme), similar to the NO, peroxynitrite and nitrosothiols.[62] Angeli's salt (AS) mediated activation of HO-1 was almost abolished by the *N*-acetylcysteine (NAC), whereas, activation of HO-1 by HNO subdued by the treatment of glutathione synthesis inhibitor (buthionine sulfoximine). These findings indisputably indicated that targeting sulfhydryl groups is crucial in controlling the expression of HO-1.

1.6. HNO donors

The most commonly used strategies to generate HNO at physiological conditions involves (i) -OH deprotonation; (ii) cleavage of PG by a specific stimulus and (iii) nucleophilic attack on acyl nitroso moiety. In the first case, -OH deprotonation takes place at physiological pH 7.4 and undergoes further decomposition to release HNO. Next, the stimulus was used for the cleavage of the protecting group to generate HNO. Finally, the formation of acyl nitroso intermediate takes place, which on nucleophilic attack or hydrolysis to release nitroxyl anion (NO^-). In the second and third strategies, different stimuli such as light, thiol, heat and enzymes were used to generate HNO (Scheme 1.10).

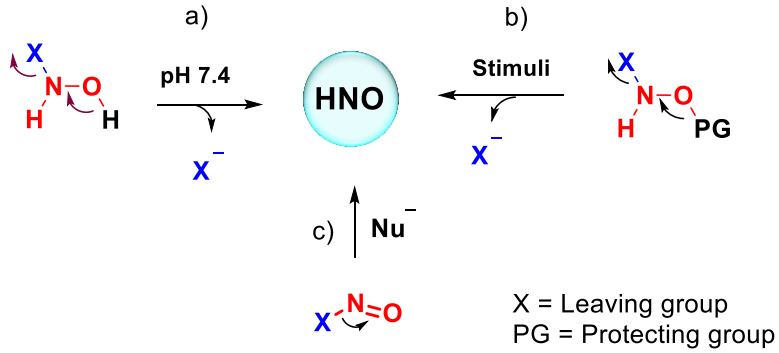

Scheme 1.10: General strategy for the HNO generation

1.6.1. HNO generation in the aqueous condition

In this category, Angeli's salt (AS, $Na_2N_2O_3$) is the priority. It is an inorganic salt that was originally discovered in 1896.[9] In physiological conditions, it rapidly generates HNO with a half-life of ~ 3 min. The interest in the biological activity of HNO has led to the development of Angeli's salt as an effective donor for understanding the chemistry and pharmacology of HNO. (Scheme 1.11).

Proposed mechanism

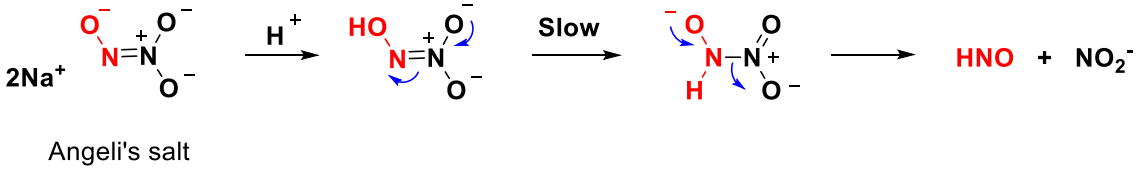

Scheme 1.11: Decomposition of Angeli's salt and proposed mechanism of HNO generation

Next, Piloty's acid and its derivatives are listed below, known to release HNO at physiological conditions.[63,64] CXL-1020 and CXL-1472 (BMS-986231) are two of the reported donors that are undergoing clinical studies for the treatment of heart failure (Figure 1.6).[65,66]

There have also been reports of other donors such as derivatives of diazeniumdiolates (IPA/NO, CPA/NO, CHA/NO, CHPA/NO and COA/NO), acyloxy nitroso, *N*,*O*-bis-acylated and carbon-based leaving group donors (Scheme 1.7).[67,68,69,70,71]

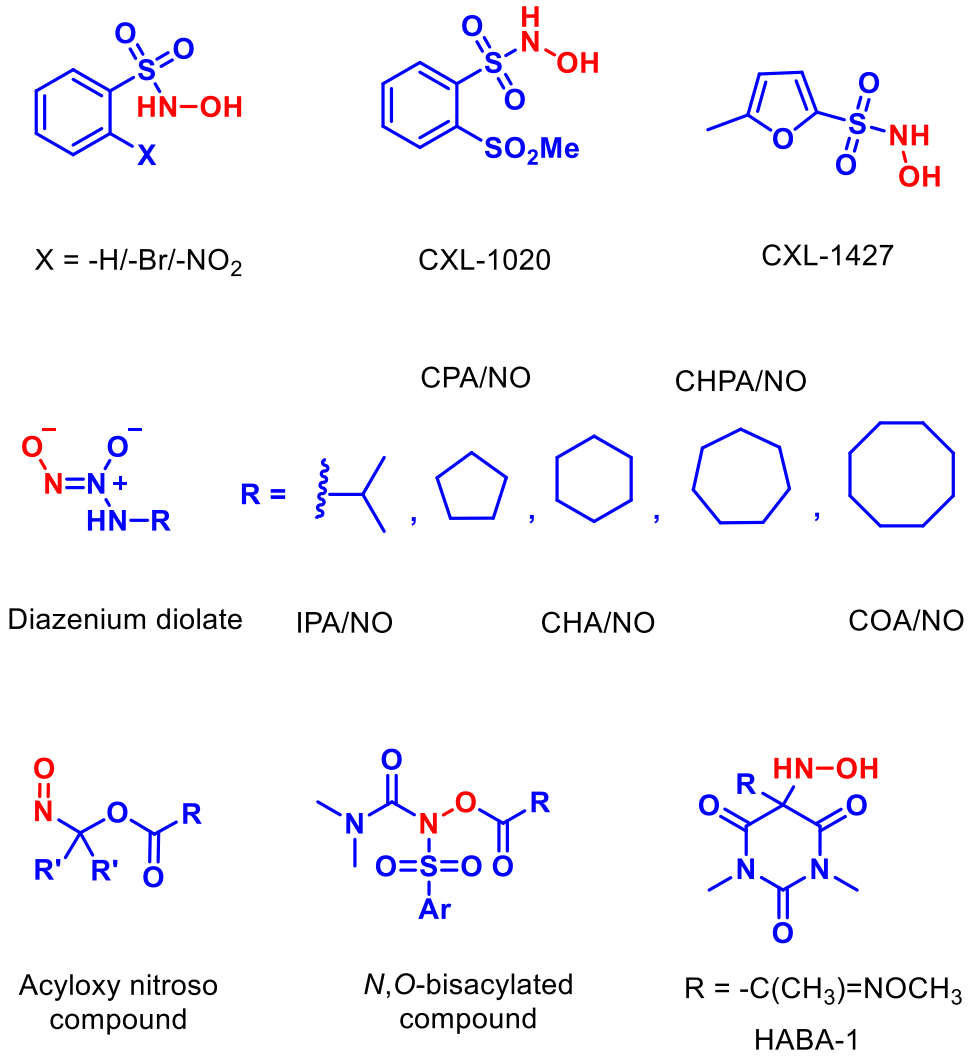

Figure 1.6: Structures of HNO donors

Unfortunately, controlled delivery of HNO would be impossible using these donors. Burst HNO generation leads to HNO dimerization which lowers the effective concentration of produced HNO. Hence, it is urgent to develop controlled HNO generators.

1.6.2. Light-triggered approach for HNO generation

Over the years, several research groups have developed a series of photo-activated HNO donors such as 3,2-HNM, 6,2-HNM and nitrobenzene-based donors.[72,73,74,75] These donors are capable of generating HNO in good to excellent yield. However, the use of these donors is limited, due to O-N bond cleavage over C-O bond, low HNO yield and phototoxicity of UV light. Hence, the development of alternative donors is necessary to overcome the aforementioned limitations (Figure 1.7).

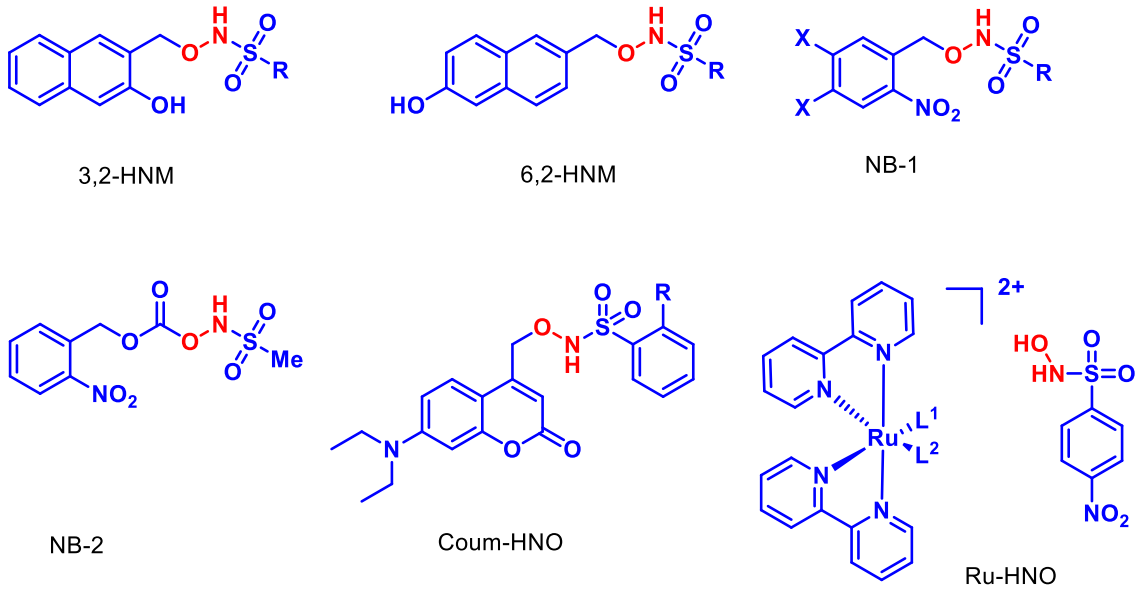

Figure 1.7: Light-activated HNO donors, L^1 = PMe_3; L^2 = Glutamate

Nakagawa group has developed a visible light-activated HNO donor, based on the 7-aminocoumarin.[76] Upon irradiation by visible light, the concomitant release of HNO with a fluorescence reporter was observed following the cleavage of the C-O bond in Coum-HNO cleavage takes place to form carbocation and N anion derivative of Piloty's acid, upon light irradiation. Interestingly, the generated carbocation reacts with the water molecule leading to the release of HNO and the formation of the fluorescent molecule (HNO-generating pathway). As well as N anion derivative of Piloty's acid also attacks the carbocation which leads to the formation of an oxime derivative (non-HNO generating pathway). The HNO-generating pathway contributes to only 7.1%, leading to low HNO generation.

Next, the Doctorovich group developed a Ru-HNO donor using 4-nitropiloty's acid as the source of HNO. Selective delivery could not be achieved using a Ru-HNO donor.[77]

1.6.3. Thiol and thermally-activated approach for HNO generation

Sadler group has reported the thiol-dependent HNO release using a Ru-based donor which showed the HIF-1α inhibition.[43] However, specific HNO delivery could not be achieved using Ru(II)-NO donor. Further, retro Dials-Alder reaction-based HNO donors as well as HNO/H_2S dual donors have been reported (Figure 1.8).[78,79,80,81,82]

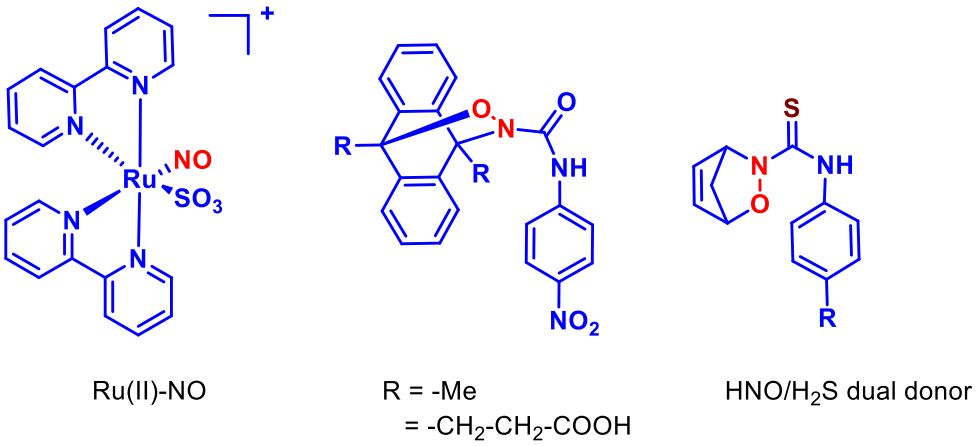

Figure 1.8: Thiol and thermally activated HNO donors

1.6.4. Chemically and enzymatically triggered approach for HNO generation

Recently, the King group reported the chemically activated self-immolating HNO donors. The nitro, azide and boronate ester were used as a protecting group, which was cleaved by the $NaBH_4$ or NTR, $NaBH_4/CuSO_4$ and hydrogen peroxide respectively.[83] In these cases, azide-containing compounds showed promising results with HNO release in high yield. However, the use of $NaBH_4/CuSO_4$ in the biological system would not be a good strategy to generate HNO. Further, the Nagasawa group developed *N*-hydroxycarboximidic acid derivatives which can be activated by esterases.[84] These donors showed low HNO yield. Next, the Miranda group developed the esterase and β-galactosidase sensitive HNO donors using IPA/NO as an HNO source.[85,86] Unfortunately, these donor act as HNO/NO dual donors. The reaction of HNO with the NO complicates further studies as several reports demonstrated that these species play opposing roles. It would not be a good choice for the donor (Figure 1.9).

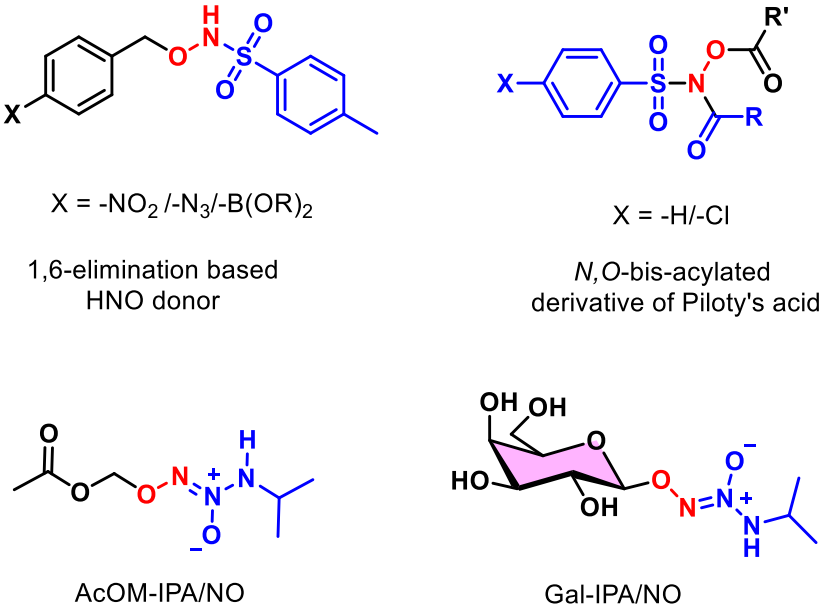

Figure 1.9: Enzymatically activated HNO donors

1.6.5. Limitations with existing HNO donors

The above-described approaches to generating HNO have some limitations. Reported HNO donors generate HNO in an uncontrolled manner (burst HNO release) leading to the dimerization of HNO. These donors have no selectivity in the delivery of HNO. To overcome these limitations, UV light-triggered HNO donors have been developed. However, UV light can enhance oxidative stress in the cellular system and affect the function of vital cellular biomolecules. Since low tissue penetration of UV light, *in vivo* studies become more challenging. Hence, UV-triggered HNO donors are unsuitable for study of the HNO biology and pharmacology. Next, thiol activated HNO donor was reported and HNO is thiophilic in nature, the effective concentration of HNO will be less and the donor is not selective. Retro Diels-Alder reaction-based HNO donor needs quite a heating condition to generate HNO, making it unsuitable in cellular studies. Recently, an esterase-triggered donor was developed, however, the issues with these donors are low HNO yield and concurrent generation of NO. To achieve the selectivity in HNO delivery, β-galactosidase sensitive IPA/NO-based HNO donors are reported. Given that, IPA/NO gives concomitant release of HNO/NO, the studies become more complicated.

Hence, to overcome these limitations of existing prodrug strategies, the development of versatile HNO donors is in urgent need.

1.7. HNO detection

Given that HNO is a short-lived species, the detection of HNO becomes crucial in cellular systems. Enormous effects were made towards the development of HNO-sensitive probes for detection. As HNO is highly reactive towards biomolecules (thiols/thiol proteins, metalloproteins), precise detection of mysterious HNO becomes quite challenging. HNO also displayed higher reactivity with the phosphines. Based on the reactivity of HNO, several probes were developed with the phosphine, thiol and metals.

1.7.1. Phosphine-based HNO probes

The reaction of phosphine and HNO follows Staudinger ligation chemistry. The fluorescence reporter is attached to the phosphine HNO recognition unit. In phosphine probes, the ester linkage is appended on the ortho position along with the latent fluorophore. Upon reaction with HNO, the release of active fluorescent molecules takes place, which attributes to the HNO generation (Figure 1.10).[87]

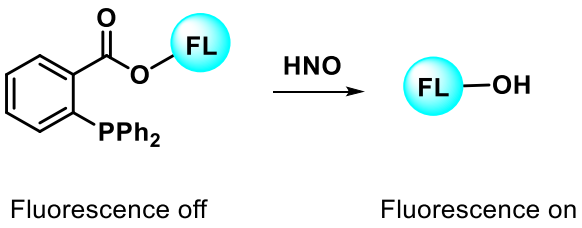

Figure 1.10: Staudinger ligation reaction of phosphine with the HNO

The following mechanism has been proposed for HNO detection by phosphine-based probes. Here, nucleophilic phosphine attacks on the electrophilic nitrogen of HNO, one molecule of phosphine is converted into phosphine oxide and another molecule forms phosphine aza-ylide which further rearranges into an ionic form. Intramolecular attack of nitrogen anion on the ester linkage results in the release of an active fluorophore. An enhancement in the fluorescence signal corresponds to the amount of HNO generation from the donor (Scheme 1.12).

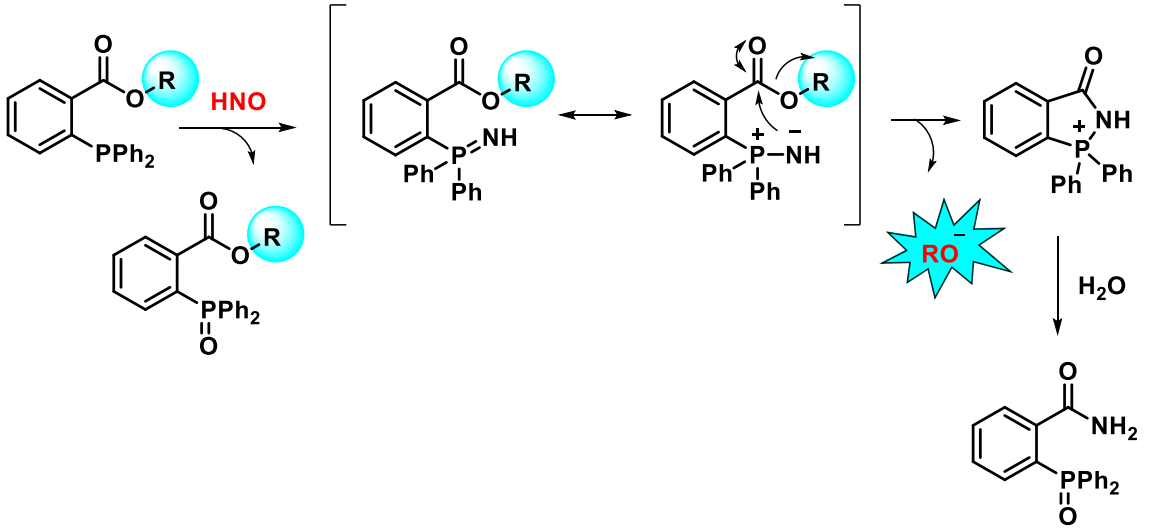

Scheme 1.12: Proposed mechanism of the HNO detection by phosphine probe

Various kinds of phosphine probes have been developed for HNO detection. Representative probes are listed below such as turn-on probes (e.g. PCM, P-Res and P-Rhod),[88,89,90] intramolecular charge transfer (ICT) ratiometric probe (e.g. HNO-TCF),[91] an excited state intramolecular proton transfer (ESIPT) mechanism-based ratiometric probes (e. g. FLA-1 and P-HBT),[92,93] two-photon activated probes (e. g. P-Np-Rhod),[94] Forster resonance energy transfer (FRET) mechanism-based ratiometric probes (e. g. CF),[95] mitochondria-targeted probes (e. g. Mito-HNO)[96] and lysosome targeted probe (e. g. Lyso-JN)[97] (Figure 1.11).

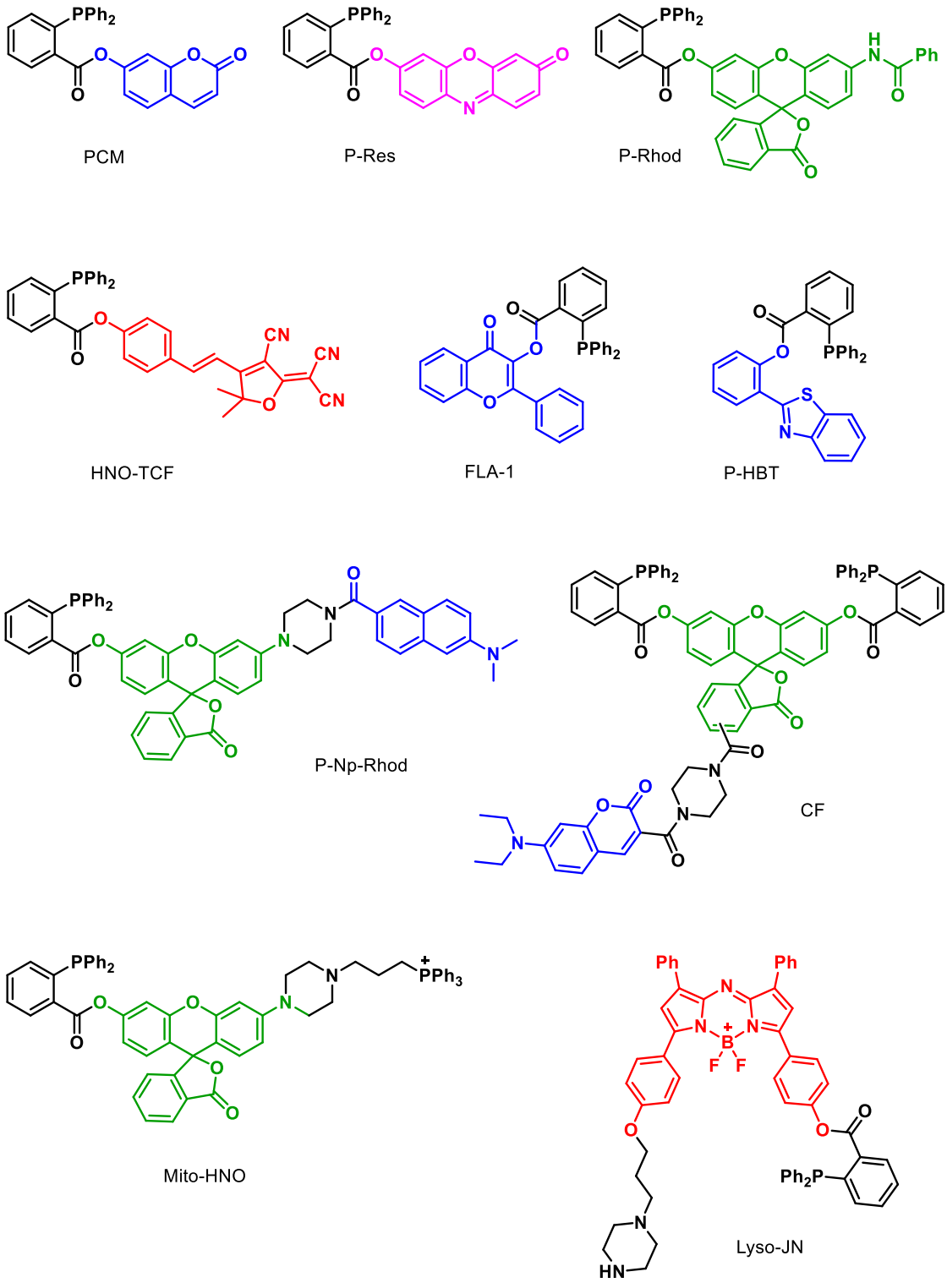

Figure 1.11: Phosphine-based HNO probes

1.7.2. Thiol-based HNO probes

As HNO is highly reactive towards thiols, the Chan group has developed a thiol-based probe to detect HNO. Here, thiol served as a recognition unit for the HNO. The nucleophilic thiol attacks the electrophilic nitrogen of HNO to generate an *N*-hydroxysulfenamide intermediate, which undergoes intramolecular cyclization to release the masked fluorophore. The amount of HNO generation from the donor was estimated based on the fluorescence increment (Scheme 1.13).[98]

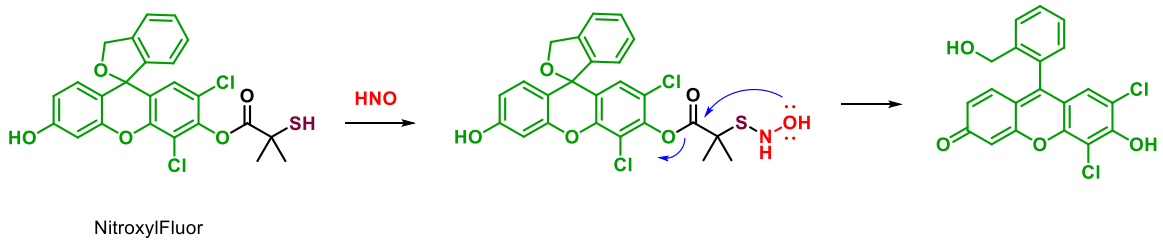

Scheme 1.13: Proposed mechanism for the HNO detection by thiol-based HNO probe

1.7.3. Prefluorescent HNO probe

HNO is known to efficiently react with radicals via a proton transfer. Based on this chemistry, the Toscano group has developed a prefluorescent probe that reacts with HNO via a net hydrogen abstraction to produce fluorophore and NO.[99] The important feature of the probe is that it can be able to differentiate the HNO from NO (Scheme 1.14). However, TEMPO-9-AC is quite unstable in aerobic conditions, making it difficult to use in physiological conditions.

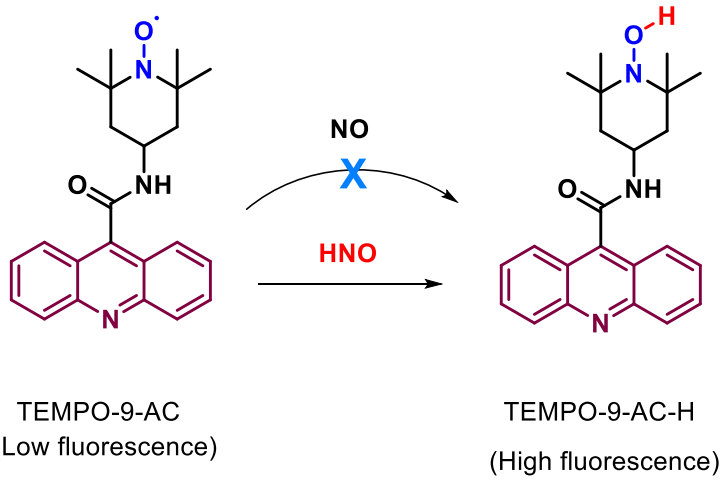

Scheme 1.14: Mechanism of HNO detection by TEMPO-9-AC

1.7.4. Copper (II) based probe for the HNO detection

As HNO is known to react with metalloproteins, copper (II) based HNO probes have been reported. Cu (II) is present in these probes with an unpaired electron in the d orbital, which causes fluorescence to be quenched by the photoinduced electron transfer (PET) mechanism. Typically, there is little to no fluorescence when the fluorescent molecules bind to the Cu (II) complex. (Figure 1.12).

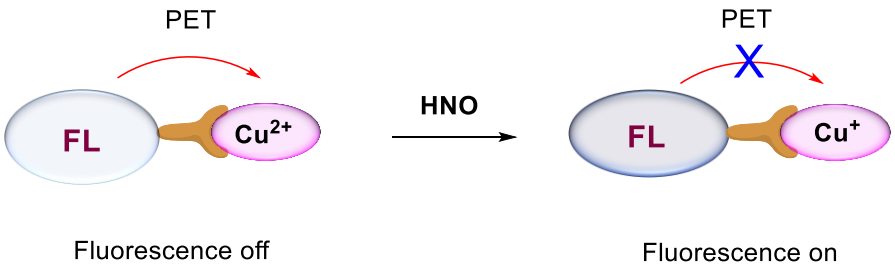

Figure 1.12: Schematic diagram for the HNO detection by the Cu(II) based probes

The representative examples of a few Cu(II) based probes (Cu(II)[BOT1] and Cu(II)[BRNO3]) used for the HNO detection are listed. Lippard group constructed the Cu(II) based probe based on the reduction of Cu(II) to Cu(I) by HNO. BODIPY moiety served as a fluorescence reporter and Cu(II) acts as the HNO recognition unit for the HNO (Figure 1.13).[100,101,102,103]

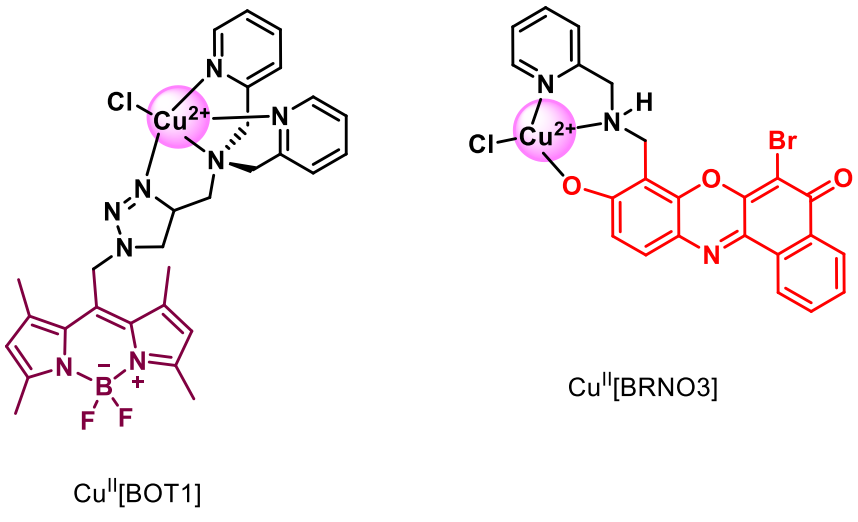

Figure 1.13: Cu(II) based probes for the HNO detection

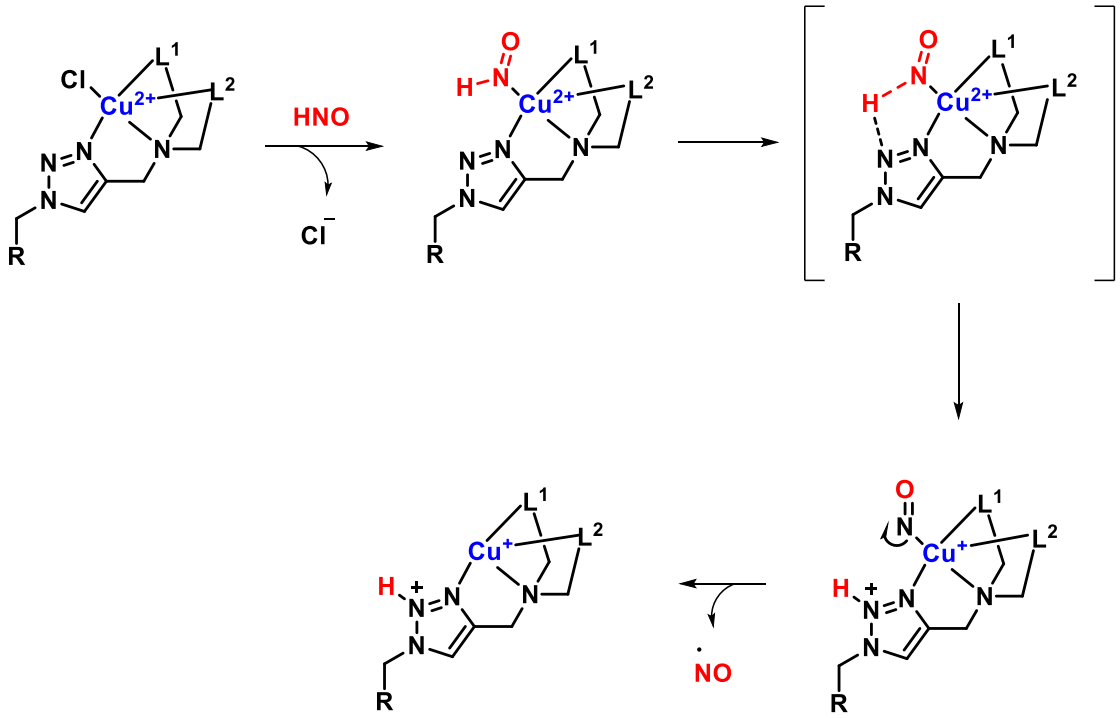

Scheme 1.15: Mechanism of HNO detection by the Cu(II) complex

Upon interaction of HNO with the Cu(II) complex, nucleophilic nitrogen of HNO attack on the Cu(II) to display chloride anion. Further, the hydrogen atom of HNO forms intramolecular hydrogen bonding with the nitrogen atom of the triazole moiety of the complex in the transition state, subsequently hydrogen atom transfer to the nitrogen atom of the triazole and Cu(II) reduce into the Cu(I). Finally, the nitric oxide radical (NO·) is released from the complex resulting in an enhancement in the fluorescence response (Scheme 1.15).

1.7.5. Detection of N_2O (HNO dimer) by GC/MS

As described above, dimerization of HNO leads to the formation of nitrous oxide (N_2O). It is quite stable and can be quantified by the GC/MS analysis (m/z = 44) (Scheme 1.1).

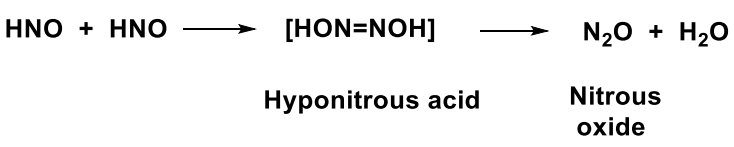

Scheme 1.1. Mechanism of HNO dimerization

Other than phosphine, thiol, Cu(II) and GC/MS-based HNO detection methods, electrochemical detection of HNO by amperometric sensors and MIMS (Membrane inlet mass spectrometry) were used to measure HNO.

1.7.6. Limitations with the existing HNO probes

Several limitations are associated with the phosphine, thiol, prefluorescent probe and Cu(II) based probes such as 1) HNO gets consumed during this process; 2) instability of certain probes in cellular conditions; 3) no selectivity between HNO and NO; 4) Dimerization can take place between thiol based probe; 5) instability in aerobic conditions.

Several limitations are associated with HNO donors and HNO probes. The HNO delivery with triggerable and tunable HNO release along with the fluorescence reporter for broad applicability is not yet reported. Therefore, the development of versatile HNO donors along with the fluorescent reporter is in urgent need.

1.8. Aim

We aim to design, synthesize and evaluate HNO donors with the following characteristics.

i) Donor should be triggerable and the trigger should be selective.

ii) HNO release should be in a controlled manner to minimize dimerization.

iii) Fluorescence reporter should be turn ON and stable for an extended period.

iv) Fluorophores should not consume HNO during the detection; but instead, report HNO generation.

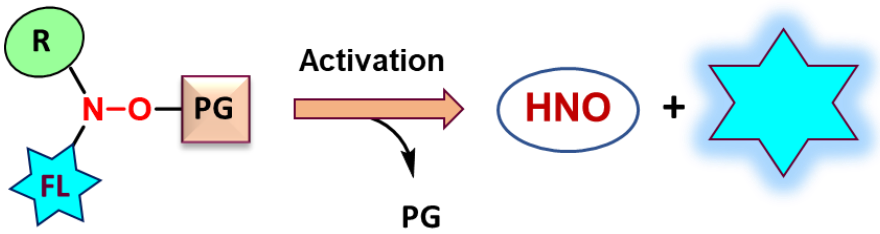

Figure 1.14: Design of the real-time monitoring of HNO

Based on the above design, in **Chapter 2**, we develop the HNO donor along with the fluorescence reporter (Figure 1.14). Upon activation by esterase, it generates HNO and fluorescence signals without the consumption of HNO during its detection. In addition, we synthesized a focused small library of compounds to achieve the tunable HNO release. Here, we used esterase as a trigger which is present ubiquitously in all types of cells. It offers a broad scope to study HNO biology and pharmacology in nearly all cell lines. Since, cancer cells produce higher levels of β-glucosidase enzyme, in **Chapter 3**, we designed β-Glu-HNO donors which can generate HNO in a controlled manner upon activation by β-glucosidase. Further, to make specific delivery of HNO in senescent cells, in **Chapter 4**, we developed a β-galactosidase sensitive HNO donors. The presence of the ASGP receptors on the aged cells allowed the specific delivery of the donor. The β-Gal-HNO donor can generate HNO in a steady state and can mitigate the ROS level in the senescent cells.

Altogether, the studies described in this thesis, address the several awaited problems associated with the existing HNO donors such as triggerable and tunable HNO release, low concurrent generation of NO, real-time monitoring of HNO in cells, site-specific delivery, and benign byproducts. These tools will play an important role in exploring HNO biology and pharmacology, which is yet to be completely understood.

1.9. References

(1) Culotta, E.; Koshland, D. E. NO News Is Good News. *Science (80).* **1992**, *258* (5090), 1862–1865.

(2) Palmer, R. M. J.; Ferrige, A. G.; Moncada, S. Nitric Oxide Release Accounts for the Biological Activity of Endothelium-Derived Relaxing Factor. *Nature* **1987**, *327* (6122), 524–526.

(3) Ignarro, L. J. Nitric Oxide: A Unique Endogenous Signaling Molecule in Vascular Biology (Nobel Lecture). *Angew. Chemie Int. Ed.* **1999**, *38* (13–14), 1882–1892.

(4) Thomas, D. D.; Ridnour, L. A.; Isenberg, J. S.; Flores-Santana, W.; Switzer, C. H.; Donzelli, S.; Hussain, P.; Vecoli, C.; Paolocci, N.; Ambs, S.; Colton, C. A.; Harris, C. C.; Roberts, D. D.; Wink, D. A. The Chemical Biology of Nitric Oxide: Implications in Cellular Signaling. *Free Radic. Biol. Med.* **2008**, *45* (1), 18–31.

(5) Esplugues, J. V. NO as a Signalling Molecule in the Nervous System. *Br. J. Pharmacol.* **2002**, *135* (5), 1079–1095.

(6) Wang, G. R.; Zhu, Y.; Halushka, P. V; Lincoln, T. M.; Mendelsohn, M. E. Mechanism of Platelet Inhibition by Nitric Oxide: In Vivo Phosphorylation of Thromboxane Receptor by Cyclic GMP-Dependent Protein Kinase. *Proc. Natl. Acad. Sci. U. S. A.* **1998**, *95* (9), 4888–4893.

(7) Urbano, R.; Karlinsey, J. E.; Libby, S. J.; Doulias, P.-T.; Ischiropoulos, H.; Warheit-Niemi, H. I.; Liggitt, D. H.; Horswill, A. R.; Fang, F. C. Host Nitric Oxide Disrupts Microbial Cell-to-Cell Communication to Inhibit Staphylococcal Virulence. *Cell Host Microbe* **2018**, *23* (5), 594-606.e7.

(8) Lymar, S. V; Shafirovich, V.; Poskrebyshev, G. A. One-Electron Reduction of Aqueous Nitric Oxide: A Mechanistic Revision. *Inorg. Chem.* **2005**, *44* (15), 5212–5221.

(9) A. Angeli, sopra la nitroidrossilammina, *Gazz. Chim. Ital.*, 1896, 26, 17

(10) Shafirovich, V.; Lymar, S. V. Nitroxyl and Its Anion in Aqueous Solutions: Spin States, Protic Equilibria, and Reactivities toward Oxygen and Nitric Oxide. *Proc. Natl. Acad. Sci.* **2002**, *99* (11), 7340–7345.

(11) Orgel, L. E. 255. The Electronic Structures and Spectra of Some Molecules Related to Oxygen. *J. Chem. Soc.* **1953**, 1276.

(12) Dalby, F. W. THE SPECTRUM AND STRUCTURE OF THE HNO MOLECULE. *Can. J. Phys.* **1958**, *36* (10), 1336–1371.

(13) Michalski, R.; Smulik-Izydorczyk, R.; Pięta, J.; Rola, M.; Artelska, A.; Pierzchała, K.; Zielonka, J.; Kalyanaraman, B.; Sikora, A. B. The Chemistry of HNO: Mechanisms and Reaction Kinetics. *Front. Chem.* **2022**, *10*.

(14) Bartberger, M. D.; Liu, W.; Ford, E.; Miranda, K. M.; Switzer, C.; Fukuto, J. M.; Farmer, P. J.; Wink, D. A.; Houk, K. N. The Reduction Potential of Nitric Oxide (NO) and Its Importance to NO Biochemistry. *Proc. Natl. Acad. Sci.* **2002**, *99* (17), 10958–10963.

(15) Adak, S.; Wang, Q.; Stuehr, D. J. Arginine Conversion to Nitroxide by Tetrahydrobiopterin-Free Neuronal Nitric-Oxide Synthase. Implications for Mechanism. *J. Biol. Chem.* **2000**, *275* (43), 33554–33561.

(16) Murphy, M. E.; Sies, H. Reversible Conversion of Nitroxyl Anion to Nitric Oxide by Superoxide Dismutase. *Proc. Natl. Acad. Sci. U. S. A.* **1991**, *88* (23), 10860–10864.

(17) Sharpe, M. A.; Cooper, C. E. Reactions of Nitric Oxide with Mitochondrial Cytochrome c: A Novel Mechanism for the Formation of Nitroxyl Anion and Peroxynitrite. *Biochem. J.* **1998**, *332 (Pt 1* (Pt 1), 9–19.

(18) Choe, C.; Lewerenz, J.; Fischer, G.; Uliasz, T. F.; Espey, M. G.; Hummel, F. C.; King, S. B.; Schwedhelm, E.; Böger, R. H.; Gerloff, C.; Hewett, S. J.; Magnus, T.; Donzelli, S. Nitroxyl Exacerbates Ischemic Cerebral Injury and Oxidative Neurotoxicity. *J. Neurochem.* **2009**, *110* (6), 1766–1773.

(19) Miljkovic, J. L.; Kenkel, I.; Ivanović-Burmazović, I.; Filipovic, M. R. Generation of HNO and HSNO from Nitrite by Heme-Iron-Catalyzed Metabolism with H 2 S. *Angew. Chemie Int. Ed.* **2013**, *52* (46), 12061–12064.

(20) Filipovic, M. R.; Miljkovic, J. L.; Nauser, T.; Royzen, M.; Klos, K.; Shubina, T.; Koppenol, W. H.; Lippard, S. J.; Ivanović-Burmazović, I. Chemical Characterization of the Smallest S -Nitrosothiol, HSNO; Cellular Cross-Talk of H 2 S and S -Nitrosothiols. *J. Am. Chem. Soc.* **2012**, *134* (29), 12016–12027.

(21) Eberhardt, M.; Dux, M.; Namer, B.; Miljkovic, J.; Cordasic, N.; Will, C.; Kichko, T. I.; de la Roche, J.; Fischer, M.; Suárez, S. A.; Bikiel, D.; Dorsch, K.; Leffler, A.; Babes, A.; Lampert, A.; Lennerz, J. K.; Jacobi, J.; Martí, M. A.; Doctorovich, F.; Högestätt, E. D.; Zygmunt, P. M.; Ivanovic-Burmazovic, I.; Messlinger, K.; Reeh, P.; Filipovic, M. R. H2S and NO Cooperatively Regulate Vascular Tone by Activating a Neuroendocrine HNO–TRPA1–CGRP Signalling Pathway. *Nat. Commun.* **2014**, *5* (1), 4381.

(22) Zarenkiewicz, J.; Khodade, V. S.; Toscano, J. P. Reaction of Nitroxyl (HNO) with

Hydrogen Sulfide and Hydropersulfides. *J. Org. Chem.* **2021**, *86* (1), 868–877.

(23) Doyle, M. P.; Mahapatro, S. N.; Broene, R. D.; Guy, J. K. Oxidation and Reduction of Hemoproteins by Trioxodinitrate(II). The Role of Nitrosyl Hydride and Nitrite. *J. Am. Chem. Soc.* **1988**, *110* (2), 593–599.

(24) Miranda, K. M.; Paolocci, N.; Katori, T.; Thomas, D. D.; Ford, E.; Bartberger, M. D.; Espey, M. G.; Kass, D. A.; Feelisch, M.; Fukuto, J. M.; Wink, D. A. A Biochemical Rationale for the Discrete Behavior of Nitroxyl and Nitric Oxide in the Cardiovascular System. *Proc. Natl. Acad. Sci.* **2003**, *100* (16), 9196–9201.

(25) Lopez, B. E.; Wink, D. A.; Fukuto, J. M. The Inhibition of Glyceraldehyde-3-Phosphate Dehydrogenase by Nitroxyl (HNO). *Arch. Biochem. Biophys.* **2007**, *465* (2), 430–436.

(26) Norris, A. J.; Sartippour, M. R.; Lu, M.; Park, T.; Rao, J. Y.; Jackson, M. I.; Fukuto, J. M.; Brooks, M. N. Nitroxyl Inhibits Breast Tumor Growth and Angiogenesis. *Int. J. cancer* **2008**, *122* (8), 1905–1910.

(27) Nagasawa, H. T.; DeMaster, E. G.; Redfern, B.; Shirota, F. N.; Goon, D. J. W. Evidence for Nitroxyl in the Catalase-Mediated Bioactivation of the Alcohol Deterrent Agent Cyanamide. *J. Med. Chem.* **1990**, *33* (12), 3120–3122.

(28) DeMaster, E. G.; Redfern, B.; Nagasawa, H. T. Mechanisms of Inhibition of Aldehyde Dehydrogenase by Nitroxyl, the Active Metabolite of the Alcohol Deterrent Agent Cyanamide. *Biochem. Pharmacol.* **1998**, *55* (12), 2007–2015.

(29) Andrews, K. L.; Irvine, J. C.; Tare, M.; Apostolopoulos, J.; Favaloro, J. L.; Triggle, C. R.; Kemp-Harper, B. K. A Role for Nitroxyl (HNO) as an Endothelium-Derived Relaxing and Hyperpolarizing Factor in Resistance Arteries. *Br. J. Pharmacol.* **2009**, *157* (4), 540–550.

(30) Ellis, A.; Li, C. G.; Rand, M. J. Differential Actions of L-Cysteine on Responses to Nitric Oxide, Nitroxyl Anions and EDRF in the Rat Aorta. *Br. J. Pharmacol.* **2000**, *129* (2), 315–322.

(31) Favaloro, J. L.; Kemp-Harper, B. K. The Nitroxyl Anion (HNO) Is a Potent Dilator of Rat Coronary Vasculature. *Cardiovasc. Res.* **2007**, *73* (3), 587–596.

(32) Fukuto, J. M.; Chiang, K.; Hszieh, R.; Wong, P.; Chaudhuri, G. The Pharmacological Activity of Nitroxyl: A Potent Vasodilator with Activity Similar to Nitric Oxide and/or Endothelium-Derived Relaxing Factor. *J. Pharmacol. Exp. Ther.* **1992**, *263* (2), 546–551.

(33) Li, C. G.; Karagiannis, J.; Rand, M. J. Comparison of the Redox Forms of Nitrogen

Monoxide with the Nitrergic Transmitter in the Rat Anococcygeus Muscle. *Br. J. Pharmacol.* **1999**, *127* (4), 826–834.

(34) Wanstall, J. C.; Jeffery, T. K.; Gambino, A.; Lovren, F.; Triggle, C. R. Vascular Smooth Muscle Relaxation Mediated by Nitric Oxide Donors: A Comparison with Acetylcholine, Nitric Oxide and Nitroxyl Ion. *Br. J. Pharmacol.* **2001**, *134* (3), 463–472.

(35) Zhu, G.; Groneberg, D.; Sikka, G.; Hori, D.; Ranek, M. J.; Nakamura, T.; Takimoto, E.; Paolocci, N.; Berkowitz, D. E.; Friebe, A.; Kass, D. A. Soluble Guanylate Cyclase Is Required for Systemic Vasodilation but Not Positive Inotropy Induced by Nitroxyl in the Mouse. *Hypertens. (Dallas, Tex. 1979)* **2015**, *65* (2), 385–392.

(36) Sidorkina, O.; Espey, M. G.; Miranda, K. M.; Wink, D. A.; Laval, J. Inhibition of Poly(ADP-RIBOSE) Polymerase (PARP) by Nitric Oxide and Reactive Nitrogen Oxide Species. *Free Radic. Biol. Med.* **2003**, *35* (11), 1431–1438.

(37) Väänänen, A. J.; Kankuri, E.; Rauhala, P. Nitric Oxide-Related Species-Induced Protein Oxidation: Reversible, Irreversible, and Protective Effects on Enzyme Function of Papain. *Free Radic. Biol. Med.* **2005**, *38* (8), 1102–1111.

(38) Väänänen, A. J.; Salmenperä, P.; Hukkanen, M.; Rauhala, P.; Kankuri, E. Cathepsin B Is a Differentiation-Resistant Target for Nitroxyl (HNO) in THP-1 Monocyte/Macrophages. *Free Radic. Biol. Med.* **2006**, *41* (1), 120–131.

(39) Väänänen, A. J.; Salmenperä, P.; Hukkanen, M.; Miranda, K. M.; Harjula, A.; Rauhala, P.; Kankuri, E. Persistent Susceptibility of Cathepsin B to Irreversible Inhibition by Nitroxyl (HNO) in the Presence of Endogenous Nitric Oxide. *Free Radic. Biol. Med.* **2008**, *45* (6), 749–755.

(40) Gao, W. D.; Murray, C. I.; Tian, Y.; Zhong, X.; DuMond, J. F.; Shen, X.; Stanley, B. A.; Foster, D. B.; Wink, D. A.; King, S. B.; Van Eyk, J. E.; Paolocci, N. Nitroxyl-Mediated Disulfide Bond Formation Between Cardiac Myofilament Cysteines Enhances Contractile Function. *Circ. Res.* **2012**, *111* (8), 1002–1011.

(41) Donald, C. E.; Hughes, M. N.; Thompson, J. M.; Bonner, F. T. Photolysis of the Nitrogen-Nitrogen Double Bond in Trioxodinitrate: Reaction between Triplet Oxonitrate(1-) and Molecular Oxygen to Form Peroxonitrite. *Inorg. Chem.* **1986**, *25* (16), 2676–2677.

(42) Bazylinski, D. A.; Hollocher, T. C. Metmyoglobin and Methemoglobin as Efficient Traps for Nitrosyl Hydride (Nitroxyl) in Neutral Aqueous Solution. *J. Am. Chem. Soc.* **1985**, *107* (26), 7982–7986.

(43) Silva Sousa, E. H.; Ridnour, L. A.; Gouveia, F. S.; Silva da Silva, C. D.; Wink, D. A.; de França Lopes, L. G.; Sadler, P. J. Thiol-Activated HNO Release from a Ruthenium Antiangiogenesis Complex and HIF-1α Inhibition for Cancer Therapy. *ACS Chem. Biol.* **2016**, *11* (7), 2057–2065.

(44) Sulc, F.; Immoos, C. E.; Pervitsky, D.; Farmer, P. J. Efficient Trapping of HNO by Deoxymyoglobin. *J. Am. Chem. Soc.* **2004**, *126* (4), 1096–1101.

(45) Lin, R.; Farmer, P. J. The HNO Adduct of Myoglobin: Synthesis and Characterization. *J. Am. Chem. Soc.* **2000**, *122* (10), 2393–2394.

(46) Abucayon, E. G.; Khade, R. L.; Powell, D. R.; Zhang, Y.; Richter-Addo, G. B. Hydride Attack on a Coordinated Ferric Nitrosyl: Experimental and DFT Evidence for the Formation of a Heme Model–HNO Derivative. *J. Am. Chem. Soc.* **2016**, *138* (1), 104–107.

(47) Subedi, H.; Hassanin, H. A.; Brasch, N. E. Kinetic and Mechanistic Studies on the Reaction of the Vitamin B12 Complex Aquacobalamin with the HNO Donor Angeli's Salt: Angeli's Salt and HNO React with Aquacobalamin. *Inorg. Chem.* **2014**, *53* (3), 1570–1577.

(48) Subedi, H.; Brasch, N. E. Studies on the Reaction of Reduced Vitamin B 12 Derivatives with the Nitrosyl -Hydride (HNO) Donor Angeli's Salt: HNO Oxidizes the Transition-Metal Center of Cob(I)Alamin. *Eur. J. Inorg. Chem.* **2015**, *2015* (23), 3825–3834.

(49) Subedi, H.; Brasch, N. E. Mechanistic Studies of the Reactions of the Reduced Vitamin B 12 Derivatives with the HNO Donor Piloty's Acid: Further Evidence for Oxidation of Cob(i)Alamin by (H)NO. *Dalt. Trans.* **2016**, *45* (1), 352–360.

(50) Martí, M. A.; Bari, S. E.; Estrin, D. A.; Doctorovich, F. Discrimination of Nitroxyl and Nitric Oxide by Water-Soluble Mn(III) Porphyrins. *J. Am. Chem. Soc.* **2005**, *127* (13), 4680–4684.

(51) Liochev, S. I.; Fridovich, I. The Mode of Decomposition of Angeli's Salt (Na2N2O3) and the Effects Thereon of Oxygen, Nitrite, Superoxide Dismutase, and Glutathione. *Free Radic. Biol. Med.* **2003**, *34* (11), 1399–1404.

(52) Goldstein, S.; Samuni, A. Oxidation Mechanism of Hydroxamic Acids Forming HNO and NO; 2015; pp 315–333.

(53) Paolocci, N.; Saavedra, W. F.; Miranda, K. M.; Martignani, C.; Isoda, T.; Hare, J. M.; Espey, M. G.; Fukuto, J. M.; Feelisch, M.; Wink, D. A.; Kass, D. A. Nitroxyl Anion Exerts Redox-Sensitive Positive Cardiac Inotropy in Vivo by Calcitonin Gene-Related Peptide Signaling. *Proc. Natl. Acad. Sci. U. S. A.* **2001**, *98* (18), 10463–10468.

(54) Cheong, E.; Tumbev, V.; Abramson, J.; Salama, G.; Stoyanovsky, D. A. Nitroxyl Triggers Ca^{2+} Release from Skeletal and Cardiac Sarcoplasmic Reticulum by Oxidizing Ryanodine Receptors. *Cell Calcium* **2005**, *37* (1), 87–96.

(55) Tocchetti, C. G.; Wang, W.; Froehlich, J. P.; Huke, S.; Aon, M. A.; Wilson, G. M.; Di Benedetto, G.; O'Rourke, B.; Gao, W. D.; Wink, D. A.; Toscano, J. P.; Zaccolo, M.; Bers, D. M.; Valdivia, H. H.; Cheng, H.; Kass, D. A.; Paolocci, N. Nitroxyl Improves Cellular Heart Function by Directly Enhancing Cardiac Sarcoplasmic Reticulum Ca 2+ Cycling. *Circ. Res.* **2007**, *100* (1), 96–104.

(56) Froehlich, J. P.; Mahaney, J. E.; Keceli, G.; Pavlos, C. M.; Goldstein, R.; Redwood, A. J.; Sumbilla, C.; Lee, D. I.; Tocchetti, C. G.; Kass, D. A.; Paolocci, N.; Toscano, J. P. Phospholamban Thiols Play a Central Role in Activation of the Cardiac Muscle Sarcoplasmic Reticulum Calcium Pump by Nitroxyl. *Biochemistry* **2008**, *47* (50), 13150–13152.

(57) Sivakumaran, V.; Stanley, B. A.; Tocchetti, C. G.; Ballin, J. D.; Caceres, V.; Zhou, L.; Keceli, G.; Rainer, P. P.; Lee, D. I.; Huke, S.; Ziolo, M. T.; Kranias, E. G.; Toscano, J. P.; Wilson, G. M.; O'Rourke, B.; Kass, D. A.; Mahaney, J. E.; Paolocci, N. HNO Enhances SERCA2a Activity and Cardiomyocyte Function by Promoting Redox-Dependent Phospholamban Oligomerization. *Antioxid. Redox Signal.* **2013**, *19* (11), 1185–1197.

(58) Pagliaro, P.; Mancardi, D.; Rastaldo, R.; Penna, C.; Gattullo, D.; Miranda, K. M.; Feelisch, M.; Wink, D. A.; Kass, D. A.; Paolocci, N. Nitroxyl Affords Thiol-Sensitive Myocardial Protective Effects Akin to Early Preconditioning. *Free Radic. Biol. Med.* **2003**, *34* (1), 33–43.

(59) Ma, X. L.; Gao, F.; Liu, G. L.; Lopez, B. L.; Christopher, T. A.; Fukuto, J. M.; Wink, D. A.; Feelisch, M. Opposite Effects of Nitric Oxide and Nitroxyl on Postischemic Myocardial Injury. *Proc. Natl. Acad. Sci. U. S. A.* **1999**, *96* (25), 14617–14622.

(60) Miller, T. W.; Cherney, M. M.; Lee, A. J.; Francoleon, N. E.; Farmer, P. J.; King, S. B.; Hobbs, A. J.; Miranda, K. M.; Burstyn, J. N.; Fukuto, J. M. The Effects of Nitroxyl (HNO) on Soluble Guanylate Cyclase Activity. *J. Biol. Chem.* **2009**, *284* (33), 21788–21796.

(61) Wink, D. A.; Feelisch, M.; Fukuto, J.; Chistodoulou, D.; Jourd'heuil, D.; Grisham, M. B.; Vodovotz, Y.; Cook, J. A.; Krishna, M.; DeGraff, W. G.; Kim, S.; Gamson, J.; Mitchell, J. B. The Cytotoxicity of Nitroxyl: Possible Implications for the Pathophysiological Role of NO. *Arch. Biochem. Biophys.* **1998**, *351* (1), 66–74.

(62) Naughton, P.; Foresti, R.; Bains, S. K.; Hoque, M.; Green, C. J.; Motterlini, R. Induction of Heme Oxygenase 1 by Nitrosative Stress. *J. Biol. Chem.* **2002**, *277* (43), 40666–40674.

(63) Piloty, O. Ueber Eine Oxydation Des Hydroxylamins Durch Benzolsulfochlorid. *Berichte der Dtsch. Chem. Gesellschaft* **1896**, *29* (2), 1559–1567.

(64) Aizawa, K.; Nakagawa, H.; Matsuo, K.; Kawai, K.; Ieda, N.; Suzuki, T.; Miyata, N. Piloty's Acid Derivative with Improved Nitroxyl-Releasing Characteristics. *Bioorg. Med. Chem. Lett.*, **2013**, *23* (8).

(65) Kamynina, A.; Guttzeit, S.; Eaton, P.; Cuello, F. Nitroxyl Donor CXL-1020 Lowers Blood Pressure by Targeting C195 in Cyclic Guanosine-3',5'-Monophosphate-Dependent Protein Kinase I. *Hypertension* **2022**, *79* (5), 946–956.

(66) Cowart, D.; Venuti, R.; Guptill, J.; Noveck, R.; Foo, S. A PHASE 1 STUDY OF THE SAFETY AND PHARMACOKINETICS OF THE INTRAVENOUS NITROXYL PRODRUG, CXL-1427. *J. Am. Coll. Cardiol.* **2015**, *65* (10), A876.

(67) Salmon, D. J.; Torres de Holding, C. L.; Thomas, L.; Peterson, K. V.; Goodman, G. P.; Saavedra, J. E.; Srinivasan, A.; Davies, K. M.; Keefer, L. K.; Miranda, K. M. HNO and NO Release from a Primary Amine-Based Diazeniumdiolate As a Function of PH. *Inorg. Chem.* **2011**, *50* (8), 3262–3270.

(68) Bharadwaj, G.; Benini, P. G. Z.; Basudhar, D.; Ramos-Colon, C. N.; Johnson, G. M.; Larriva, M. M.; Keefer, L. K.; Andrei, D.; Miranda, K. M. Analysis of the HNO and NO Donating Properties of Alicyclic Amine Diazeniumdiolates. *Nitric oxide Biol. Chem.* **2014**, *42*, 70–78.

(69) Shoman, M. E.; DuMond, J. F.; Isbell, T. S.; Crawford, J. H.; Brandon, A.; Honovar, J.; Vitturi, D. A.; White, C. R.; Patel, R. P.; King, S. B. Acyloxy Nitroso Compounds as Nitroxyl (HNO) Donors: Kinetics, Reactions with Thiols, and Vasodilation Properties. *J. Med. Chem.* **2011**, *54* (4), 1059–1070.

(70) Sutton, A. D.; Williamson, M.; Weismiller, H.; Toscano, J. P. Optimization of HNO Production from N, O - Bis -Acylated Hydroxylamine Derivatives. *Org. Lett.* **2012**, *14* (2), 472–475.

(71) Guthrie, D. A.; Kim, N. Y.; Siegler, M. A.; Moore, C. D.; Toscano, J. P. Development of N -Substituted Hydroxylamines as Efficient Nitroxyl (HNO) Donors. *J. Am. Chem. Soc.* **2012**, *134* (4), 1962–1965.

(72) Zhou, Y.; Cink, R. B.; Dassanayake, R. S.; Seed, A. J.; Brasch, N. E.; Sampson, P. Rapid Photoactivated Generation of Nitroxyl (HNO) under Neutral PH Conditions.

Angew. Chemie Int. Ed. **2016**, *55* (42), 13229–13232.

(73) Zhou, Y.; Cink, R. B.; Fejedelem, Z. A.; Cather Simpson, M.; Seed, A. J.; Sampson, P.; Brasch, N. E. Development of Photoactivatable Nitroxyl (HNO) Donors Incorporating the (3-Hydroxy-2-naphthalenyl)Methyl Phototrigger. *European J. Org. Chem.* **2018**, *2018* (15), 1745–1755.

(74) Zhou, Y.; Cink, R. B.; Seed, A. J.; Simpson, M. C.; Sampson, P.; Brasch, N. E. Stoichiometric Nitroxyl Photorelease Using the (6-Hydroxy-2-Naphthalenyl)Methyl Phototrigger. *Org. Lett.* **2019**, *21* (4), 1054–1057.

(75) Zhou, Y.; Bharadwaj, V.; Rahman, M. S.; Sampson, P.; Brasch, N. E.; Seed, A. J. Synthesis and Photochemical Studies of 2-Nitrobenzyl-Caged N-Hydroxysulfonamides. *J. Photochem. Photobiol. A Chem.* **2019**, *384*, 112033.

(76) Kawaguchi, M.; Tani, T.; Hombu, R.; Ieda, N.; Nakagawa, H. Development and Cellular Application of Visible-Light-Controllable HNO Releasers Based on Caged Piloty's Acid. *Chem. Commun.* **2018**, *54* (73), 10371–10374.

(77) Carrone, G.; Pellegrino, J.; Doctorovich, F. Rapid Generation of HNO Induced by Visible Light. *Chem. Commun.* **2017**, *53* (38), 5314–5317.

(78) Xu, Y.; Alavanja, M.-M.; Johnson, V. L.; Yasaki, G.; King, S. B. Production of Nitroxyl (HNO) at Biologically Relevant Temperatures from the Retro-Diels–Alder Reaction of N-Hydroxyurea-Derived Acyl Nitroso-9,10-Dimethylanthracene Cycloadducts. *Tetrahedron Lett.* **2000**, *41* (22), 4265–4269.

(79) Zheng, Y.; Yu, B.; Ji, K.; Pan, Z.; Chittavong, V.; Wang, B. Esterase-Sensitive Prodrugs with Tunable Release Rates and Direct Generation of Hydrogen Sulfide. *Angew. Chemie Int. Ed.* **2016**, *55* (14), 4514–4518.

(80) Zeng, B.-B.; Huang, J.; Wright, M. W.; King, S. B. Nitroxyl (HNO) Release from New Functionalized N-Hydroxyurea-Derived Acyl Nitroso-9,10-Dimethylanthracene Cycloadducts. *Bioorg. Med. Chem. Lett.* **2004**, *14* (22), 5565–5568.

(81) Adachi, Y.; Nakagawa, H.; Matsuo, K.; Suzuki, T.; Miyata, N. Photoactivatable HNO-Releasing Compounds Using the Retro-Diels–Alder Reaction. *Chem. Commun.* **2008**, No. 41, 5149.

(82) Kelly, S. S.; Ni, X.; Yuen, V.; Radford, M. N.; Xian, M. C -Nitrosothioformamide: A Donor Template for Dual Release of HNO and H 2 S. *ChemBioChem* **2022**, *23* (13).

(83) Long, Y.; Xia, Z.; Rice, A. M.; King, S. B. Para-Substituted O-Benzyl Sulfohydroxamic Acid Derivatives as Redox-Triggered Nitroxyl (HNO) Sources. *Molecules* **2022**, *27* (16), 5305.

(84) Lee, M. J. C.; Shoeman, D. W.; Goon, D. J. W.; Nagasawa, H. T. N-Hydroxybenzenecarboximidic Acid Derivatives: A New Class of Nitroxyl-Generating Prodrugs. *Nitric Oxide* **2001**, *5* (3), 278–287.

(85) Andrei, D.; Salmon, D. J.; Donzelli, S.; Wahab, A.; Klose, J. R.; Citro, M. L.; Saavedra, J. E.; Wink, D. A.; Miranda, K. M.; Keefer, L. K. Dual Mechanisms of HNO Generation by a Nitroxyl Prodrug of the Diazeniumdiolate (NONOate) Class. *J. Am. Chem. Soc.* **2010**, *132* (46), 16526–16532.

(86) Holland, R. J.; Paulisch, R.; Cao, Z.; Keefer, L. K.; Saavedra, J. E.; Donzelli, S. Enzymatic Generation of the NO/HNO-Releasing IPA/NO Anion at Controlled Rates in Physiological Media Using β-Galactosidase. *Nitric Oxide* **2013**, *35*, 131–136.

(87) Reisz, J. A.; Zink, C. N.; King, S. B. Rapid and Selective Nitroxyl (HNO) Trapping by Phosphines: Kinetics and New Aqueous Ligations for HNO Detection and Quantitation. *J. Am. Chem. Soc.* **2011**, *133* (30), 11675–11685.

(88) Mao, G. J.; Zhang, X. B.; Shi, X. L.; Liu, H. W.; Wu, Y. X.; Zhou, L. Y.; Tan, W.; Yu, R. Q. A Highly Sensitive and Reductant-Resistant Fluorescent Probe for Nitroxyl in Aqueous Solution and Serum. *Chem. Commun.* **2014**, *50* (43).

(89) Bobba, K. N.; Zhou, Y.; Guo, L. E.; Zang, T. N.; Zhang, J. F.; Bhuniya, S. Resorufin Based Fluorescence 'Turn-on' Chemodosimeter Probe for Nitroxyl (HNO). *RSC Adv.* **2015**, *5* (103), 84543–84546.

(90) Kawai, K.; Ieda, N.; Aizawa, K.; Suzuki, T.; Miyata, N.; Nakagawa, H. A Reductant-Resistant and Metal-Free Fluorescent Probe for Nitroxyl Applicable to Living Cells. *J. Am. Chem. Soc.* **2013**, *135* (34), 12690–12696.

(91) Liu, C.; Wang, Y.; Tang, C.; Liu, F.; Ma, Z.; Zhao, Q.; Wang, Z.; Zhu, B.; Zhang, X. A Reductant-Resistant Ratiometric, Colorimetric and Far-Red Fluorescent Probe for Rapid and Ultrasensitive Detection of Nitroxyl. *J. Mater. Chem. B* **2017**, *5* (19).

(92) Jin, X.; Sun, X.; Di, X.; Zhang, X.; Huang, H.; Liu, J.; Ji, P.; Zhu, H. Novel Fluorescent ESIPT Probe Based on Flavone for Nitroxyl in Aqueous Solution and Serum. *Sensors Actuators B Chem.* **2016**, *224*, 209–216.

(93) Lv, H.-M.; Yi Chen, Y. C.; Lei, J.; Au, C.-T.; Yin, S.-F. An ESIPT-Based Ratiometric Fluorescent Probe for the Imaging of Nitroxyl in Living Cells. *Anal. Methods* **2015**, *7* (9), 3883–3887.

(94) Zhu, X.; Xiong, M.; Liu, H.; Mao, G.; Zhou, L.; Zhang, J.; Hu, X.; Zhang, X.-B.; Tan, W. A FRET-Based Ratiometric Two-Photon Fluorescent Probe for Dual-Channel Imaging of Nitroxyl in Living Cells and Tissues. *Chem. Commun.* **2016**, *52* (4), 733–

736.

(95) Zhang, H.; Liu, R.; Tan, Y.; Xie, W. H.; Lei, H.; Cheung, H.-Y.; Sun, H. A FRET-Based Ratiometric Fluorescent Probe for Nitroxyl Detection in Living Cells. *ACS Appl. Mater. Interfaces* **2015**, *7* (9), 5438–5443.

(96) Ren, M.; Deng, B.; Zhou, K.; Wang, J.-Y.; Kong, X.; Lin, W. A Targetable Fluorescent Probe for Imaging Exogenous and Intracellularly Formed Nitroxyl in Mitochondria in Living Cells. *J. Mater. Chem. B* **2017**, *5* (10), 1954–1961.

(97) Jing, X.; Yu, F.; Chen, L. Visualization of Nitroxyl (HNO) in Vivo via a Lysosome-Targetable near-Infrared Fluorescent Probe. *Chem. Commun.* **2014**, *50* (91), 14253–14256.

(98) Pino, N. W.; Davis, J.; Yu, Z.; Chan, J. NitroxylFluor: A Thiol-Based Fluorescent Probe for Live-Cell Imaging of Nitroxyl. *J. Am. Chem. Soc.* **2017**, *139* (51), 18476–18479.

(99) Cline, M. R.; Toscano, J. P. Detection of Nitroxyl (HNO) by a Prefluorescent Probe. *J. Phys. Org. Chem.* **2011**, *24* (10), 993–998. https://doi.org/10.1002/poc.1871.

(100) Rosenthal, J.; Lippard, S. J. Direct Detection of Nitroxyl in Aqueous Solution Using a Tripodal Copper(II) BODIPY Complex. *J. Am. Chem. Soc.* **2010**, *132* (16), 5536–5537.

(101) Apfel, U.-P.; Buccella, D.; Wilson, J. J.; Lippard, S. J. Detection of Nitric Oxide and Nitroxyl with Benzoresorufin-Based Fluorescent Sensors. *Inorg. Chem.* **2013**, *52* (6), 3285–3294.

(102) Zhou, Y.; Liu, K.; Li, J.-Y.; Fang, Y.; Zhao, T.-C.; Yao, C. Visualization of Nitroxyl in Living Cells by a Chelated Copper(II) Coumarin Complex. *Org. Lett.* **2011**, *13* (6), 1290–1293.

(103) Lv, H.; Ma, R.; Zhang, X.; Li, M.; Wang, Y.; Wang, S.; Xing, G. Surfactant-Modulated Discriminative Sensing of HNO and H2S with a Cu2+-Complex-Based Fluorescent Probe. *Tetrahedron* **2016**, *72* (35), 5495–5501.

Chapter 2: Esterase triggered Nitroxyl (HNO) Donors with a Fluorescence Reporter

2.1. Introduction

As mentioned in **Chapter 1**, reported donors spontaneously release HNO *in vitro* and intracellularly. As HNO is highly reactive towards biomolecules, controlled and site-directed generation is required. Being a transient species, precise detection and quantification of HNO are quite challenging. Thus, a strategy where small molecules can generate HNO in a controlled manner along with the concurrent release of a fluorescence reporter is an urgent need. In this chapter, we utilized a reliable strategy of masking HNO with the esterase-sensitive trigger. Esterase (ES) is known to cleave the carbonyl ester bonds. Owing to the wide occurrence of esterase in all the cells, this tool can be used in a wide range of cell types and would hence have a broad scope.

Further, we chose Piloty's acid and its derivatives as HNO donors, as it is known to generate HNO in an excellent yield.[1] Piloty's acid offers the opportunity to install the different groups (EDG and EWG) at different positions (*o*/*m*/*p*) on aromatic systems which may help to tune the HNO generation. As well as it would help to understand the mechanistic insights.

Here, we designed an HNO prodrug based on *N*,*N*,*O*-protected hydroxylamine. The oxygen of hydroxylamine was protected with cyclopropyl carboxylic ester, and on the nitrogen, a leaving group and Boc/H substituent was placed. Esterase is expected to cleave the ester linkage and further decomposition leads to HNO release.

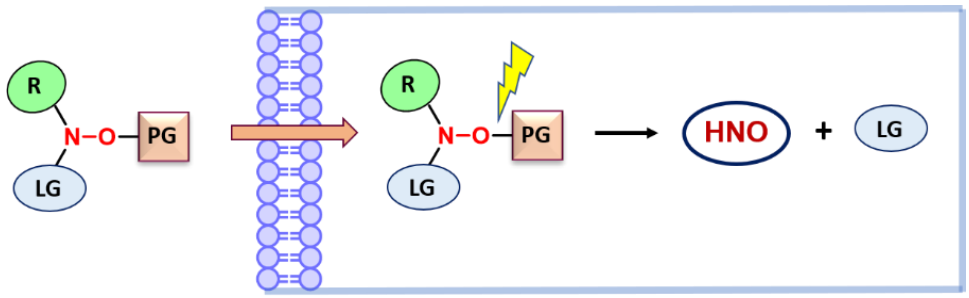

Figure 2.1. Design of stimuli-responsive Nitroxyl (HNO) donor

Next, we developed a modular scaffold with two series of esterase-activated nitroxyl donors (Figure 2.1). In series 1, upon esterase activation, compound **2** produces *N*-Boc Piloty's acid intermediate I. Further, it cleaved to produce arylsulfinic acid and a common

intermediate, which upon hydrolysis, it produces HNO, CO_2 and ^tBuOH. In series 2, the cyclopropyl carbonyl ester will cleave in the presence of esterase and produce a derivative of Piloty's acid which further dissociates to produce HNO and arylsulfinic acid. (Scheme 2.1).

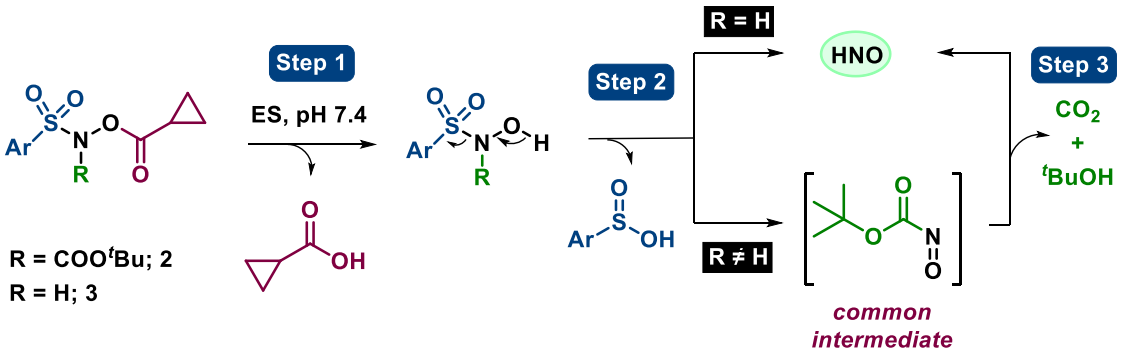

Scheme 2.1. Proposed mechanism of HNO generation upon activation by esterase

2.2. Result and discussion

2.2.1. Synthesis

In order to test our hypothesis of esterase-activated HNO donors, compounds were synthesized in three steps. First, treatment of cyclopropylcarbonyl chloride with *N*-Boc-hydroxylamine under basic conditions afforded compound **1** (Scheme 2.2).[2] which on *N*-sulfonation by respective arylsulfonyl chlorides and sodium hydride afforded compound **2a-2g** (Scheme 2.3).[3] Boc deprotection of **2a-2g** using trifluoroacetic acid gave compound **3a-3g** (Scheme 2.4).[3]

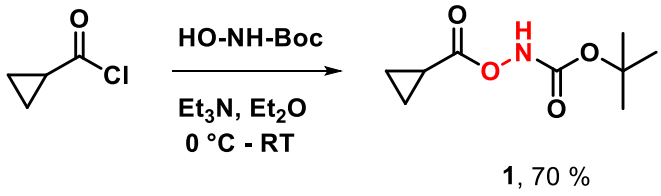

Scheme 2.2. Synthesis of compound **1**

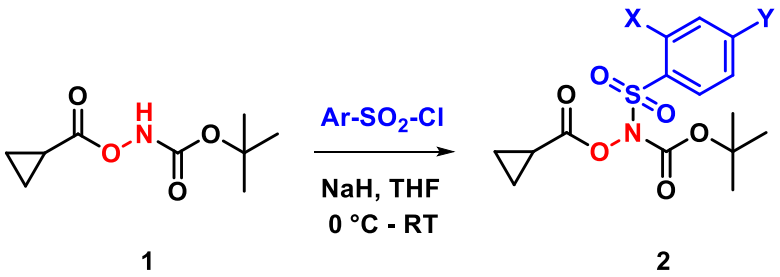

Scheme 2.3. Synthesis of compound **2**

Table 2.1: Synthesis of Boc-protected compounds **2a-2g** from **1**

Entry	Product	X	Y	Yield, %
1	**2a**	H	H	56
2	**2b**	Br	H	64
3	**2c**	H	Br	37
4	**2d**	CF_3	H	41
5	**2e**	Br	CF_3	59
6	**2f**	NO_2	H	48
7	**2g**	H	NO_2	48

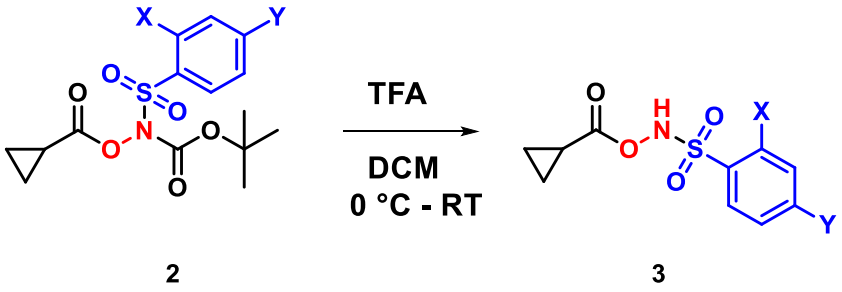

Scheme 2.4. Synthesis of compound **3**

Table 2.2: Synthesis of compounds **3a-3g** from **2**

Entry	Product	X	Y	Yield, %
1	**3a**	H	H	56
2	**3b**	Br	H	53
3	**3c**	H	Br	92
4	**3d**	CF_3	H	41
5	**3e**	Br	CF_3	40
6	**3f**	NO_2	H	95
7	**3g**	H	NO_2	61

Next, we synthesized the 2-bromopiloty's acid as a control compound by following a reported procedure.[1] Condensation reaction of hydroxylamine hydrochloride with 2-bromo-benzenesulfonyl chloride at 0 ˚C afforded compound **4** in good yield (Scheme 2.5).

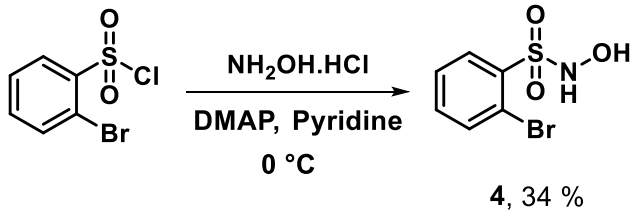

Scheme 2.5. Synthesis of 2-bromopiloty's acid

Next, we synthesized the HNO probes using a reported procedure. EDC-mediated esterification with 2-(diphenylphosphino)benzoic acid with 7-hydroxycoumrin afforded the compound **5** (PCM).[4] **6** (HNO-TCF) was also synthesized following a similar methodology in moderate to good yield (Scheme 2.6).[5]

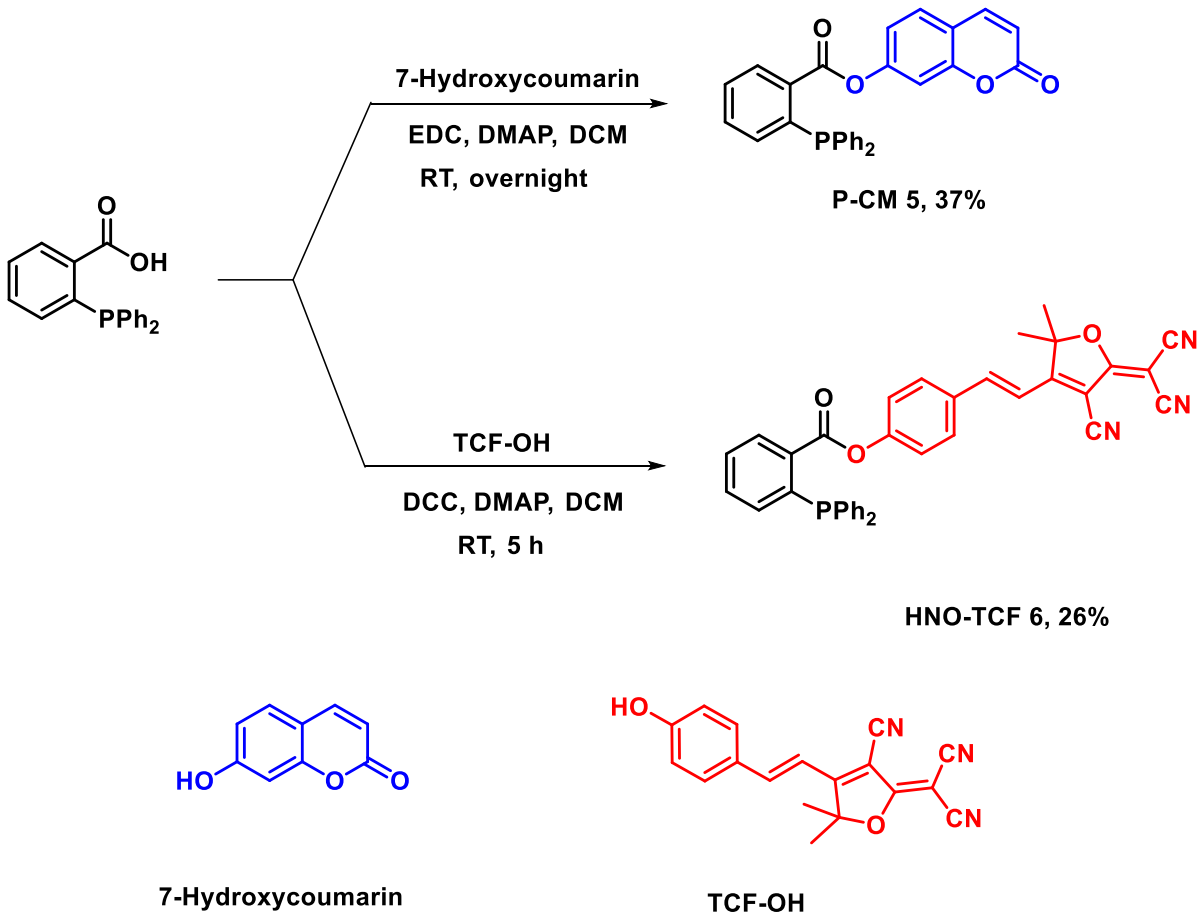

Scheme 2.6. Synthesis of **5** and **6** probes

2.2.2. HNO generation and fluorescence emission study

2.2.2.1. *In vitro* HNO generation

The ability of compounds to generate HNO was tested using a fluorescence-based assay using **5**. HNO probes work on the principle of photoinduced electron transfer (PET) mechanism. **5** can trap the HNO and release the active fluorophore umbelliferone (Scheme 2.7).

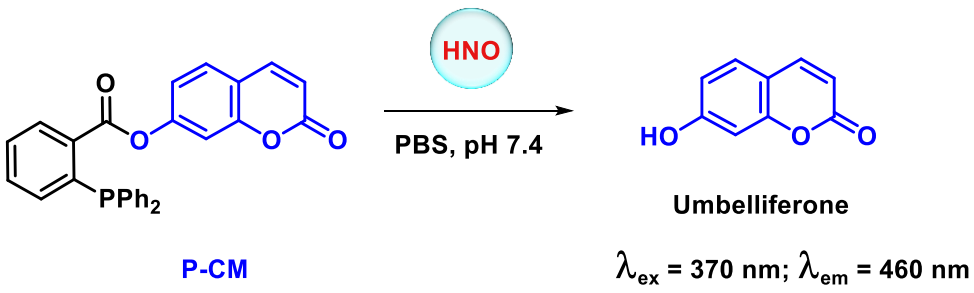

Scheme 2.7. Mechanism of HNO trapping by **5** to release highly fluorescent product umbelliferone

When compounds from series **2** and **3** were incubated independently with **5** and esterase from the porcine liver in phosphate buffer saline (PBS pH 7.4), fluorescence enhancement was recorded using an Ensight Multimode Plate Reader (excitation 370 nm; emission 460 nm). In the absence of esterase, no significant fluorescence signal was observed at 460 nm. This suggests that the compounds were stable in buffer and elicit an enhancement in the fluorescence signal upon activation by esterase (Figure 2.2).

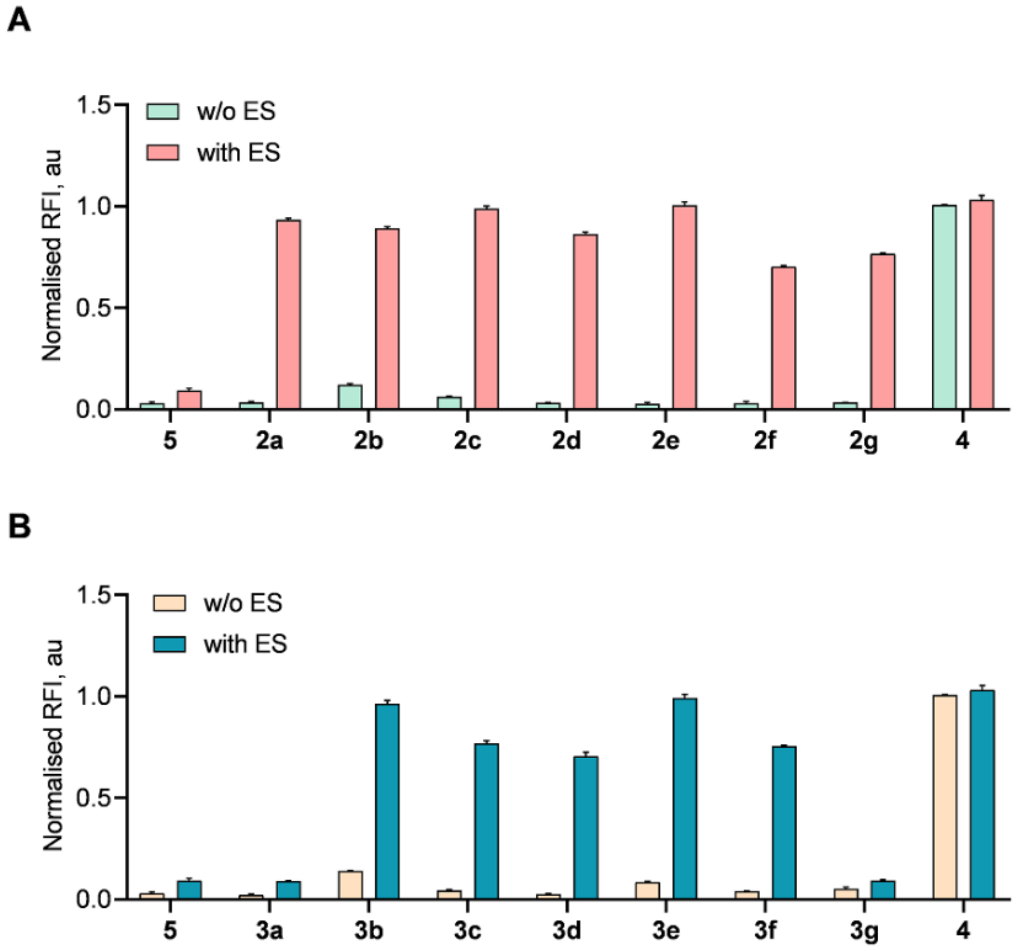

Figure 2.2. Enhancement in fluorescence signal corresponding to the generation of HNO from compounds **2a-2g** (50 µM) and **3a-3g** (50 µM) in the presence of **5** and esterase (0.5 U/mL) in PBS (10 mM, pH 7.4) at 37 ˚C for 30 minutes. **5** refers to PCM dye; **4** refers to 2-bromopiloty's acid; (λ_{ex} = 370 nm; λ_{em} = 460 nm).

2.2.2.2. Time course of HNO generation

We synthesized the focused small library of HNO donors. To check the tunable HNO generation from these donors, compounds from series **2** and **3** were incubated with **5** in the

presence of esterase in buffer and fluorescence signal (λ_{ex} = 370 nm; λ_{em} = 460 nm) was recorded over 30 min (Figure 2.3). Interestingly, these donors demonstrated different release profiles, indicative of tunable HNO generation.

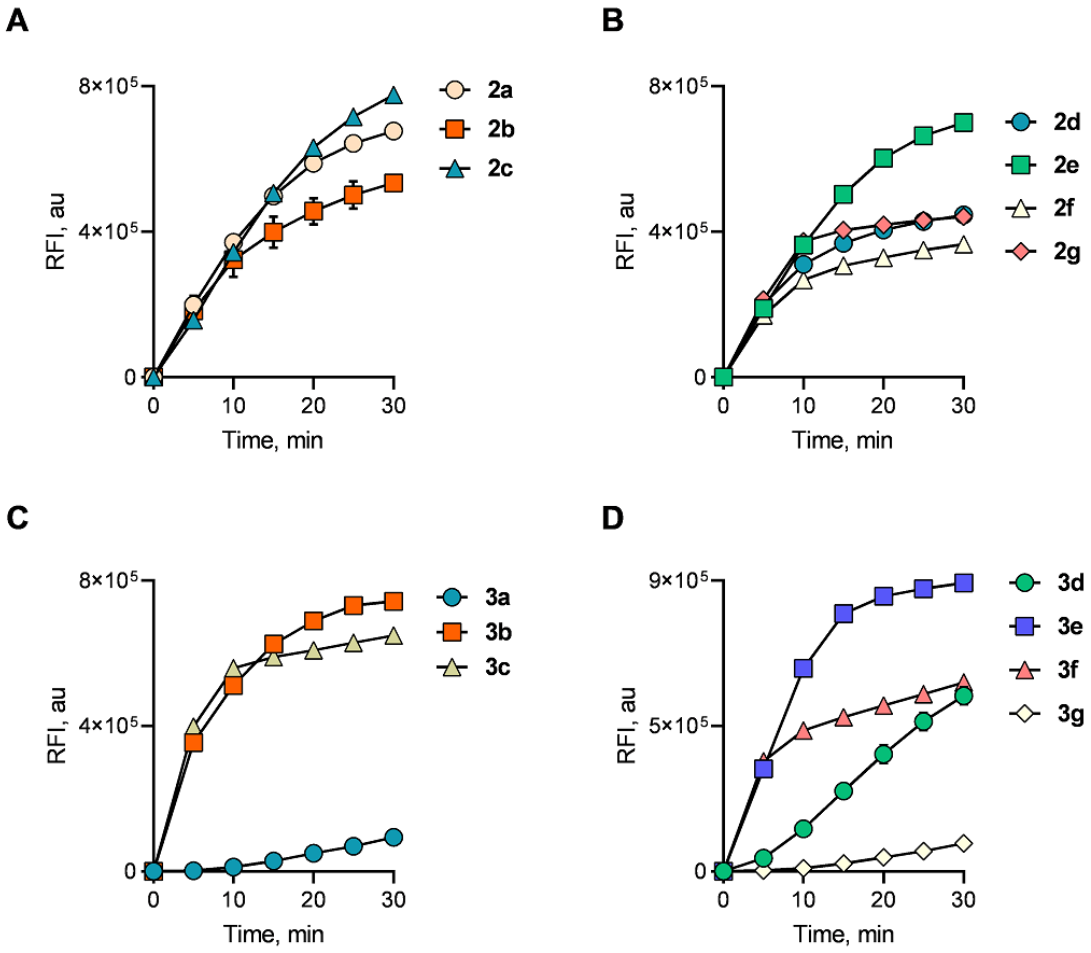

Figure 2.3. Time-dependent HNO generation from compounds (a) **2a-2c,** (b) **2d-2g,** (c) **3a-3c** and (d) **2d-2g** (50 µM) using **5** were incubated in the presence of esterase (0.5 U/mL) in PBS (10 mM, pH 7.4) at 37 ˚C and fluorescence enhancement was monitored over 30 min. (λ_{ex} = 370 nm; λ_{em} = 460 nm).

However, **5** was unstable in the experimental conditions for an extended period. In the presence of esterase (0.5 U/mL), further cleavage of **5** was observed after 30 minutes. **5** is not suitable for slow HNO-generating donors and may provide false positive results. As HNO is a transient species and highly reactive towards biomolecules (thiols protein, selenoproteins and metalloproteins), precise detection of HNO in biological systems becomes more challenging. Furthermore, the measurement of HNO is invariably associated with the

consumption of HNO. Thus, a strategy where a small molecule can generate HNO along with a fluorescence reporter would be useful, which will eliminate the need for secondary assays to monitor the release of HNO.

To address this issue, next, we designed esterase-triggered HNO donors along with a fluorescence reporter (Figure 2.4). In the first strategy, we made the aryl sulfonamides where aryl sulfinic acid is the leaving group. To tune the HNO generation, we used the different derivatives of arylsufinic acid as a leaving group. Instead of arylsulfinic acid, the incorporation of a latent fluorophore would be useful. The donors are expected to have weak fluorescence, and upon esterase cleavage, a donor will release HNO along with fluorescent dansylsulfinic acid. The fluorescence quantum yield of dansylsulfinic acid is 83%.[6] The higher the fluorescence quantum yield values, the fluorescence signal intensity of the fluorophore will be high. Hence, in the second strategy, dansyl was incorporated as leaving group. Due to the presence of the cyclopropylcarbonyl ester group, HNO donors were expected to be fluorescence turn-off. The concurrent release of HNO and fluorescence reporter can eliminate the need for a secondary assay for the detection of HNO generation.

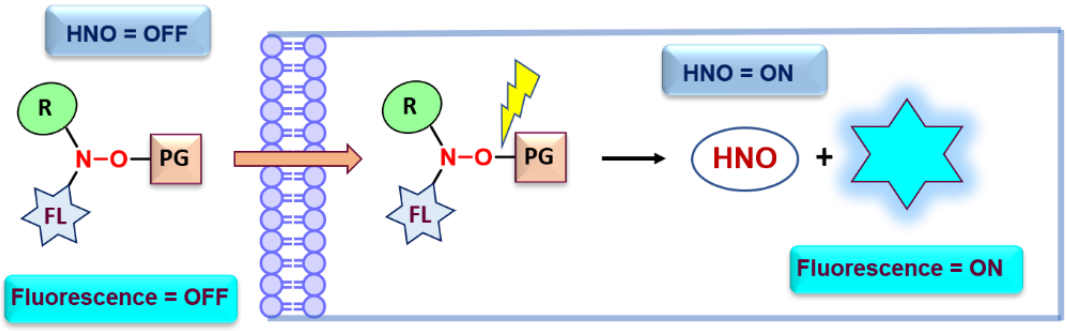

Figure 2.4. Design of stimuli-responsive concomitant release of nitroxyl (HNO) and fluorescence reporter by the HNO donor. The incorporation of latent fluorophore in the donor eliminates the need for a secondary assay for monitoring HNO.

Compounds **2h** and **3h** were synthesized using the above-mentioned protocols. Compound **1** was treated with dansyl chloride in the presence of sodium hydride to get compound **2h** which was further treated with TFA to afford **3h** in good yield (Scheme 2.8).[3]

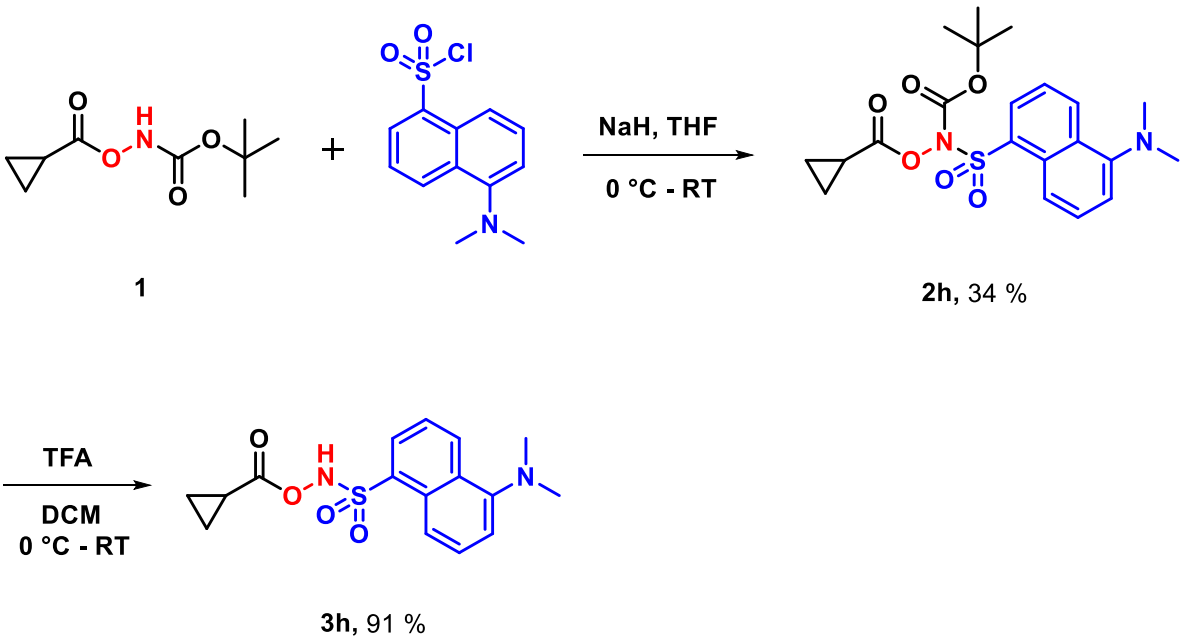

1

2h, 34 %

3h, 91 %

Scheme 2.8. Synthesis of **2h** and **3h**

Next, we synthesized the control compound. Dansylsulfinic acid was reduced by sodium borohydride to afford compound **7** (Scheme 2.9).[1]

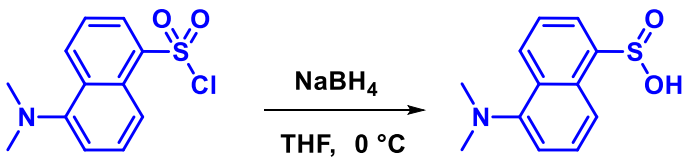

7, 47 %

Scheme 2.9. Synthesis of **7**

2.2.3. Photophysical properties of 7

Firstly, we studied the photophysical properties of **7** such as absorbance and fluorescence profiles in buffer (pH 7.4), photostability in different pH (8.0 – 5.0) and time course in buffer (pH 7.4) and fluorescence lifetime in the excited state.

2.2.3.1. Measurement of UV absorbance of 7

The UV absorbance spectrum of **7** was recorded in buffer (pH 7.4) at room temperature. The absorbance maximum (λ_{ex}) of **7** was observed at 308 nm in buffer (pH 7.4) (Figure 2.5).

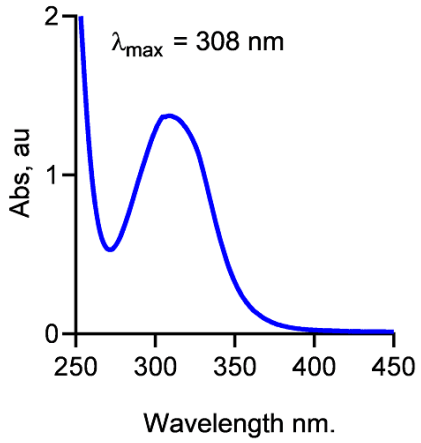

Figure 2.5. The UV absorption spectrum of **7** (100 µM) was measured in buffer (pH 7.4).

2.2.3.2. Measurement of fluorescence of 7

The fluorescence spectrum of **7** was recorded in buffer (pH 7.4). The fluorescence emission (λ_{em}) of **7** was observed at 497 nm (Figure 2.6).

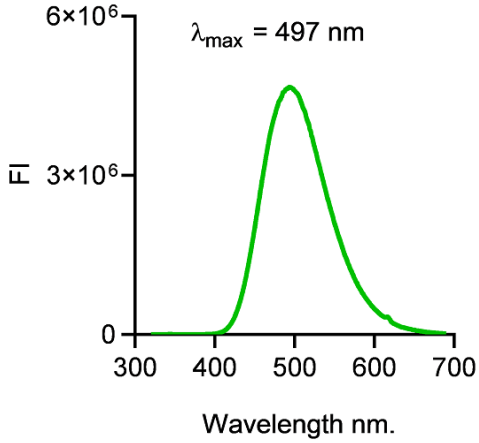

Figure 2.6. The fluorescence spectrum of **7** was measured in buffer (pH 7.4) (λ_{ex} = 308 nm; λ_{em} = 320 - 700 nm).

2.2.3.3. Stability of fluorescence of 7 in different pH

The stability of fluorescence signals in different pH is important for bioimaging purposes. The reason is that cancerous and non-cancerous cells have different pH. If a fluorophore shows fluorescence stability in different pH, it would be an ideal probe for bioimaging. Next, the fluorescence stability of **7** was monitored at varying pH ranging from 5.0 to 8.0. The

fluorescence of **7** was quite stable at different pH. **7** would be the best tool for bioimaging. Fluorescence measurement was carried out by using excitation at 308 and emission spectrum was obtained using 320-700 nm (Figure 2.7).

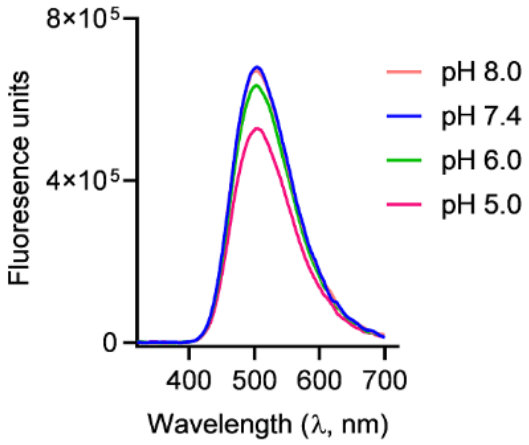

Figure 2.7: Fluorescence stability of **7** (50 µM) was measured in buffer (pH 7.4) upon excitation at 308 nm.

2.2.3.4. Stability of fluorescence of 7

The stability of fluorescence signals at physiological pH for an extended period is also an important property of an ideal fluorophore. To check the fluorescence stability, **7** was incubated in a buffer (pH 7.4) and fluorescence intensity was monitored over 12 h. The fluorescence of **7** was quite stable for 6 h and a small decrease in intensity over 12 h was recorded (Figure 2.8).

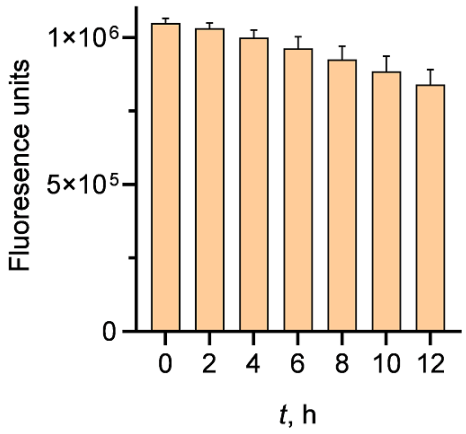

Figure 2.8: Fluorescence stability of **7** (50 µM) was measured in buffer (pH 7.4) for 12 h. (λ_{ex} = 308 nm; λ_{em} = 497 nm).

2.2.3.5. Time-resolved photoluminescence (PL) measurements

Time-Correlated Single Photon Counting (TCSPC) is a commonly used method for carrying out time-resolved photoluminescence (PL) measurements. TCSPC works by measuring the time between sample excitation by a laser pulse and the arrival of the emitted photon at the detector. The fluorescence lifetime is an intrinsic characteristic of fluorophore that can provide insight into the excited state dynamics of the species. Time-Resolved Photoluminescence (TRPL) is the tool of choice for studying fast electronic deactivation processes that result in the emission of photons, a process called fluorescence. The lifetime of a molecule in its lowest excited singlet state usually ranges from a few picoseconds up to nanoseconds. If the fluorescence lifetime of a fluorophore is higher, it will be very useful for imaging. A few fluorophores are listed below with their respective fluorescence lifetimes which are used for bioimaging (Table 2.3).

Table 2.3: Fluorescence lifetime of known fluorophores

Entry	Fluorophore	Media	Fluorescence lifetime, ns
1	DAPI[7]	H_2O	2.78
2	Sodium fluorescein[8]	PBS pH 7.4	4.05
3	Umbelliferone[9]	H_2O	5.0
4	Rhodamine B[10]	H_2O	1.74

Further, a Time-resolved PL study of **7** was performed by using a 292 nm nanoLED as the excitation source a time-to-amplitude converter (TAC) range of 200 ns for 10,000 counts and a fluorescence lifetime of **7** was monitored in the excited state (Figure 2.9).[11] It was observed that fluorescence in the excited state was stable for a longer time. The average lifetime (τ_{avg}) was calculated using the following equation.

$$\tau_{avg} = \frac{\alpha_1\tau_1 + \alpha_2\tau_2}{\alpha_1 + \alpha_2}$$

α = Relative amplitude; τ = Excited state

The average lifetime (τ_{avg}) of **7** was 13.82 ns (Table 2.4).

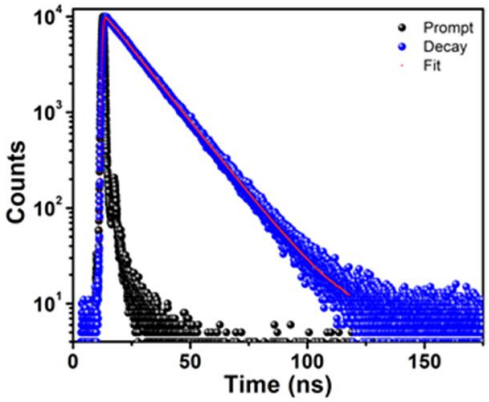

Figure 2.9: Time-resolved (lifetime) PL studies of **7** (10 µM) was measured by TCSPC (Time-Correlated Single Photon Counting) in PBS pH 7.4 for 200 ns. The data were fitted by second exponential and the τ_{avg} was 13.82 ns. CHISQ is a chi-square, used to compare observed results with expected results.

Table 2.4: Fluorescence lifetime of **7**

Compound	τ_1 (ns)	α_1 (%)	τ_2 (ns)	α_2 (%)	τ_{avg} (ns)	CHISQ
7 (10 µM)	6.8	4.01	14.12	95.99	13.82	1.07256

2.2.4. HNO generation and release of 7 from 2h and 3h

2.2.4.1. HNO generation from 2h and 3h

It is expected that upon activation by esterase, **2h** and **3h** concomitantly release HNO and fluorescent reporter **7** (Scheme 2.10).

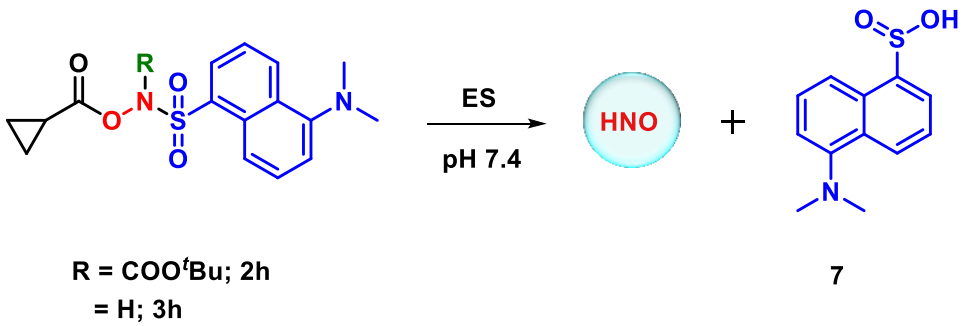

Scheme 2.10. Proposed mechanism of generation of HNO and fluorescent reporter **7**

To test the hypothesis, compounds **2h** and **3h** were independently co-incubated with **5** in the absence or presence of esterase. As anticipated, compounds **2h** and **3h** did not release HNO in buffer. However, an enhancement in the fluorescence signal (fluorescence signals correspond to HNO release) was observed in the presence of esterase with compounds **2h** and **3h.** Compound **2h** was able to generate a higher level of HNO as compared to compound **3h**. In this experiment, **4** was used as a positive control, a known HNO generator and the yield of HNO from this compound was assigned as 1 (Figure 2.10A). In a control experiment, esterase inhibitor PMSF (phenylmethylsulfonyl fluoride) was used to inhibit the esterase activity.[12] As a result, diminished HNO release was observed from compounds **2h** and **3h**. Overall, these results suggest that donors were specifically activated by esterase to release HNO (Figure 2.10A). Next, by using similar experimental conditions, the time course of HNO generation from **2h** and **3h** were monitored over 30 min using **5**. Time-dependent fluorescence enhancement was observed, which suggested the controlled HNO release (Figure 2.10B).

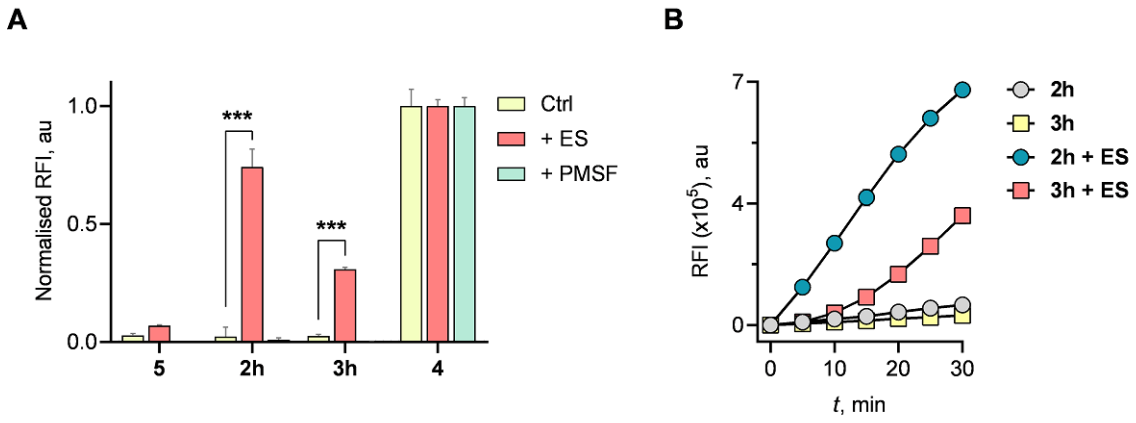

Figure 2.10: (A) Monitoring of fluorescence signals (λ_{ex} = 370 nm; λ_{em} = 460 nm) corresponding to HNO generation using **5** from compounds **2h** and **3h** (50 µM) were incubated in the absence and presence of esterase (0.5 U/mL) in buffer (pH 7.4) at 37 ˚C for 30 min. **5** refers to PCM dye; **4** refers to 2-bromopiloty's acid; + PMSF refers to esterase inhibitor; (B) Time course of HNO generation from compounds **2h** and **3h** (50 µM) over 30 min.

2.2.4.2. Concentration-dependent release of 7 in buffer

Next, the concentration-dependent release of **7** from **2h** and **3h** were studied. The fluorescence enhancement (λ_{ex} = 308 nm; λ_{em} = 497 nm) from compounds **2h** and **3h** were monitored in the absence and presence of esterase. A quantitative release of **7** was observed from

compounds **2h** and **3h**. In this experiment, compound **7** was used as positive control and the yield of fluorescence signals of **7** was assigned as 1 (Figure 2.11). In a control experiment, an esterase inhibitor (PMSF) was used to inhibit the esterase activity. As a result, fluorescence signals were diminished. Overall, these results suggest that donors were specifically activated by esterase to release fluorescence reporter **7**. Also, it was observed that PMSF did not affect the fluorescence signals of **7** (Figure 2.11).

Also, the time course generation of **7** was monitored in the presence of esterase for 180 min. Formation of **7** was observed from **2h** and **3h** with different rate constants 1.06 $\pm$ 0.05 h^{-1} and 1.77 $\pm$ 0.010 h^{-1}. Data were fitted in pseudo-first-order kinetics (Figure 2.12).

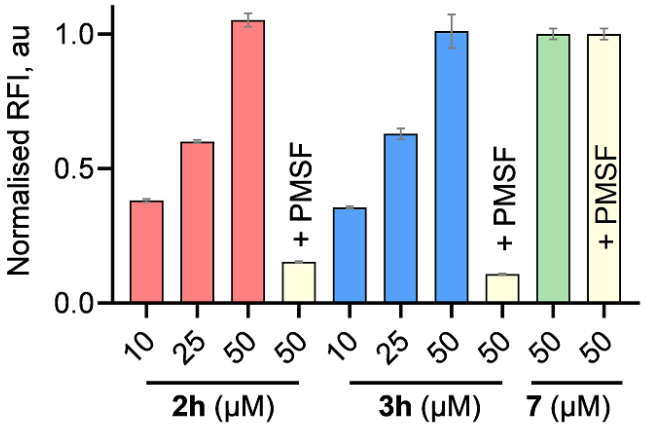

Figure 2.11. Concentration-dependent release of compound **7**: (A) Compounds **2h** and **3h** (50 μM) were incubated in the presence of esterase (0.5 U/mL) in buffer (pH 7.4) at 37 ˚C for 2 hours. **7** refers to dansylsulfinic acid; + PMSF refers to esterase inhibitor; (λ_{ex} = 308 nm; λ_{em} = 497 nm).

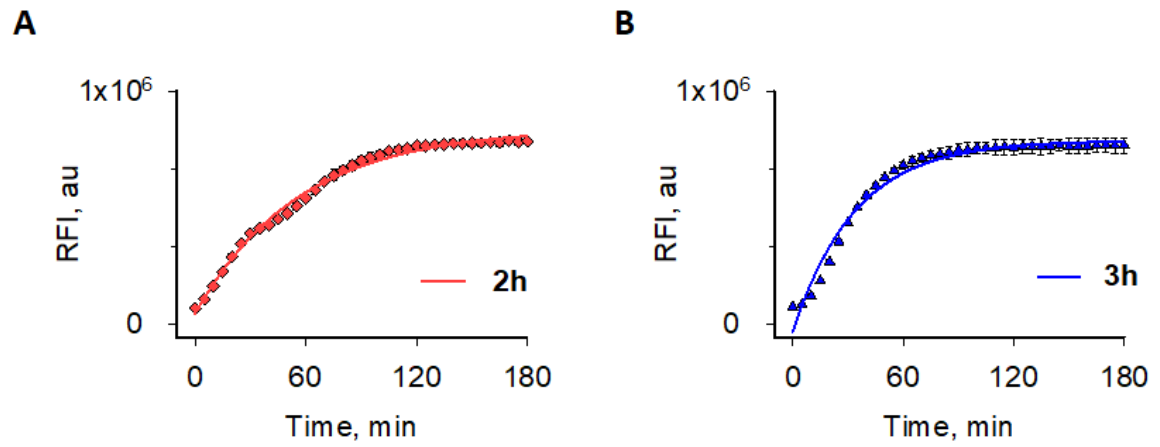

Figure 2.12. (A) Time-dependent release of **7** from **2h** in the presence of esterase in buffer; (B) Time-dependent release of **7** from **3h** in the presence of esterase in buffer.

2.2.4.3. Concomitant release of HNO and 7

Next, the time course of HNO generation and release of **7** in the presence of esterase were monitored by independent assays. HNO detection was performed by using HNO probe **5** and fluorescence was monitored at 460 nm for 30 min (Figure 2.10). Formation of **7** was monitored by fluorescence enhancement at 497 nm for 30 min (Figure 2.11). The time course of HNO generation corresponded well with the time course of fluorescence enhancement of **7** (Figure 2.13), thus suggesting that the release of HNO and fluorescence reporter **7** are concomitant. (Scheme 2.11). Together, these data demonstrate that fluorescence emission at 497 nm is a convenient signal to demonstrate HNO release. Real-time monitoring of HNO is possible by using **2h** and **3h**, it would eliminate the use of secondary assays (using HNO probes) to monitor the HNO release.

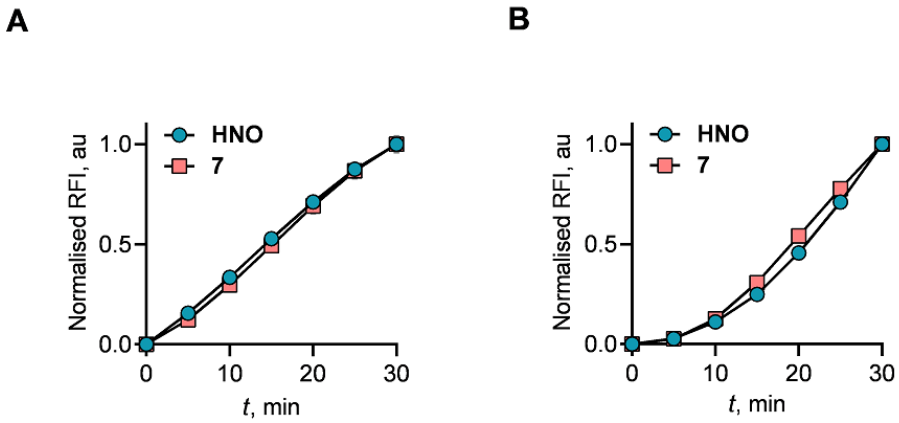

Figure 2.13. Time-dependent release of HNO and **7**: (A) Compounds **2h** (50 µM); (B) **3h** (50 µM) were incubated in the presence of esterase (0.5 U/mL) in buffer (pH 7.4) at 37 ˚C. The fluorescence enhancement was monitored over 30 min.

2.2.5. Nitric oxide (NO) generation

Since nitroxyl (HNO) donors are known to concurrently generate NO (Nitric oxide) at physiological conditions. Nitric oxide is a gasotransmitter and has been involved in several biological functions. These reactive nitrogen species (HNO and NO) have different activities in cells. NO is known to react with HNO and formed other reactive nitrogen species. The concurrent release of NO along with HNO, complicates the study of HNO and may provide false positive results. Hence, selectivity towards the generation of HNO *vs* NO, became an important feature of HNO donors.

Next, nitric oxide generation from esterase-triggered HNO donors was studied by using a colorimetric Griess assay. In this assay, NO is measured indirectly as nitrite (NO_2^-), a product of the autooxidation of NO.[13] The generated NO is converted into nitrite, which further reacts with Griess reagent (i.e. Sulfinamide) to form a diazonium salt and subsequently reacts with *N*-(1-naphthyl) ethylene diamine to form azo dye (pink color solution) with an absorbance maximum at 540 nm (Scheme 2.11). The amount of nitrite released was estimated from a standard calibration curve generated using sodium nitrite ($NaNO_2$) solution (Figure 2.14).

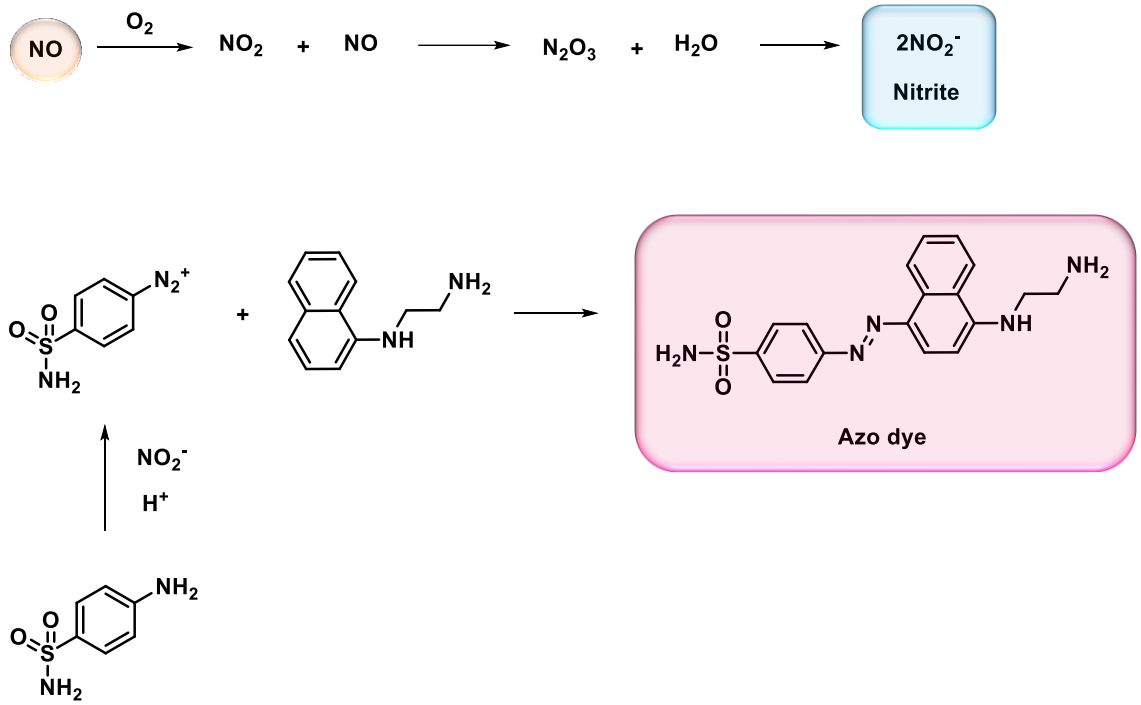

Scheme 2.11: The reaction of nitrite (NO_2^-) with Griess reagents forms an azo dye

The calibration curve was generated by using varying concentrations of $NaNO_2$ (0 – 50 µM). $NaNO_2$ and Griess's reagent was added to buffer (pH 7.4) and incubated at 37 ˚C for 25 min. Absorbance was measured at 540 nm (Figure 2.14).

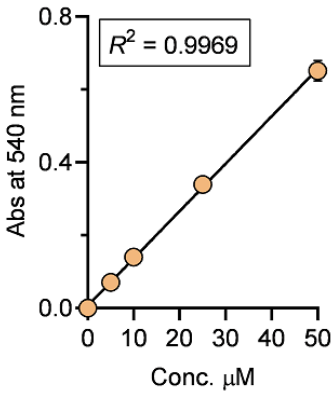

Figure 2.14: Calibration curve for varying concentrations of $NaNO_2$

Compounds **2a-2h** and **3a-3h** were incubated with esterase in buffer (pH 7.4) for 30 min in aerobic conditions and then incubated with Griess reagent for 25 min. The reaction mixture became light pink to dark pink, suggesting the formation of azo dye. The dark pink color of the reaction mixture corresponds to the formation of a high level of nitric oxide (NO). In this

experiment, **4** was used as the control compound and $NaNO_2$ was used as a positive control in similar reaction conditions and the absorbance was measured at 540 nm (Figure 2.15).

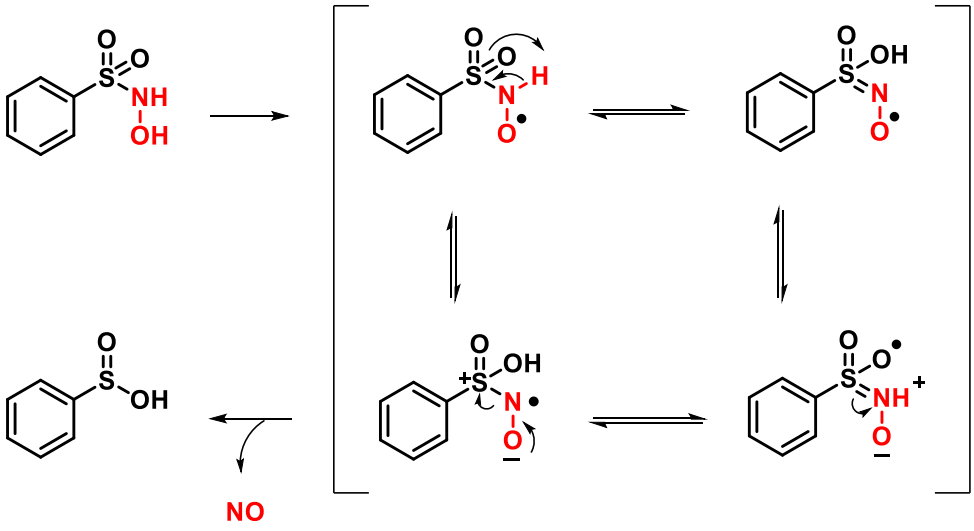

Scheme 2.12: Proposed mechanism for NO release from Piloty's acid

In the NO release mechanism, both oxygen and nitrogen atoms of Piloty's acid are in unprotected form. Radical formation on the oxygen atom and subsequently, on the nitrogen atom takes place which led to the NO formation in aerobic conditions (Scheme 2.12).[14,15] Sine, compound **4** is a derivative of Piloty's acid and both oxygen and nitrogen atoms are unprotected form which led to the formation of a higher amount of NO. However, in the case of compounds **3a-3h** oxygen atom is in protected form with the cyclopropylcarbonyl group which results in lower NO formation as compared to **4**. In another case, in **2a-2h,** both oxygen and nitrogen atoms are in protected forms which led to the lowest NO formation as compared to compounds **3a-3h** and **4**. This result suggests that to achieve the selectivity of the formation of HNO over NO, both oxygen and nitrogen atoms should be in protected form. Together, compounds **2a-2h** and **3a-3h** showed diminished NO formation compared to the **4** (Figure 2.15).

Order of NO formation: **4** > **3** > **2**

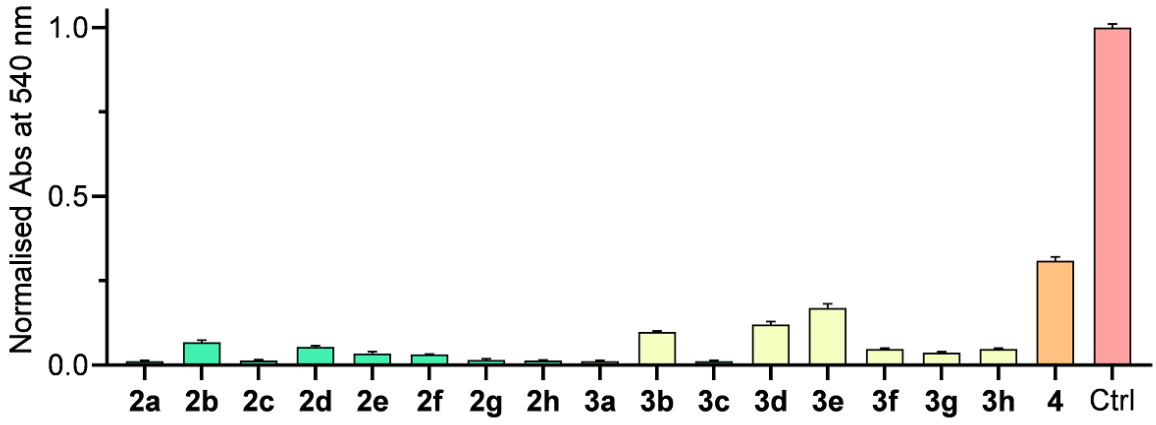

Figure 2.15: Griess assay for NO detection. Compounds **2a-2h** and **3a-3h** were incubated with esterase in buffer (pH 7.4) at 37 ˚C for 30 min and NO release was at 540 nm. Ctrl refers to the $NaNO_2$ and the data was normalized with $NaNO_2$ (50 µM).

2.2.6. LC/MS analysis

2.2.6.1. Decomposition of 2h

Following this assessment, the decomposition of **2h** was analyzed in the presence of esterase by LC/MS. Compound **2h** was incubated with esterase (0.5 U/mL) in pH 7.4 buffer and LC/MS profile was recorded at different time points. Compound **2h** disappeared within 10 min in the presence of esterase (Figure 2.16). A new peak at 12.0 min was recorded, it was intermediate **II**, and the concentration was built up over time and gradually consumed over 5 h (Figure 2.17). Surprisingly, two more peaks were eluted at 10.9 min and 7.81 min which was ascribed to the formation of compound **3h** (Figure 2.18) and dansyl Piloty's acid **8** (Figure 2.19). This was accompanied by the formation of a new peak at 5.99 corresponding to the formation of dansyl sulfinic acid **7** (Figure 2.20).

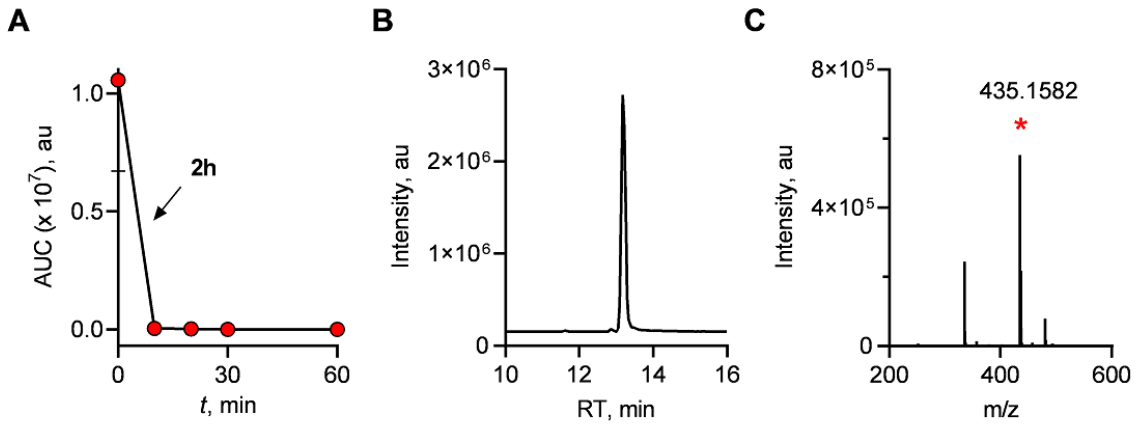

Figure 2.16: LC/MS study. (A) Decomposition of **2h** upon incubation with esterase (0.5 U/mL) as monitored by LC/MS. (B) Extracted ion chromatograms from an LC/MS analysis of **2h** (C) Mass spectra for compound **2h** (expected, m/z = 435.1584 $[M + H]^+$; observed, m/z = 435.1582).

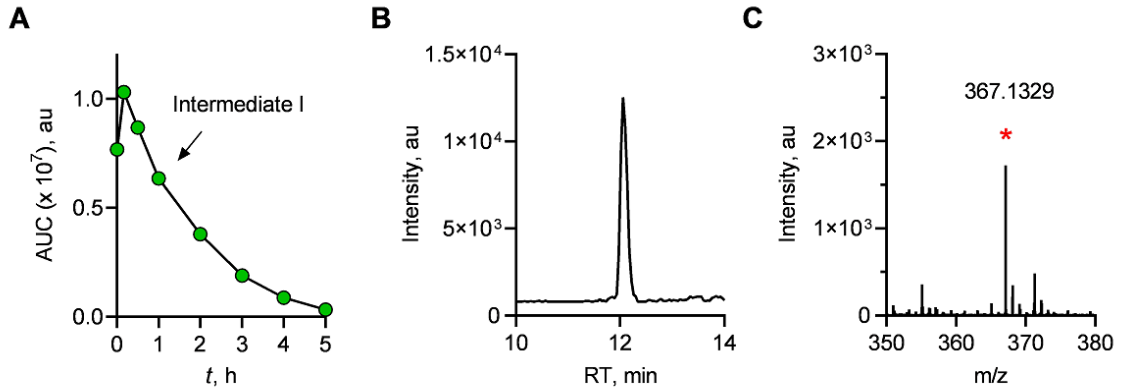

Figure 2.17: LC/MS study. (A) Formation of intermediate **I** (or **II**) during the decomposition of **2h** upon incubation with esterase (0.5 U/mL) as monitored by LC/MS. (B) Extracted ion chromatograms from an LC/MS analysis of intermediate **I** (or **II**) (C) mass spectra for intermediate **I** (or **II**) (expected, m/z = 367.1322 $[M + H]^+$; observed, m/z = 367.1329).

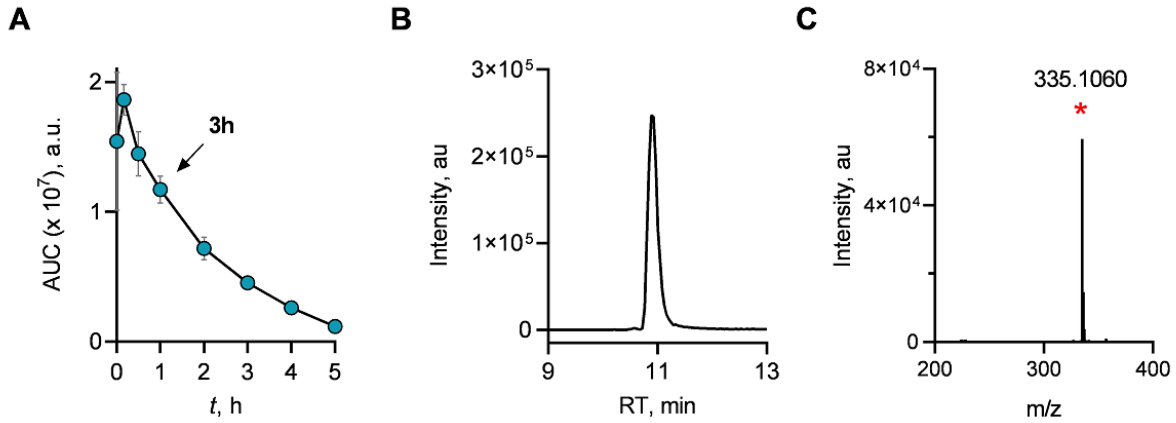

Figure 2.18: LC/MS study. (A) Formation of **3h** during the decomposition of **2h** upon incubation with esterase (0.5 U/mL) as monitored by LC/MS. (B) Extracted ion chromatograms from an LC/MS analysis of intermediate **3h**; (C) Mass spectra for **3h** (expected, m/z = 335.1058 $[M + H]^+$; observed, m/z = 335.1060).

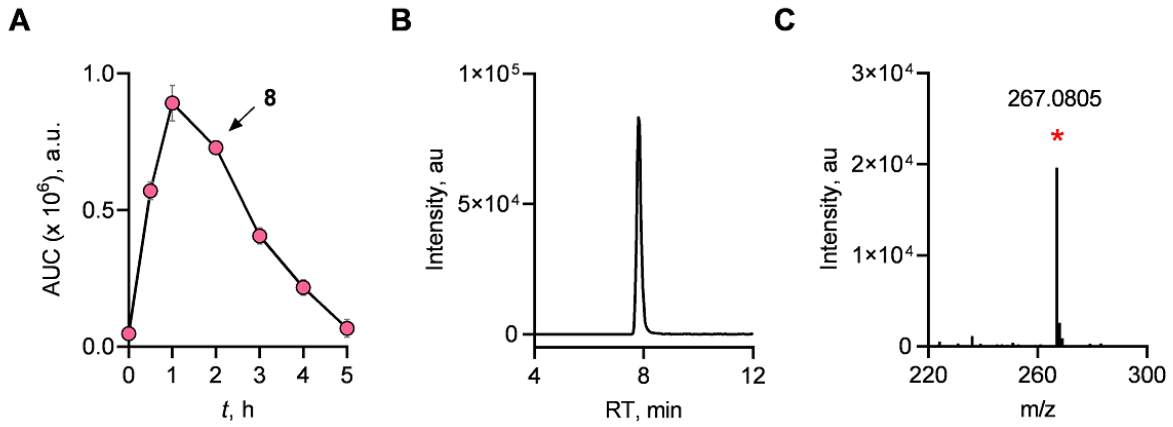

Figure 2.19: LC/MS study. (A) Formation of **8** during the decomposition of **2h** upon incubation with esterase (0.5 U/mL) as monitored by LC/MS. (B) Extracted ion chromatograms from an LC/MS analysis of **8**; (C) Mass spectra for **8** (expected, m/z = 267.0798 $[M + H]^+$; observed, m/z = 267.0805).

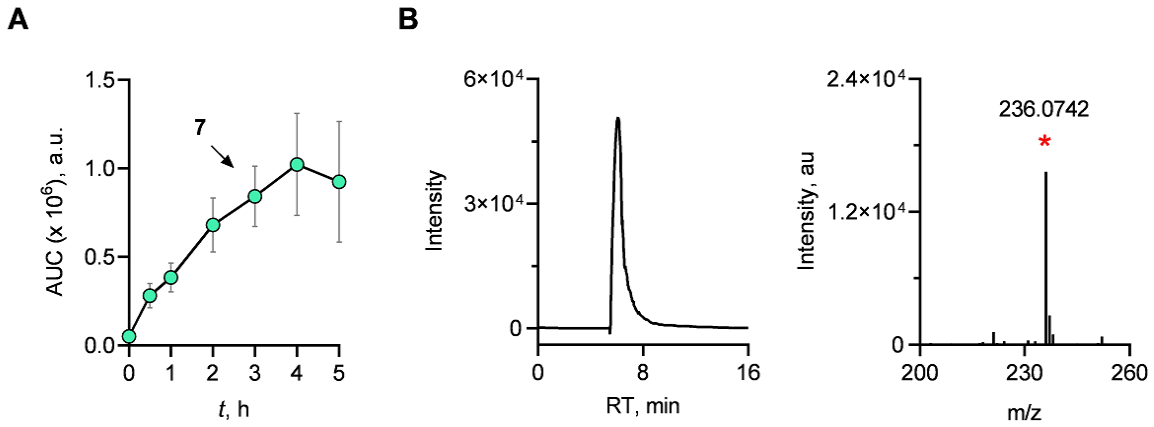

Figure 2.20: LC/MS study. (A) Formation of **7** during the decomposition of **2h** upon incubation with esterase (0.5 U/mL) as monitored by LC/MS; (B) Extracted ion chromatograms from an LC/MS analysis of **7**; (C) Mass spectra for **7** (expected, m/z = 236.0739 $[M + H]^+$; observed, m/z = 236.0742).

2.2.6.2. Stability of 3h

Similarly, stability and decomposition of **3h** were analyzed by LC/MS. Compound **3h** was found to be stable in buffer for 5 h (Figure 2.21).

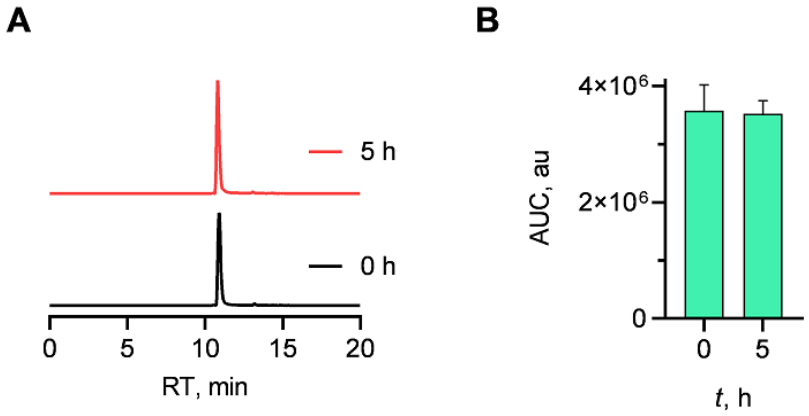

Figure 2.21: LC/MS study. Stability of compound **3h** in buffer (pH 7.4) for 0 and 5 h.

2.2.6.3. Decomposition of 3h

Next, a time-dependent LC/MS study was conducted to investigate the decomposition of **3h** in the presence of esterase. Compound **3h** was decomposed gradually over 240 min (Figure 2.22). A new peak ascribed to **8** eluted at 7.81 min and another peak at 5.99 was recorded which is **7** (Figure 2.23).

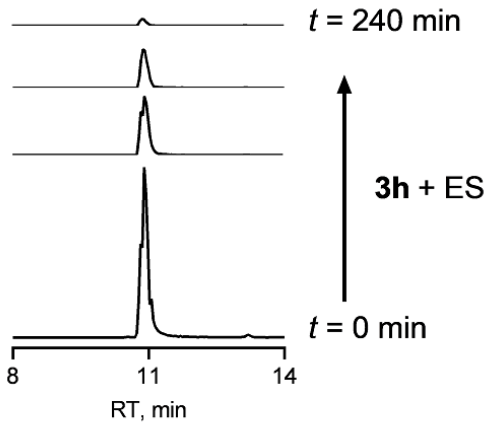

Figure 2.22: Extracted ion chromatograms from an LC/MS analysis of decomposition of **3h** upon incubation with esterase (0.5 U/mL) in buffer (pH 7.4). The time points considered were 0 min, 60 min, 120 min and 240 min.

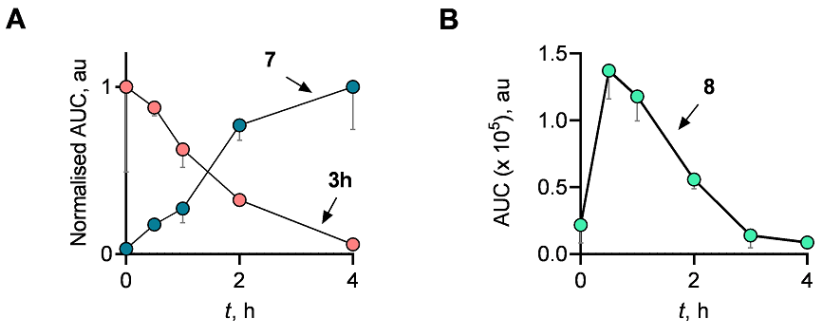

Figure 2.23: LC/MS study. (A) Decomposition of **3h** and formation of **7** upon incubation with esterase (0.5 U/mL) in buffer (pH 7.4) at 37 ˚C as monitored by LC/MS. **3h** (expected, m/z = 335.1060 $[M + H]^+$; observed, m/z = 335.1058), **7** (expected, m/z = 236.0739 $[M + H]^+$; observed, m/z = 236.0742). (B) Formation of **8** during the decomposition of **3h** upon incubation with esterase (0.5 U/mL) as monitored by LC/MS. **8** (expected, m/z = 267.0798 $[M + H]^+$; observed, m/z = 267.0805). All data are presented as mean ± SD (n = 3 per group).

2.2.7. Mechanism

Based on the above observations, a mechanism for the generation of HNO from esterase-triggered HNO prodrugs was postulated (Scheme 2.13). The cyclopropyl carbonyl ester of **2h** is cleaved by the attack of nucleophilic serine residue of esterase enzyme to form an intermediate I, which decomposes to liberate dansyl sulfinic acid **7** and common intermediate (Acyl nitroso intermediate). The latter intermediate releases HNO upon hydrolysis. Along with this mechanism, compound **2h** followed another mechanism where the Boc group of **2h** is cleaved in the presence of esterase and or in buffer (pH 7.4) to generate **3h**. Further, cyclopropylcarbonyl ester of **3h** is cleaved by an esterase enzyme to form **8** which is further cleaved to release HNO and dansyl sulfinic acid **7** (Scheme 2.13).

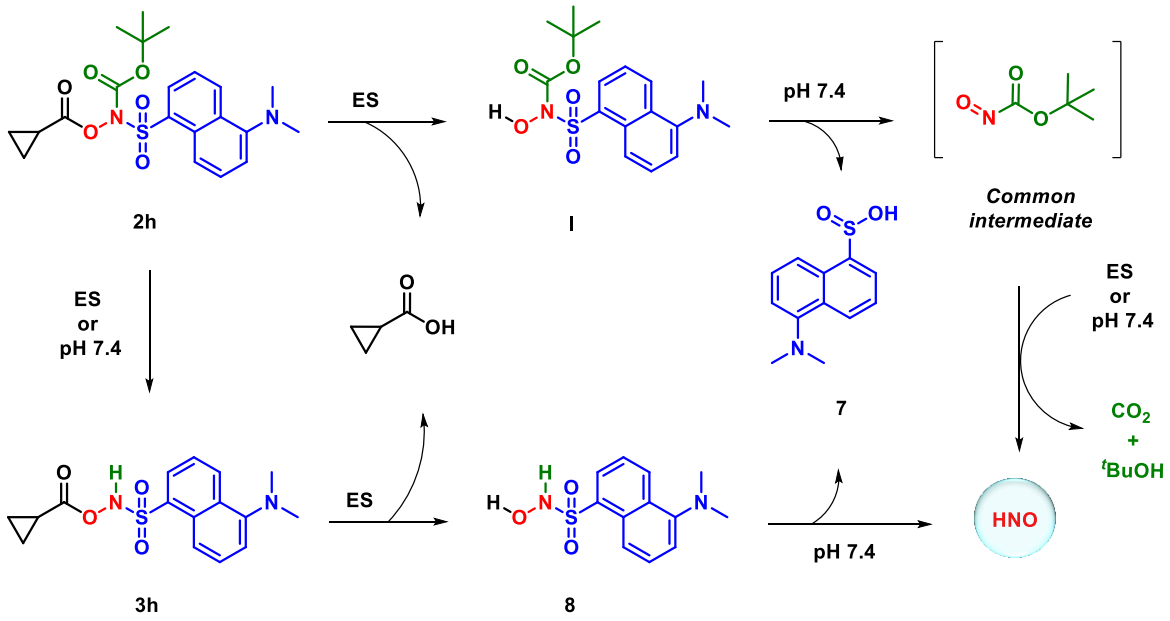

Scheme 2.13: Proposed mechanism of generation of HNO and **7**

2.2.8. Polysulfide measurement by LC/MS analysis

The objective was to study the cross-talk between HNO and H_2S and the ability of **2h** and **3h** to generate persulfides/polysulfides in the presence of H_2S.[16] Persulfides/polysulfides are sulfane sulfur pools, a cellular antioxidant reservoir. It can prevent overoxidation of proteins by different mechanisms such as directly scavenging the oxidants,[17] persulfidation of thiol proteins and upregulation of antioxidant genes.[18,19] Therefore, enhancing persulfides has emerged as an important therapeutic strategy in countering oxidative stress. Hence, it is important to study the redox biology of reactive sulfur species.

In order to study the cross-talk between HNO with H_2S, **2h** and **3h** were co-incubated independently with Na_2S and esterase in buffer (pH 7.4) for 15 min. The aliquots of the reaction mixture were subjected to the LC/MS analysis and the generation of persulfides/polysulfides was monitored. Since persulfide/polysulfide is known to have high nucleophilicity and can be trapped by using electrophiles. In this study, HPE-IAM was used as an electrophile to trap the generated persulfide/polysulfide (Scheme 2.14).[17]

2.2.8.1. Mechanism of polysulfide generation and trapping of polysulfide

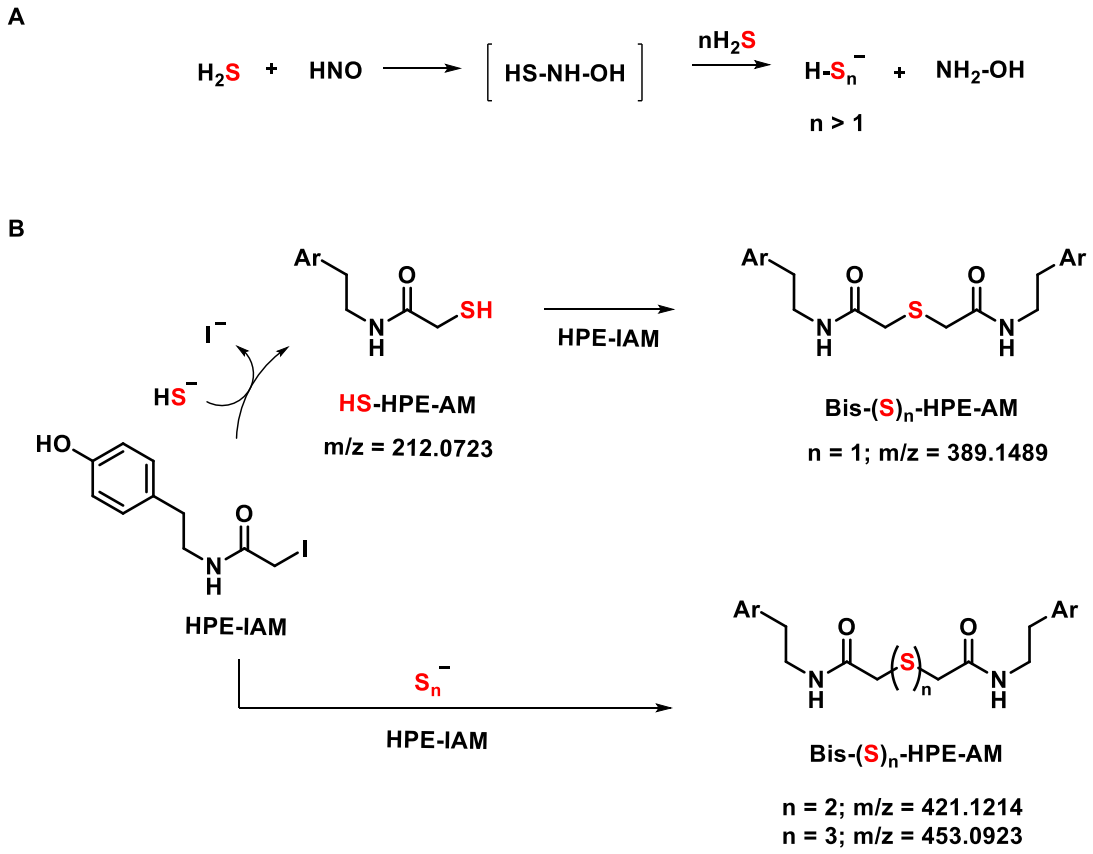

Scheme 2.14: LC/MS study. (A) Proposed mechanism of HNO reaction with H_2S; (B) Proposed mechanism of polysulfide formation; Ar refers to 4-hydroxyphenyl

2.2.8.2. Structures of sulfur species trapped by HPE-IAM

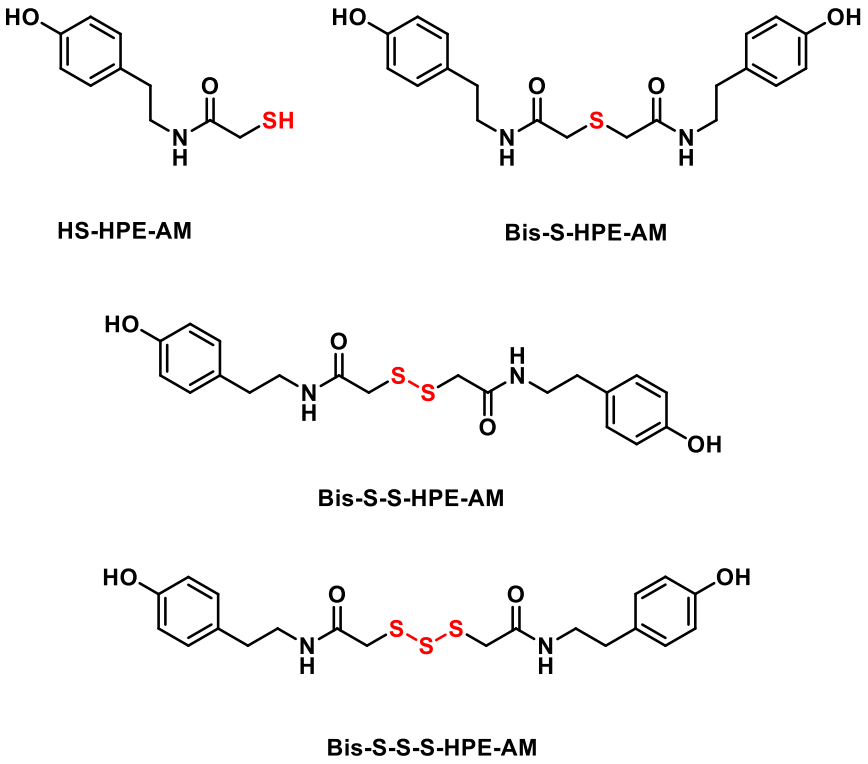

Scheme 2.15: Structures of sulfur species trapped by HPE-IAM probe

Results suggested that compounds **2h** and **3h** reacts with H_2S to generate persulfide/polysulfide (Scheme 2.15; Figure 2.24 - 2.28).

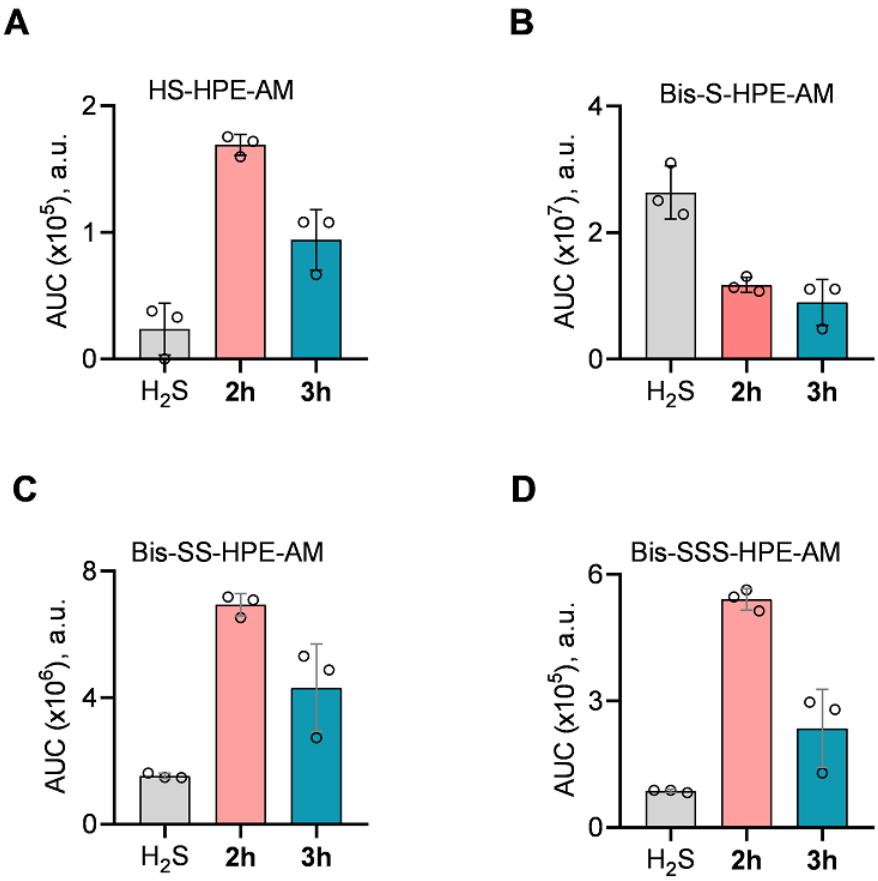

Figure 2.24: LC/MS study. Polysulfide formation was measured by detection of trapped HPE-IAM species from Na_2S, **2h** and **3h** upon incubation with esterase in buffer (pH 7.4) at 37 ˚C for 15 min; (A) Formation of HS-HPE-AM (expected, m/z = 212.0740 $[M + H]^+$; observed, m/z = 212.0719); (B) Formation of Bis-S-HPE-AM (expected, m/z = 389.1530 $[M + H]^+$; observed, m/z = 389.1489); (C) Formation of Bis-SS-HPE-AM (expected, m/z = 421.1205 $[M + H]^+$; observed, m/z = 421.1214); (D) Formation of Bis-SSS-HPE-AM (expected, m/z = 453.0971 $[M + H]^+$; observed, m/z = 453.0923).

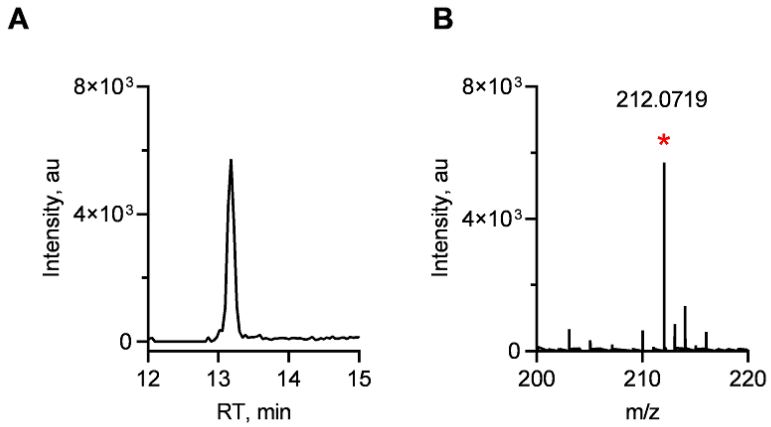

Figure 2.25: (A) Representative LC trace for the HS-HPE-AM; (B) Mass spectra for the HS-HPE-AM adduct from Na_2S with HPE-IAM (expected, m/z = 212.0740 $[M + H]^+$; observed, m/z = 212.0719).

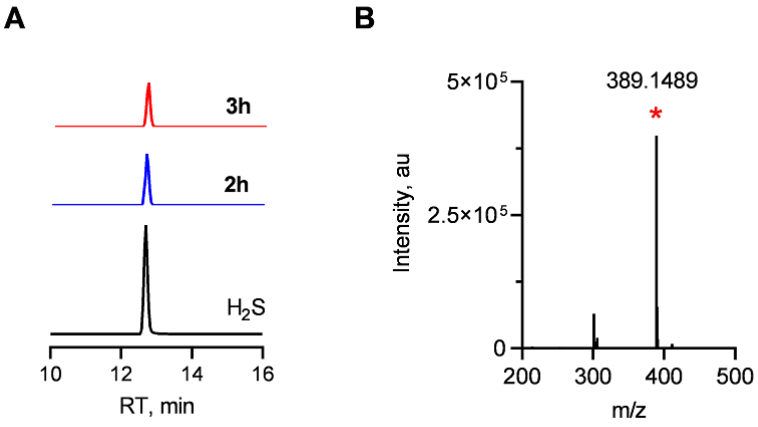

Figure 2.26: (A) Extracted ion chromatograms from an LC/MS analysis of Bis-S-HPE-AM formation from Na_2S, **2h** and **3h**; (B) Mass spectra for Bis-S-HPE-AM (expected, m/z = 389.1530 $[M + H]^+$; observed, m/z = 389.1489).

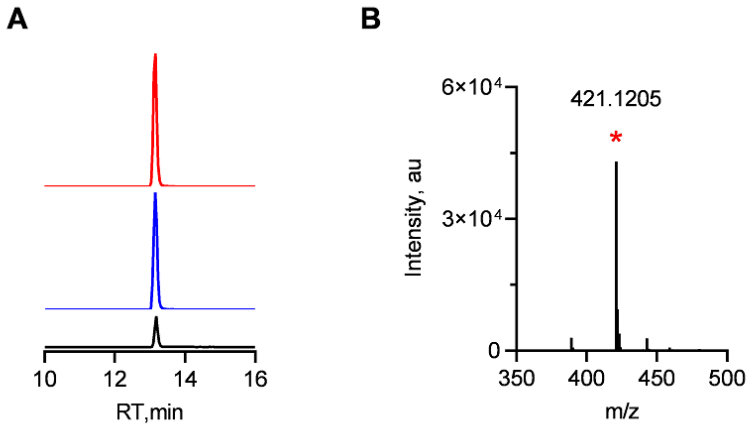

Figure 2.27: (A) Extracted ion chromatograms from an LC/MS analysis of Bis-SS-HPE-AM formation from Na_2S, **2h** and **3h**; (B) Mass spectra for Bis-SS-HPE-AM (expected, m/z = 421.1250 $[M + H]^+$; observed, m/z = 421.1205).

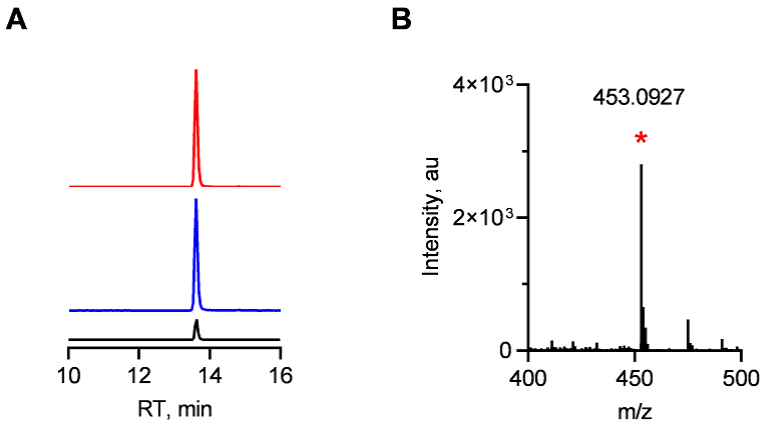

Figure 2.28: (A) Extracted ion chromatograms from an LC/MS analysis of Bis-SSS-HPE-AM formation from Na_2S, **2h** and **3h**; (B) Mass spectra for Bis-SSS-HPE-AM (expected, m/z = 453.0971 $[M + H]^+$; observed, m/z = 453.0927).

2.2.8.3. Polysulfide formation from 4

In this study, compound **4** was used as the positive control. Compound **4** (a known HNO generator) was co-incubated with Na_2S for 15 min and further incubated with an HPE-IAM probe for 15 min. The aliquots of the reaction mixture were subjected to LC/MS analysis and the formation of persulfide and polysulfide was monitored. As expected, Bis-SS-HPE-AM and Bis-SSS-HPE-AM formation was observed in higher quantities (Figure 2.29). Taken

together, these studies suggest that the production of persulfide/polysulfides are depend on the rate of production of HNO.

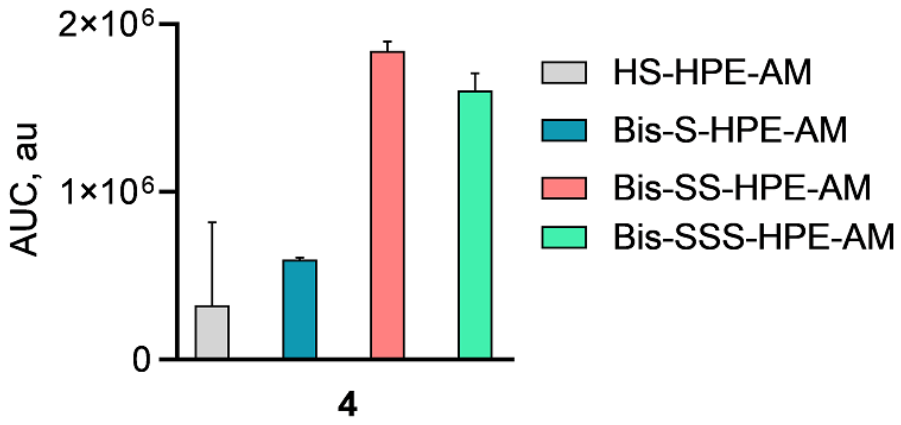

Figure 2.29: A comparison of sulfur species measured by detection of trapped HPE-AM species from H_2S with **4** and structures of polysulfide adduct with HPE-IAM. HS-HPE-AM (expected, m/z = 212.0740 $[M + H]^+$; observed, m/z = 212.0720); Bis-S-HPE-AM (expected, m/z = 389.1530 $[M + H]^+$; observed, m/z = 389.1489); Bis-SS-HPE-AM (expected, m/z = 421.1250 $[M + H]^+$; observed, m/z = 421.1203): Bis-SSS-HPE-AM (expected, m/z = 453.0971 $[M + H]^+$; observed, m/z = 453.0923).

2.2.9. Concentration-dependent release of 7 in A549 cell lysate

To test the hypothesis of the release of fluorescent reporter **7** in cell lysate, compounds **2h** and **3h** were independently incubated in cell lysate. In cell lysate, compounds were cleaved to release **7** and a concentration-dependent fluorescence enhancement was observed

Next, cell lysate was treated with PMSF to inhibit the esterase activity for 30 min. These PMSF-pretreated cell lysates were incubated with **2h** and **3h** for 3 h. As expected, diminished fluorescence signals were observed (Figure 2.30).

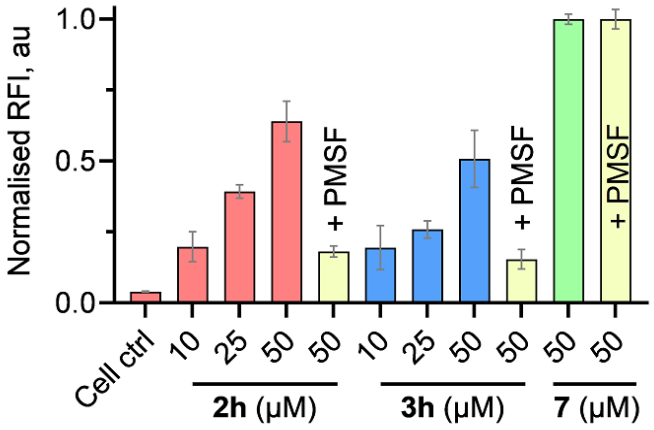

Figure 2.30: Compounds **2h, 3h** and **7** were incubated in A549 cell lysate (1 mg/mL) in the presence and absence of PMSF (esterase inhibitor) for 3 h; cell ctrl refers to untreated cell lysate; + PMSF refers to cell lysate were preincubated with PMSF for 30 min. Fluorescence measurement (λ_{ex} = 308 nm; λ_{em} = 497 nm) was carried out by varying concentrations of **2h** and **3h; 7** refers to dansyl sulfinic acid.

2.2.10. MTT assay for cell viability

The cytotoxicity of compounds **2h, 3h** and **7** were evaluated using a standard MTT assay to estimate the cell viability. Mouse embryonic fibroblasts (MEF) cells, lung carcinoma cells (A549) and breast cancer cells (MCF-7) were treated with varying concentrations of **2h, 3h** and **7** and incubated for 24 h following which cell viability was measured. The compounds **2h** and **3h** were found to be well tolerated up to 25 μM by the MCF-7 cells and but higher toxicity in MEF and A549 cells was observed. Compound **7** was found to be well tolerated by MCF-7, MEF and A549 cells (Figure 2.31-2.33).

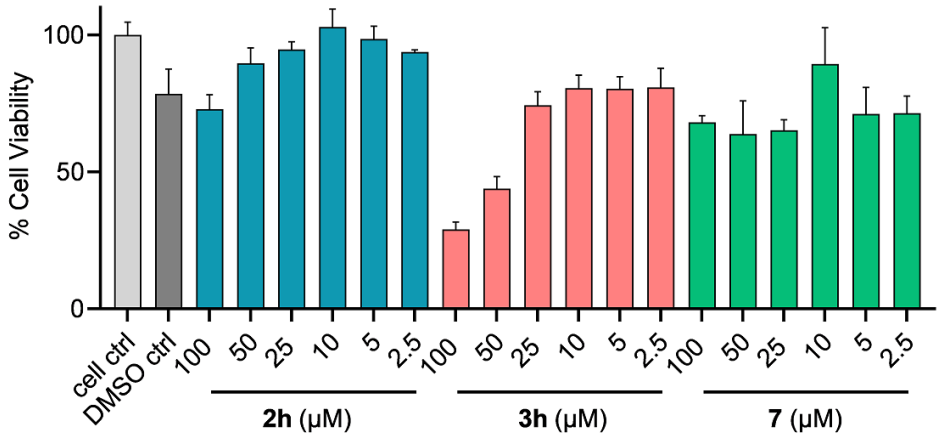

Figure 2.31: Cell viability assay carried out with varying concentrations of compounds **2h**, **3h** and **7** on MCF-7 cells for 24 h. All data are presented as mean ± SD (n =3/group).

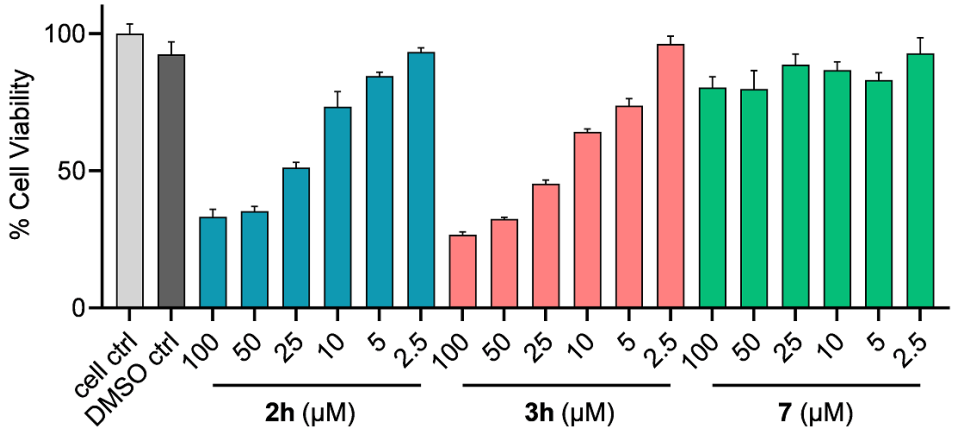

Figure 2.32: Cell viability assay carried out with varying concentrations of compounds **2h**, **3h** and **7** on MEF cells for 24 h. All data are presented as mean ± SD (n =3/group).

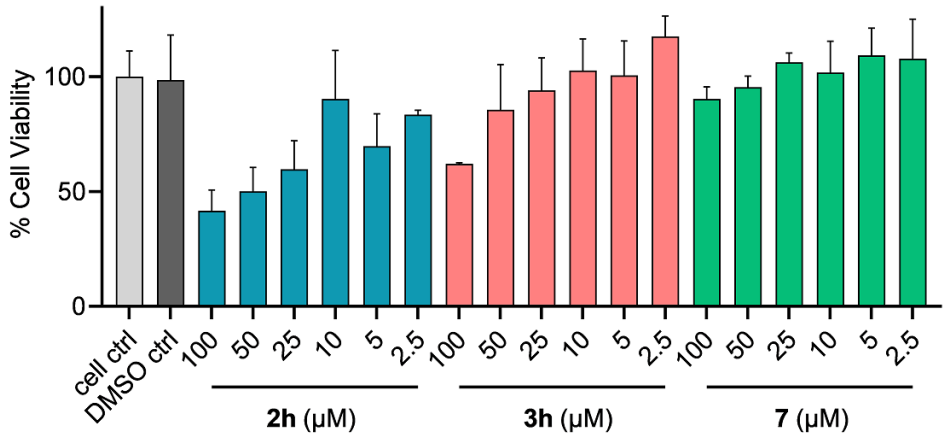

Figure 2.33: Cell viability assay carried out with varying concentrations of compounds **2h**, **3h** and **7** on A549 cells for 24 h. All data are presented as mean ± SD (n =3/group).

2.2.11. Intracellular generation of HNO and 7 in MCF-7 cells

Prodrugs **2h** and **3h** were chosen to assess the intracellular generation of HNO. To detect intracellular HNO, the previously reported probe **6** was used.[5] The probe reacts with HNO to release TCF-OH which produces a distinct fluorescent signal at 614 nm with excitation at 560 nm (Scheme 2.16).

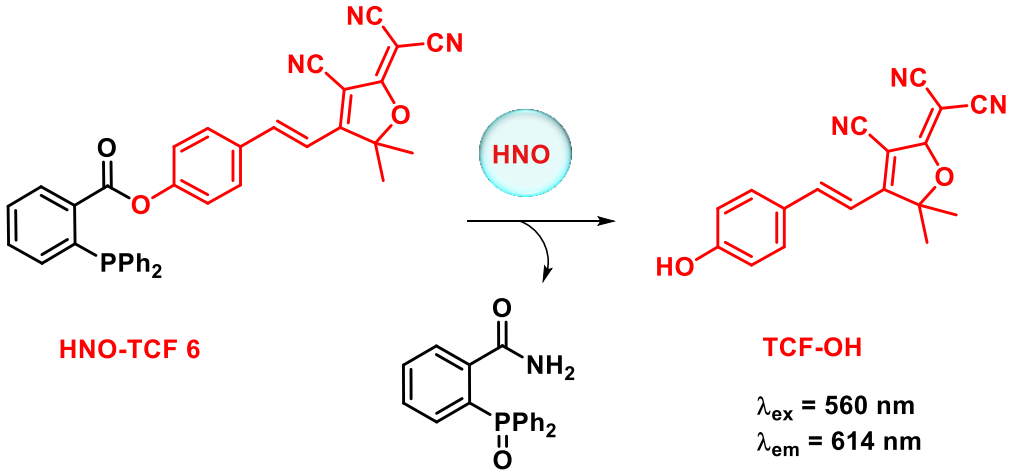

Scheme 2.16: Proposed mechanism for HNO detection by **6** and release of TCF-OH

MCF-7 cells were pre-treated with 20 μM of **6** and incubated for 30 min followed by incubation with **2h** and **3h** independently for 2 h. Fluorescence imaging was carried out in the Alexa fluor 568 (Red channel) on Carl Zeiss LSM710 laser scanning confocal microscope with anisotropy with a 63x oil filter. A significant increment in fluorescence, corresponding

to the generation of HNO was observed at a concentration of 200 μM of **2h** and **3h** (Figure 2.34). The release of **7** from **2h** and **3h** in MCF-7 cells were imaged in a DAPI channel on Carl Zeiss LSM710 laser scanning confocal microscope with anisotropy with a 63x oil filter (Figure 2.34). Bright field images for **4**, **2h**, **3h** and **7** were imaged on Carl Zeiss LSM710 laser scanning confocal microscope with anisotropy (Figure 2.35).

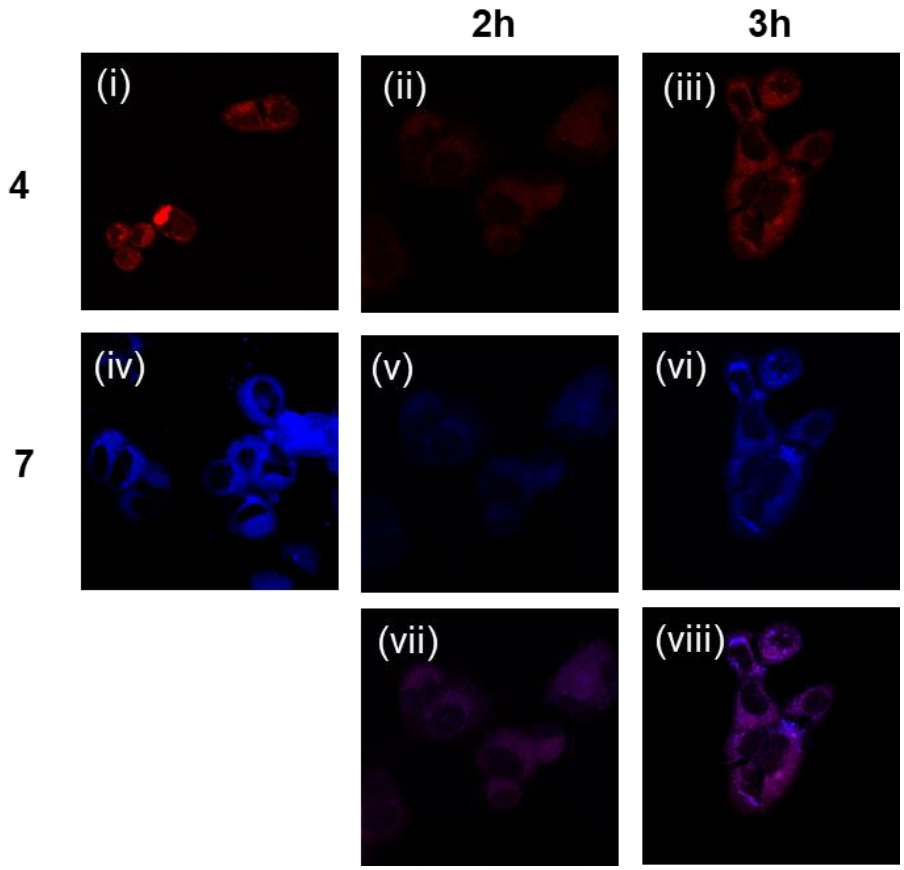

Figure 2.34: Confocal microscopy images of HNO and **7** in breast cancer cells (MCF-7). **HNO detection:** MCF-7 cells were pre-incubated with **6 (**20 μM) for 30 min followed by treatment of (i) **4**; (ii) **2h** (iii) **3h** (200 μM) independently for 2 h. The cells were imaged on Carl Zeiss LSM710 laser scanning confocal microscope with anisotropy. The cells were imaged in the RED channel (Alexa fluor 568 for HNO detection). (iv) **7** (200 μM); (v) **2h** (vi) **3h**. The cells were imaged in the DAPI channel (Detection of **7**). (vii) Merged image of (ii and v); (viii) Merged image of (iii and vi).

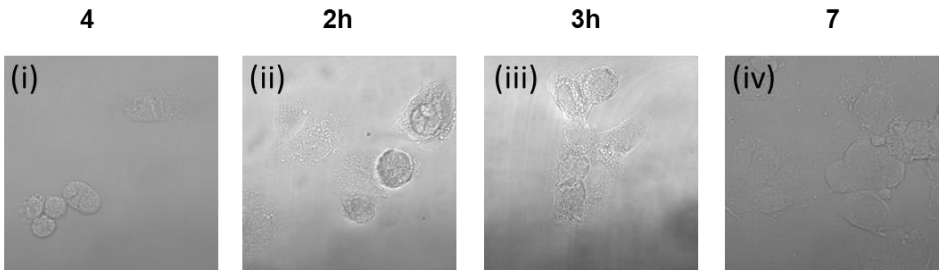

Figure 2.35: Bright field images for (i) **4**; (ii) **2h**; (iii) **3h** and (iv) **7** were imaged on Carl Zeiss LSM710 laser scanning confocal microscope with anisotropy.

2.3. Summary

To summarize, esterase-triggered HNO generators were designed and two series of donors were synthesized. Firstly, HNO release was monitored for both the series of compounds using **5**. All tested compounds were able to generate a significant amount of HNO except compounds **3a** and **3g**. In the presence of esterase, the cleavage of **5** was observed after 30 min. Hence, HNO detection could not be performed beyond 30 min.

To address this issue, we designed and synthesized HNO donors with a dansyl-based fluorescence reporter. Firstly, we studied the photophysical properties of dansyl probes such as UV-absorbance and fluorescence properties (Emission, fluorescence lifetime in excited state, stability of fluorescence in different pH related to cellular conditions). HNO detection assay was performed with **2h** and **3h**. Compound **2h** was able to generate a significant amount of HNO in the presence of esterase compared to **3h**. Further, the release of fluorescence reporter **7** was monitored with compounds **2h** and **3h** for 2 h and a quantitative release of **7** was observed from these compounds. Next, we compare the release of HNO and **7** with compounds **2h** and **3h** and the concomitant release was observed with both the series of compounds. Together, these data demonstrate that fluorescence emission of fluorescence reporter **7** at 497 nm is a convenient signal to demonstrate HNO release. Real-time monitoring of HNO is possible by using **2h** and **3h**, it will eliminate the use of secondary assays (using HNO probes) to monitor the HNO release.

Since the reaction of H_2S and HNO is known to enhance the persulfide/polysulfide levels in vitro. We studied the persulfide/polysulfide formation with **2h** and **3h** by reacting with Na_2S (source of H_2S) and the formation of these sulfur species was monitored. Compounds **2h** and **3h** were able to enhance persulfide/polysulfide in vitro.

Next, cell viability of **2h**, **3h** and **7** were performed in MEF, MCF-7 and A549 cells. The byproduct **7** was benign and well tolerated by the cells. Compounds **2h** and **3h** were quite toxic to the cells. Compounds **2h** and **3h** were subjected to the cells and compounds were able to enhance the cellular HNO level which was detected using **6**. Also, these compounds were able to enhance the level of fluorescent reporter **7** in cells. Together, the data suggest that real-time monitoring of HNO *in vitro* and cells are possible by using these donors. Having these tools in hand, triggerable and tunable HNO generation can achieve.

2.4. Experimental Protocols

2.4.1. Synthesis and characterization:

Synthesis of *tert*-butyl ((cyclopropanecarbonyl)oxy)carbamate (1): From cyclopropylcarbonyl chloride, *tert*-butyl ((cyclopropanecarbonyl)oxy)carbamate (**1**) was synthesized by using reported protocol.[2]

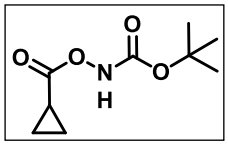

N-Boc hydroxylamine (764 mg, 5.74 mmol, 1.0 eq.) was dissolved in DCM (4 mL) and NEt_3 (0.74 mL, 7.31 mmol, 1.1 eq.) was added. At 0 ˚C, cyclopropanecarbonyl chloride (600 mg, 5.74 mmol, 1.0 eq.) was added dropwise and the reaction was warmed to reach room temperature. After 2 h of stirring, the reaction mixture was vacuum filtered and the residue was washed with DCM. The filtrate was washed with water (20 mL), satd. $NaHCO_3$ solution (20 mL) and brine (20 mL). The organic layer was dried over Na_2SO_4, filtered and the filtrate was concentrated to yield the corresponding carbamate **1** as a colorless crystalline solid (800 mg, 70%). ^{1}H-NMR ($CDCl_3$, 400 MHz): δ 7.93 (s, 1H), 1.81 - 1.75 (m, 1H), 1.49 (s, 9H), 1.16 - 1.12 (m, 2H), 1.05 - 1.0 (m, 2H); ^{13}C-NMR ($CDCl_3$, 100 MHz): δ 174.5, 155.7, 83.3, 28.2, 11.1, 9.6; HRMS (ESI-TOF) for $[C_9H_{15}NO_4 + H]^+$: Calcd., 202.1078, Found, 202.1083.

General procedure for the synthesis of *N*-sulfonyl-*N*-(cyclopropanecarbonyl)oxy-*tert*-butyl-carbamate (2): From *tert*-butyl ((cyclopropanecarbonyl)oxy)carbamate (**1**), *N*-sulfonyl-*N*-(cyclopropanecarbonyl)oxy-*tert*-butyl-carbamate (**2**) was synthesized by using reported protocol.[3]

tert-butyl ((cyclopropanecarbonyl)oxy) carbamate (**1**) was dissolved in anhydrous THF. To this solution, 2.5 eq. of NaH was added and the reaction stirred for 5 minutes until the completion of gas evolution. To this solution, 1 eq. of the sulfonyl chloride derivatives ($ArSO_2Cl$) was added. Upon completion of the reaction (TLC analysis) the solvent was

evaporated under reduced pressure to the yield crude product, which was further purified using silica gel column chromatography to yield an *N*-sulfonyl-*N*-(cyclopropanecarbonyl)oxy-*tert*-butyl-carbamate (**2**).

***tert*-butyl ((cyclopropanecarbonyl)oxy)(phenylsulfonyl)carbamate (2a):**

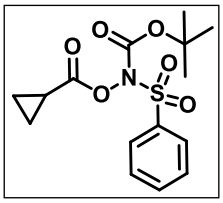

Yield (380 mg, 56%); FT-IR (υ_{max}, cm^{-1}): 1736, 1669; ^{1}H-NMR ($CDCl_3$, 400 MHz): δ 7.99 – 7.97 (m, 2H), 7.63 – 7.59 (m, 1H), 7.51 – 7.47 (m, 2H), 1.81 – 1.74 (m, 1H), 1.32 (s, 9H), 1.19 – 1.13 (m, 2H), 1.04 – 1.01 (m, 2H); ^{13}C-NMR ($CDCl_3$, 100 MHz): δ 170.7, 147.6, 136.9, 133.3, 127.9, 127.8, 85.4, 26.8, 9.4, 8.8; HRMS (ESI-TOF) for $[C_{15}H_{19}NO_6S + Na]^+$: Calcd., 364.0800, Found, 364.0839.

***tert*-butyl ((2-bromo-phenyl)sulfonyl)((cyclopropanecarbonyl)oxy)carbamate (2b):**

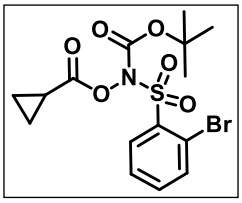

Yield (533 mg, 64%); FT-IR (υ_{max}, cm^{-1}): 1794, 1761; ^{1}H-NMR ($CDCl_3$, 400 MHz): δ 8.29 – 8.26 (m, 1H), 7.79 – 7.77 (m, 1H), 7.53 – 7.46 (m, 2H), 1.91 – 1.85 (m, 1H), 1.36 (s, 9H), 1.27 – 1.23 (m, 2H), 1.11 – 1.09 (m, 2H); ^{13}C-NMR ($CDCl_3$, 100 MHz): δ 171.9, 148.2, 138.1, 135.8, 134.9, 133.6, 127.5, 121.0, 86.6, 27.9, 10.5, 10.0; HRMS (ESI-TOF) for $[C_{15}H_{18}BrNO_6S + Na)]^+$: Calcd., 441.9935, Found, 441.9940.

***tert*-butyl ((4-bromophenyl)sulfonyl)((cyclopropanecarbonyl)oxy)carbamate (2c):**

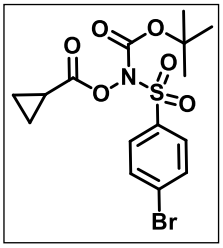

Yield (305 mg, 37%); FT-IR (υ_{max}, cm^{-1}): 1748; ^{1}H-NMR ($CDCl_3$, 400 MHz): δ 7.92 – 7.90 (m, 2H), 7.71 – 7.68 (m, 2H), 1.86 – 1.80 (m, 1H), 1.41 (s, 9H), 1.23 – 1.19 (m, 2H), 1.12 – 1.09 (m, 2H); ^{13}C-NMR ($CDCl_3$, 100 MHz): δ 171.9, 148.6, 137.0, 132.3, 130.7, 129.9, 86.8, 28, 10.6, 10.0; HRMS (ESI-TOF) for $[C_{15}H_{18}BrNO_6S + Na]^+$: Calcd., 441.9936, Found, 441.9940.

***tert*-butyl ((cyclopropanecarbonyl)oxy)((2-(trifluoromethyl)phenyl)sulfonyl)carbamate (2d):**

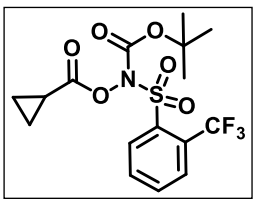

Yield (340 mg, 41%); FT-IR (υ_{max}, cm^{-1}): 1717; ^{1}H-NMR ($CDCl_3$, 400 MHz): δ 8.42 – 8.39 (m, 1H), 7.78 – 7.84 (m, 1H), 7.74 – 7.67 (m, 2H), 1.82 – 1.75 (m, 1H), 1.31 (s, 9H), 1.18 – 1.14 (m, 2H), 1.05 – 1.00 (m, 2H); ^{13}C-NMR ($CDCl_3$, 100 MHz): δ 170.8, 147.1, 136.5, 133.0, 132.3, 131.2, 127.6, 127.2 (q, $J_{C,F}$ = 5.9 Hz), 119.8, 85.7, 26.7, 9.4, 8.8; HRMS (ESI-TOF) for $[C_{16}H_{18}F_3NO_6S + Na]^+$: Calcd., 432.0697, Found, 432.0708.

***tert*-butyl ((2-bromo-4-(trifluoromethyl)phenyl)sulfonyl)((cyclopropanecarbonyl)oxy)carbamate (2e):**

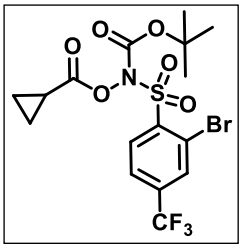

Yield (573 mg, 59%); FT-IR (υ_{max}, cm^{-1}): 1799, 1765; ^{1}H-NMR ($CDCl_3$, 400 MHz): δ 8.34 (d, *J* = 8.2 Hz, 1H), 7.96 (d, *J* = 0.8 Hz, 1H), 7.69 (dd, *J* = 8.3 Hz, 1.1 Hz, 1H), 1.84 – 1.77 (m, 1H), 1.32 (s, 9H), 1.21 – 1.16 (m, 2H), 1.07 – 1.04 (m, 2H); ^{13}C-NMR ($CDCl_3$, 100 MHz): δ 170.8, 146.9, 140.4, 135.4, 135.1, 132.9, 131.7 (q, $J_{C,F}$ = 3.7 Hz), 123.3, 120.6, 86.1, 26.8, 9.3, 9.0; HRMS (ESI-TOF) for $[C_{16}H_{17}BrF_3NO_6S + H]^+$: Calcd., 486.9900, Found, 486.8889.

***tert*-butyl ((cyclopropylcarbonyl)oxy)((2-nitrophenyl)sulfonyl)carbamate (2f):**

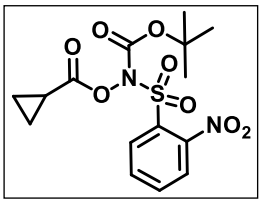

Yield (364 mg, 48%); FT-IR (υ_{max}, cm^{-1}): 1793, 1762; ^{1}H-NMR ($CDCl_3$, 400 MHz): δ 8.39 – 8.37 (m, 1H), 7.79 – 7.77 (m, 3H), 1.92 – 1.85 (m, 1H), 1.43 (s, 9H), 1.27 – 1.23 (m, 2H), 1.14 – 1.10 (m,2H); ^{13}C-NMR ($CDCl_3$, 100 MHz): δ 171.9, 148.2, 148.0, 135.1, 132.8, 132.0, 131.7, 124.6, 87.1, 27.9, 10.5, 10.0; HRMS (ESI-TOF) for $[C_{15}H_{18}N_2O_8S + Na]^+$: Calcd., 409.0697, Found, 409.0683.

***tert*-butyl ((cyclopropanecarbonyl)oxy)((4-nitrophenyl)sulfonyl)carbamate (2g):**

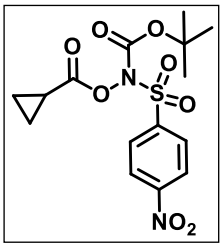

Yield (300 mg, 48%); FT-IR (υ_{max}, cm^{-1}): 1794, 1762; ^{1}H-NMR ($CDCl_3$, 400 MHz): δ 8.40 – 8.36 (m, 2H), 8.25 – 8.22 (m, 2H), 1.87 – 1.81 (m, 1H), 1.40 (s, 9H), 1.24 – 1.20 (m, 2H), 1.15 – 1.12 (m, 2H); ^{13}C-NMR ($CDCl_3$, 100 MHz): δ 172.0, 151.0, 148.2, 143.5, 130.7, 124.1, 87.4, 28.0, 10.5, 10.2; HRMS (ESI-TOF) for $[C15H18N_2O8S + H]^+$: Calcd., 387.0900, Found, 387.0720.

***tert*-butyl ((cyclopropanecarbonyl)oxy)((5-(dimethylamino)naphthalen-1-yl)sulfonyl)carbamate (2h):** From dansyl chloride, *tert*-butyl ((cyclopropanecarbonyl)oxy)((5-(dimethylamino)naphthalen-1-yl)sulfonyl)carbamate **(2h)** was synthesized by using the general procedure for the synthesis of **2**.[3]

Yield (220 mg, 34%); FT-IR (υ_{max}, cm^{-1}): 1795, 1756; ^{1}H-NMR ($CDCl_3$, 400 MHz): δ 8.57 (m, 1H), 8.37 (dd, *J* = 7.4, 1.2 Hz, 1H), 8.22 (m, 1H), 7.52 (m, 2H), 7.14 (d, *J* = 7.1 Hz, 1H), 2.80 (s, 6H), 1.87 – 1.81 (m, 1H), 1.20 (s, 9H), 1.19 – 1.16 (m, 2H), 1.06 – 1.01 (m, 2H); ^{13}C-NMR ($CDCl_3$, 100 MHz): δ 171.8, 152.0, 148.8, 133.6, 132.6, 132.3, 130.1, 129.9, 129.1,

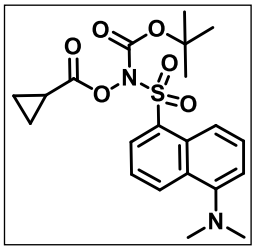

123.0, 119.1, 115.7, 86.4, 45.6, 27.9, 10.6, 10.0; HRMS (ESI-TOF) for $[C_{21}H_{26}N_2O_6S + Na]^+$: Calcd., 435.1590, Found, 435.1583.

General procedure for the synthesis of *N*-cyclopropanecarbonyloxy-sulfonamide (3): From *N*-sulfonyl-*N*-(cyclopropanecarbonyl)oxy-*tert*-butyl-carbamate (**2**), *N*-cyclopropanecarbonyloxy-sulfonamide (**1**) was synthesized by using reported protocol.[3]

The *N*-sulfonyl-*N*-(cyclopropanecarbonyl)oxy-*tert*-butyl-carbamate (**2**), 5 eq. of trifluoroacetic acid was added and the mixture was stirred for 2 – 3 h. Upon completion of the reaction (TLC analysis), the mixture was washed with hexane several times and the resultant solvent mixture was evaporated under reduced pressure to yield crude product, which was further purified using silica gel column chromatography to yield an *N*-(cyclopropanecarbonyl)oxy-sulfonamide (**3**).

***N*-((cyclopropanecarbonyl)oxy)benzenesulfonamide (3a):**

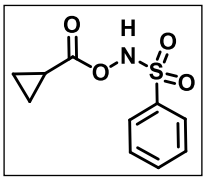

Yield (380 mg, 56%); FT-IR (υ_{max}, cm^{-1}): 1757; ^{1}H-NMR ($CDCl_3$, 400 MHz): δ 8.95 (s, 1H), 7.90 – 7.88 (m, 2H), 7.64 – 7.60 (m, 1H), 7.52 – 7.48 (m, 2H), 1.59 – 1.51 (m, 1H), 0.89 – 0.86 (m, 2H), 0.81 – 0.78 (m, 2H); ^{13}C-NMR ($CDCl_3$, 100 MHz): δ 172.4, 134.3, 133.4, 128.2, 127.9, 9.7, 8.7; HRMS (ESI-TOF) for $[C_{10}H_{11}NO_4S + H]^+$: Calcd., 242.0478, Found, 242.0466.

2-bromo-*N*-((cyclopropanecarbonyl)oxy)benzenesulfonamide (3b):

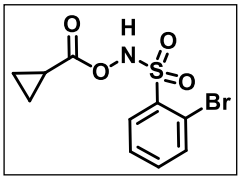

Yield (80 mg, 53%); FT-IR (υ_{max}, cm^{-1}): 1714; ^{1}H-NMR ($CDCl_3$, 400 MHz): δ 9.45 (s, 1H), 8.14 – 8.10 (m, 1H), 7.73 – 7.69 (m, 1H), 7.47 – 7.41 (m, 2H), 1.53 – 1.46 (m, 1H), 0.86 – 0.81 (m, 2H), 0.80 – 0.76 (m, 2H); ^{13}C-NMR ($CDCl_3$, 100 MHz): δ 171.9, 134.6, 134.1, 133.9, 132.5, 126.7, 120.3, 9.6, 8.7; HRMS (ESI-TOF) for $[C_{10}H_{10}BrNO_4S + Na]^+$: Calcd., 343.9400, Found, 343.9407.

4-bromo-*N*-((cyclopropanecarbonyl)oxy)benzenesulfonamide (3c):

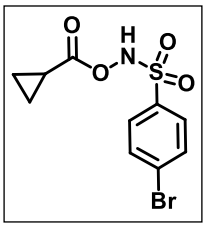

Yield (140 mg, 92%); FT-IR (υ_{max}, cm^{-1}): 1750; ^{1}H-NMR ($CDCl_3$, 400 MHz): δ 9.0 (s, 1H), 7.82 – 7.79 (m, 2H), 7.73 – 7.69 (m, 2H), 1.67 – 1.59 (m, 1H), 1.02 – 0.96 (m, 2H), 0.94 – 0.90 (m, 2H); ^{13}C-NMR ($CDCl_3$, 100 MHz): δ 173.5, 134.5, 132.7, 130.4, 130.0, 10.8, 10.0; HRMS (ESI-TOF) for $[C_{10}H_{10}BrNO_4S + H]^+$: Calcd., 319.9592, Found, 319.9637.

***N*-((cyclopropanecarbonyl)oxy)-2-(trifluoromethyl)benzenesulfonamide (3d):**

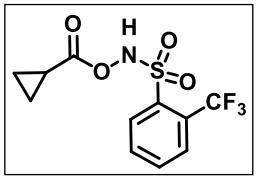

Yield (340 mg, 41%); FT-IR (υ_{max}, cm^{-1}): 1756; ^{1}H-NMR ($CDCl_3$, 400 MHz): δ 9.20 (s, 1H), 8.27 (d, *J* = 7.5 Hz, 1H), 7.93 (d, *J* = 7.5 Hz, 1H), 7.82 – 7.74 (m, 2H), 1.62 – 1.56 (m, 1H), 0.95 – 0.88 (m, 2H), 0.82 – 0.78 (m, 2H); ^{13}C-NMR ($CDCl_3$, 100 MHz): δ 173.4, 134.5, 134.1, 133.9, 132.1, 129.3, 129.0 (q, J_{C-F} = 6.3 Hz), 123.8, 10.6, 9.9; HRMS (ESI-TOF) for $[C_{11}H_{10}F_3NO_4S + Na]^+$: Calcd., 332.0197, Found, 323.0191.

2-bromo-*N*-((cyclopropanecarbonyl)oxy)-4-(trifluoromethyl)benzenesulfonamide (3e):

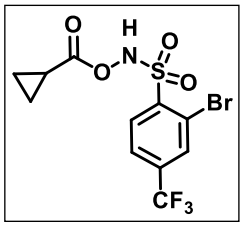

Yield (60 mg, 40%); FT-IR (υ_{max}, cm^{-1}): 1759; ^{1}H-NMR ($CDCl_3$, 400 MHz): δ 9.40 (s, 1H), 8.25 (d, *J* = 8.24 Hz, 1H), 7.97 (s, 1H), 7.71 (d, *J* = 7.68 Hz, 1H), 1.54 – 1.48 (m, 1H), 0.89 – 0.81 (m, 4H); ^{13}C-NMR ($CDCl_3$, 100 MHz): δ 172.0, 137.7, 135.9, 135.5, 132.9, 131.6 (q, J_{C-F} = 3.5 Hz), 122.6, 121.2, 119.8, 9.5, 8.9; HRMS (ESI-TOF) for $[C_{11}H_9BrF_3NO_4S + Na]^+$: Calcd., 409.9297, Found, 409.9260.

***N*-((cyclopropanecarbonyl)oxy)-2-nitrobenzenesulfonamide (3f):**

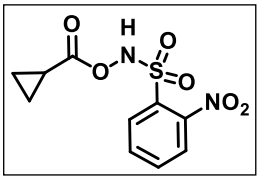

Yield (205 mg, 95%); FT-IR (υ_{max}, cm^{-1}): 1760; ^{1}H-NMR ($CDCl_3$, 400 MHz): δ 9.90 (s, 1H), 8.20 (dd, *J* = 7.6, 1.5 Hz, 1H), 7.98 (d, *J* = 7.6 Hz, 2H), 7.88 – 7.81 (m, 2H), 1.66 (br s, 1H), 0.99 – 0.93 (m, 2H), 0.90 – 0.86 (m, 2H); ^{13}C-NMR ($CDCl_3$, 100 MHz): δ 173.1, 148.4, 135.5, 133.0, 130.2, 126.3, 10.7, 10.0; HRMS (ESI-TOF) for $[C_{10}H_{10}N_2O_6S + H]^+$: Calcd., 287.0300, Found, 287.0327.

***N*-((cyclopropanecarbonyl)oxy)-4-nitrobenzenesulfonamide (3g):**

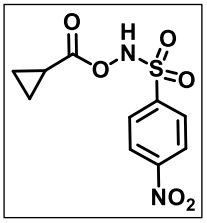

Yield (90 mg, 61%); FT-IR (υ_{max}, cm^{-1}): 1759; ^{1}H-NMR ($CDCl_3$, 400 MHz): δ 9.05 (s, 1H), 8.41 (d, *J* = 8.8 Hz, 2H), 8.16 (d, *J* = 8.8 Hz, 2H), 1.69 – 1.62 (m, 1H), 1.06 – 0.99 (m, 2H), 0.97 – 0.93 (m, 2H); ^{13}C-NMR ($CDCl_3$, 100 MHz): δ 172.4, 150.1, 140.4, 129.2, 123.3, 9.7, 9.1; HRMS (ESI-TOF) for $[C_{10}H_{10}N_2O_6S + H]^+$: Calcd., 287.0300, Found, 287.0335.

***N*-((cyclopropanecarbonyl)oxy)-5-(dimethylamino)naphthalene-1-sulfonamide (3h):** From compound **2h**, *N*-((cyclopropanecarbonyl)oxy)-5-(dimethylamino)naphthalene-1-sulfonamide **(3h)** was synthesized by using general procedure for the synthesis of **3**. Yield (70 mg, 91%); FT-IR (υ_{max}, cm^{-1}): 1756; ^{1}H-NMR ($CDCl_3$, 400 MHz): δ 9.11 (s, 1H), 8.58 (d, *J* = 8.3 Hz, 1H), 8.35 (d, *J* = 8.6 Hz, 1H), 8.28 (d, *J* = 7 Hz, 1H), 7.56 – 7.46 (m, 2H), 7.14

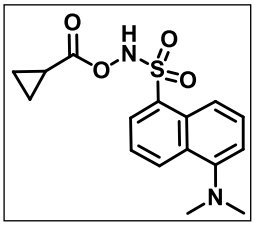

(d, *J* = 7.4 Hz, 1H), 2.82 (s, 6H), 1.43 (s, 1H), 0.76 – 0.68 (m, 4H); ^{13}C-NMR ($CDCl_3$, 100 MHz): δ 172.4, 150.9, 131.4, 131.2, 129.6, 129.4, 128.8, 128.0, 122.0, 117.9, 114.6, 44.4, 9.6, 8.5; HRMS (ESI-TOF) for $[C_{16}H_{18}N_2O_4S + H]^+$: Calcd., 335.1066, Found, 335.1057.

Synthesis of 5-(dimethylamino)naphthalene-1-sulfinic acid (7): From dansyl chloride, 5-(dimethylamino)naphthalene-1-sulfinic acid (**7**) was synthesized by using the reported protocol.[1] To a solution of dansyl chloride (50 mg, 0.185 mmol) in THF (5 mL) was added $NaBH_4$ (35 mg, 0.926 mmol) in portions at 0 ˚C. Upon completion of the reaction (TLC analysis), the solvent was evaporated under reduced pressure to afford the crude product which was further purified by prep-HPLC (H_2O:MeOH) to give 5-(dimethylamino)naphthalene-1-sulfinic acid **7** as a white solid. Yield (20 mg, 47%). FT-IR (υ_{max}, cm^{-1}): 3372; ^{1}H-NMR (Methanol-d4, 400 MHz): δ 8.37 (d, *J* = 8.4 Hz, 1H), 8.28 (d, *J* = 7.6 Hz, 1H), 8.01 (dd, *J* = 7.2, 1.2 Hz, 1H), 7.55 (dd, *J* = 8.4, 7.1 Hz, 1H), 7.45 (dd, *J* = 8.5, 7.7 Hz, 1H), 7.16 (d, *J* = 7.1 Hz, 1H), 2.86 (s, 6H); ^{13}C-NMR (Methanol-d4, 100 MHz): δ 152.4, 132.8, 130.5, 127.1, 126.9, 125.4, 121.2, 119.8, 115.2, 47.5; HRMS (ESI-TOF) for $[C_{12}H_{13}NO_2S + H]^+$: Calcd., 236.0745, Found, 236.0739.

Synthesis of 2-bromo-*N*-hydroxybenzenesulfonamide (4): From 2-bromobenzenesulfonyl chloride, 2-bromo-*N*-hydroxybenzenesulfonamide (**4**) was synthesized by using the reported protocol.[1]

To a mixture of hydroxylamine hydrochloride (164 mg, 1.17 mmol) and DMAP (245 mg, 2.34 mmol) in pyridine (20 mL) was added 2-bromobenzenesulfonyl chloride (300 mg, 1.17 mmol) on an ice-bath. Then, the mixture was stirred for 5 min at room temperature. The resulting suspension was poured into EtOAc (100 mL) and 1 N HCl aq. (100 mL). The EtOAc layer was separated, washed with brine (100 mL), dried over Na_2SO_4, filtered and the filtrate was concentrated. The crude product was purified by prep-HPLC (ACN:H_2O) to give 2-bromo-*N*-hydroxybenzenesulfonamide **4** as a light yellow solid. Yield (100 mg, 34%). The analytical data are consistent with previously reported values.

Synthesis of 5 (PCM)**:** From 2-(diphenylphosphino) benzoic acid, **5** was synthesized by using the reported protocol.[4]

2-(diphenylphosphino) benzoic acid (306 mg, 0.33 mmol) was dissolved in 15 mL of anhydrous CH_2Cl_2 under an N_2 atmosphere. 4-(dimethylamino) pyridine (3 mg, 0.01 mmol)

and 1-ethyl-3- (3-dimethylaminopropyl) carbodiimide hydrochloride (64 mg, 0.36 mmol) were added at 0 °C and the reaction mixture was stirred for 30 min. 7-hydroxycoumarin (65 mg, 0.33 mmol) was added and the resulting mixture was warmed to room temperature and stirred overnight. Upon completion of the reaction (TLC analysis), the solvent was evaporated under reduced pressure to yield the crude product, which was purified by prep-HPLC (ACN:H_2O) to afford compound **5** as a faint yellow solid. Yield (55 mg, 37%). The analytical data are consistent with previously reported values.

Synthesis of 6 (HNO-TCF probe)**:** From 2-(diphenylphosphino) benzoic acid, **6** was synthesized by using the reported protocol.[5]

A mixture of 2-(diphenylphosphino) benzoic acid (149 mg, 0.489 mmol), 4-dimethylaminopyridine (DMAP, 41 mg, 0.326 mmol) and dicyclohexylcarbodiimide (DCC, 137 mg, 0.652 mmol) in anhydrous CH_2Cl_2 (10 mL) was stirred at 0 °C for 30 min in a nitrogen atmosphere. To the mixture added 1-(3-cyano-2-dicyanomethylen-5,5-dimethyl-2,5-dihydrofuran-4-yl)-2-(4-hydroxylphenyl) ethane (100 mg, 0.326 mmol) and reaction mixture was allowed to stir at RT for 5 h. Upon completion of the reaction (TLC analysis) the solvent was evaporated under reduced pressure to yield crude product, which was purified by prep-HPLC (ACN:H_2O) to afford compound **6** as an orange solid. Yield (50 mg, 26%). The analytical data are consistent with previously reported values.

2.4.2. HNO detection by using 5

Stock solutions of **5** (1 mM), **2a-2h** (5 mM)**,** and **3a-3h** (5 mM) in DMSO and esterase (1 U/mL) in phosphate buffer saline (10 mM, pH 7.4) were prepared. The reaction mixture was prepared by adding 10 μM of **5** (2 μL, 1 mM), 50 μM of **2a-2h** and **3a-3h** (2 μL, 5 mM) along with 0.5 U/mL esterase (100 μL, 1 U/mL stock) and the volume was adjusted to 200 μL using phosphate buffer saline (10 mM, pH 7.4) in a 96-well plate and then incubated for 30 min at 37 ˚C. The fluorescence (excitation at 370 nm; emission at 460 nm) was measured using an Ensight Multimode Plate Reader (PerkinElmer) (Figure 2.2, Figure 2.3 and Figure 2.10).

Stock solutions of PMSF (100 mM) in isopropanol, and esterase (1 U/mL) in phosphate buffer saline (PBS), pH 7.4 were prepared. The reaction mixture was prepared by adding 1 mM of PMSF (7.5 μL, 100 mM) along with 0.5 U/mL esterase (100 μL, 1 U/mL stock) and the volume was adjusted to 750 μL using phosphate buffer saline (10 mM, pH 7.4) in a 96-well plate. Measurements were carried out after incubation for 30 min at 37 ˚C.

Stock solutions of **5** (1 mM), **2h** and **3h** (5 mM) in DMSO and esterase (1 U/mL, pre-treated with PMSF) in phosphate buffer saline (10 mM, pH 7.4) were prepared independently. Measurements were carried out by using the above-described protocol. (Figure 2.2, Figure 2.3 and Figure 2.10).

2.4.3. Photophysical properties of 7

2.4.3.1. Measurement of absorbance

A stock solution of **7** (10 mM) in DMSO was prepared. The solution was prepared by adding 100 μM of **7** (10 μL, 10 mM) with 990 μL phosphate buffer saline (10 mM, pH 7.4) into a cuvette. UV-vis spectra were recorded by using SHIMADZU, UV-2600 UV-Vis spectrophotometer at room temperature. (Figure 2.5).

2.4.3.2. Measurement of fluorescence

A stock solution of **7** (10 mM) in DMSO was prepared. The solution was prepared by adding 100 μM of **7** (10 μL, 10 mM) with 990 μL phosphate buffer saline (10 mM, pH 7.4) into a cuvette. Fluorescence spectra were recorded by using HORIBA Scientific Fluoromax-4 spectrofluorometer at room temperature. (Figure 2.6).

The fluorescence measurement of 7 at different pH: A stock solution of **7** (10 mM) in DMSO was prepared. The solution was prepared by adding 50 μM of **7** (5 μL, 10 mM) with 995 μL phosphate buffer saline (10 mM, pH 8.0, 7.4, 6.0 and 5.0) independently into a cuvette. Fluorescence spectra were recorded by using HORIBA Scientific Fluoromax-4 spectrofluorometer at room temperature. (Figure 2.7).

The stability of fluorescence intensity of 7: A stock solution of **7** (5 mM) in DMSO was prepared. The solution was prepared by adding 50 μM of **7** (2 μL, 5 mM) with 198 μL phosphate buffer saline (10 mM, pH 7.4) in a 96-well plate and then incubated for 12 h at 37 ˚C. The stability of fluorescence intensity (excitation at 308 nm; emission at 497 nm) was measured using an Ensight Multimode Plate Reader (PerkinElmer) (Figure 2.8).

2.4.3.3. Time-resolved photoluminescence (PL) measurements

Time-resolved PL studies were performed using Horiba Jobin Yvon Flurolog-3 spectrofluorometer (HORIBA Scientific) and Time-Correlated Single Photon Counting (TCSPC) system using a 292 nm nanoLED as the excitation source with a time-to-amplitude converter (TAC) range of 200 ns for 10,000 counts.

A stock solution of **7** (10 mM) in DMSO was prepared. The reaction was prepared by adding 10 μM (1 μL, 10 mM) and the volume was adjusted to 1 mL using phosphate buffer saline (10 mM, pH 7.4) in the cuvette. The lifetime of the excited state of **7** was measured using the above-mentioned protocol. (Figure 2.9).

2.4.4. Detection of 7

Stock solutions of **7** (5 mM), **2h** and **3h** (1 mM, 2.5 mM and 5 mM) in DMSO and esterase (1 U/mL) in phosphate buffer saline (10 mM, pH 7.4) were prepared. The reaction mixture was prepared by adding 10 μM, 25 μM and 50 μM of **2h** or **3h** (2 μL, 1 mM, 2.5 mM and 5 mM) independently along with 0.5 U/mL esterase (100 μL, 1 U/mL stock) and the volume was adjusted to 200 μL using phosphate buffer saline (10 mM, pH 7.4) in a 96-well plate and then incubated for 120 min at 37 ˚C. The fluorescence corresponding to **7** was measured (excitation at 308 nm; emission at 497 nm) using an Ensight Multimode Plate Reader (PerkinElmer) (Figure 2.11 and Figure 2.12).

Stock solutions of **7** (5 mM), **2h** and **3h** (5 mM) in DMSO and esterase (1 U/mL, pre-treated with PMSF) in phosphate buffer saline (10 mM, pH 7.4) were prepared. Measurements were carried out by using the above-described protocol (Figure 2.11).

2.4.5. Griess assay for nitrite detection

Stock solutions of $NaNO_2$ (1 mM), **2a-2h** (5 mM), **3a-3h** (5 mM) in DMSO and esterase (1 U/mL) in phosphate buffer saline (10 mM, pH 7.4) were prepared. The reaction mixture was prepared by adding 50 μM of **2a-2h** and **3a-3h** (2 μL, 5 mM) independently along with 0.5 U/mL esterase (100 μL, 1 U/mL stock) and the volume was adjusted to 200 μL using phosphate buffer saline (10 mM, pH 7.4) in a 96-well plate and then incubated for 30 min at 37 ˚C. After 30 min incubation, Griess reagent (14 μL) was added to each well and further incubated for 30 min at 37 ˚C in an incubator. The absorbance (at 540 nm) was measured using an Ensight Multimode Plate Reader (PerkinElmer). (Figure 2.14 and Figure 2.15).

2.4.6. Decomposition of 2h and 3h using LC/MS

Stock solutions of **2h** (1 mM), **3h** (1 mM) and **7** (1 mM) were prepared in DMSO. A stock solution of esterase (2 U/mL) was prepared in PBS pH 7.4. The reaction mixture was prepared by adding 10 μM **2h** or **3h** or **7** (2 μL, 1 mM) independently along with 0.1 U/mL esterase (50 μL, 2 U/mL stock) and the volume was adjusted to 1 mL using phosphate buffer saline

(10 mM, pH 7.4) in an eppendorf then incubated for 5 h at 37 ˚C on thermomixer (300 rpm). 100 µL aliquots of the reaction mixture were taken at pre-determined time points and the reaction was quenched by adding 100 µL of methanol. The samples were centrifuged at 10000g for 4 min at 4 ˚C, the supernatant was collected and assessed thereafter by LC/MS. All measurements were done using the following protocol: 0.1% formic acid in methanol (A) and 0.1% formic acid in water (B) was used as the mobile phase. A multistep gradient was used with the flow rate of 0.3 mL/min starting with 75:25 → 0 min, 75:25 to 60:40 → 0 - 3 min, 60:40 to 40:60 → 3 - 7 min, 40:60 to 30:70 → 7 - 9 min, 30:70 to 0:100 → 9 - 12 min, 0:100 to 0:100 → 12 - 14 min, 0:100 to 75:25 → 14 - 18 min, 75:25 to 75:25 → 18 - 20 min. Measurements were carried out in the positive ion mode using high-resolution multiple reaction monitoring (MRM-HR) analysis on a Sciex X500R quadrupole time-of-flight (QTOF) mass spectrometer fitted with an Exion UHPLC system using a Kinetex 2.6 mm hydrophilic interaction liquid chromatography (HILIC) column with 100 Å particle size, 150 mm length and 3 mm internal diameter (Phenomenex). Nitrogen was the nebulizer gas, with the nebulizer pressure set at 50 psi, declustering potential =80 V, entrance potential = 10 V, collision energy = 20 V, and collision exit potential = 5 V. The MRM-HR mass spectrometry parameters for measuring compounds are m/z precursor ion mass ($M + H^+$) 435.1582 (**2h**), 367.1332 (**Intermediate I**), 335.1060 (**3h**), 236.0744 (**7**), 267.0802 (**8**) (Figure 2.16 - Figure 2.23).

2.4.7. Polysulfide measurement using LC/MS

Stock solutions of **2h** (5 mM), **3h** (5 mM), **4** (5 mM) and HPE-IAM (100 mM) were prepared in DMSO. A stock solution of Na_2S (20 mM) was prepared in DI water. A stock solution of esterase (2 U/mL) was prepared in PBS pH 7.4. The reaction mixture was prepared by adding 50 µM of **2h** or **3h** or **4** (10 µL, 5 mM) independently with 200 µM Na_2S (10 µL, 20 mM) along with (1 U/mL esterase (20 µL, 50 U/mL stock) and the volume was adjusted to 1 mL using phosphate buffer saline (10 mM, pH 7.4) in an eppendorf then incubated for 15 min at 37 ˚C on thermomixer (400 rpm). 100 µL aliquots of the reaction mixture were taken and then incubated with HPE-IAM (2 µL, 100 mM) for a further 15 min. The reaction was quenched by adding 100 µL of acetonitrile. The samples were centrifuged at 10000g for 10 min at 4 ˚C, the supernatant was collected and assessed thereafter by LC/MS. All measurements were done using the following protocol: Acetonitrile (A) and 0.1% formic acid in water (B) were used as the mobile phase. A gradient was used with the flow rate of 0.3 mL/min starting with 100:0

→ 0 min, 100:0 to 0:100 → 0 - 30 min. The IDA-HR mass spectrometry parameters for measuring compounds are: m/z precursor ion mass ($M + H^+$) 435.1582 (**2h**), 335.1060 (**3h**), 305.9985 (HPE-IAM), 215.0740 (HS-HPE-AM), 389.1530 (Bis-S-HPE-AM), 421.1250 (Bis-SS-HPE-AM), 453.0971 (Bis-SSS-HPE-AM) (Figure 2.24 - Figure 2.29).

2.4.8. Detection of 7 releases in A549 cell lysate

Lung carcinoma cells (A549) were cultured in 10 cm plates in complete DMEM medium supplemented with 5% FBS (fetal bovine serum) and 1% antibiotic solution in an atmosphere of 5% CO_2 at 37 ˚C. When the cells were 70% confluent, old media was removed and the cells were washed with serum-free DMEM media. The cells were trypsinized and subsequently resuspended in DMEM. The cells were harvested by centrifugation at 1000 rpm/min at 4 ˚C. Pellets were washed twice with PBS (1x), resuspended in PBS (1x, 2 mL) and transferred to a microcentrifuge tube. Cells were lysed by sonication using (a 130 W ultrasonic processor, VX 130W) stepped microtip for 2 min (with 3 sec. ON and 3 sec. OFF pulse, 60% amplitude) under ice-cold conditions. The total protein concentration of the whole cell lysate was determined by Bradford assay and further adjusted to 1 mg/mL with PBS (1x). Stock solutions of **7** (2.5 mM), **2h, 3h** (0.5 mM, 1.25 mM, 2.5 mM) independently in DMSO and 1 mg/mL stock solution of cell lysate in phosphate buffer saline (10 mM, pH 7.4) were prepared. The reaction mixture was prepared by adding 10 μM, 25 μM and 50 μM of **2h** or **3h** (2 μL, 0.5 mM, 1.25 mM and 2.5 mM) independently along with cell lysate (98 μL, 1 mg/mL) in a 96-well plate and incubated at 37 ˚C. The fluorescence corresponding to the release of **7** (excitation at 308 nm; emission at 497 nm) was measured for 3 h using an Ensight Multimode Plate Reader (PerkinElmer).

Stock solutions of PMSF (100 mM) in isopropanol and cell lysate (1 mg/mL) in phosphate buffer saline (10 mM, pH 7.4) were prepared. The reaction mixture was prepared by adding 5 mM PMSF (50 μL, 100 mM) along with cell lysate (1 mL, 1 mg/mL) in a 96-well plate and incubated at 37 ˚C on a thermomixer (300 rpm).

Stock solutions of **7** (2.5 mM), **2h, 3h** (2.5 mM) independently in DMSO and 1 mg/mL stock solution of cell lysate (Pre-treated with PMSF) in phosphate buffer saline (10 mM, pH 7.4) were prepared and release of **7** was measured by above-described protocol (Figure 2.30).

2.4.9. Cell viability Assay

Mouse embryonic fibroblasts (MEF) cells, Lung carcinoma cells (A549) and MCF-7 cells were seeded at a concentration of 1×10^4 cells/well overnight in a 96-well plate in complete

DMEM medium supplemented with 5% FBS (fetal bovine serum) and 1% antibiotic solution in an atmosphere of 5% CO_2 at 37 ˚C. Cells were exposed to varying concentrations of the test compounds prepared as a DMSO stock solution so that the final concentration of DMSO was 0.5%. The cells were incubated for 24 h at 37 ˚C. A 0.5 mg/mL stock solution of 3-(4, 5-dimethylthiazol-2-yl)-2, 5-diphenyl tetrazolium bromide (MTT) was prepared in DMEM and 100 μL of the resulting solution was added to each well. After 4 h incubation, the media was removed carefully and 100 μL of DMSO was added. Spectrophotometric analysis of each well using a microplate reader (Thermo Scientific Varioscan) at 570 nm was carried out to estimate cell viability (Figure 2.31-Figure 2.33).

2.4.10. Detection of HNO and 7 in MCF-7 cells

MCF-7 cells were seeded at 1×10^5 cells/well in a 6-well Corning plate for overnight in DMEM medium supplemented with 10% FBS (fetal bovine serum) and 1% antibiotic solution in an atmosphere of 5% CO_2 at 37 ˚C. After incubation, the media was removed and the cells were washed with 1 mL of PBS. Then 1 mL of fresh DMEM media was added along with 20 μM of HNO-TCF probe for 30 min at 37 ˚C. After 30 min, 1 mL of fresh DMEM media was added along with test compounds (200 μM). The cells were incubated for 2 h at 37 ˚C. After 2 h, old media was removed, cells were washed with 1 mL of PBS and then imaged on Carl Zeiss LSM710 laser scanning confocal microscope with anisotropy with 63x oil filter. The cells were imaged in two different channels. (RED channel-Alexa fluor 568 for HNO detection and DAPI channel for **7** detections) (Figure 2.34-Figure 2.35).

2.5. NMR spectra

^{1}H NMR spectra of **1**

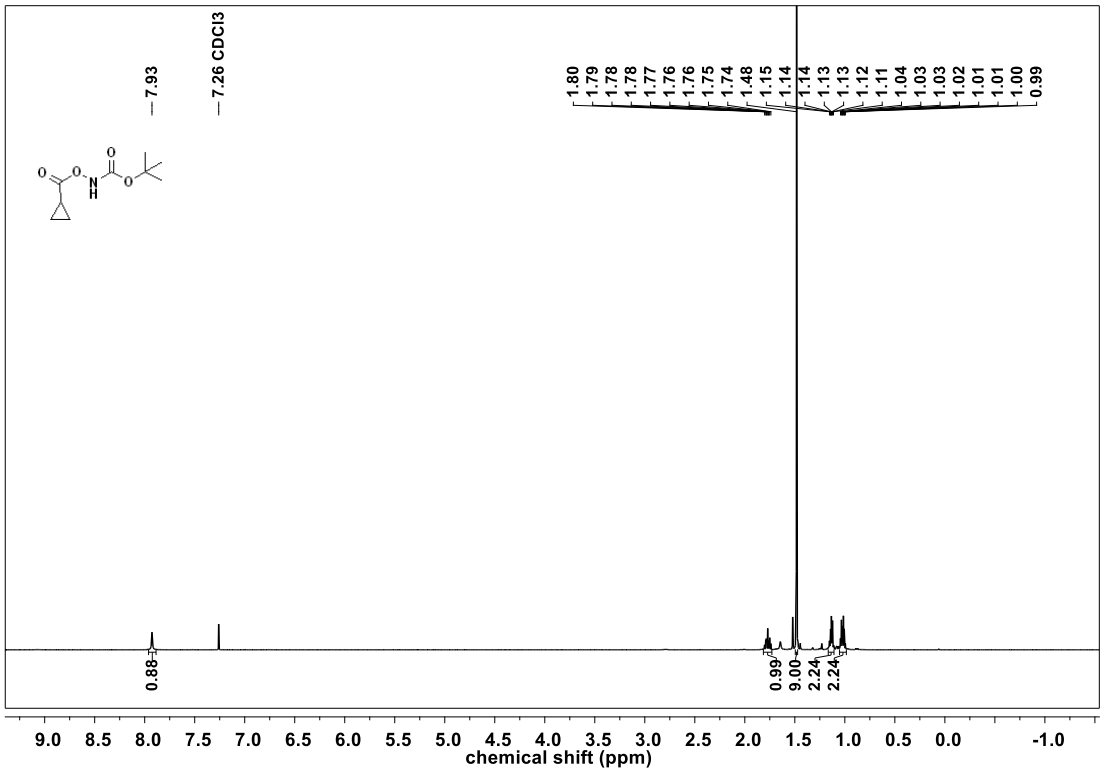

^{13}C NMR spectra of **1**

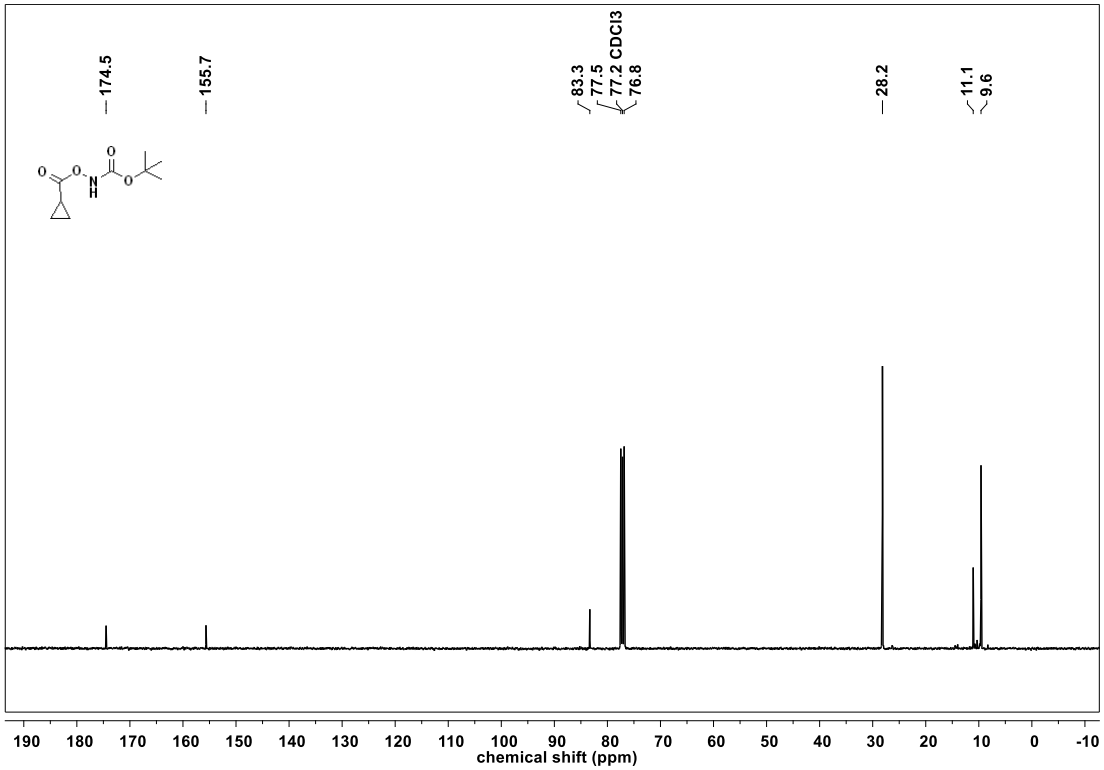

^{1}H NMR spectra of **2a**

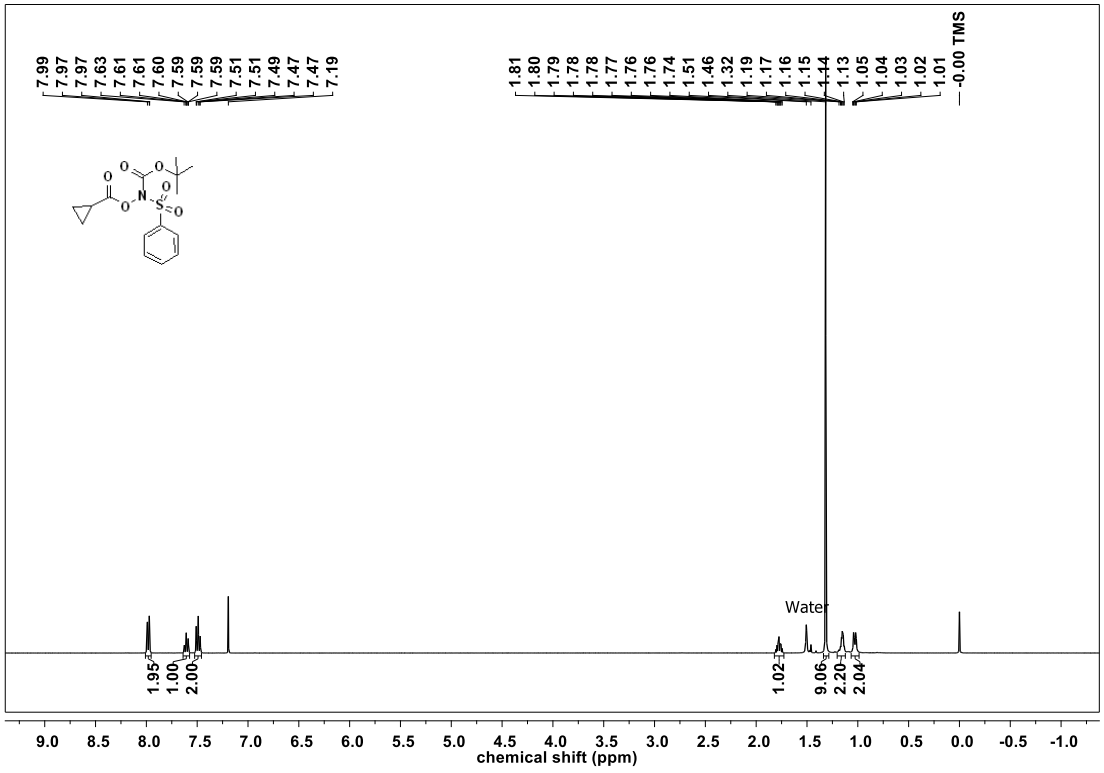

^{13}C NMR spectra of **2a**

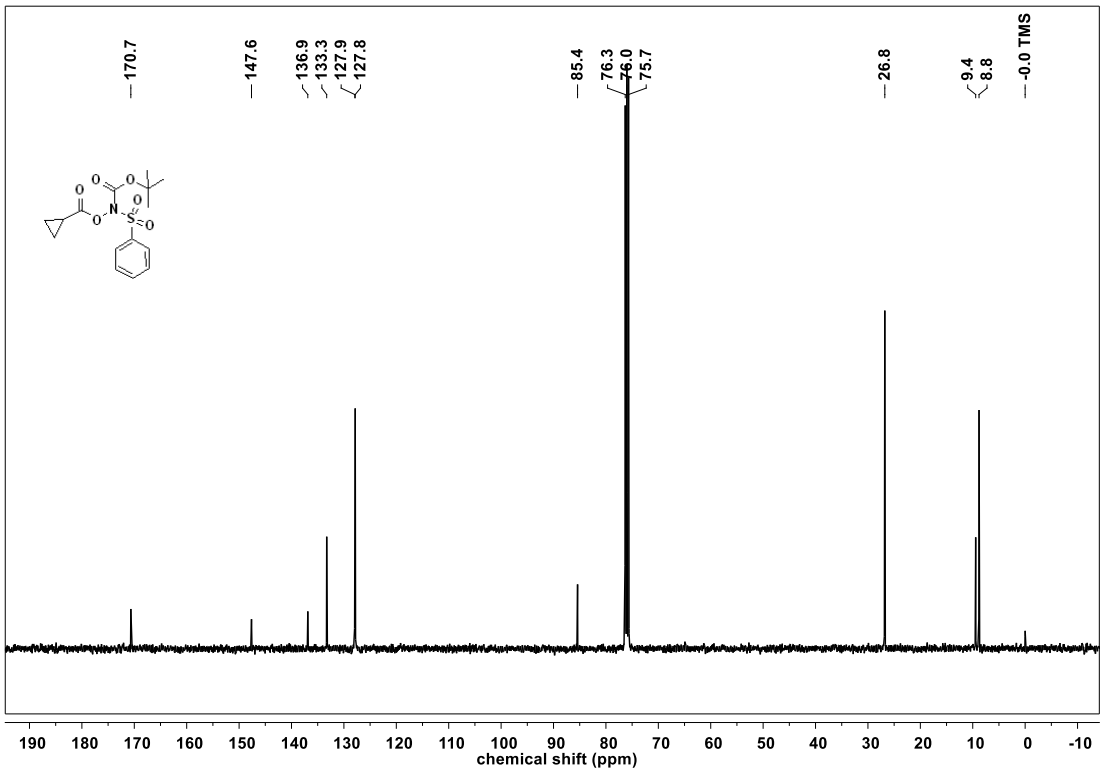

^{1}H NMR spectra of **2b**

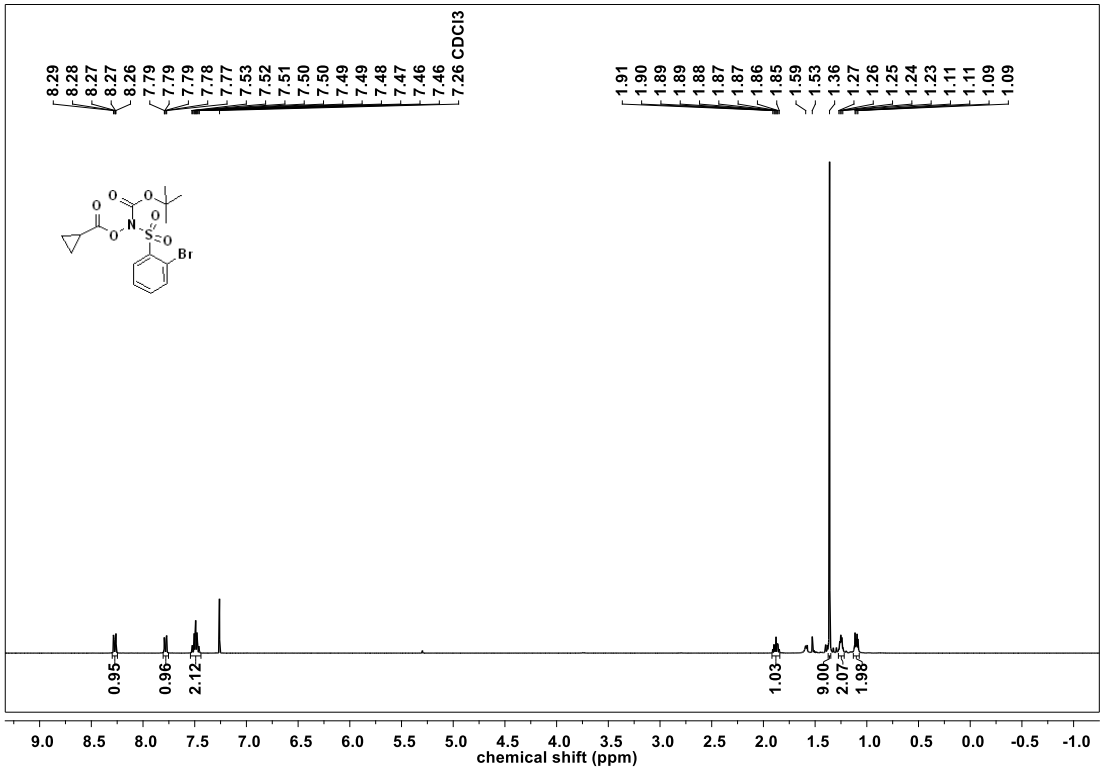

^{13}C NMR spectra of **2b**

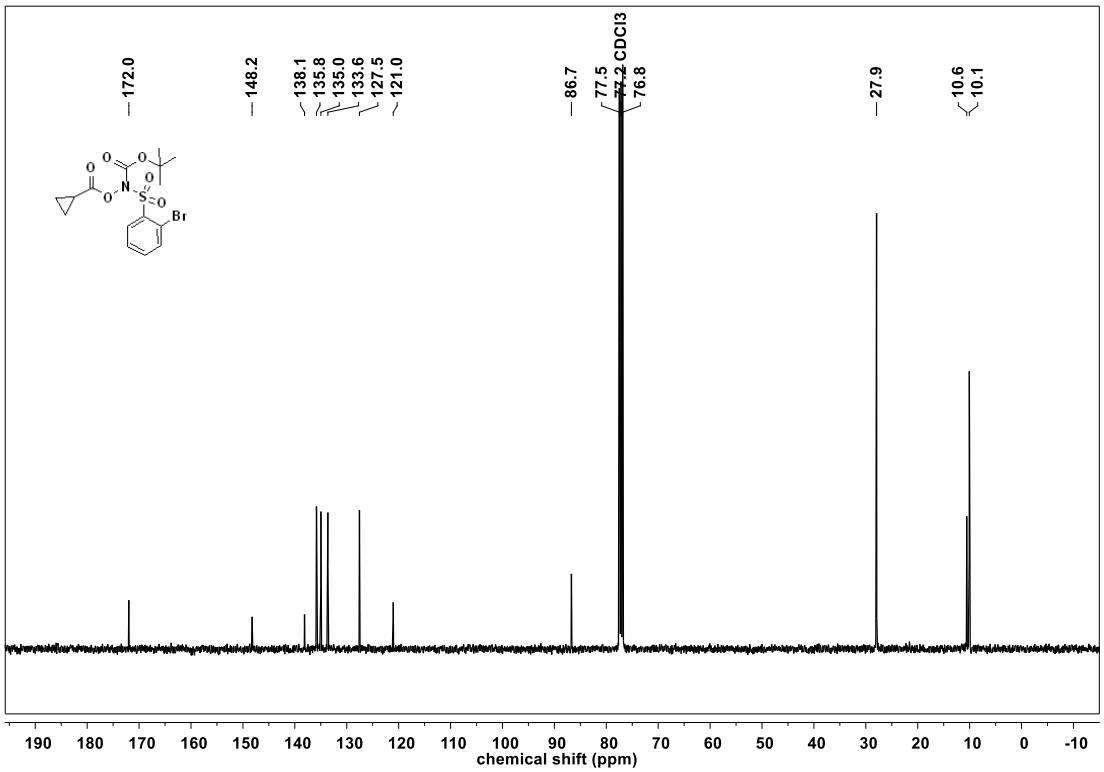

^{1}H NMR spectra of **2c**

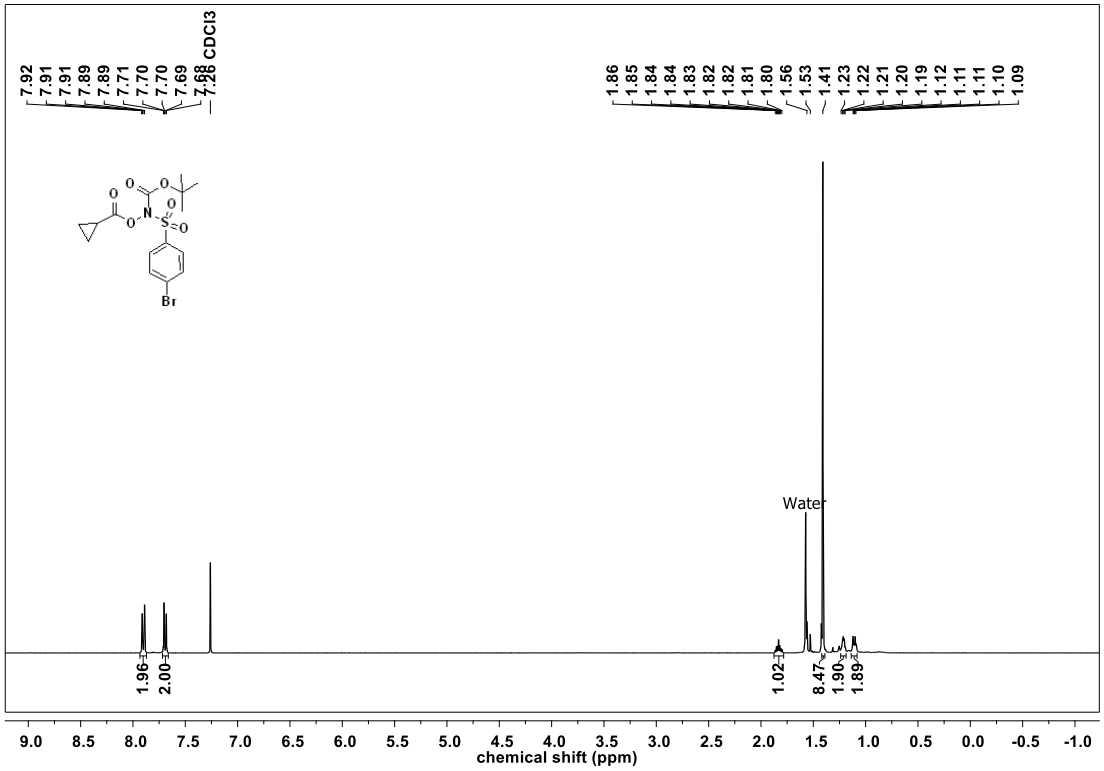

^{13}C NMR spectra of **2c**

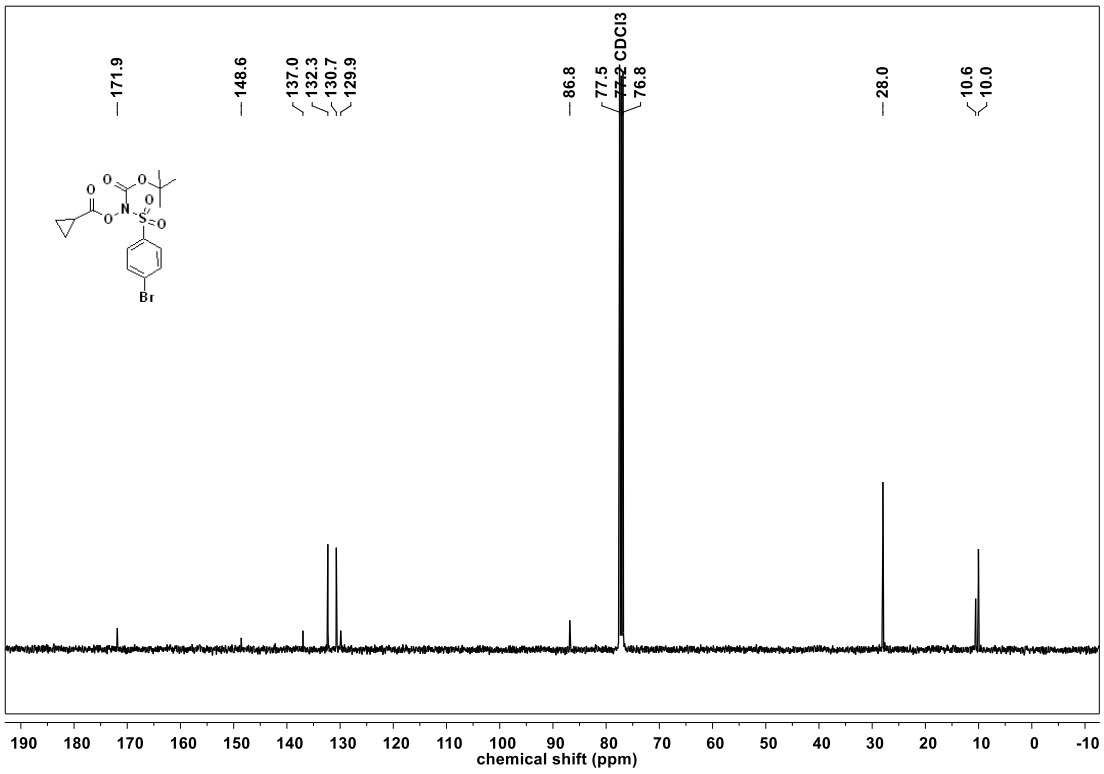

^{1}H NMR spectra of **2d**

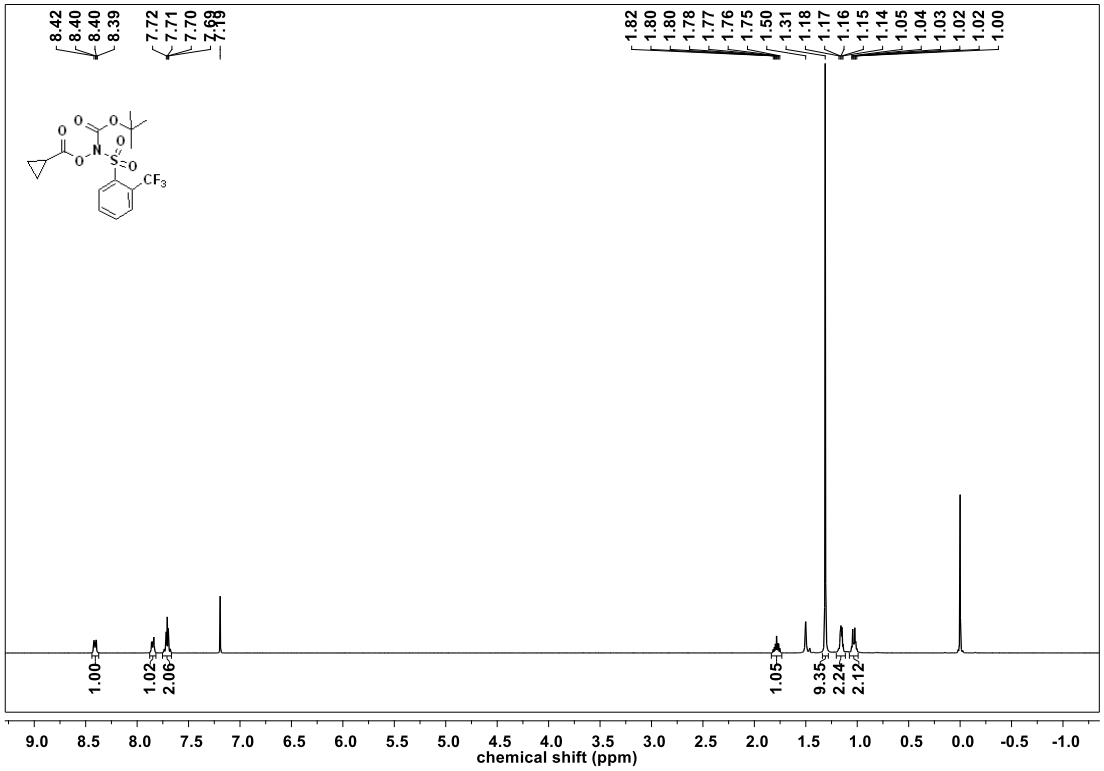

^{13}C NMR spectra of **2d**

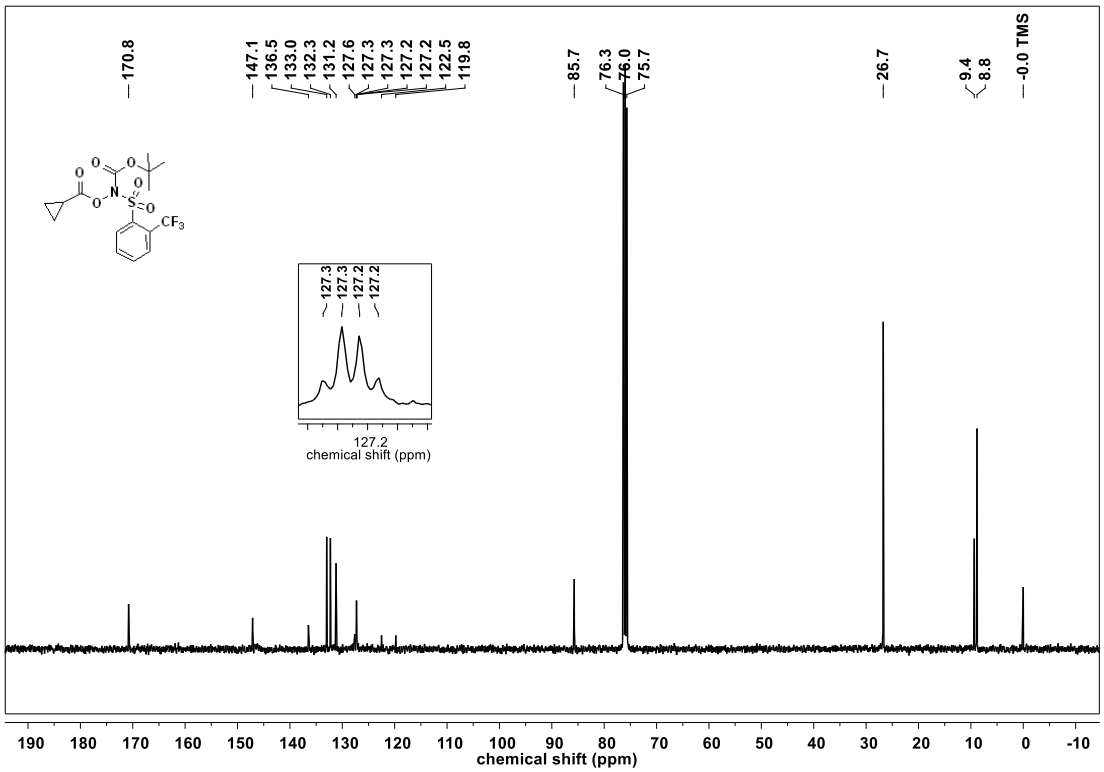

^{1}H NMR spectra of **2e**

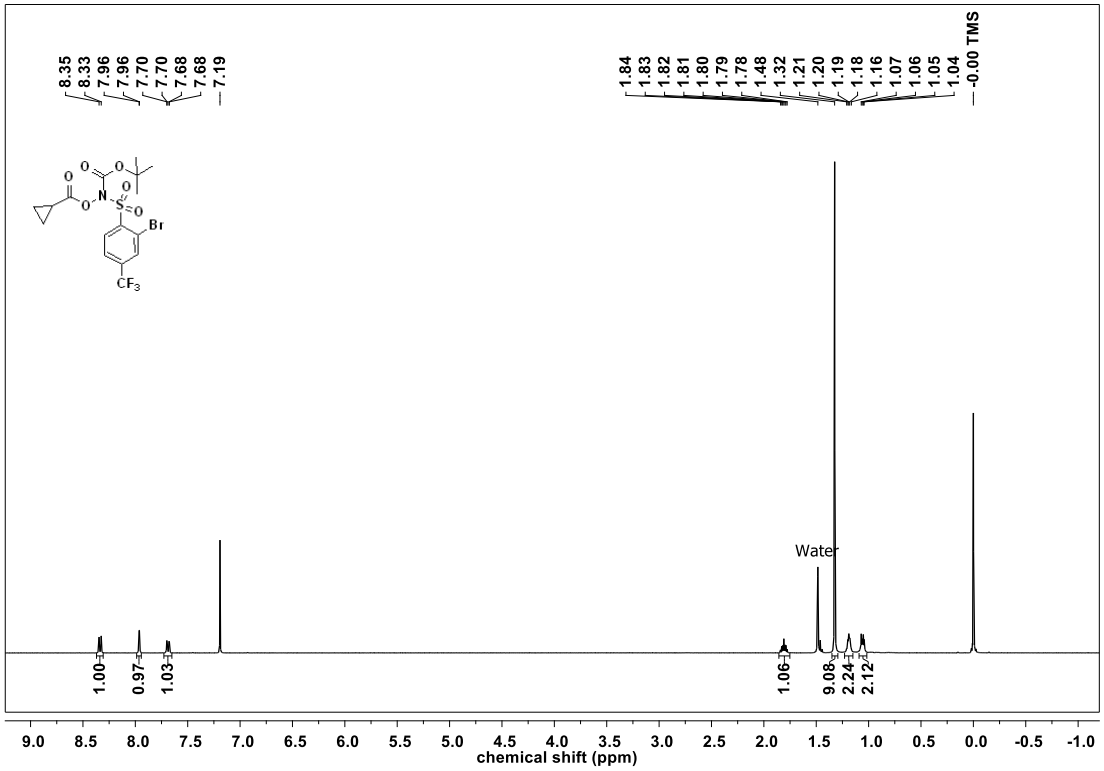

^{13}C NMR spectra of **2e**

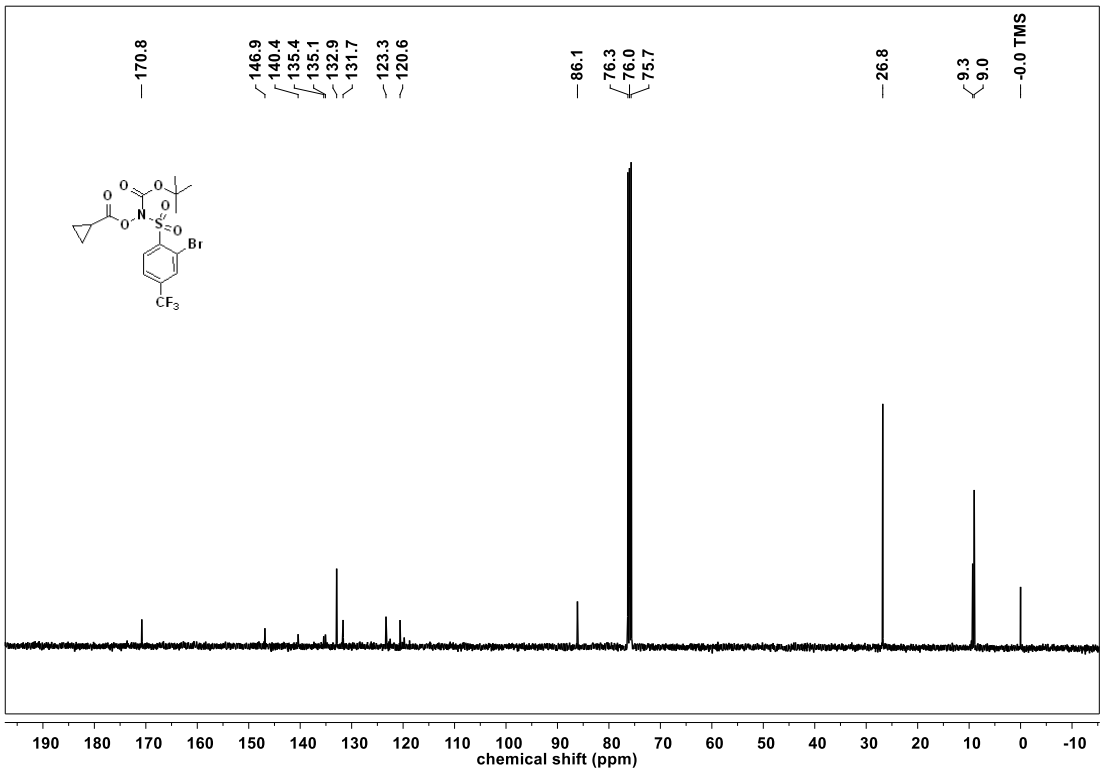

^{1}H NMR spectra of **2f**

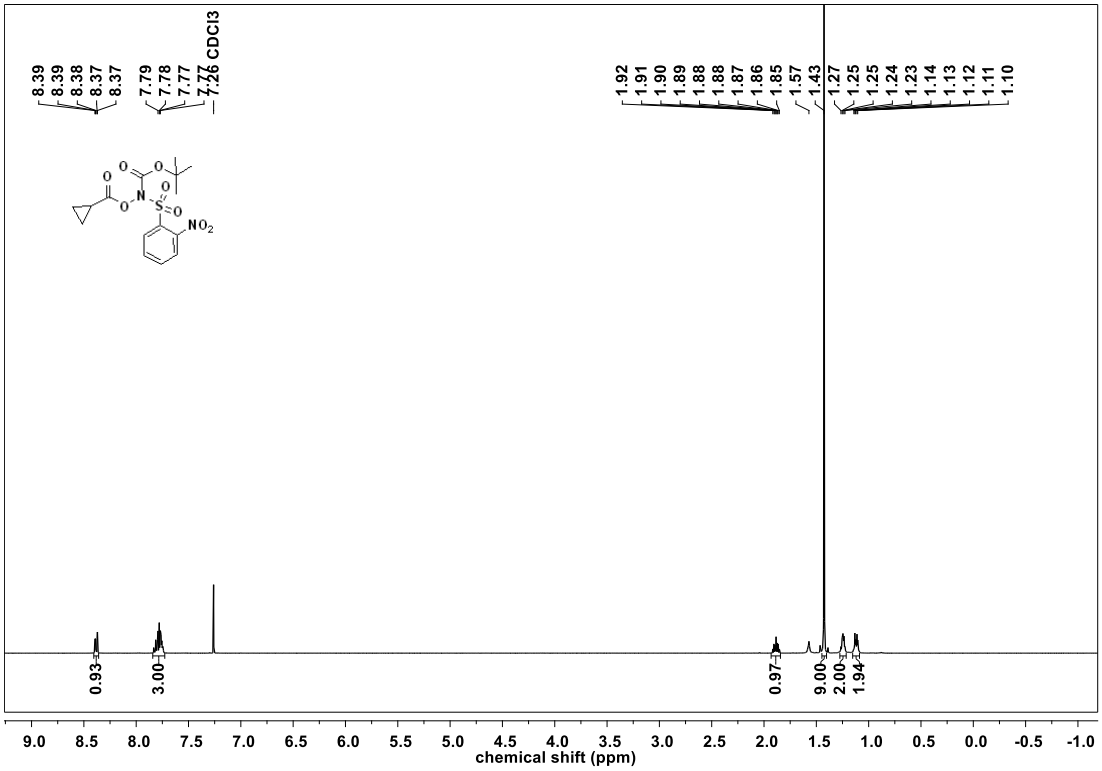

^{13}C NMR spectra of **2f**

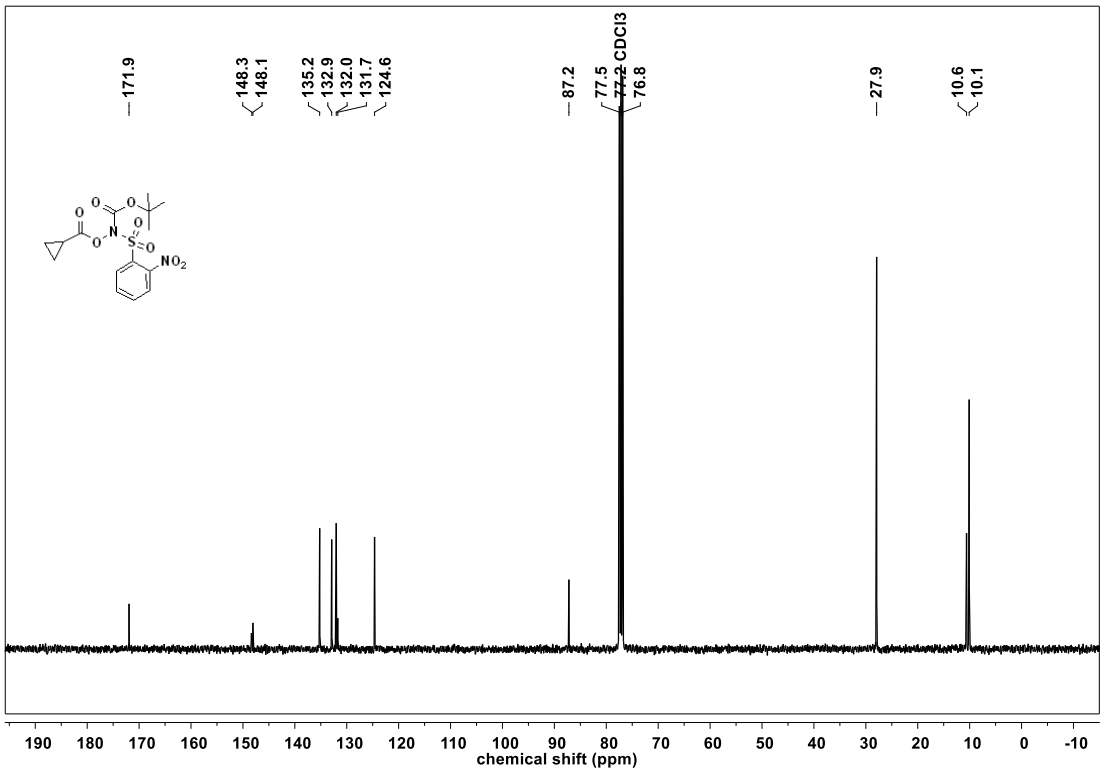

^{1}H NMR spectra of **2g**

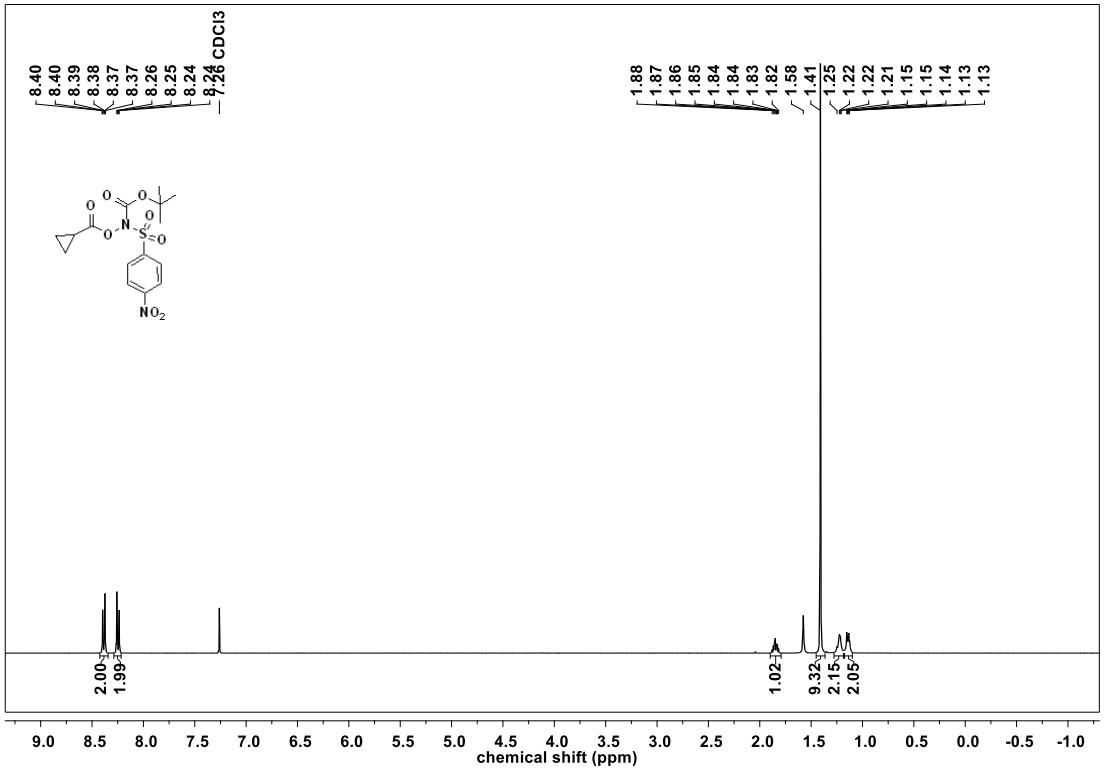

^{13}C NMR spectra of **2g**

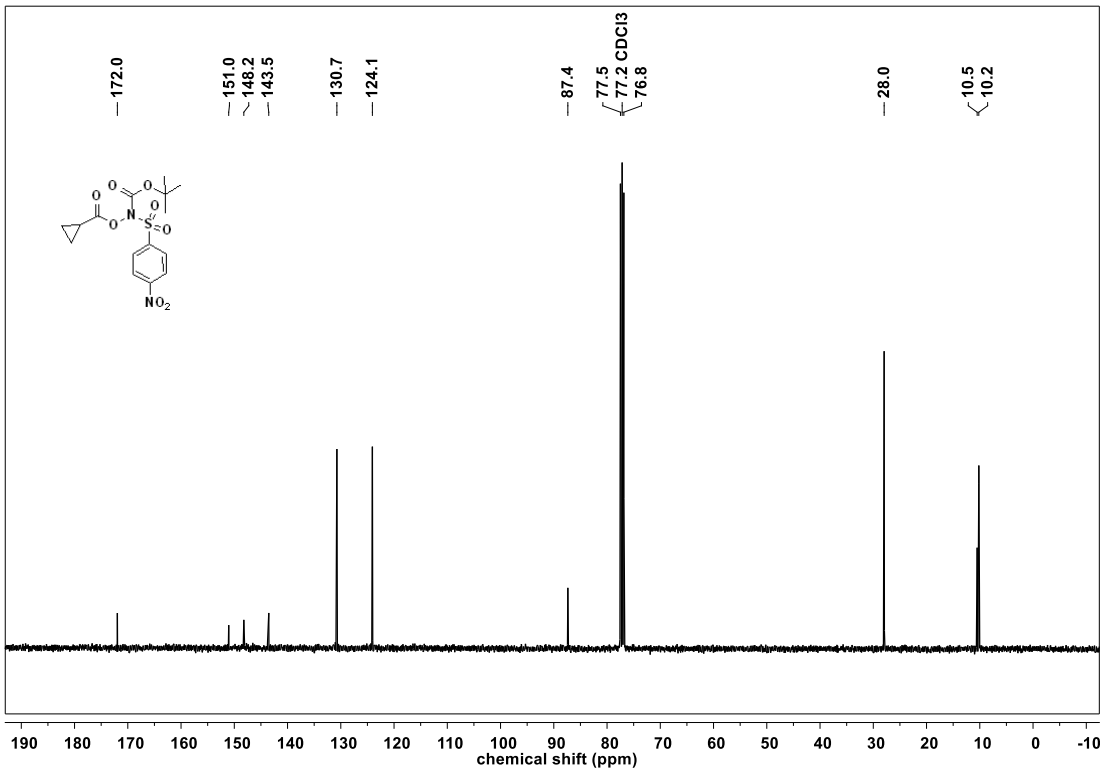

^{1}H NMR spectra of **2h**

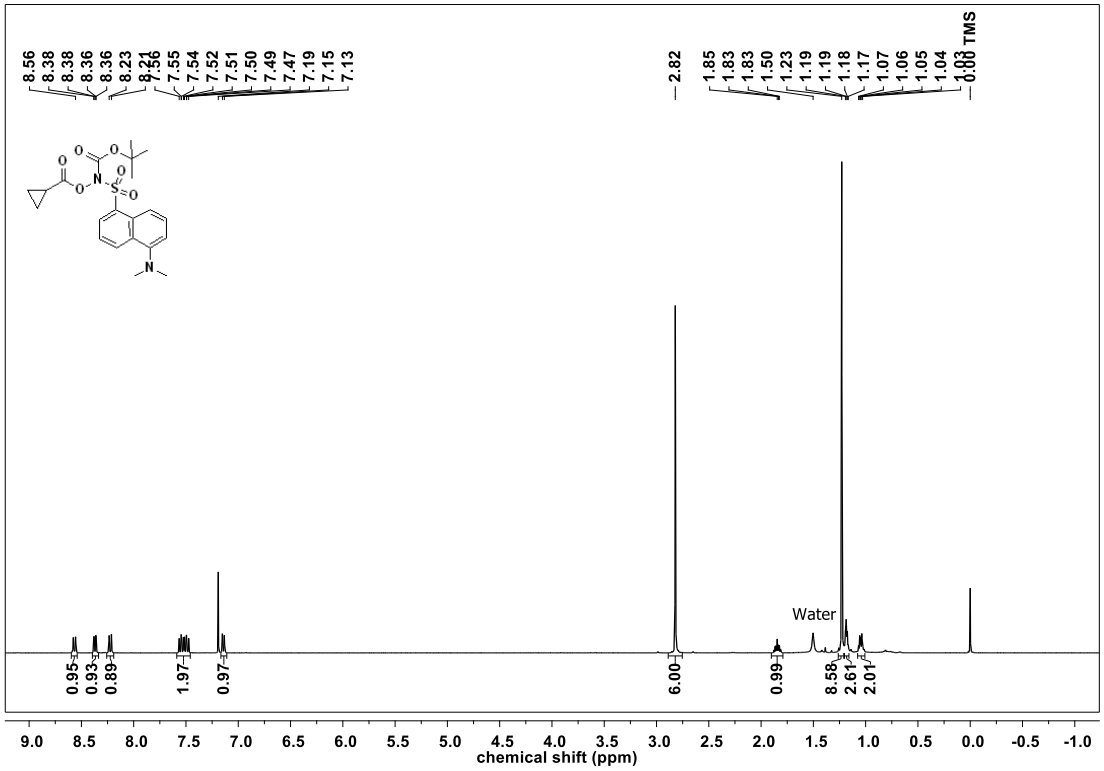

^{13}C NMR spectra of **2h**

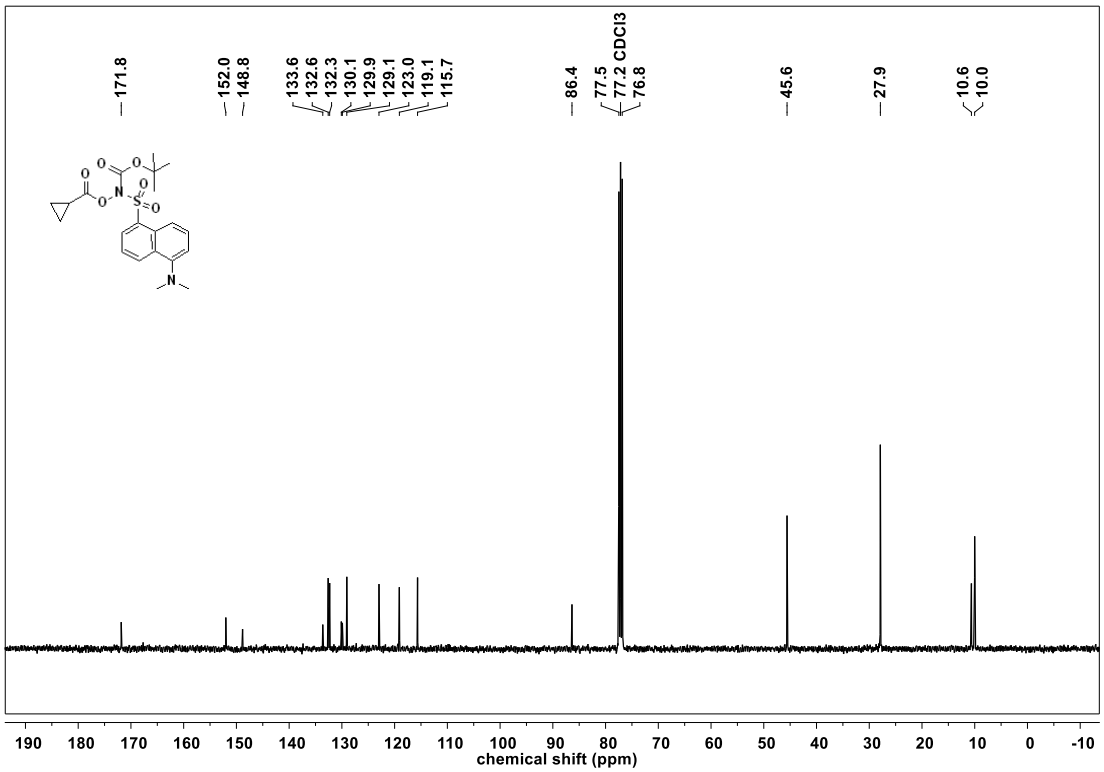

^{1}H NMR spectra of **3a**

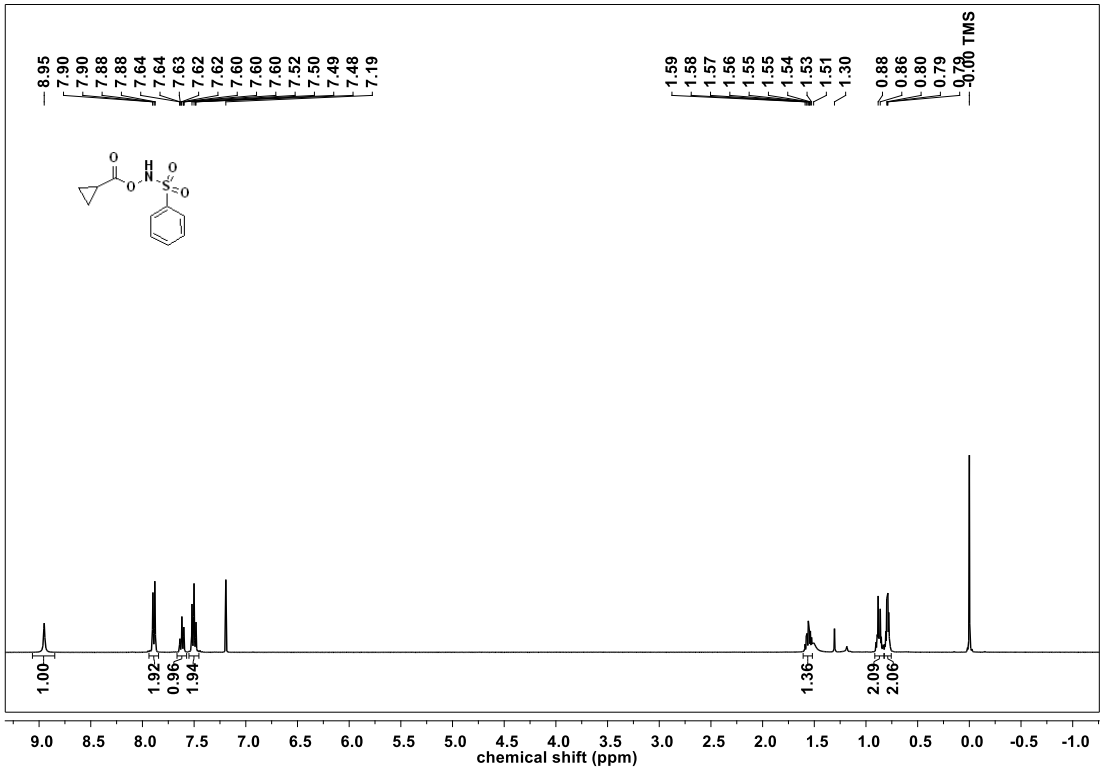

^{13}C NMR spectra of **3a**

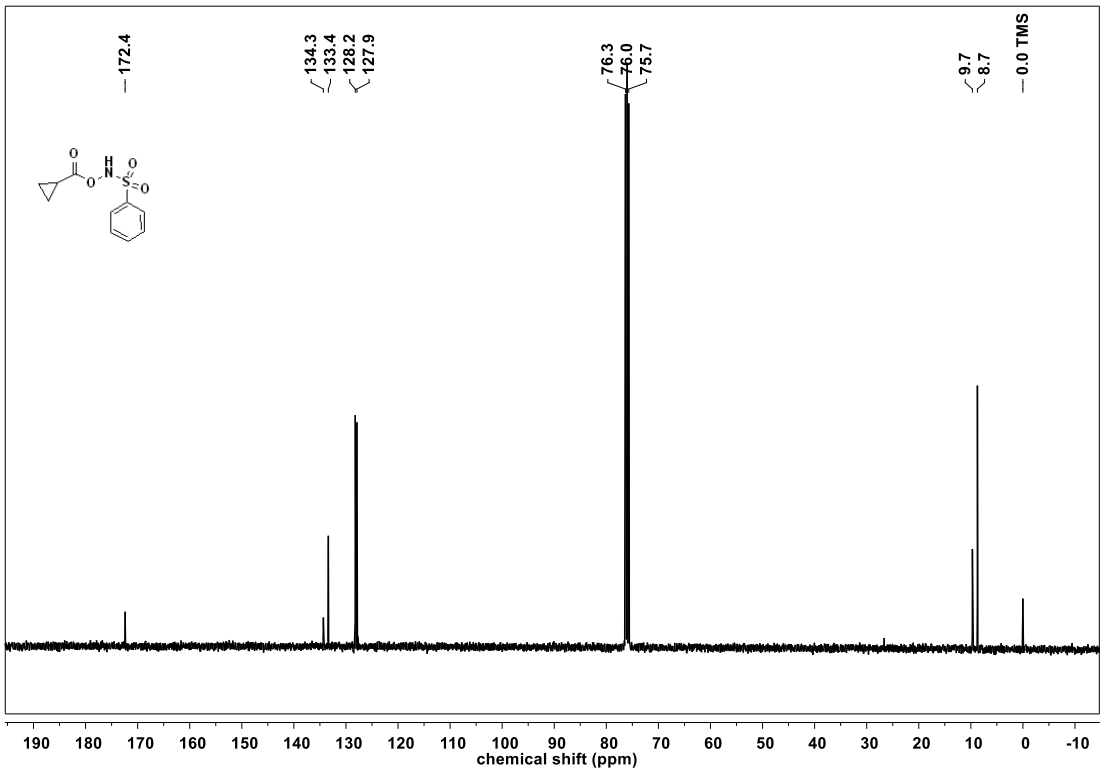

^{1}H NMR spectra of **3b**

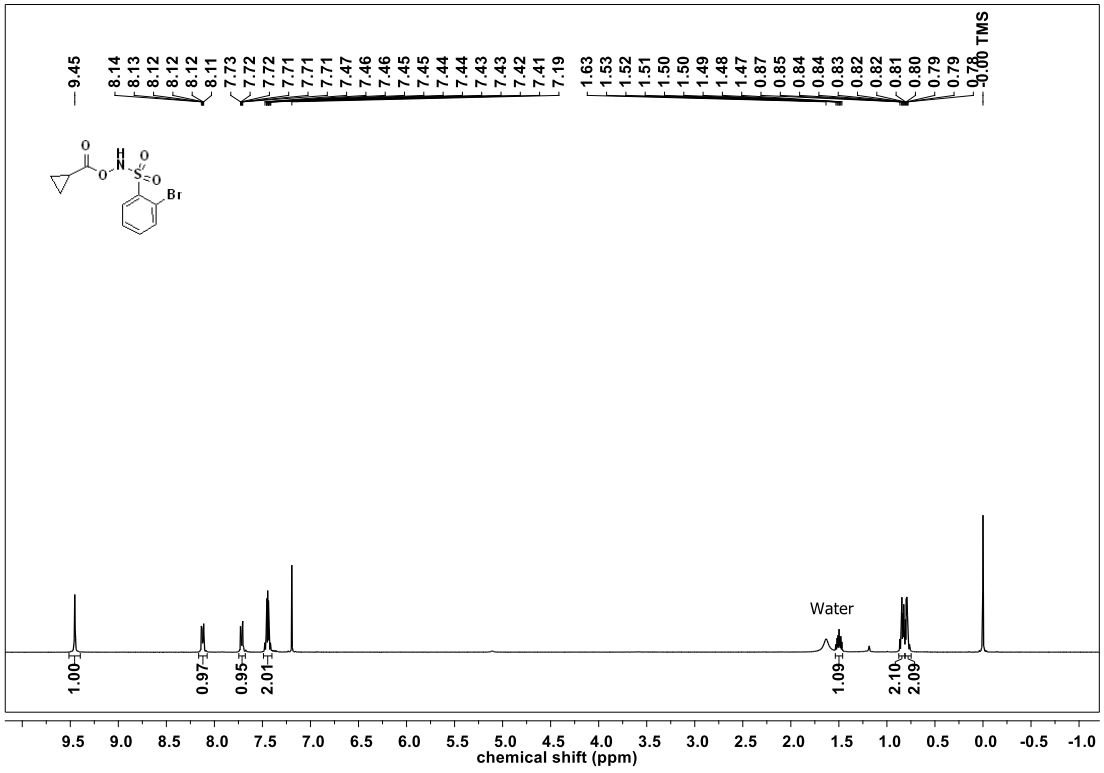

^{13}C NMR spectra of **3b**

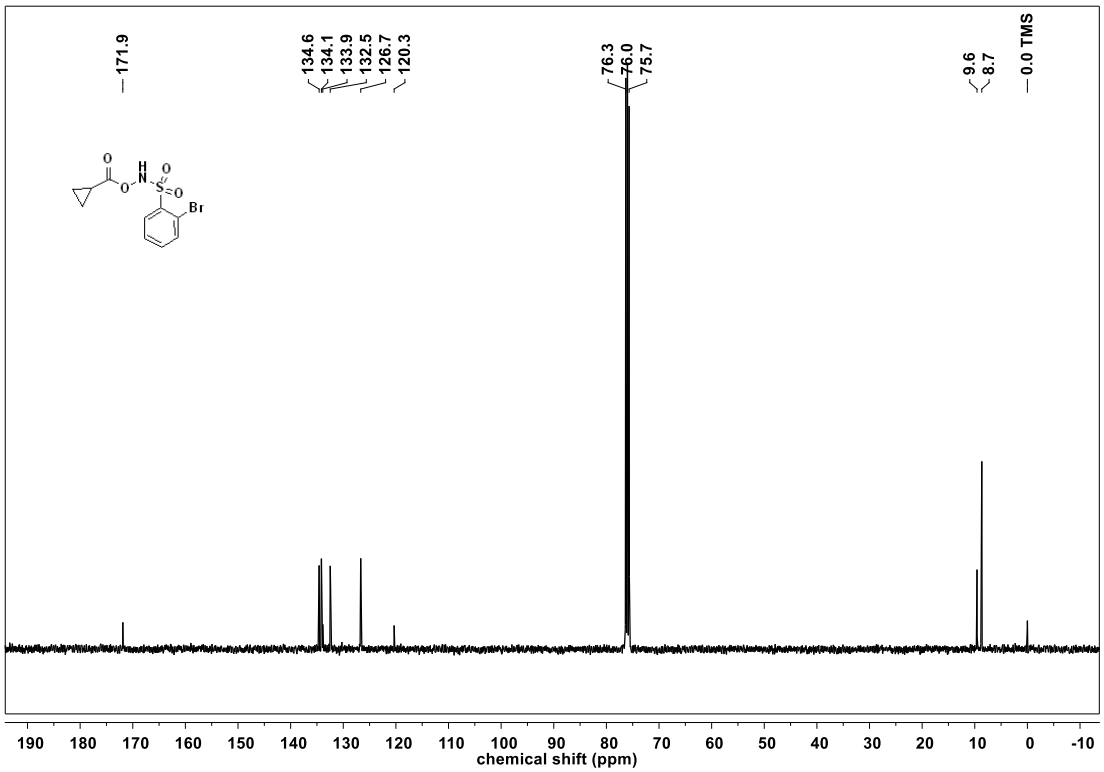

^{1}H NMR spectra of **3c**

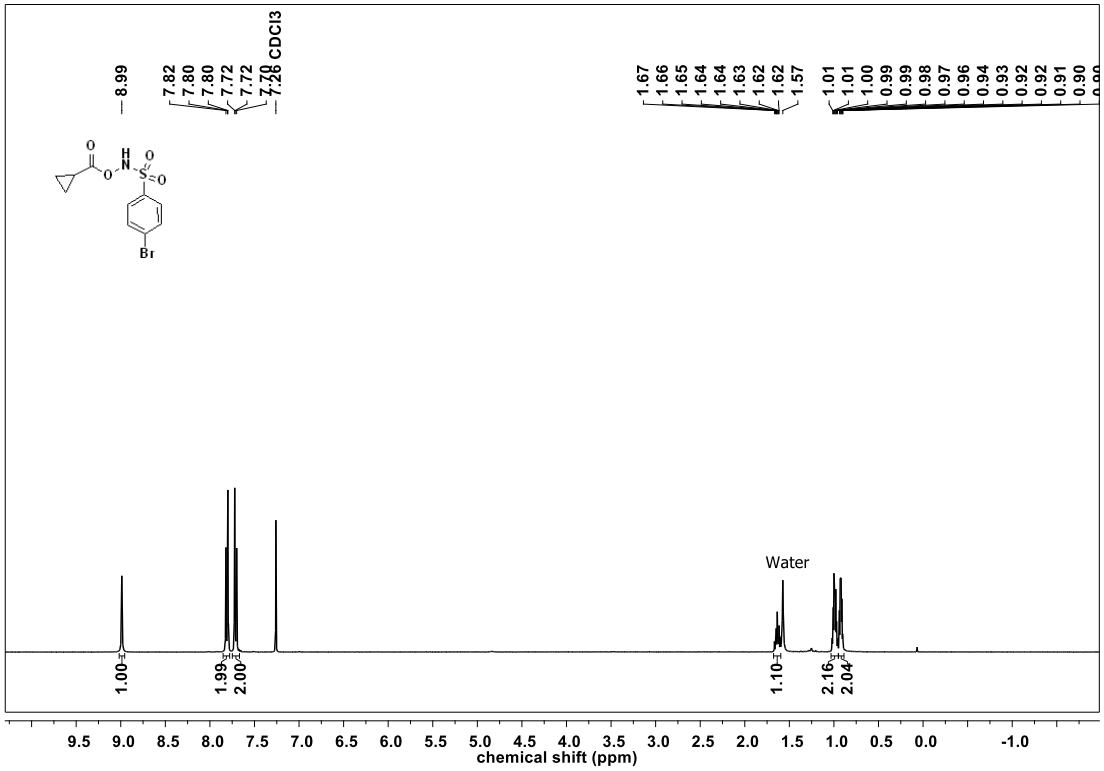

^{13}C NMR spectra of **3c**

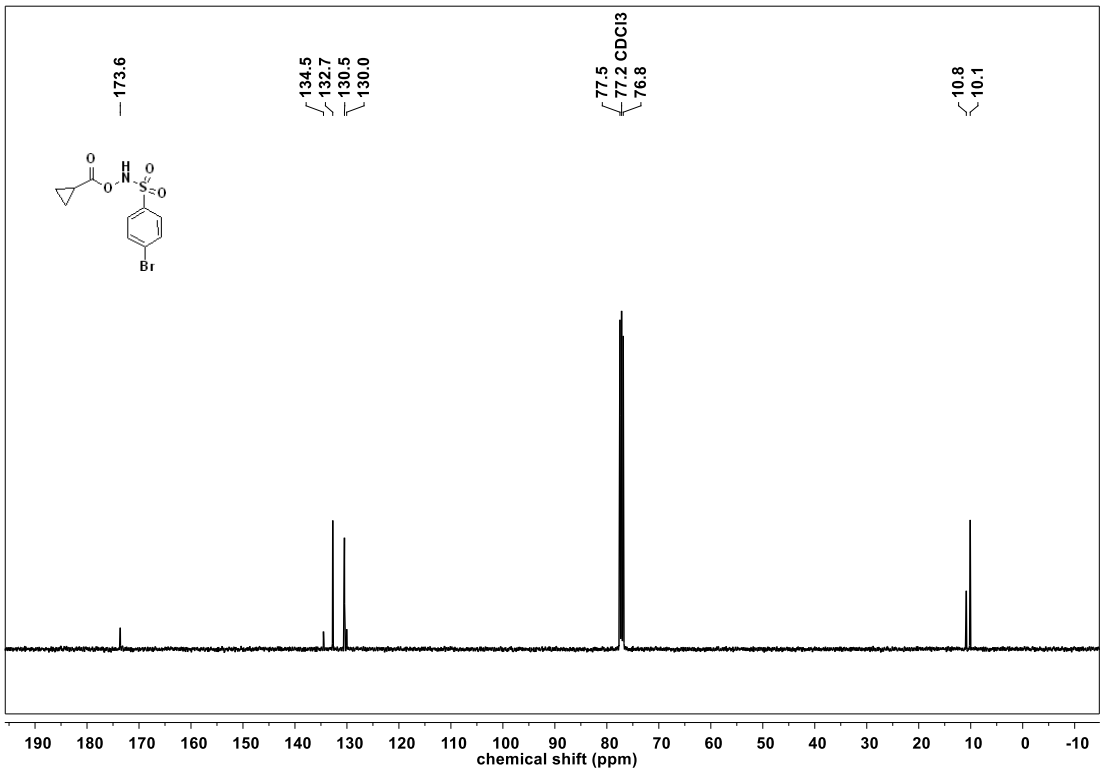

^{1}H NMR spectra of **3d**

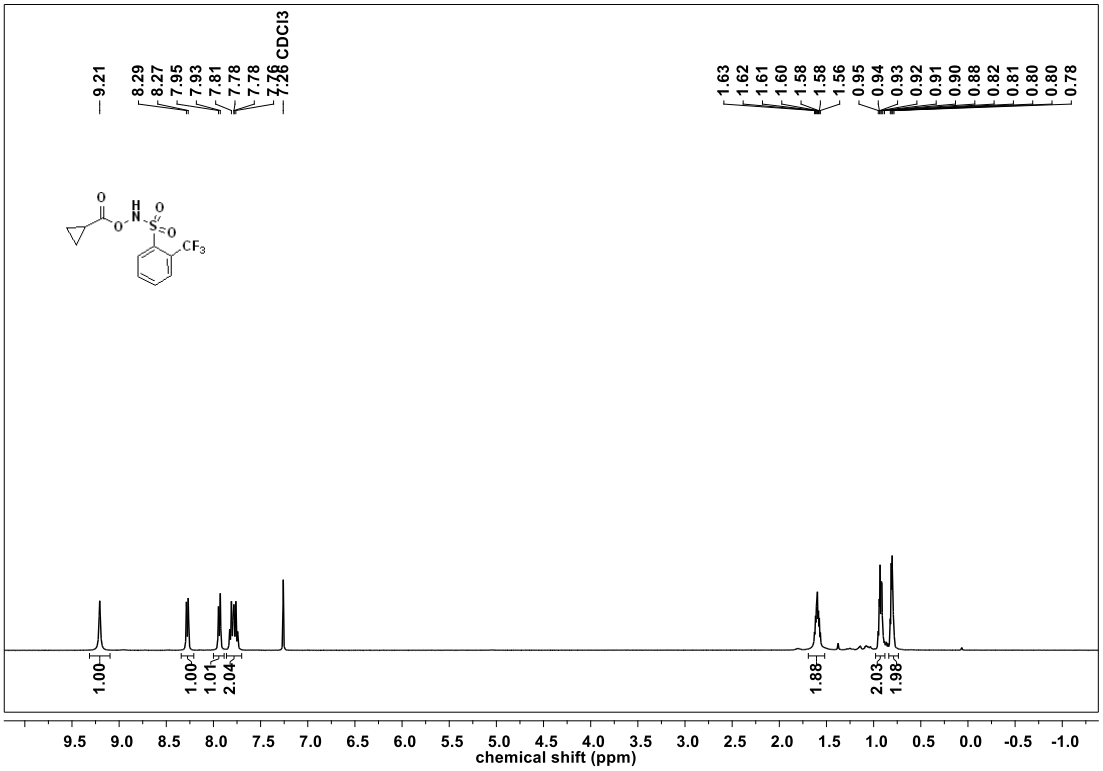

^{13}C NMR spectra of **3d**

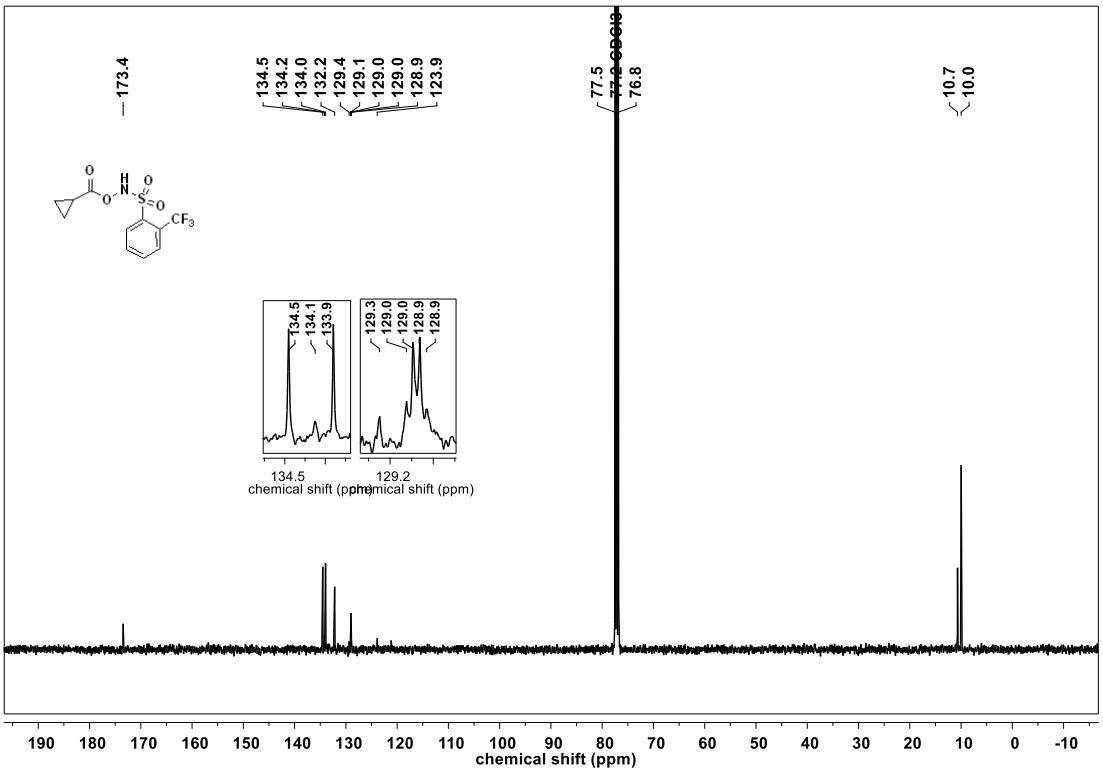

^{1}H NMR spectra of **3e**

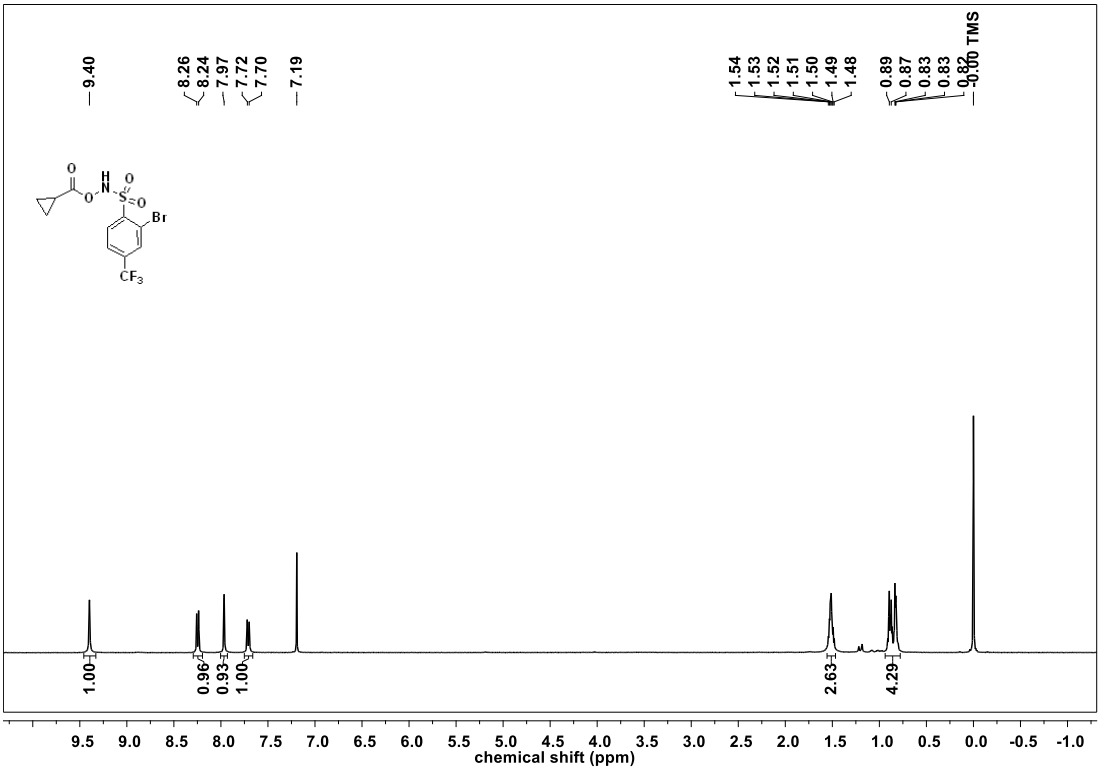

^{13}C NMR spectra of **3e**

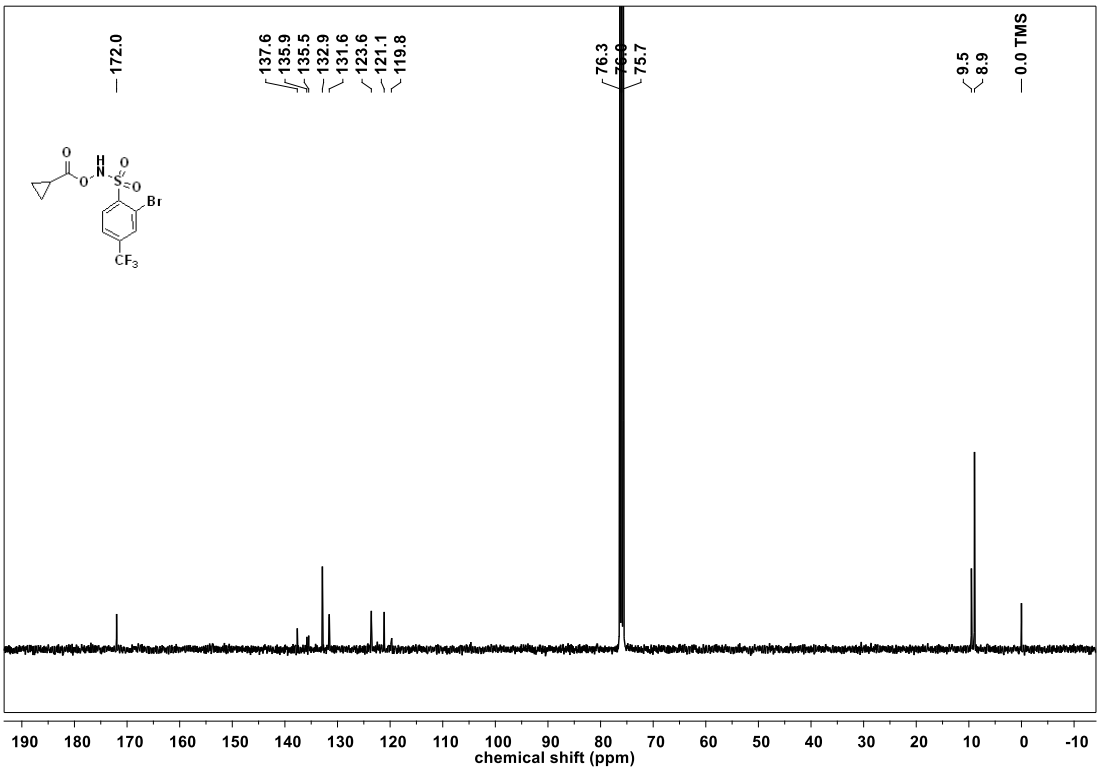

^{1}H NMR spectra of **3f**

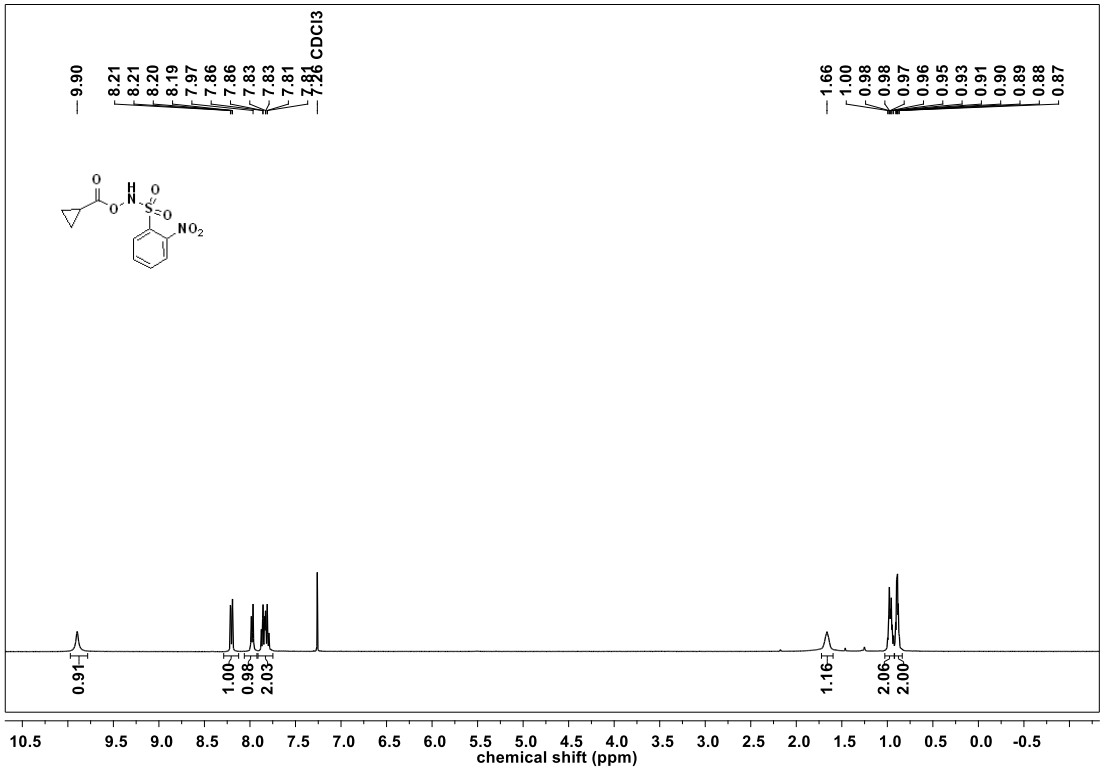

^{13}C NMR spectra of **3f**

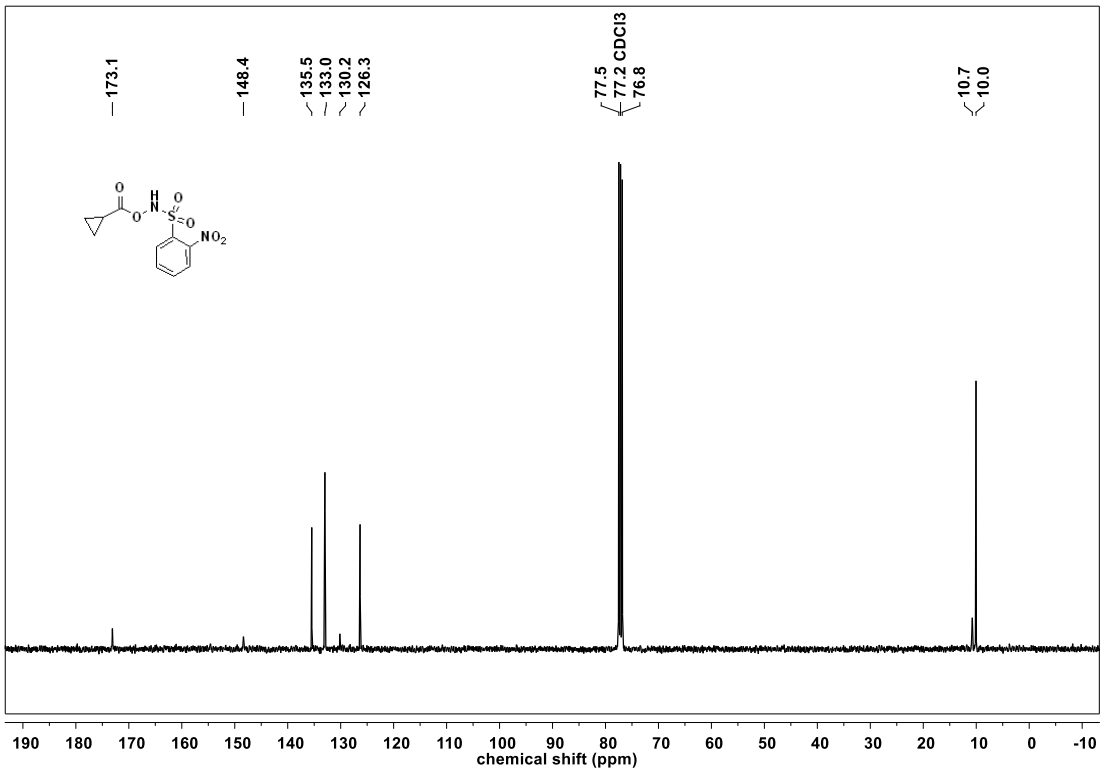

^{1}H NMR spectra of **3g**

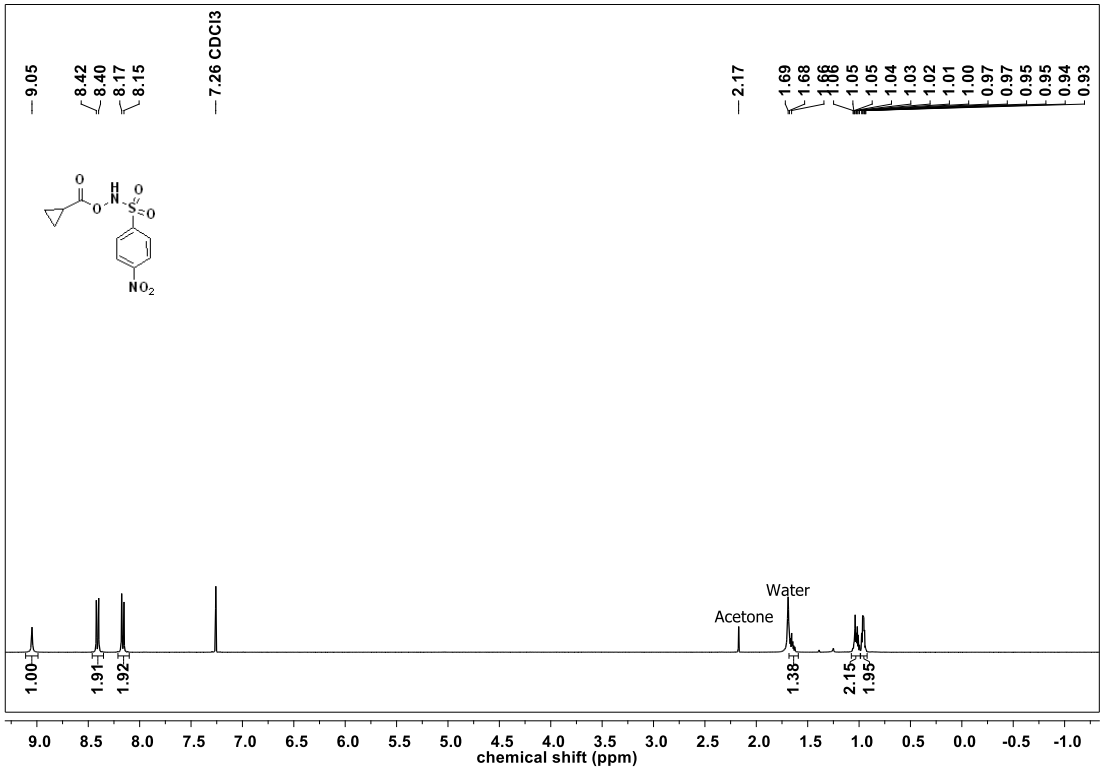

^{13}C NMR spectra of **3g**

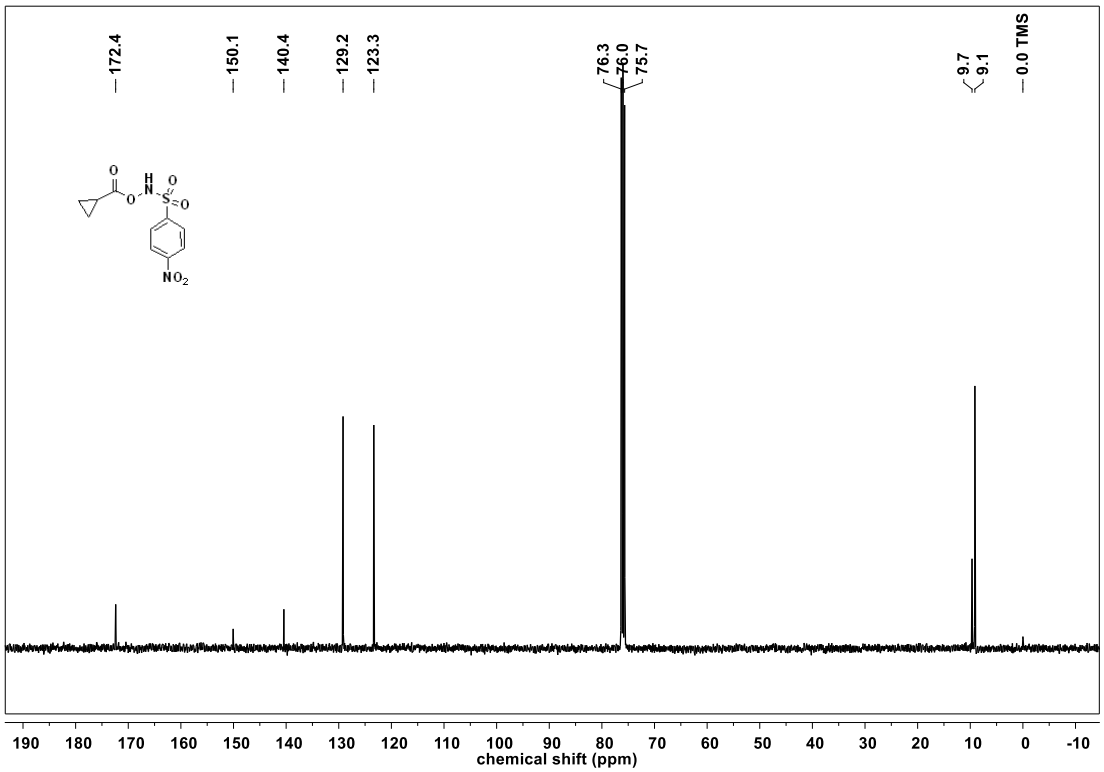

^{1}H NMR spectra of **3h**

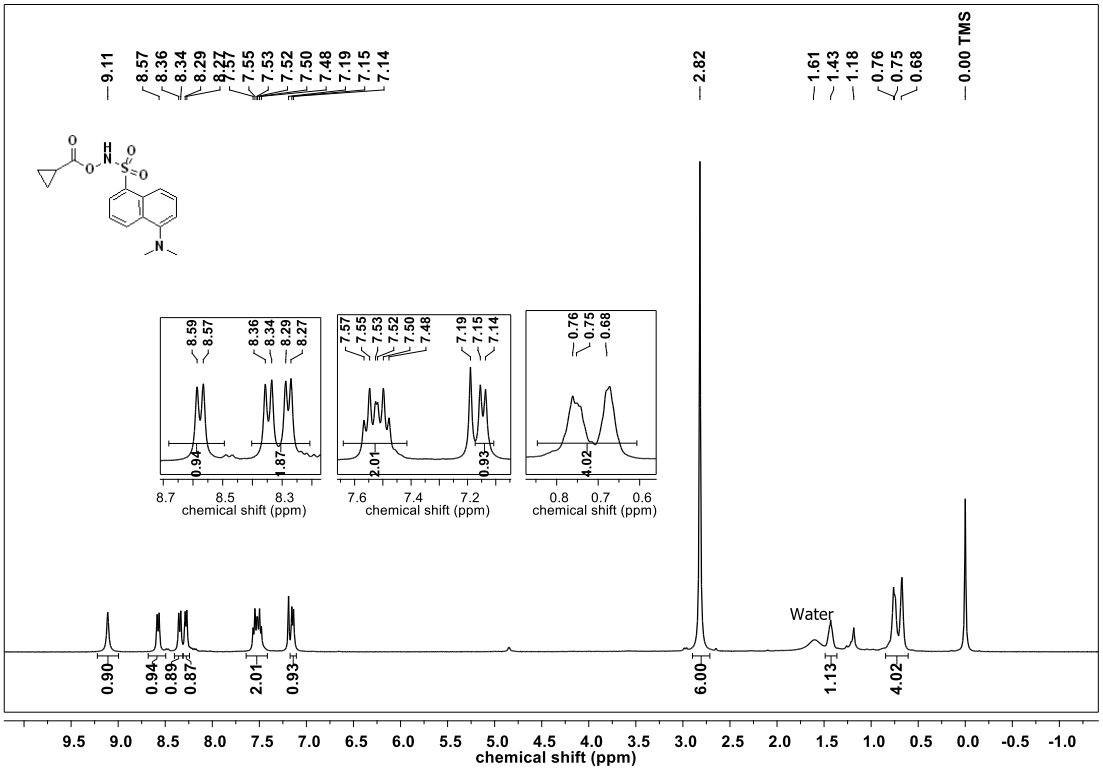

^{13}C NMR spectra of **3h**

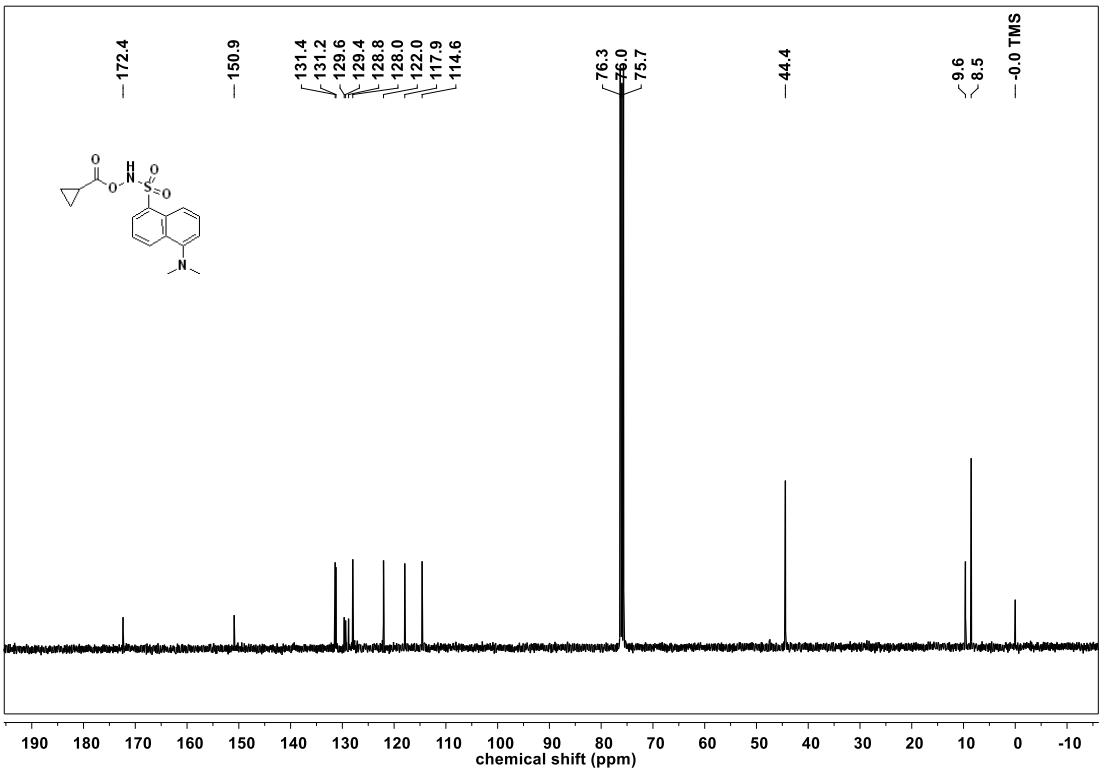

^{1}H NMR spectra for compound **4**

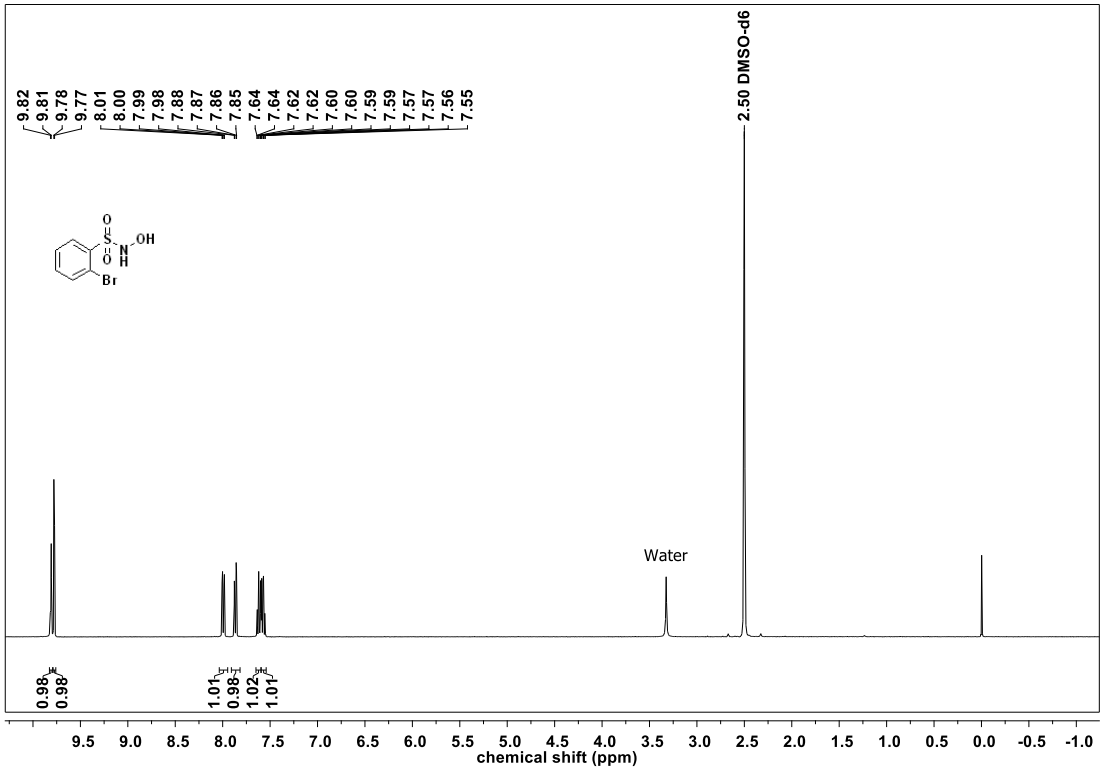

^{1}H NMR spectra for compound **5**

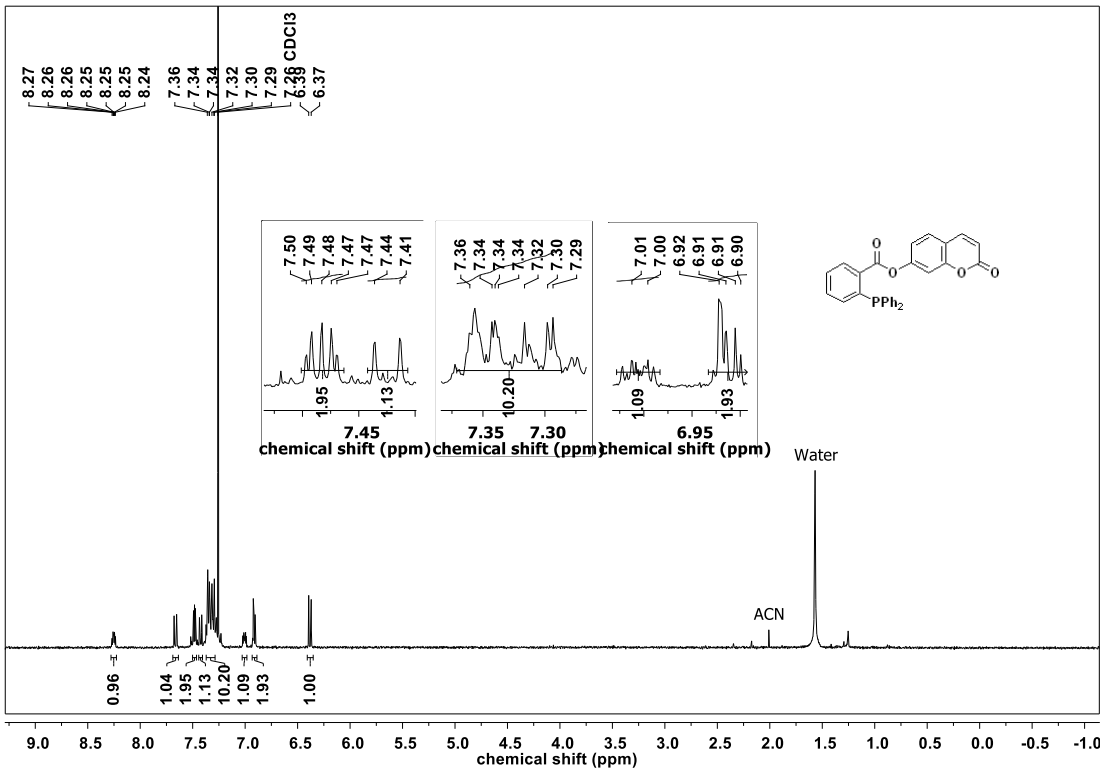

^{1}H NMR spectra for compound **6**

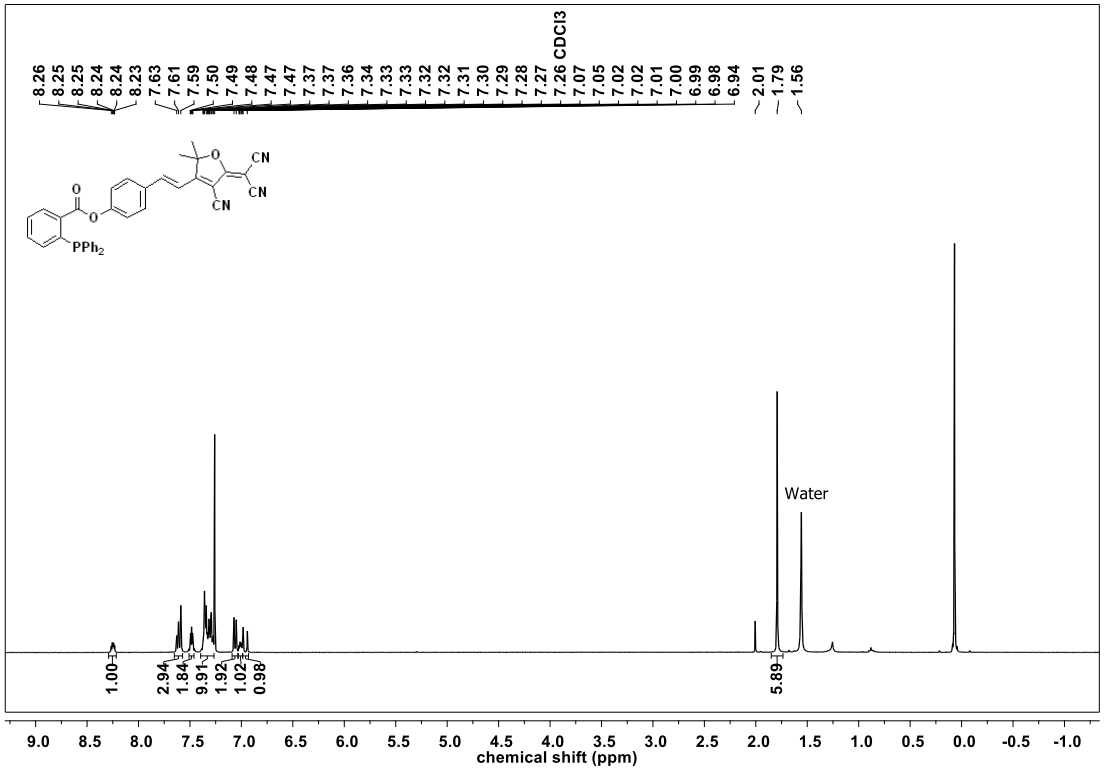

^{1}H NMR spectra of **7**

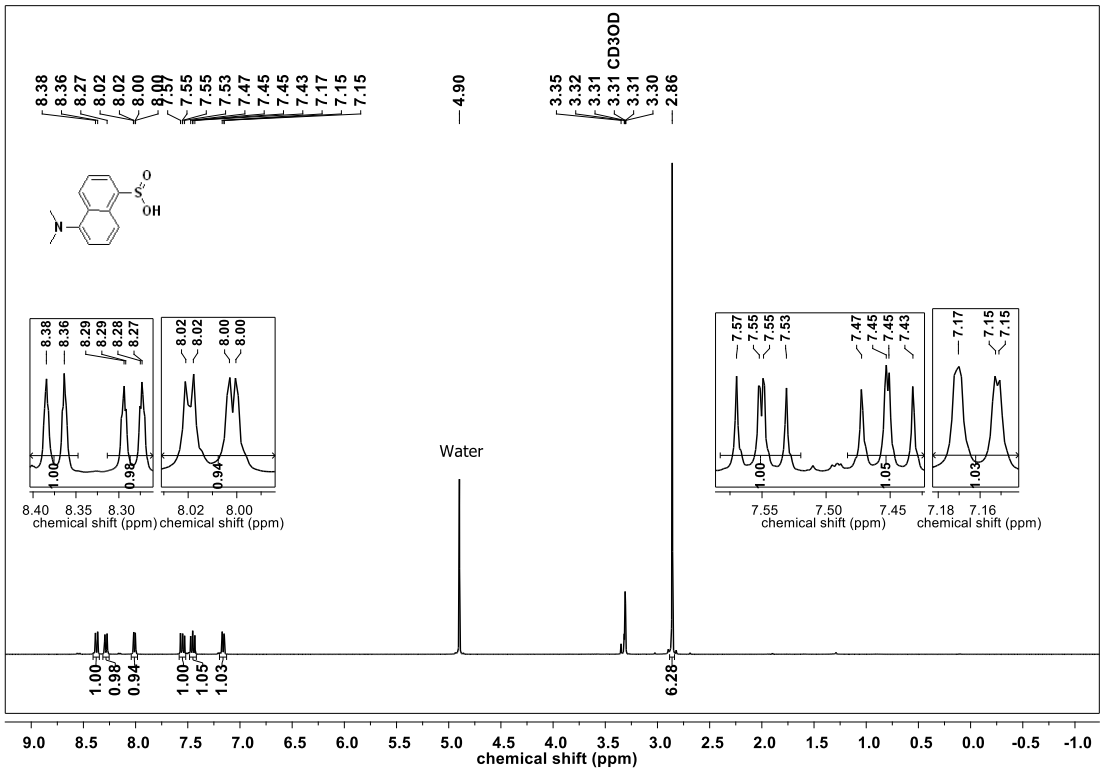

^{13}C NMR spectra of **7**

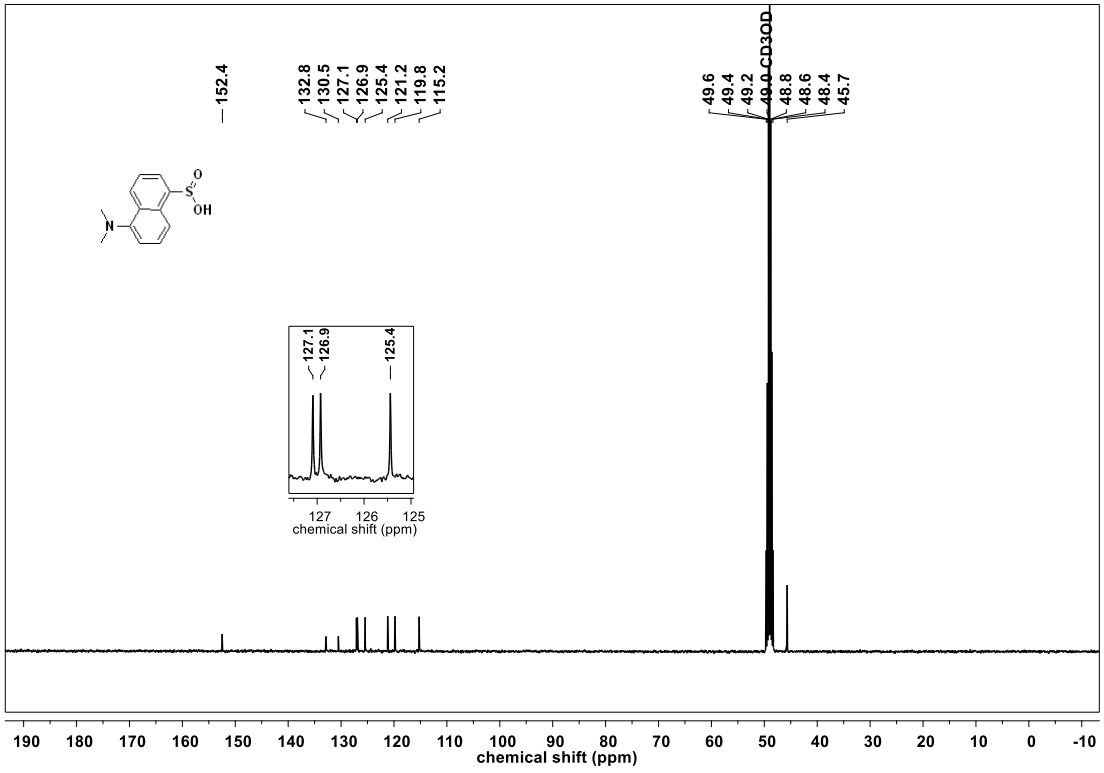

2.6. References

(1) Aizawa, K.; Nakagawa, H.; Matsuo, K.; Kawai, K.; Ieda, N.; Suzuki, T.; Miyata, N. Piloty's Acid Derivative with Improved Nitroxyl-Releasing Characteristics. *Bioorg. Med. Chem. Lett.* **2013**, *23* (8), 2340–2343.

(2) Correia, J. T. M.; Piva da Silva, G.; André, E.; Paixão, M. W. Photoredox Decarboxylative Alkylation/(2+2+1) Cycloaddition of 1,7-Enynes: A Cascade Approach Towards Polycyclic Heterocycles Using N-(Acyloxy)Phthalimides as Radical Source. *Adv. Synth. Catal.* **2019**, *361* (24), 5558–5564..

(3) Sutton, A. D.; Williamson, M.; Weismiller, H.; Toscano, J. P. Optimization of HNO Production from N , O - Bis -Acylated Hydroxylamine Derivatives. *Org. Lett.* **2012**, *14* (2), 472–475.

(4) Mao, G. J.; Zhang, X. B.; Shi, X. L.; Liu, H. W.; Wu, Y. X.; Zhou, L. Y.; Tan, W.; Yu, R. Q. A Highly Sensitive and Reductant-Resistant Fluorescent Probe for Nitroxyl in Aqueous Solution and Serum. *Chem. Commun.* **2014**, *50* (43).

(5) Liu, C.; Wang, Y.; Tang, C.; Liu, F.; Ma, Z.; Zhao, Q.; Wang, Z.; Zhu, B.; Zhang, X. A Reductant-Resistant Ratiometric, Colorimetric and Far-Red Fluorescent Probe for Rapid and Ultrasensitive Detection of Nitroxyl. *J. Mater. Chem. B* **2017**, *5* (19).

(6) Guo, Q.; Wu, Y.; Zhang, L.; Qin, Y.; Bao, J.; Feng, Y.; Liu, Y.; Zhou, Y. Real-Time Visualization of Efficient Nitroxyl (HNO) Releasing Using Fluorescence Technique. *Sensors Actuators B Chem.* **2022**, *369*, 132309.

(7) Wawilow, S. J. Die Fluoreszenzausbeute von Farbstoffl**?**sungen. *Zeitschrift f**?**r Phys.* **1924**, *22* (1), 266–272. https://doi.org/10.1007/BF01328130.

(8) Hammer, M.; Schweitzer, D.; Richter, S.; Königsdörffer, E. Sodium Fluorescein as a Retinal PH Indicator? *Physiol. Meas.* **2005**, *26* (4), N9–N12.

(9) Simkovitch, R.; Huppert, D. Photoprotolytic Processes of Umbelliferone and Proposed Function in Resistance to Fungal Infection. *J. Phys. Chem. B* **2015**, *119* (46), 14683–14696.

(10) Kristoffersen, A. S.; Erga, S. R.; Hamre, B.; Frette, Ø. Testing Fluorescence Lifetime Standards Using Two-Photon Excitation and Time-Domain Instrumentation: Rhodamine B, Coumarin 6 and Lucifer Yellow. *J. Fluoresc.* **2014**, *24* (4), 1015–

(11) Chakraborty, I. N.; Roy, S.; Devatha, G.; Rao, A.; Pillai, P. P. InP/ZnS Quantum Dots as Efficient Visible-Light Photocatalysts for Redox and Carbon–Carbon Coupling Reactions. *Chem. Mater.* **2019**, *31* (7), 2258–2262.

(12) Smith, P. C.; McDonagh, A. F.; Benet, L. Z. Effect of Esterase Inhibition on the Disposition of Zomepirac Glucuronide and Its Covalent Binding to Plasma Proteins in the Guinea Pig. *J. Pharmacol. Exp. Ther.* **1990**, *252* (1), 218–224.

(13) Griess, P. Bemerkungen Zu Der Abhandlung Der HH. Weselsky Und Benedikt „Ueber Einige Azoverbindungen". *Berichte der Dtsch. Chem. Gesellschaft* **1879**, *12* (1), 426–428.

(14) Zamora, R.; Grzesiok, A.; Weber, H.; Feelisch, M. Oxidative Release of Nitric Oxide Accounts for Guanylyl Cyclase Stimulating, Vasodilator and Anti-Platelet Activity of Piloty's Acid: A Comparison with Angeli's Salt. *Biochem. J.* **1995**, *312 (Pt 2* (Pt 2), 333–339.

(15) Sanna, D.; Rocchitta, G.; Serra, M.; Abbondio, M.; Serra, P. A.; Migheli, R.; De Luca, L.; Garribba, E.; Porcheddu, A. Synthesis of Nitric Oxide Donors Derived from Piloty's Acid and Study of Their Effects on Dopamine Secretion from PC12 Cells. *Pharmaceuticals (Basel).* **2017**, *10* (3).

(16) Zarenkiewicz, J.; Khodade, V. S.; Toscano, J. P. Reaction of Nitroxyl (HNO) with Hydrogen Sulfide and Hydropersulfides. *J. Org. Chem.* **2021**, *86* (1), 868–877.

(17) Ida, T.; Sawa, T.; Ihara, H.; Tsuchiya, Y.; Watanabe, Y.; Kumagai, Y.; Suematsu, M.; Motohashi, H.; Fujii, S.; Matsunaga, T.; Yamamoto, M.; Ono, K.; Devarie-Baez, N. O.; Xian, M.; Fukuto, J. M.; Akaike, T. Reactive Cysteine Persulfides and S-Polythiolation Regulate Oxidative Stress and Redox Signaling. *Proc. Natl. Acad. Sci.* **2014**, *111* (21), 7606–7611.

(18) Wedmann, R.; Onderka, C.; Wei, S.; Szijártó, I. A.; Miljkovic, J. L.; Mitrovic, A.; Lange, M.; Savitsky, S.; Yadav, P. K.; Torregrossa, R.; Harrer, E. G.; Harrer, T.; Ishii, I.; Gollasch, M.; Wood, M. E.; Galardon, E.; Xian, M.; Whiteman, M.; Banerjee, R.; Filipovic, M. R. Improved Tag-Switch Method Reveals That Thioredoxin Acts as Depersulfidase and Controls the Intracellular Levels of Protein Persulfidation. *Chem. Sci.* **2016**, *7* (5), 3414–3426.

(19) Yang, G.; Zhao, K.; Ju, Y.; Mani, S.; Cao, Q.; Puukila, S.; Khaper, N.; Wu, L.; Wang, R. Hydrogen Sulfide Protects Against Cellular Senescence via S -Sulfhydration of Keap1 and Activation of Nrf2. *Antioxid. Redox Signal.* **2013**, *18.*

Chapter 3: β-glucosidase activated Nitroxyl (HNO) donors

3.1. Introduction

In **Chapter 2**, the development of esterase-activated HNO generators was described. As esterase is ubiquitous, delivery of HNO is not selective towards a particular cell type. Designing a tool for specific HNO delivery is desirable to overcome the limitations associated with the esterase-based strategy. In order to achieve this goal, glucoside was chosen as protecting group for hydroxylamine. Sugars are natural biomolecules with free hydroxyl groups that are expected to enhance aqueous solubility. β-glucosidase is a lysosomal enzyme known to catalyze the hydrolysis of the glycosidic bond to release an active drug.

The expression and activity of β-glucosidase enzymes were significantly upregulated in breast cancer tissues and hepatocellular carcinoma (HCC) cell lines.[1,2] The overexpression of β-glucosidase activates PI3K/Akt/mTOR signaling, leading to increased cell growth. In contrast, β-glucosidase inhibition by siRNA depletion and pharmacological approach using conduritol B epoxide (selective β-glucosidase inhibitor) suppressed growth and induced apoptosis in breast cancer cells.[1] Importantly, β-glucosidase inhibition significantly sensitized breast cancer cells to chemotherapy, suggesting that inhibiting β-glucosidase effectively targeted breast cancer cells that were resistant to elimination by the chemotherapeutic agent when administered alone.

The elevated level of β-glucosidase is associated with certain pathophysiology of the GI tract. Therefore, prodrug strategies based on β-glucosidase as the trigger have been widely used for drug delivery to the colon. Several prodrugs have been developed using β-glucosidase as a trigger for the delivery of drugs to the colon[3,4,5], Parkinson's disease[6], Alzheimer's disease[7] and cancer.[8] It was observed that the prodrug showed better absorption and bioavailability. Also, reduced the side effects without compromising efficacy. Similarly, for the treatment of ulcerative colitis, β-glucosidase triggered prodrug of 4-aminosalicylic acid (NSAID-non-steroidal anti-inflammatory drug) was developed (Figure 3.1).[9]

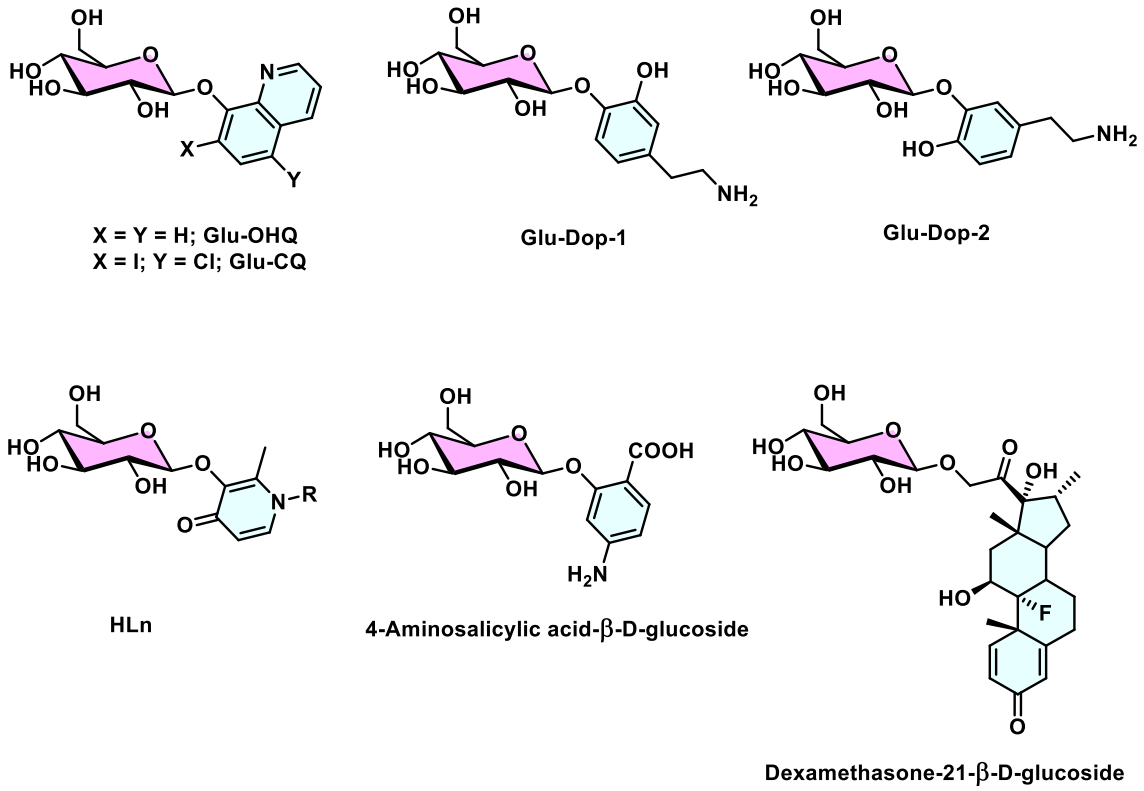

Figure 3.1. β-glucosidase activated prodrugs

Design and development of β-glucosidase sensitive HNO prodrug were considered. Since glucose transporters were overexpressed in cancer cells. The design consisted of three different parts, β-glucose was used as protecting group, HNO and aryl sulfinate (Figure 3.2).

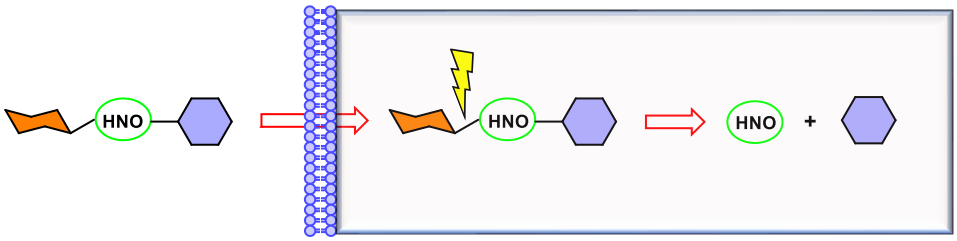

Figure 3.2. Design of β-glucosidase stimulated nitroxyl (HNO) donor

The following mechanism was proposed for HNO generation from donors. Firstly, the nucleophilic attack of β-glucosidase takes place on the anomeric carbon of glycoside resulting in the cleavage of the glucosidic bond to release an anionic intermediate. Further, the intermediate undergoes subsequent decomposition in pH 7.4 to release HNO and aryl sulfinic acid (Scheme 3.1).

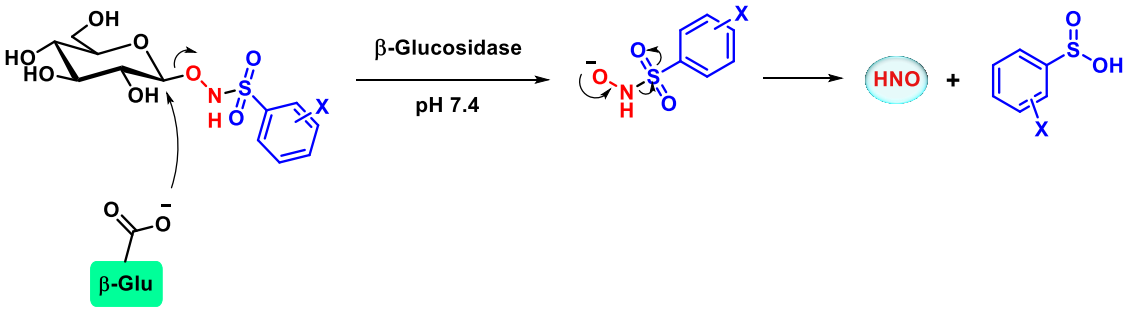

Scheme 3.1. Proposed mechanism of HNO generation upon activation by β-glucosidase

3.2. Result and discussion

3.2.1. Synthesis

To test the hypothesis, HNO prodrugs were synthesized in five steps. Synthesis of prodrugs commenced with glucose pentaacetate. Bromination with hydrobromic acid afforded compound **9**[10] which was later coupled with *N*-hydroxyphthalimide in basic conditions to provide compound **10**.[11] Next, deprotection was performed using hydrazine hydrate to obtain **11**[11], which upon *N*-sulfonation by respective arylsulfonyl chlorides in basic conditions furnished compounds **12a-12e** (Scheme 3.2).[12]

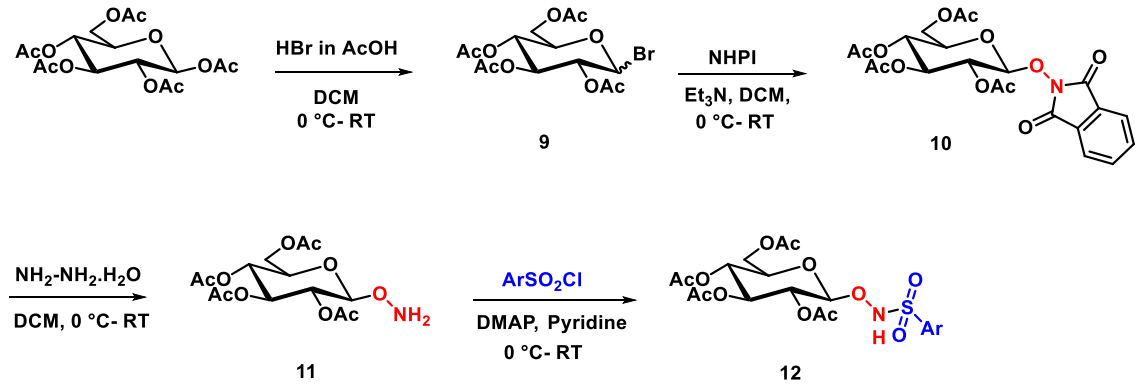

Scheme 3.2. Synthesis of compound **12**

Table 3.1: Synthesis of compounds **12a-12e**

Entry	Product	Ar	Yield, %
1	**12a**	2-Br-Ph	96
2	**12b**	Dansyl	93
3	**12c**	4-OMe-Ph	86
4	**12d**	2- NO_2-4-CF_3-Ph	33
5	**12e**	2,4,6-trifluoro-Ph	80

Next, deacetylation of compound **12a-12e** was achieved using sodium methoxide condition (Scheme 3.3).[13]

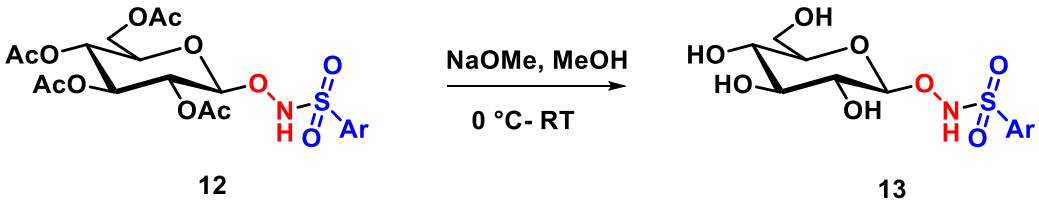

Scheme 3.3. Synthesis of compound **13**

Table 3.2: Synthesis of compounds **13a-13e** from **12**

Entry	Product	Ar	Yield, %
1	**13a**	2-Br-Ph	20
2	**13b**	Dansyl	22
3	**13c**	4-OMe-Ph	21
4	**13d**	2- NO_2-4- CF_3-Ph	98
5	**13e**	2,4,6-trifluoro-Ph	13

Jishnu, C. V. has contributed in the synthesis of derivatives of compound **13**.

Next, we synthesized the 2-bromosulfinic acid as a control compound by following a reported procedure. 2-bromosulfonyl chloride was reduced by sodium borohydride at 0 ˚C gave compound **14** in good yield (Scheme 3.4).[13]

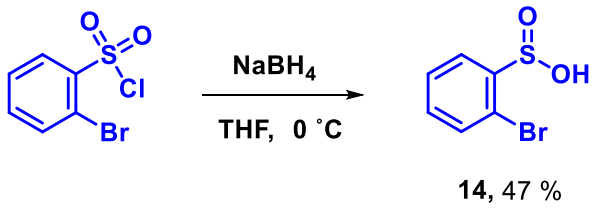

Scheme 3.4. Synthesis of compound **14**

3.2.2. HNO generation study

3.2.2.1. Evaluation of HNO generation using 5

To test the HNO generation from prodrug, a fluorescence-based experiment was performed using β-glucosidase from almonds and **5**.[14] Compounds **13a-13e** are expected to the cleaved by β-glucosidase to release HNO, which can be trapped by **5** to release fluorescent umbelliferone (excitation = 370 nm; emission = 460 nm) (Scheme 3.5).

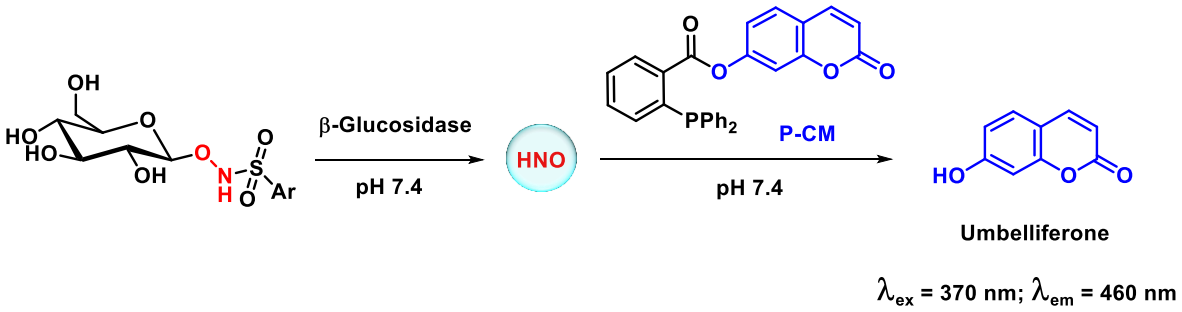

Scheme 3.5: Proposed mechanism for HNO trapping by **5** and release of fluorescent umbelliferone

Compounds **13a-13e** were incubated with **5** in the presence and absence of β-glucosidase (10 U/mL) in buffer (pH 7.4) and the fluorescence signal was recorded at 460 nm over 6 h. In the absence of an enzyme, no significant fluorescence signal was observed from compounds **13a-13e**. However, in the presence of β-glucosidase only compound **13a** was able to significantly generate HNO comparable to compound **4** (2-bromo-piloty's acid, a known HNO donor), as determined by the fluorescence signal of umbelliferone while others did not generate HNO (Figure 3.3).

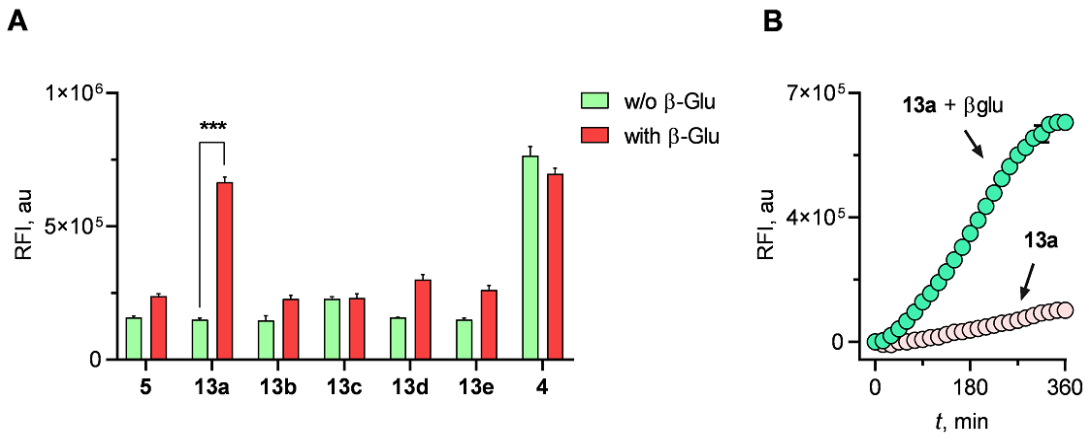

Figure 3.3: Detection of HNO using **5.** (A) Compounds **13a-13e** were incubated with **5** and in the presence and absence of the β-glucosidase in buffer (pH 7.4) at 37 ˚C for 6 h; (B) Time-dependent release of HNO from compound **13a** in the absence and presence of β-glucosidase in buffer (pH 7.4) at 37 ˚C for 6 h. **5** refers to PCM dye; **4** refers to 2-bromo-piloty's acid (λ_{ex} = 370 nm; λ_{em} = 460 nm).

3.2.3. NO detection

Next, NO release from prodrug **13a** was measured by a colorimetric assay (Griess assay). A calibration curve was generated using $NaNO_2$ and was used to quantify NO release. The amount of NO released from prodrug **13a** was measured by generating the sodium nitrite calibration curve (similar to Figure 2.14). Compound **13a** was incubated with β-glucosidase in buffer (pH 7.4) at 37 ˚C for 6 h. The release of NO was determined using Griess reagent, which upon reaction results in the formation of a pink color azo product that absorbs strongly at 540 nm. The diminished yield of NO was observed from compound **13a** as compared to **4** (Figure 3.4).

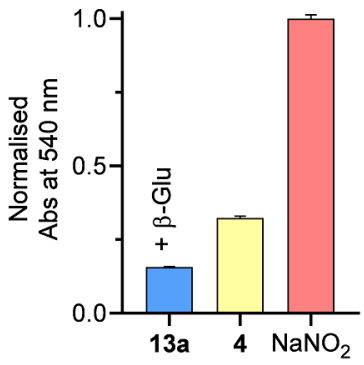

Figure 3.4: NO detection by Griess assay

3.2.4. HPLC study

In order to study the stability of compound **13a**, these compounds were incubated in the absence and presence of β-glucosidase. HPLC analysis of this mixture gave an estimate of stability and yield in the presence of the enzyme. In the absence of β-glucosidase, compound **13a** was stable over an extended period (Figure 3.5). As expected, the decomposition of compound **13a** with concomitant formation of **14** was observed in the presence of β-glucosidase (Figure 3.6).

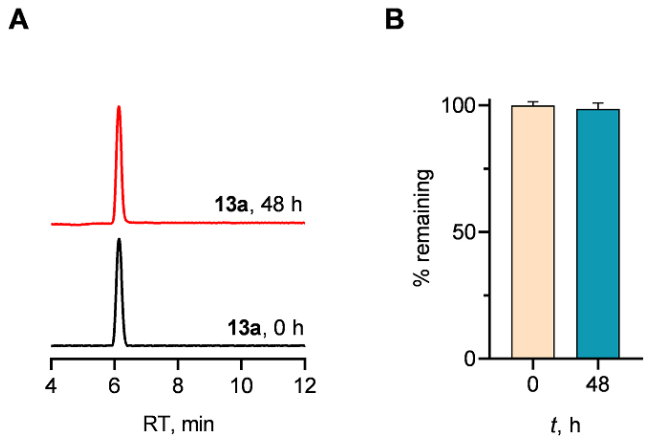

Figure 3.5: Stability of prodrug **13a** in buffer. (A) HPLC trace of stability of **13a** (RT = 6.1 min; (B) Area under the curve corresponding to **13a** (absorbance 230 nm).

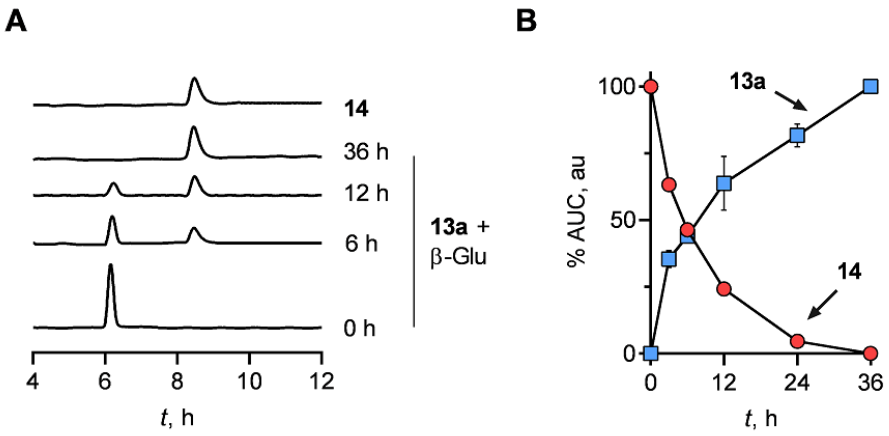

Figure 3.6: HPLC traces and AUC for decomposition of **13a** (RT = 6.1 min) and formation of **14** (RT = 8.4 min) in the presence of β-glucosidase in buffer (pH 7.4).

The decomposition of a compound depends on the interaction with the active residues of the enzyme. In an effort to unravel the plausible binding of compounds into the active site of β-glucosidase, computational studies were performed.

3.2.5. Computational studies

The structure of β-glucosidase from almonds shares a 60% sequence identity with β-glucosidase from white clover leaf. Given the higher sequence similarity, we used β-glucosidase (Clover leaf; PDB ID: 1CBG with a resolution of 2.15 Å) for molecular docking study (Figure 3.7).

```
Clover      ---------------LL--SITTTHIHAFKPLPISFDDFSDLNRSCFAPGFVFGTASSAF      43
Almonds     MAMQLRSLLLCVLLLLLGFALADTNAAARIHPPVVCANLSRANFDTLVPGFVFGAATASY      60
                          **  ::: *:  *    *:   ::*  * . :.******:*::::

Clover      QYEGAAFEDGKGPSIWDTFTHKYPEKIKDRTNGDVAIDEYHRYKEDIGIMKDMNLDAYRF      103
Almonds     QVEGAANLDGRGPSIWDTFTHKHPEKIADGSNGDVAIDQYHRYKEDVAIMKDMGLESYRF      120
            * ****  **:***********:**** * :*******:*******:.*****.*::***

Clover      SISWPRVLPKGKLSGGVNREGINYYNNLINEVLANGMQPYVTLFHWDVPQALEDEYRGFL      163
Almonds     SISWSRVLPNGTLSGGINKKGIEYYNNLINELLHNGIEPLVTLFHWDVPQTLEDEYGGFL      180
            **** ****:*.****:*::**:********:* **::* **********:***** ***

Clover      GRNIVDDFRDYAELCFKEFGDRVKHWITLNEPWGVSMNAYAYGTFAPGRCSDWLKLNCTG      223
Almonds     SNRIVNDFEEYAELCFKKFGDRVKHWTTLNEPYTFSSHGYAKGTHAPGRCSAWYNQTCFG      240
            ...**:**.:*******:******** *****: .* :.** **.****** * : .* *

Clover      GDSGREPYLAAHYQLLAHAAAARLYKTKYQASQNGIIGITLVSHWFEPASKEKADVDAAK      283
Almonds     GDSATEPYLVTHNLLLAHAAAVKLYKTKYQAYQKGVIGITVVTPWFEPASEAKEDIDAVF      300
            ***. ****.:*  *******.:******** *:*:****:*: ******: * *:**.

Clover      RGLDFMLGWFMHPLTKGRYPESMRYLVRKRLPKFSTEESKELTGSFDFLGLNYYSSYYAA      343
Almonds     RALDFIYGWFMDPLTRGDYPQSMRSLVGERLPNFTKKESKSLSGSFDYIGINYYSARYAS      360
            *.***: ****.***:* **:*** ** :***:*:.:***.*:****::*:****: **:

Clover      KAPRIPNARPAIQTDSLINATFEHNGKPLGPMAASSWLCIYPQGIRKLLLYVKNHYNNPV      403
Almonds     ASKNY-SGHPSYLNDVNVDVKSELNGVPIGPQAASSWLYFYPKGLYDLLRYTKEKYNDPI      419
             : .  ..:*:  .*  ::.. * ** *:** ****** :**:*: .** *.*::**:*:

Clover      IYITENGRNSSTINTVTS----------RIPF----------------------------      425
Almonds     IYITENGVDEFNQPNPKLSLCQLLDDSNRIYYYYHHLCYLQAAIKEGVKVKGYFAWSLLD      479
            ******* :. .  . .           ** :

Clover      ------------------------------------------------------------      425
Almonds     NFEWDNGYTVRFGINYVDYDNGLKRHSKHSTHWFKSFLKKSSRNTKKIRRCGNNNTSATK      539


Clover      ---        425
Almonds     FVF        542
```

Figure 3.7. Sequence alignment of β-glucosidase from white clover leaf (Uniprot no. P26205) and almonds (Uniprot no. H9ZGD8). Computational studies were performed by T. Anand Kumar (Prof. Harinath Chakrapani Lab**,** IISER Pune).

The first pocket with the active site residues is shown in Figure 3.8.

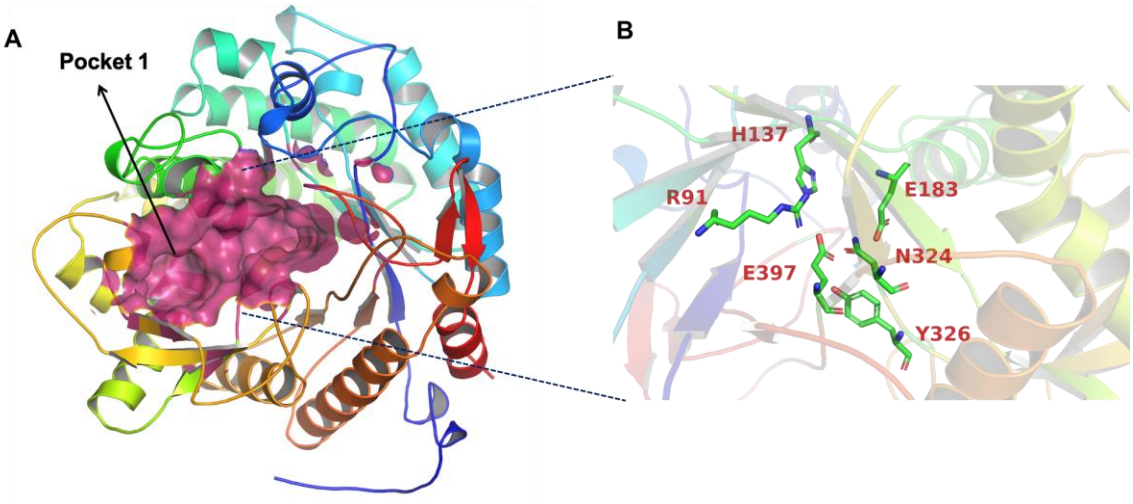

Figure 3.8. (A) The ligand binding pocket of β-glucosidase (PDB: 1CBG from white clover [*Trifolium repens*]) was predicted using the CASTp web server with a cartoon representation of the protein and probe radius 1.4 Å. The pocket was shown as surface colored as warm pink. (B) Zoom view of the active site of pocket 1 containing catalytic residues of β-glucosidase.

The mechanism for cleavage of glucosidic bonds by β-glucosidase has been documented in a detailed crystallographic study by Hughes and coworkers.[15] As shown in Figure 3.7, the active site pocket contains two highly conserved Glu residues (Glu183 or E183 and Glu397 or E397) that have been assigned the respective roles of proton donor and nucleophile based on inhibitor-binding and mutagenesis experiments.

E397 performs a nucleophilic attack at the anomeric carbon resulting in the formation of a glucose-enzyme tetrahedral intermediate. The departure of the aglucone moiety is facilitated by the protonation of the oxygen by the acidic residue (**E183**). During the second catalytic step, a water molecule activated by the catalytic base (**E183**) serves as a nucleophile for hydrolysis of the glucosidic bond to regenerate the free enzyme (Scheme 3.6).

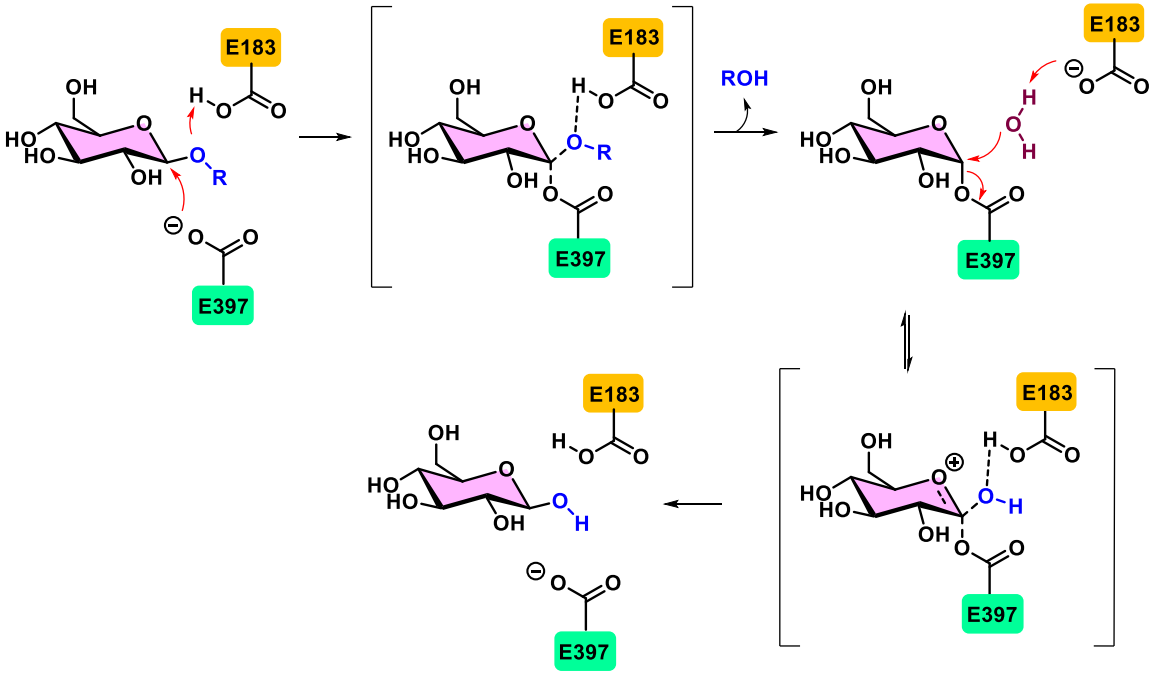

Scheme 3.6. A plausible mechanism of hydrolysis of the glucosidic bond by β-glucosidase

To investigate the propensity of hydrolysis of the compounds **13a-13e** mediated by β-glucosidase, *in silico* molecular docking studies were performed (Figure 3.9). In this study, 4-nitrophenol- β-glucopyranoside **15** was used as a positive control to validate the docking simulations. The protein and ligand PDBQT files were prepared using AutoDock Tools 1.5.6 (ADT) following the standard protocol.[16] A grid box (24.375 × 24.375 × 24.375 $Å^3$) defined for Pocket 1 (Table 3.3, entry A) of the chain A in β-glucosidase centered at the coordinates (x = 40.217, y = 30.310, z = 83.613) was used for docking into the active site with default settings: exhaustiveness = 64, energy range = 3 kcal/mol and number of modes = 20. The best-scored docking pose for all the compounds with the lowest binding energy (Table 3.3) was selected for analysis and figures were visualized using PyMOL (The PyMOL Molecular Graphics System, Version 2.0 Schrodinger, LLC) (Figure 3.10). LigPLOT was used to depict the 2D interactions of ligands and proteins (Figure 3.11).[17]

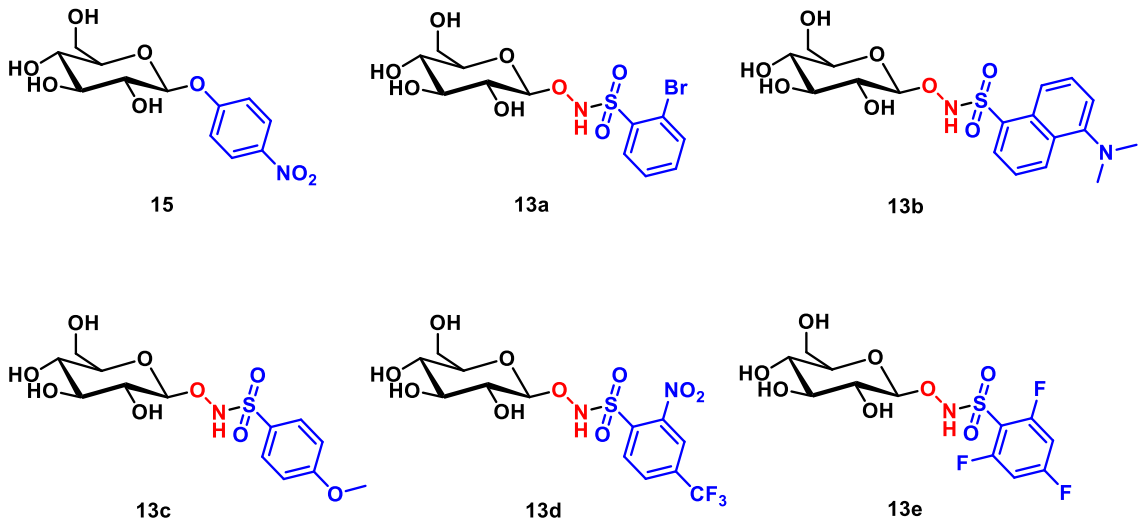

Figure 3.9. Structures of compounds **15** and **13a-13e** used for docking analysis

Table 3.3: Comparative analysis of the docking results of prodrugs **13a-13e**

Entry	Ligand/ Prodrug	Affinity (kcal/mol)	Distance from O (RCOOH) of E183 (Å)*	Distance from O (RCOOH) of E397 (Å)*
1	**15**	-7.4	3.6	5.6
2	**13a**	-8.3	5.3	6.9
3	**13b**	-8.7	9.0	10.9
4	**13c**	-8.3	8.6	10.9
5	**13d**	-8.7	9.2	11.2
6	**13e**	-8.1	8.3	9.9

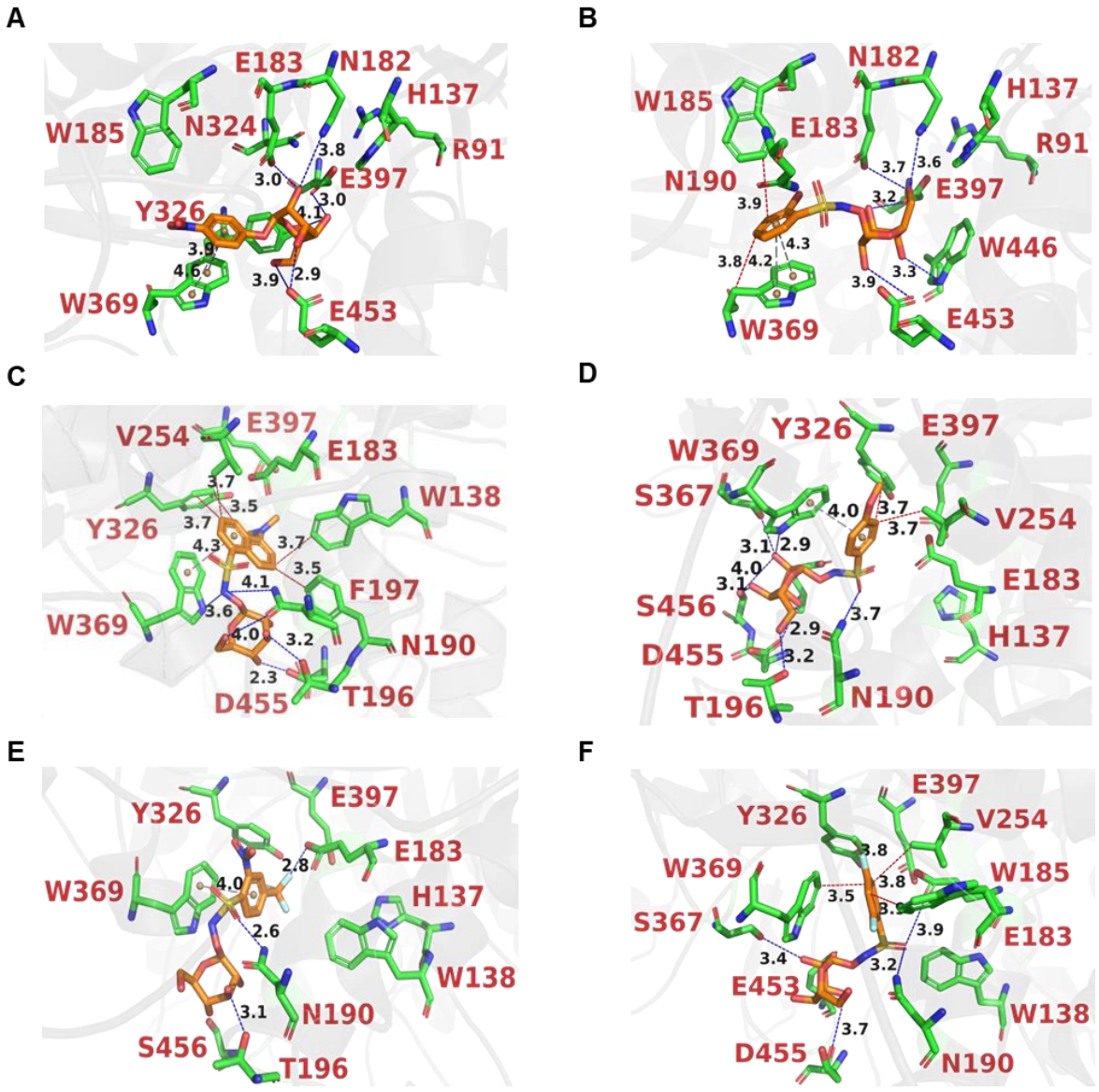

Figure 3.10: Cartoon representation of docked compounds (A) **15**; (B) **13a**; (C) **13b**; (D) **13c**; (E) **13d**; (F) **13e** into the active site of cyanogenic β-glucosidase from white clover (Trifolium repens L.; PDB = 1CBG). The docked ligands were shown in the stick model and the active site residues are indicated by a 1-letter code. The hydrogen, hydrophobic and pi-pi interactions are drawn as blue, red and gray dotted lines, and the lengths are indicated. The figures were generated using PyMOL v 2.0.

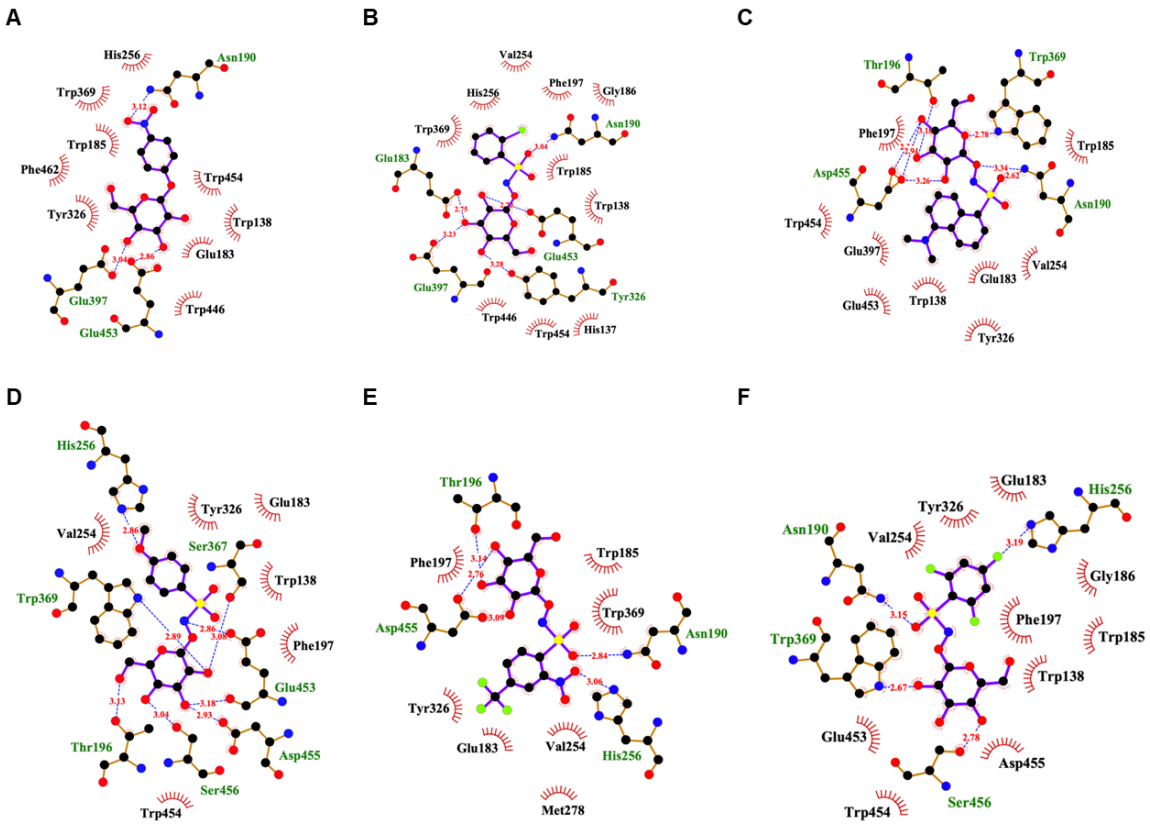

Figure 3.11: LigPlot showing the 2D interactions of compounds (A) **15**; (B) **13a**; (C) **13b**; (D) **13c**; (E) **13d**; (F) **13e** with β-glucosidase. The molecule is represented in a stick model. Active site residues are labeled by a 3-letter code and represented as a ball and stick model. The residues forming hydrophobic interactions are shown as red arcs while the hydrogen bonds are shown as blue dashed lines with indicated bond lengths (Table 3.4).

As anticipated, positive control **15** fitted into the active site (ΔG = -7.4 kcal/mol) and was found closer to catalytic active site residues (3.6 Å from E183 and 5.6 Å from E397 respectively). This enables favorable orientation and spacing for hydrolysis of glucosidic bond and plausible release of 4-nitrophenol from **15**. Similarly, compounds **13a-13e** were also fitted into the active site with a varying docking score ranging from -8.1 to -8.7 kcal/mol. It was noteworthy that the glucosidic moiety of **13a** was in proximity to active site residues (5.3 Å from E183 and 6.9 Å from E397 respectively) than other docked analogs. (Table 3.4, Figure 3.9 and Figure 3.10). Altogether, the docking studies revealed that **13a** binds well to the β-glucosidase over other derivatives (**13b-13e**). The residues involved in catalysis were also appropriately aligned. Together, these model data suggest the importance of binding of the substrate to the active site and also permit to the sensitivity of the active site to minor modification in the substrate.

3.2.6. MTT assay for the cell viability

Next, the cell viability of compounds **13a-13e** was determined using an MTT assay. Breast cancer cells (MCF-7) were treated with varying concentrations of compounds **13a-13e** for 24 h. Compounds **13a-13e** were found to be well tolerated by the MCF-7 cells (Figures 3.12 and 3.13).

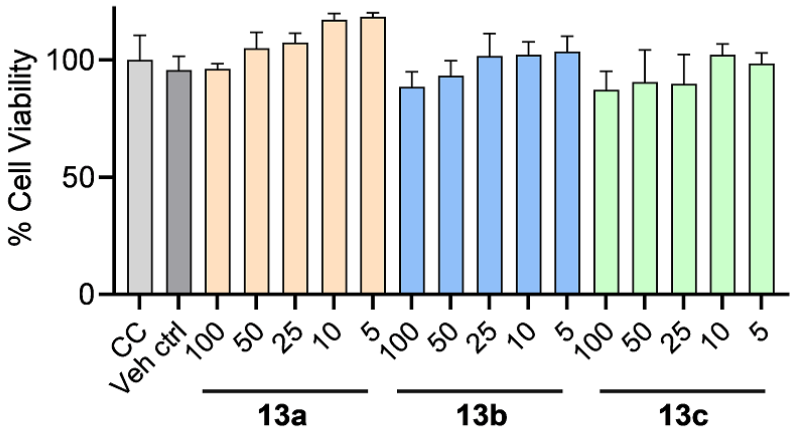

Figure 3.12: Cell viability assay carried out with varying concentrations of compound **13a-13c** on MCF-7 cells for 24 h. All data are presented as mean ± SD (n =3/group).

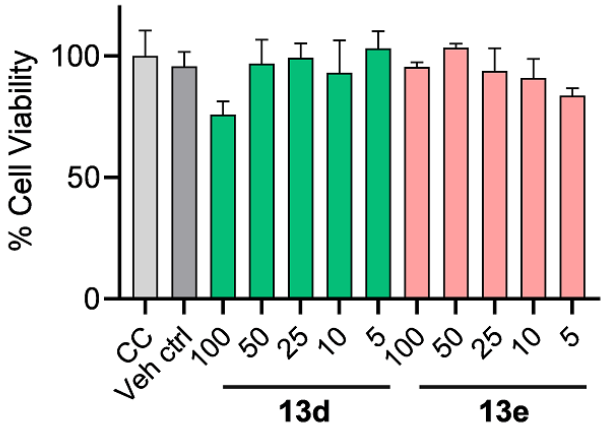

Figure 3.13: Cell viability assay carried out with varying concentrations of compound **13d-13e** on MCF-7 cells for 24 h. All data are presented as mean ± SD (n =3/group).

3.3. Summary

To summarize, β-glucosidase activated HNO donors were designed and derivatives of donors were synthesized. Firstly, we studied the HNO generation from compounds **13a-13e** using **5** and HNO generation was observed with compound **13a** only. Next, we studied the nitric oxide (NO) release from compound **13a** by Griess assay and diminished NO release was observed compared to compound **4**. The amount of NO generation was measured by using a calibration curve which was generated by using $NaNO_2$. Further, the decomposition of compound **13a** was studied by HPLC analysis. It was observed that compound **13a** was stable in physiological conditions. In the presence of β-glucosidase, the disappearance of compound **13a** with concomitant formation of **14** was observed over an extended period. These results were validated by docking studies and it was observed that only compound **13a** was able to interact with the active site residues (E424 and E211) of the enzyme, which probably led to enzyme-mediated decomposition to liberate HNO. While compounds **13b-13e** were shown hydrophobic interactions with the other residues of the enzyme rather than E424 and E211 residues which led to no HNO release. Finally, the cytotoxicity of compounds **13a-13e** were evaluated in MCF-7 cells and all compounds were well tolerated by cells.

Together, the data suggest that triggerable and controlled HNO generation can be achieved using water-soluble β-glucosidase activated nitroxyl (HNO) donors.

3.4. Experimental protocols

3.4.1. Synthesis and characterization

Synthesis of (2R,3R,4S,5R)-2-(acetoxymethyl)-6-bromotetrahydro-2H-pyran-3,4,5-triyl triacetate (9):

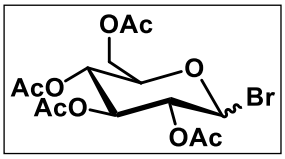

To a solution of β-D-galactose pentaacetate (2 g, 5.12 mmol) in anhydrous DCM (20 mL), HBr in acetic acid (8 mL) was added dropwise at 0 ˚C under N_2 atmosphere and stirred at RT for 2 h. After completion of the reaction (TLC analysis), the reaction mixture was quenched with NaHCO3 followed by extraction with DCM (3 × 20 mL). The combined organic layers were washed with brine, dried over anhydrous Na_2SO_4, filtered and the filtrate was concentrated under reduced pressure to afford the crude product (1.9 g, 90%). The product was immediately used in the next step without further purification.

Synthesis of (2*R*,3*R*,4*S*,5*R*,6*S*)-2-(acetoxymethyl)-6-((1,3-dioxoisoindolin-2-yl)oxy)tetrahydro-2*H*-pyran-3,4,5-triyl triacetate (10):

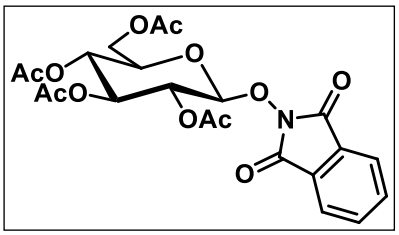

N-hydroxyphthalimide (2.8 g, 17.16 mmol, 3.5 eq.) and Et_3N (2 mL, 4 eq.) were dissolved in anhydrous DCM (30 mL). To this solution, compound **9** (1.9 g, 4.62 mmol, 1 eq.) was added and the reaction mixture was stirred for 16 h at RT. Upon completion of the reaction (TLC analysis), the reaction mixture was quenched by adding water and extracted with DCM (3 x 50 mL). The combined organic extracts were dried over Na_2SO_4 and the filtrate was concentrated under reduced pressure. The crude product was purified by silica column chromatography. Product **10** was isolated as a white solid (1 g, 44%); ^{1}H NMR (400 MHz, $CDCl_3$): δ 7.88 - 7.85 (m, 2H), 7.81 - 7.78 (m, 2H), 5.32 - 5.22 (m, 3H), 5.12 - 5.10 (m, 1H), 4.34 (dd, *J* = 12.3, 4.8 Hz, 1H), 4.16 – 4.12 (dd, *J* = 12.3, 2.5 Hz, 1H), 3.79 – 3.75 (m, 1H), 2.20 (s, 3H), 2.06 (s, 3H), 2.05 (s, 3H), 2.03 (s, 3H); ^{13}C NMR (100 MHz, $CDCl_3$): δ 150.1, 135.5, 134.9, 130.3, 123.3, 122.4, 108.8, 79.5, 77.0, 75.0, 70.7, 70.0, 62.2; HRMS (ESI): m/z for $C_{22}H_{23}NO_{12}$ $[M+Na]^+$ calc., 516.1117, found, 516.1113.

Synthesis of (2R,3R,4S,5R,6S)-2-(acetoxymethyl)-6-(aminooxy)tetrahydro-2H-pyran-3,4,5-triyl triacetate (11):

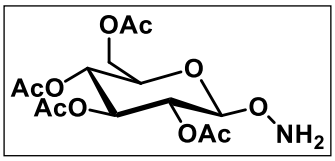

To a solution of compound **10** (300 mg, 0.6 mmol, 1 eq.) in anhydrous DCM (5 mL), hydrazine monohydrate (0.06 mL, 1 eq.) was added dropwise at 0 ˚C. The reaction mixture was slowly warmed to room temperature and stirred for ~1 h. The white suspension was filtered. The filtrate was washed with water and the aqueous layer was extracted with DCM. The combined organic extracts were dried over Na_2SO_4, filtered and the filtrate was concentrated under reduced pressure to a yield crude product **11** (150 mg, 68%), which was used for the next step without further purification.

General procedure A: Synthesis of 12a-12e:

A mixture of compound **11** (1 eq.) and DMAP (1.2 eq.) in pyridine (5 mL) was independently added to aryl sulfonyl chloride derivatives (1.2 eq.) at 0 ˚C. The reaction mixture was warmed to RT and stirred for 2 - 3 h. Upon completion of the reaction (TLC analysis), the reaction was quenched by adding 1 N HCl and extracted with EtOAC. The combined organic extracts were dried over Na_2SO_4, filtered and the filtrate was concentrated under reduced pressure to yield a crude product, which was purified by silica column chromatography.

Synthesis of 2*R*,3*R*,4*S*,5*R*,6*S*)-2-(acetoxymethyl)-6-(((2-bromophenyl)sulfonamido)oxy) tetrahydro-2*H*-pyran-3,4,5-triyl triacetate (12a):

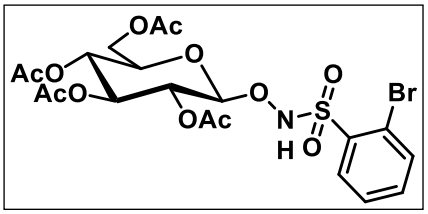

Starting with compound **11** (150 mg, 0.41 mmol), 2-bromobenzenesulfonyl chloride (125 mg, 0.49 mmol), DMAP (50 mg, 0.49 mmol) and the desired product **12a** was isolated as a pale yellow solid (230 mg, 96%); ^{1}H NMR (400 MHz, $CDCl_3$): δ 8.36 (s, 1H), 8.06 – 8.04 (m, 1H), 7.78 – 7.75 (m, 1H), 7.52 – 7.49 (m, 2H), 5.20 (d, *J* = 9.5 Hz, 1H), 5.02 (dd, *J* = 10.3, 8.2 Hz, 2H), 4.84 (dd, *J* = 9.5, 8.2 Hz, 1H), 4.27 (dd, *J* = 12.5, 4.5 Hz, 1H), 4.13 (dd, *J* = 12.5, 2.2 Hz, 1H), 3.78 – 3.74 (m, 1H), 2.09 (s, 3H), 2.05 (s, 3H), 2.01 (s, 3H), 1.97 (s, 3H); ^{13}C NMR (100 MHz, $CDCl_3$) : δ 170.8, 170.1, 169.6, 169.2, 135.5, 135.4, 134.4, 133.1, 127.9, 120.2, 104.6, 72.6, 72.4, 69.4, 67.8, 61.6, 20.9, 20.8, 20.7, 20.7; HRMS (ESI): m/z for $C_{20}H_{24}BrNO_{12}S$ $[M+Na]^+$ calcd., 604.0100, found, 604.0089.

Synthesis of (2*R*,3*R*,4*S*,5*R*,6*S*)-2-(acetoxymethyl)-6-(((5-(dimethylamino)naphthalene)-1-sulfonamido)oxy) tetrahydro-2*H*-pyran-3,4,5-triyl triacetate (12b):

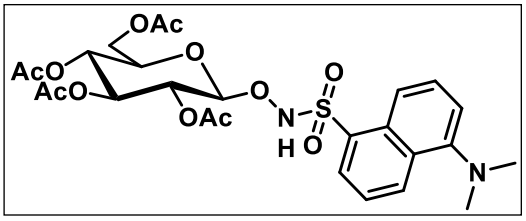

Starting with compound **11** (150 mg, 0.41 mmol), dansyl chloride (137 mg, 0.50 mmol), DMAP (50 mg, 0.50 mmol) and product **12b** was isolated as a yellow solid (228 mg, 93%); ^{1}H NMR (400 MHz, $CDCl_3$): δ 8.63 (d, *J* = 8.4 Hz, 1H), 8.21 – 8.16 (m, 2H), 7.80 (br s,1H), 7.61 – 7.52 (m, 2H), 7.21 (d, *J* = 7.56 Hz, 1H), 5.18 (t, *J* = 9.4 Hz, 1H), 4.97 (d, *J* = 8.3 Hz, 1H), 4.92 (t, *J* = 9.7 Hz, 1H), 4.82 – 4.87 (dd, *J* = 9.4, 8.5 Hz, 1H), 4.11 – 4.07 (dd, *J* = 12.5, 4.5 Hz, 1H), 4.03 – 3.99 (dd, *J* = 12.4, 2.2 Hz, 1H), 3.69 – 3.65 (m, 1H), 2.89 (s, 6H), 2.14 (s, 3H), 2.03 (s, 3H), 1.99 (s, 3H), 1.97 (s, 3H); ^{13}C NMR (100 MHz, $CDCl_3$): δ 170.7, 170.1, 169.5, 169.4, 152.6, 132.4, 132.3, 130.9, 130.0, 129.9, 129.4, 123.1, 117.8, 115.7, 104.4, 72.6, 72.2, 69.5, 67.8, 61.5, 45.5, 20.9, 20.8, 20.7; HRMS (ESI): m/z for $C_{26}H_{32}BrN_2O_{12}S$ $[M+H]^+$ calcd., 597.1749, found, 597.1743.

(2*R*,3*R*,4*S*,5*R*,6*S*)-2-(acetoxymethyl)-6-(((4-methoxyphenyl)sulfonamido)oxy)tetrahydro-2*H*-pyran-3,4,5-triyl triacetate (12c):

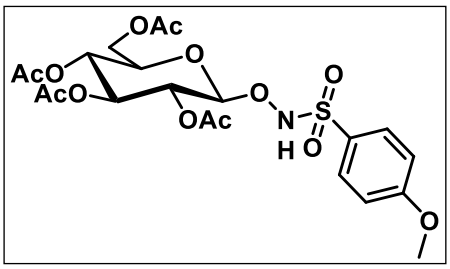

Starting with compound **11** (150 mg, 0.41 mmol), 4-methoxybenzenesulfonyl chloride (120 mg, 0.49 mmol), DMAP (50 mg, 0.49 mmol) and product **12c** was isolated as a white solid (100 mg, 86%); ^{1}H NMR (400 Hz , $CDCl_3$): δ 7.78 – 7.74 (m, 2H), 7.44 (s, 1H), 7.02 – 6.98 (m, 2H), 5.27 – 5.23 (m, 1H), 5.05 – 4.97 (m, 3H), 4.23 (dd, *J* = 7.9 and 4.6 Hz, 1H), 4.13 – 4.09 (m, 1H), 3.89 (s, 3H), 3.76 – 3.72 (m, 1H), 2.18 (s, 3H), 2.07 (s, 3H), 2.02 (s, 3H), 2.01 (s, 3H); ^{13}C NMR (100 MHz, $CDCl_3$): δ 170.8, 170.1, 169.9, 169.6, 130.8, 127.8, 114.6, 104.9, 72.6, 72.2, 69.6, 67.9, 61.6, 55.9, 20.9, 20.8, 20.7; HRMS (ESI): m/z for $C_{21}H_{27}NO_{13}S$ $[M+Na]^+$ calcd., 556.1100, found, 556.1093.

(2*R*,3*R*,4*S*,5*R*,6*S*)-2-(acetoxymethyl)-6-(((2-Nitro-4-(trifluoromethyl)phenyl)sulfonamido)oxy)tetrahydro-2*H*-pyran-3,4,5-triyl triacetate (12d):

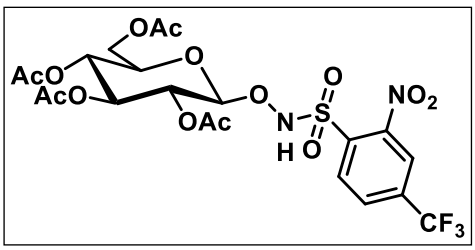

Starting with compound **11** (1.5 g, 1.1 mmol), 2-nitro-4-(trifluoromethyl)benzenesulfonyl chloride (1.436 g, 1.32 mmol), DMAP (0.516 g, 1.32 mmol) and product **12d** was isolated as orange solid (830 mg, 33%); ^{1}H NMR (400 Hz, $CDCl_3$): δ 8.69 (s, 1H), 8.19 (d, 8.1H),

8.15 (d, J = 0.9 Hz, 1H), 8.06 (dd, J = 8.2 Hz, 1H), 5.28 (t, J = 9.4 Hz, 1H), 5.09 – 5.02 (m, 2H), 4.94 (dd, J = 8.2, 1.1 Hz, 1H), 4.31 (dd, J = 7.8, 4.6 Hz, 1H), 4.18 (dd, J = 10.2, 2.2 Hz, 1H), 3.84 – 3.79 (m, 1H), 2.19 (s, 3H), 2.10 (s, 3H), 2.04 (s, 3H), 2.01 (s, 3H); ^{13}C NMR (100 MHz, $CDCl_3$): δ 170.7, 170.1, 169.7, 169.6, 148.7, 137.5, 137.2, 134.5, 133.3, 129.8, 123.1, 105.5, 72.5, 72.4, 69.8, 67.8, 61.6, 21.0, 20.8, 20.7; HRMS (ESI): m/z for $C_{21}H_{23}F_3N_2O_{14}S$ $[M+Na]^+$ calcd., 639.0719, found, 639.0725.

(2*R*,3*R*,4*S*,5*R*,6*S*)-2-(acetoxymethyl)-6-(((2,4,6-trifluorophenyl)sulfonamido)oxy)tetrahydro-2*H*-pyran-3,4,5-triyl triacetate (12e):

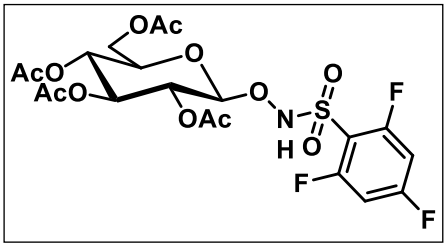

Starting with compound **11** (280 mg, 0.77 mmol), 2,4,6-trifluorobenzenesulfonyl chloride (213 mg, 0.92 mmol), DMAP (97 mg, 0.92 mmol) and product **12e** was isolated as a pale yellow solid (200 mg, 80%); ^{1}H NMR (400 MHz, $CDCl_3$): 7.98 (s, 1H), 6.86 – 6.82 (t, *J* = 8.5 Hz, 2H), 5.25 (t, *J* = 9.5 Hz, 1H), 5.06 - 5.01 (m, 2H), 4.88 (dd, *J* = 8.5, 1.0 Hz, 1H), 4.29 (dd, *J* = 7.9, 4.5 Hz, 1H), 4.16 (dd, *J* = 10.2, 2.2 Hz, 1H), 3.80 – 3.76 (m, 1H), 2.10 (s, 3H), 2.06 (s, 3H), 2.03 (s, 3H), 1.99 (s, 3H); ^{13}C NMR (100 MHz, $CDCl_3$): δ 170.8, 170.0, 169.6, 169.6, 105.2, 102.9, 102.6, 102.3, 72.5, 72.4, 70.4, 69.4, 67.9, 61.6, 20.9, 20.7, 20.7; HRMS (ESI): m/z for $C_{20}H_{22}F_3NO_{12}S$ $[M+Na]^+$ calcd., 558.0712, found, 558.0711.

General procedure B: Synthesis of 13a-13e:

Compound **13a-13e** (1 eq.) was dissolved in methanol (5 mL) under a nitrogen atmosphere. Sodium methoxide (4 eq.) in methanol (2 mL) was added to the solution at 0 ˚C. The mixture was warmed at RT and stirred for ~3 h. Upon completion of the reaction (TLC analysis), cation-exchange resin (H^+) was added, filtered and washed with MeOH. The solvent was evaporated under reduced pressure. The crude product was purified by prep-HPLC column chromatography (MeOH/H_2O) to give the desired compounds.

2-bromo-*N*-(((2*S*,3*R*,4*S*,5*S*,6*R*)-3,4,5-trihydro-6-(hydroxymethyl)tetrahydro-2*H*-pyran-2-yl)oxy)benzenesulfonamide (13a):

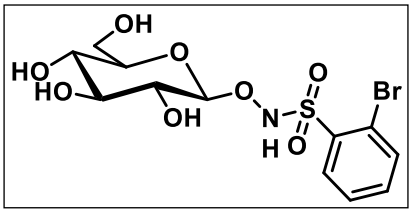

Starting with compound **12a** (210 mg, 0.36 mmol), sodium methoxide (78 mg, 1.44 mmol), product **13a** was isolated as a white solid (30 mg, 20%); ^{1}H NMR (400 MHz, CD_3OD): δ 8.21- 8.17 (m, 1H), 7.85 – 7.83 (m, 1H), 7.59 - 7.54 (m,

2H), 4.65 (d, *J* = 8.2 Hz, 1H), 3.82 (dd, *J* = 11.3, 1.9 Hz, 1H), 3.64 (dd, *J* = 11.9, 5.0 Hz, 1H), 3.34 (d, *J* = 8.9 Hz, 1H), 3.28 – 3.22 (m, 2H), 3.16 (dd, *J* = 8.9, 8.3 Hz, 1H) ; ^{13}C NMR (100 MHz, CD_3OD): δ 137.8, 136.5, 136.0, 134.6, 129.1, 123.3, 107.9, 78.1, 77.9, 73.0, 71.2, 62.5; HRMS (ESI): m/z for $C_{12}H_{16}BrNO_8S$ $[M+Na]^+$ calcd., 435.9672, found, 435.9678.

5-(dimethylamino)-*N*-(((2*S*,3*R*,4*S*,5*S*,6*R*)-3,4,5-trihydro-6-(hydroxymethyl)tetrahydro-2*H*-pyran-2-yl)oxy)naphthalene-1-sulfonamide (13b):

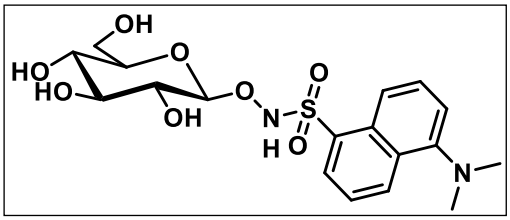

Starting with compound **12b** (210 mg, 0.35 mmol), sodium methoxide (76 mg, 1.40 mmol), product **13b** was isolated as a yellow solid (33 mg, 22%); ^{1}H NMR (400 MHz, CD_3OD): δ 8.61 (d, *J* = 8.5 Hz, 1H), 8.51 (d, *J* = 8.6 Hz, 1H), 8.37 (d, *J* = 7.2 Hz, 1H), 7.65 (q, *J* = 10.1Hz, 2H), 7.42 (d, *J* = 7.5 Hz, 1H), 4.52 (d, *J* = 8.1 Hz, 1H), 3.72 (d, *J* = 10.8 Hz, 1H), 3.55 (dd, *J* = 11.8, 4.9 Hz, 1H), 3.26 – 3.09 (m, 4H), 2.99 (s, 6H); ^{13}C NMR (100 MHz, CD_3OD): δ 134.1, 133.3, 131.5, 131.4, 130.4, 129.2, 125.1, 122.2, 117.2, 107.7, 78.0, 77.9, 73.1, 71.1, 62.5, 46.1; HRMS (ESI): m/z for $C_{18}H_{24}N_2O_8S$ $[M+H]^+$ calcd., 429.1326, found, 429.1331.

4-methoxy-*N*-(((2*S*,3*R*,4*S*,5*S*,6*R*)-3,4,5-trihydroxy-6-(hydroxymethyl)tetrahydro-2*H*-pyran-2-yl)oxy)benzenesulfonamide (13c):

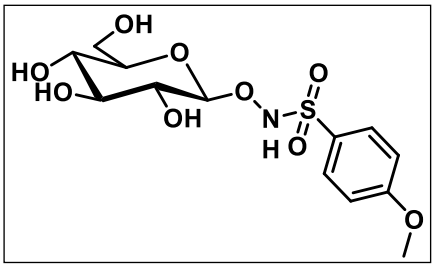

Starting with compound **12c** (300 mg, 1.3 mmol), sodium methoxide (150 mg, 3.09 mmol), product **13c** was isolated as a white solid (30 mg, 21%); ^{1}H NMR (400 MHz, CD_3OD): δ 7.94 – 7.92 (m, 2H), 7.11 – 7.07 (m, 2H), 4.69 (d, *J* = 8.2 Hz, 1H), 3.89 (s, 3H), 3.85 (dd, *J* = 11.9, 1.6 Hz, 1H), 3.69 – 3.64 (m, 1H), 3.37 (t, *J* = 9.0 Hz, 1H), 3.29 – 3.27 (m, 2H), 3.21 (dd, *J* = 9.0, 8.3 Hz, 1H); ^{13}C NMR (100 MHz, CD_3OD): δ 132.1, 129.8, 115.2, 107.6, 78.2, 78.1, 73.2, 71.3, 62.6, 56.3, 30.7; HRMS (ESI): m/z for $C_{13}H_{19}NO_9S$ $[M+H]^+$ calc., 366.0859, found, 366.0858.

2-nitro-4-(trifluoromethyl)-*N*-(((2*S*,3*R*,4*S*,5*S*,6*R*)-3,4,5-trihydroxy-6-(hydroxymethyl)tetrahydro-2*H*-pyran-2-yl)oxy)benzenesulfonamide (13d):

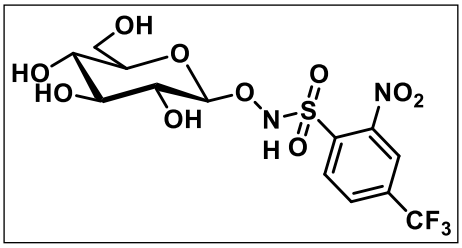

Starting with compound **12d** (800 mg, 1.3 mmol), sodium methoxide (281 mg, 5.2 mmol), product **13d** was isolated as a pale yellow solid (600 mg, 98%); ^{1}H NMR (400 MHz, CD_3OD): δ 8.46 (d, *J* = 8.2 Hz, 1H), 8.32 (d, *J* = 1.1 Hz), 8.17 (dd, *J* = 8.2, 1.1 Hz, 1H), 4.76 (d, *J* = 8.2 Hz, 1H), 3.85 (dd, *J* = 11.8, 2.0 Hz, 1H), 3.67 (dd, *J* = 11.8, 5.1 Hz, 1H), 3.40 – 3.34 (m, 2H), 3.27 – 3.25 (m, 1H), 3.17 (dd, *J* = 9.0, 8.2 1H)); ^{13}C NMR (100 MHz, CD_3OD): δ 150.1, 135.4, 135.1, 130.2, 123.3, 122.5, 78.1, 78.0, 73.3, 71.2, 62.5; HRMS (ESI): m/z for $C_{13}H_{15}F_3N_2O_{10}S$ $[M+Na]^+$ calcd., 471.0292, found,471.0299.

2,4,6-trifluoro-*N*-(((2*S*,3*R*,4*S*,5*S*,6*R*)-3,4,5-trihydroxy-6-(hydroxymethyl)tetrahydro-2*H*-pyran-2-yl)oxy)benzenesulfonamide (13e):

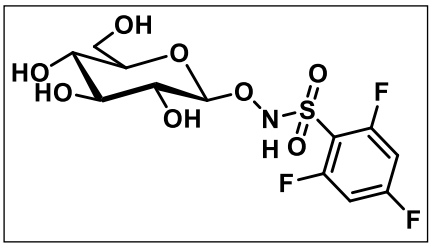

Starting with compound **12e** (350 mg, 1.3 mmol), sodium methoxide (145 mg, 3.09 mmol), product **13e** was isolated as pale yellow solid (32 mg, 13%); ^{1}H NMR (400 MHz, CD_3OD): δ 7.12 (t, *J* = 9.0 Hz, 2H), 4.68 (d, *J* = 8.1 Hz, 1H), 3.85 (dd, *J* = 11.9, 1.9 Hz, 1H), 3.66 (dd, *J* = 11.9, 5.1 Hz, 1H), 3.39 – 3.34 (m, 1H), 3.27 – 3.29 (m, 2H), 3.23 – 3.19 (m, 1H); ^{13}C NMR (100 MHz, CD_3OD): δ 107.9, 103.5, 103.3, 103.0, 78.2, 77.9, 73.1, 71.2; ^{19}F NMR (376 MHz, CD_3OD): δ -103.4 (d, *J* = 11.8 Hz), -99.5 (t, *J* = 11.9 Hz); HRMS (ESI): m/z for $C_{12}H_{14}F_3NO_8S$ $[M+H]^+$ calcd., 390.0465, found, 390.0427.

Synthesis of 2-bromobenzenesulfinic acid (14):

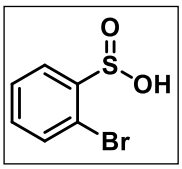

To a solution of 2-bromobenzenesulfonyl chloride (100 mg, 0.39 mmol) in THF (5 mL) was added $NaBH_4$ (85 mg, 2.24 mmol) in portion at 0 ˚C. The reaction mixture was stirred for 2- 3 h. Upon completion of the reaction (TLC analysis), the reaction mixture was quenched by aqueous HCl to maintain acidic pH <2 on an ice bath and the resulting mixture was extracted with $CHCl_3$. The organic layer was washed with brine, dried over Na_2SO_4, filtered and the filtrate was concentrated under reduced pressure to yield the crude product which was purified by prep-HPLC to give compound **14** as white crystalline solid (60 mg, 69%): ^{1}H NMR (400 MHz, DMSO-d_6): δ 7.85 – 7.82 (dd, *J* = 7.7, 1.6 Hz, 1H), 7.70 (d, *J* = 7.7 Hz, 1H), 7.61 (t, *J* = 7.3 Hz, 1H), 7.51 – 7.47 (m, 1H); ^{13}C NMR (100 MHz, DMSO-d_6): δ 147.2, 133.4, 133.2, 128.4, 125.2, 119.9; HRMS (ESI): m/z for $C_6H_5BrO_2S$ $[M+H]^+$ calcd., 220.9266, found, 220.9268.

3.4.2. HNO detection by fluorescence study

Stock solutions of **5** (1 mM), **13a-13e**, and **4** (5 mM) in DMSO. A stock solution of β-glucosidase from almonds (50 U/mL) in phosphate buffer saline (10 mM, pH 7.4) was prepared. The reaction mixture was prepared by adding 10 μM of **5** (2 μL, 1 mM), 50 μM **of 13a-13e** (2 μL, 5 mM) along with 10 U/mL β-glucosidase (40 μL, 50 U/mL) from the stock solution and the volume was adjusted to 200 μL using phosphate buffer saline (10 mM, pH 7.4) in a 96-well plate and then incubated for 6 h at 37 ˚C. The fluorescence (excitation at 370 nm; emission at 460 nm) was measured using an Ensight Multimode Plate Reader (PerkinElmer) (Figure 3.2).

3.4.3. Nitric oxide detection by Griess assay

5 mM stock solution of compound **13a** and **4** in DMSO was prepared. A typical reaction mixture consisted of compounds **13a** or **4** by mixing 2 μL from 5 mM stock solution and in the presence or absence of 10 U/mL β-glucosidase (40 μL, 50 U/mL) with phosphate buffer saline (pH 7.4, 10 mM) to make 200 μL final volume in 96 well plates (with lid) and incubated for 6 h at 37 ºC. To this, 14 μL of Griess reagent was added in each well and incubated for 25 min at 37 ºC. Absorbance was measured at 540 nm on the Ensight Varioskan microtiter plate reader. The amount of NO released was estimated using a standard calibration curve generated with different concentrations of sodium nitrite ($NaNO_2$) solution (0 – 50 μM) using Ensight Multimode Plate Reader (PerkinElmer). The data represented here is average of 3 repeats (Figure 3.3).

3.4.4. Decomposition study by HPLC

A stock solution of **13a** and **14** (10 mM) was prepared in DMSO and β-glucosidase (10 U/mL from 50 U/mL stock solution in PBS pH 7.4). The reaction mixture contained compound **13a** (5 μL, 10 mM), in the presence or absence of β-glucosidase (200 μL, 50 U/mL) in PBS pH 7.4 (1mL) and incubated at 37 ºC. 100 μL aliquots of the reaction mixture were taken out at pre-determined time points and the reaction mixture was quenched by adding 100 μL of methanol. The samples were centrifuged at 10000 rpm for 10 min at 4 ºC and injected (100 μL) in high-performance liquid chromatography (HPLC Agilent Technologies 1260 Infinity) at different time points. The mobile phase was water (0.1% TFA)/Acetonitrile (0.1% TFA). The stationary phase was a C-18 reverse phase column (Phenomenex, 5 μm, 4.6 x 250 mm). A multistep gradient was used with the flow rate of 1 mL/min starting with 70:30 → 0 min, 70:30 to 60: 40 → 0 - 3 min, 60:40 to 50: 50 → 3 - 6 min, 50:50 to 40: 60 → 6 – 9 min, 40:60

to 30: 70 → 9 - 10 min, 30:70 to 50: 50 → 10 - 12 min, 50:50 to 60: 40 → 12 - 13 min, 60:40 to 70: 30 → 13 - 15 min, 70:30 to 70: 30 → 15 - 18 min. The retention time for **13a** is 6.1 min and for **14** is 8.4 min. The decomposition of **13a** and formation of **14** was monitored at 230 nm. Authentic **14** (50 μM) in phosphate buffer saline was injected in HPLC and used as a control (Figure 3.6).

3.4.5. Cell viability Assay

Breast cancer cells (MCF-7) were seeded at a concentration of 1×10^4 cells/well overnight in a 96-well plate in complete DMEM medium supplemented with 5% FBS (fetal bovine serum) and 1% antibiotic solution in an atmosphere of 5% CO_2 at 37 ˚C. Cells were exposed to varying concentrations of the test compounds prepared as a DMSO stock solution so that the final concentration of DMSO was 0.5%. The cells were incubated for 24 h at 37 ˚C. A 0.5 mg/mL stock solution of 3-(4, 5-dimethylthiazol-2-yl)-2, 5-diphenyl tetrazolium bromide (MTT) was prepared in DMEM and 100 μL of the resulting solution was added to each well. After 4 h incubation, the media was removed carefully and 100 μL of DMSO was added. Spectrophotometric analysis of each well using a microplate reader (Thermo Scientific Varioscan) at 570 nm was carried out to estimate cell viability (Figure 3.12 – Figure 3.13).

3.5. NMR spectra

^{1}H NMR spectra for compound **10**

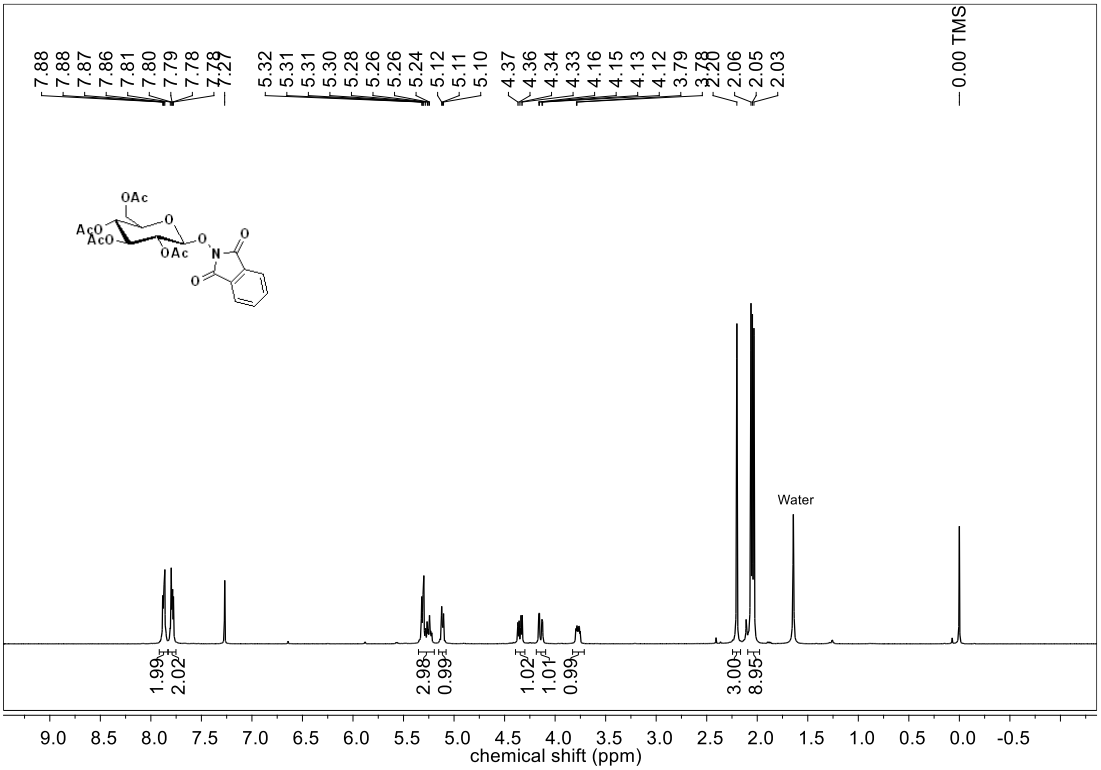

^{13}C NMR spectra for compound **10**

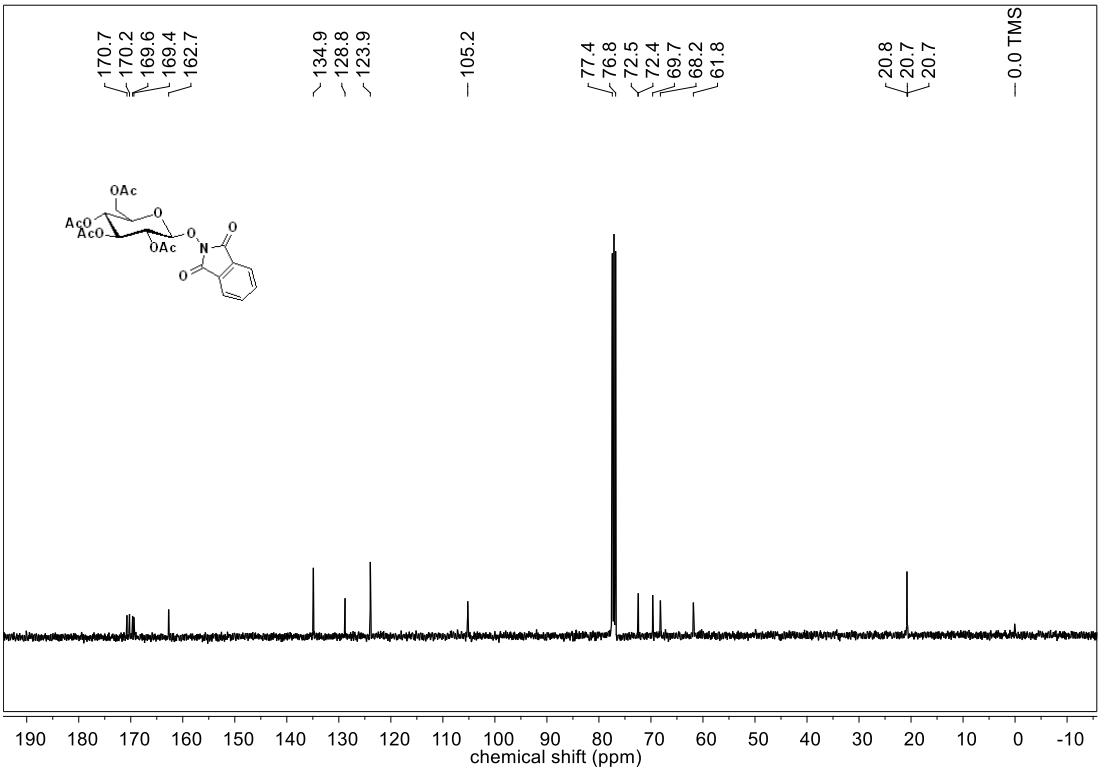

^{1}H NMR spectra for compound **12a**

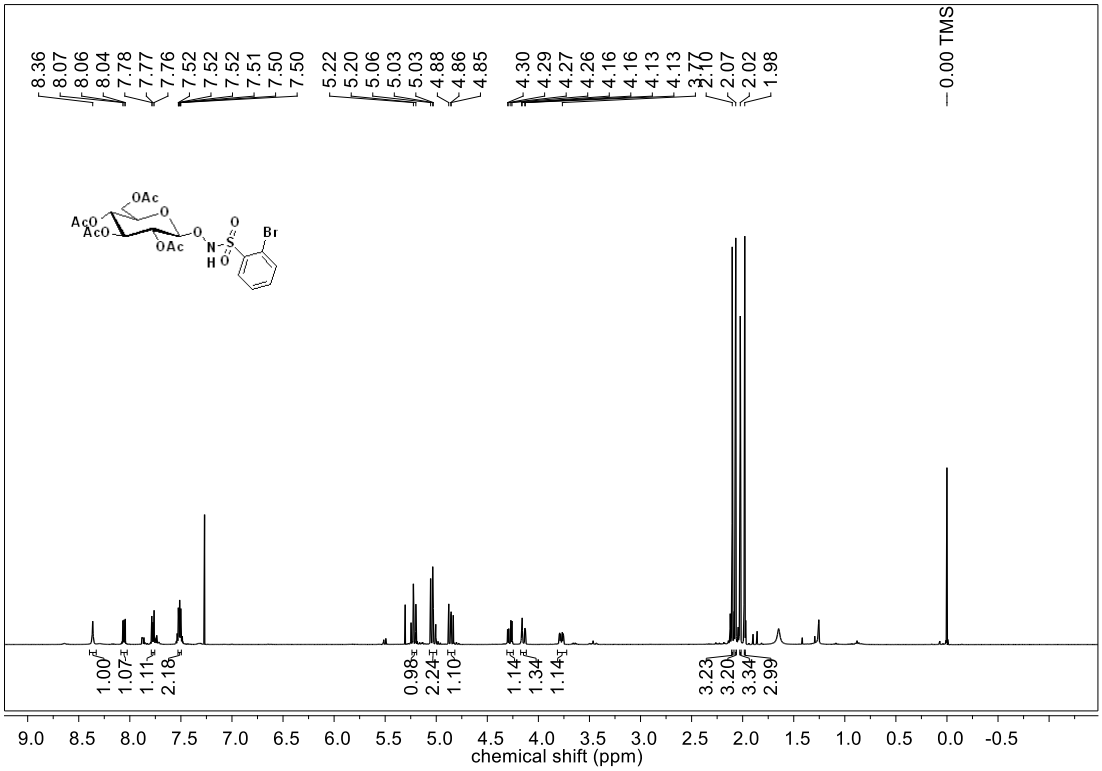

^{13}C NMR spectra for compound **12a**

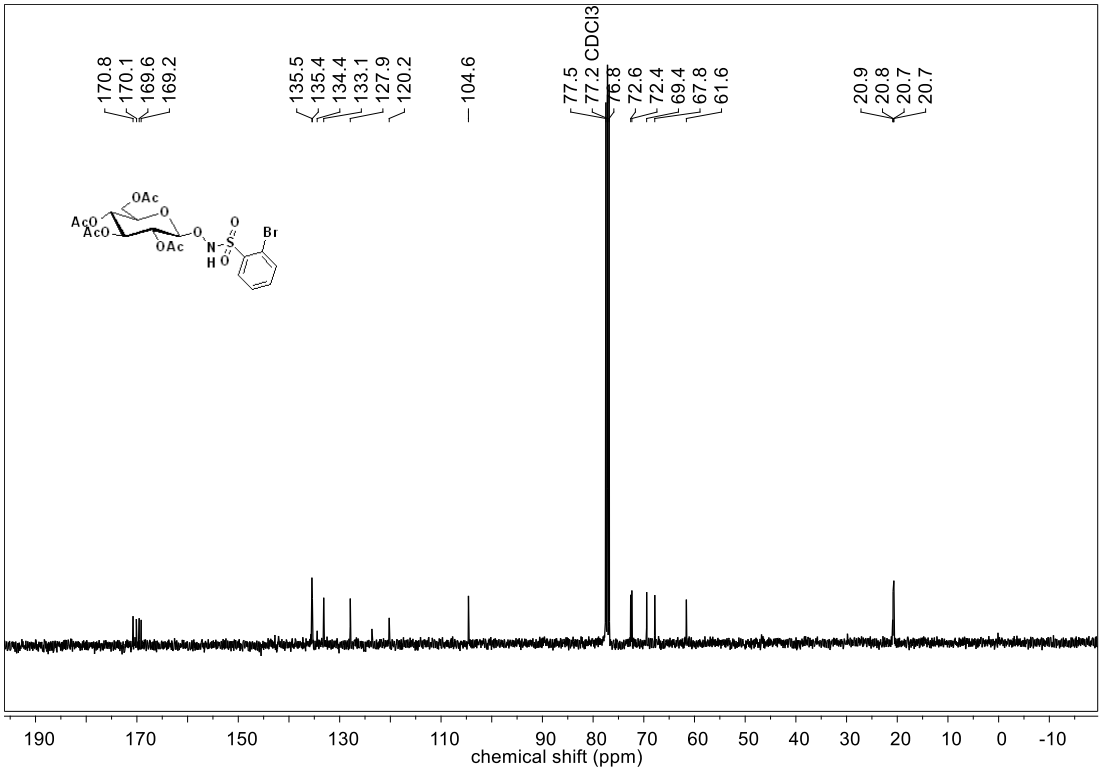

^{1}H NMR spectra for compound **12b**

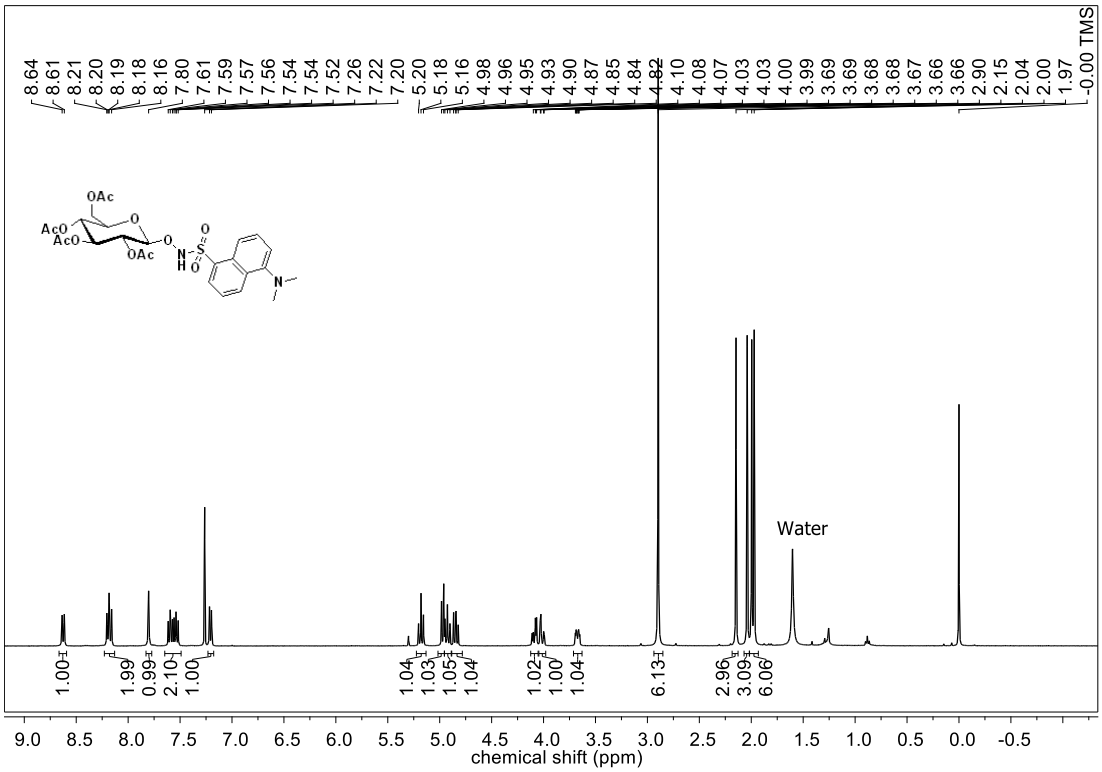

^{13}C NMR spectra for compound **12b**

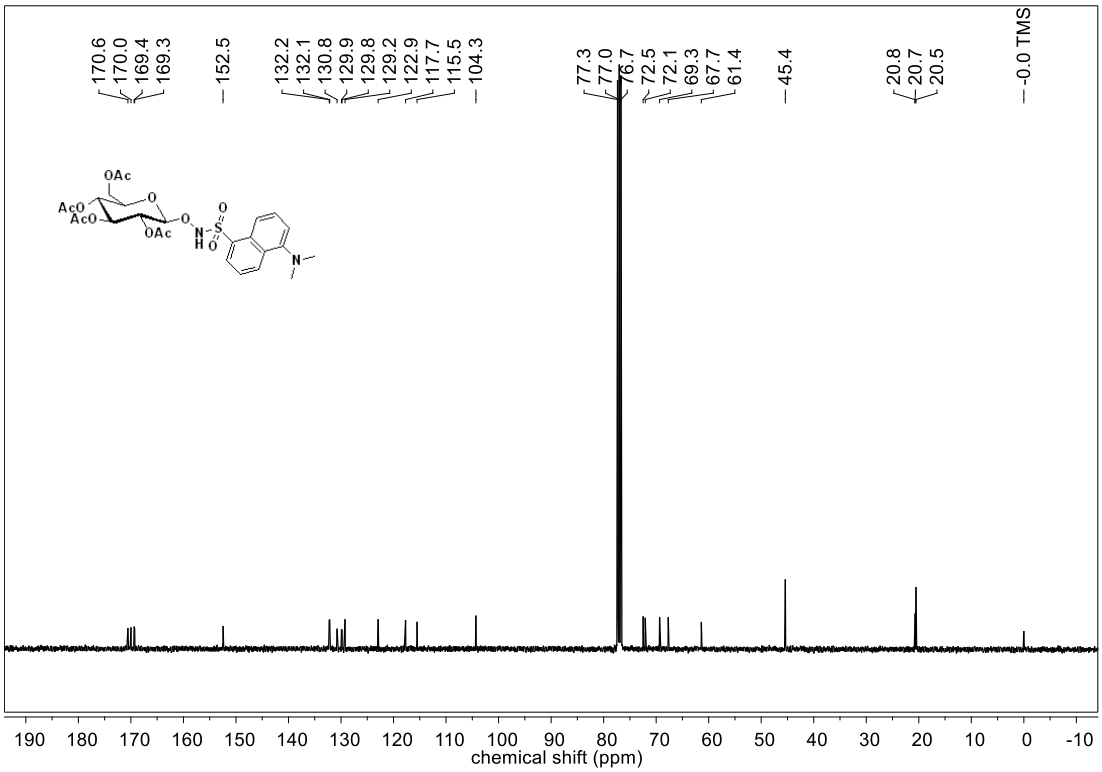

^{1}H NMR spectra for compound **12c**

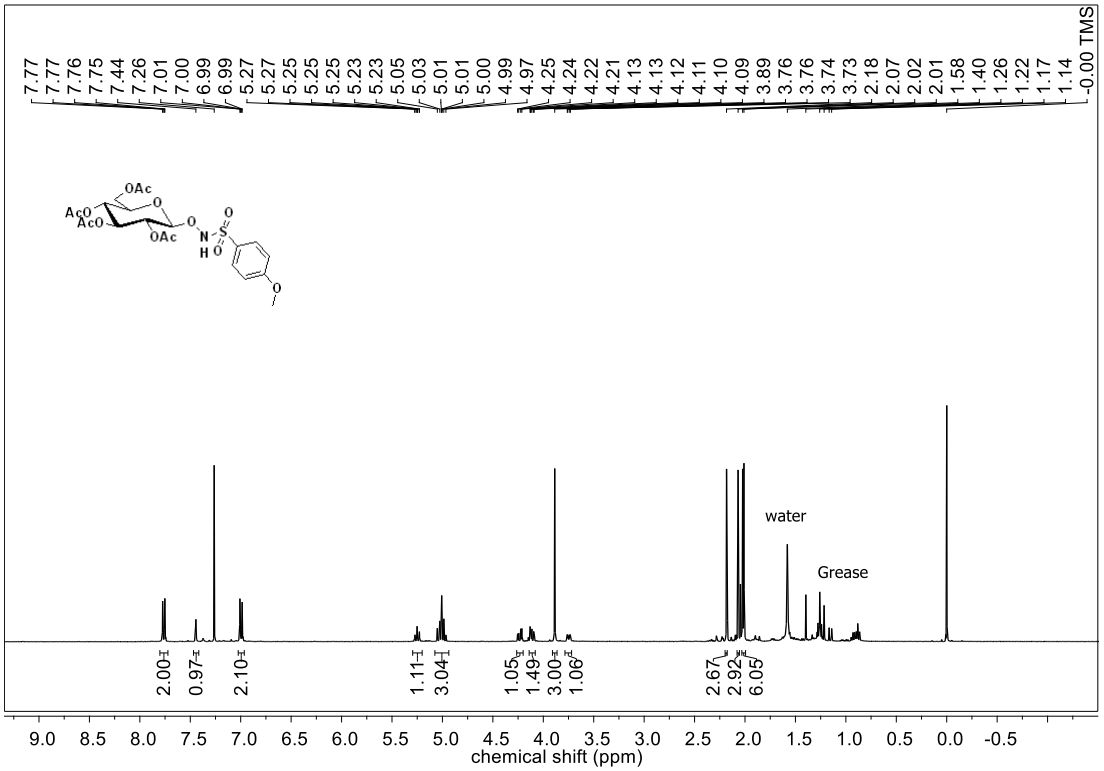

^{13}C NMR spectra for compound **12c**

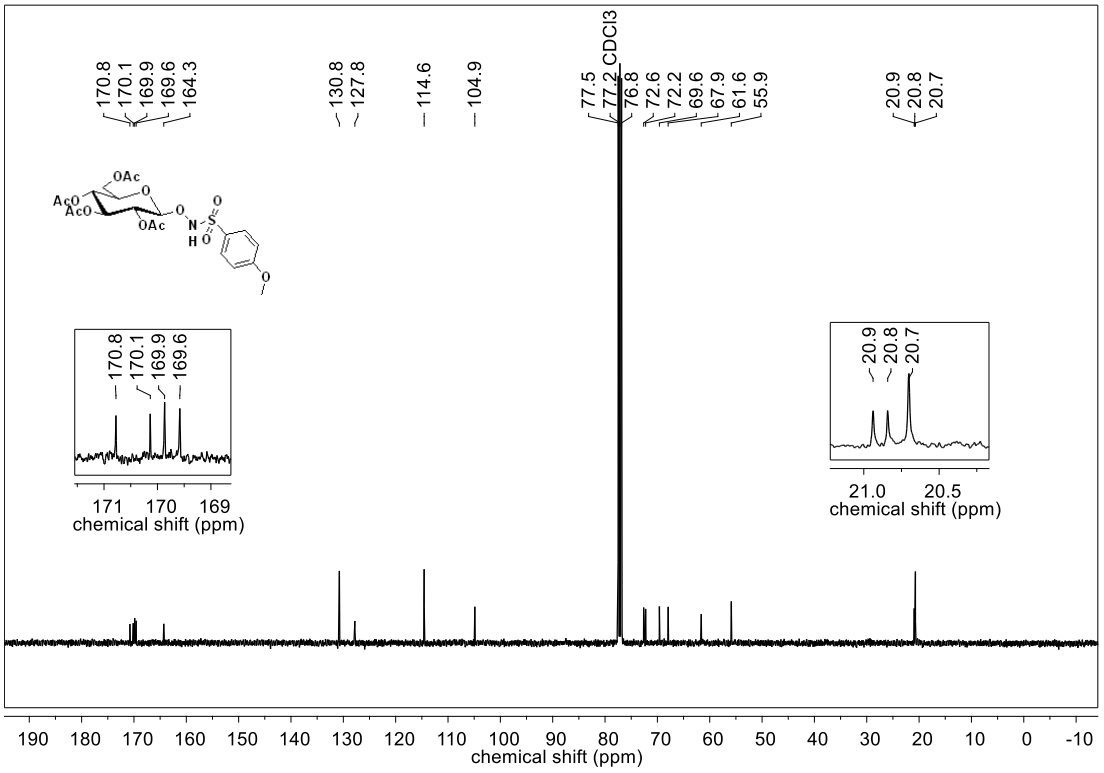

^{1}H NMR spectra for compound **12d**

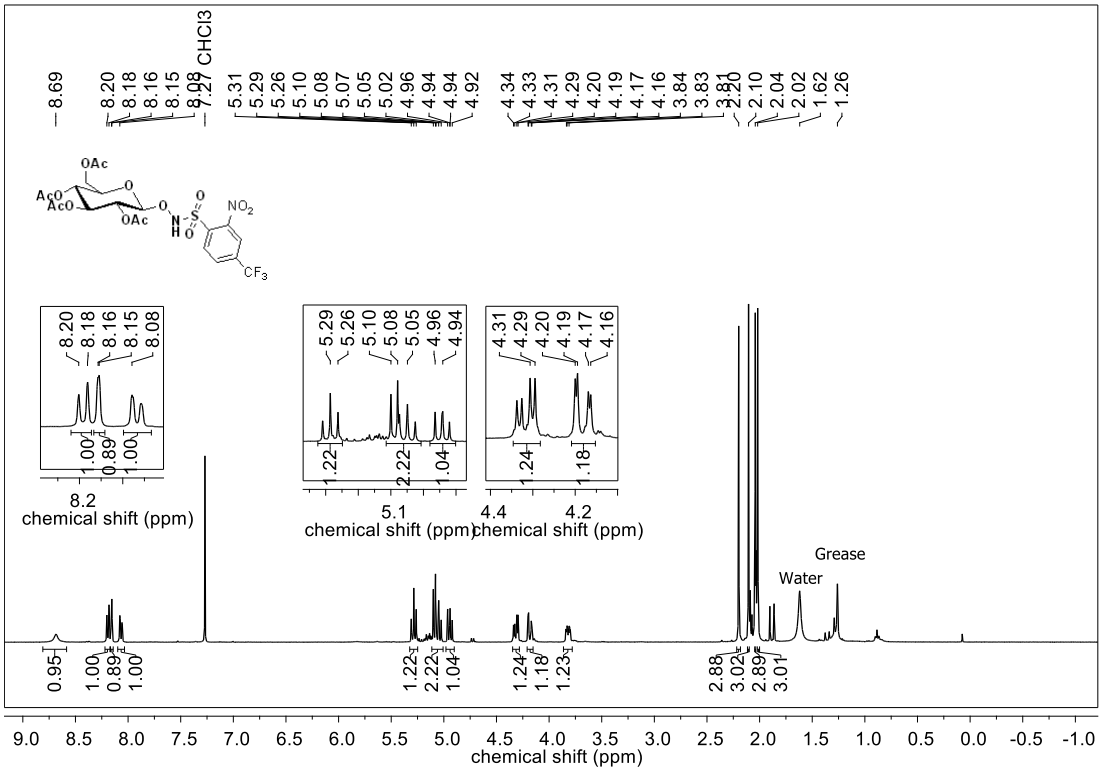

^{13}C NMR spectra for compound **12d**

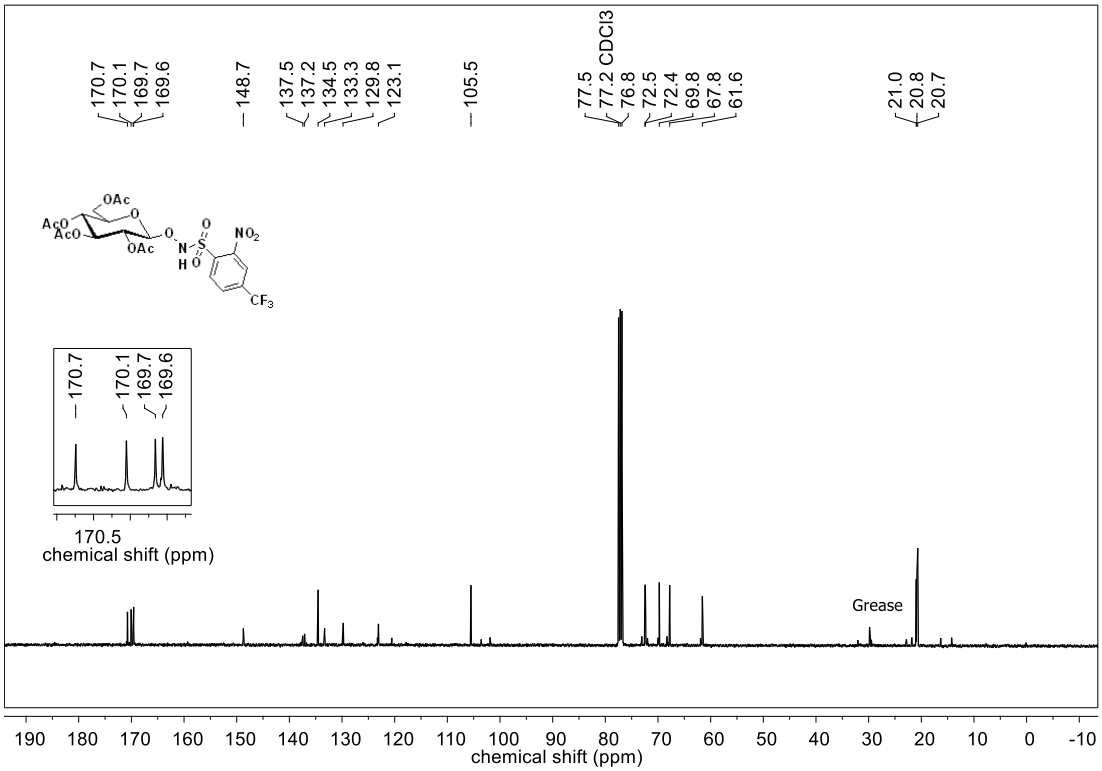

^{1}H NMR spectra for compound **12e**

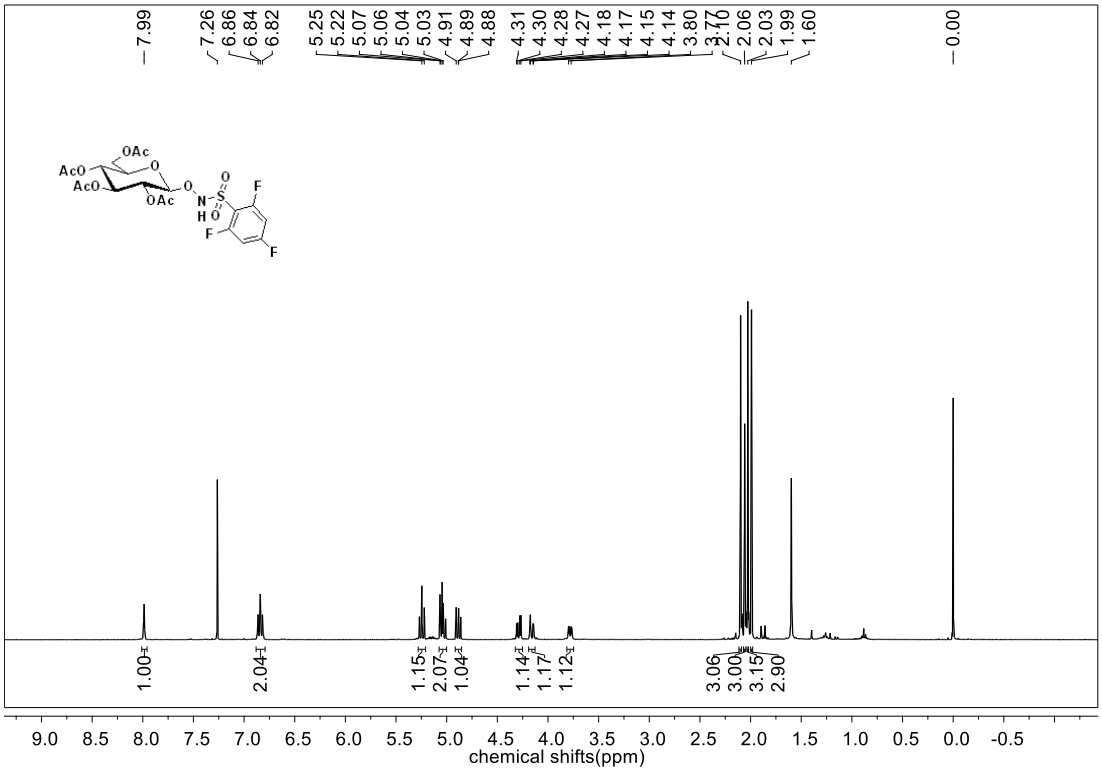

^{13}C NMR spectra for compound **12e**

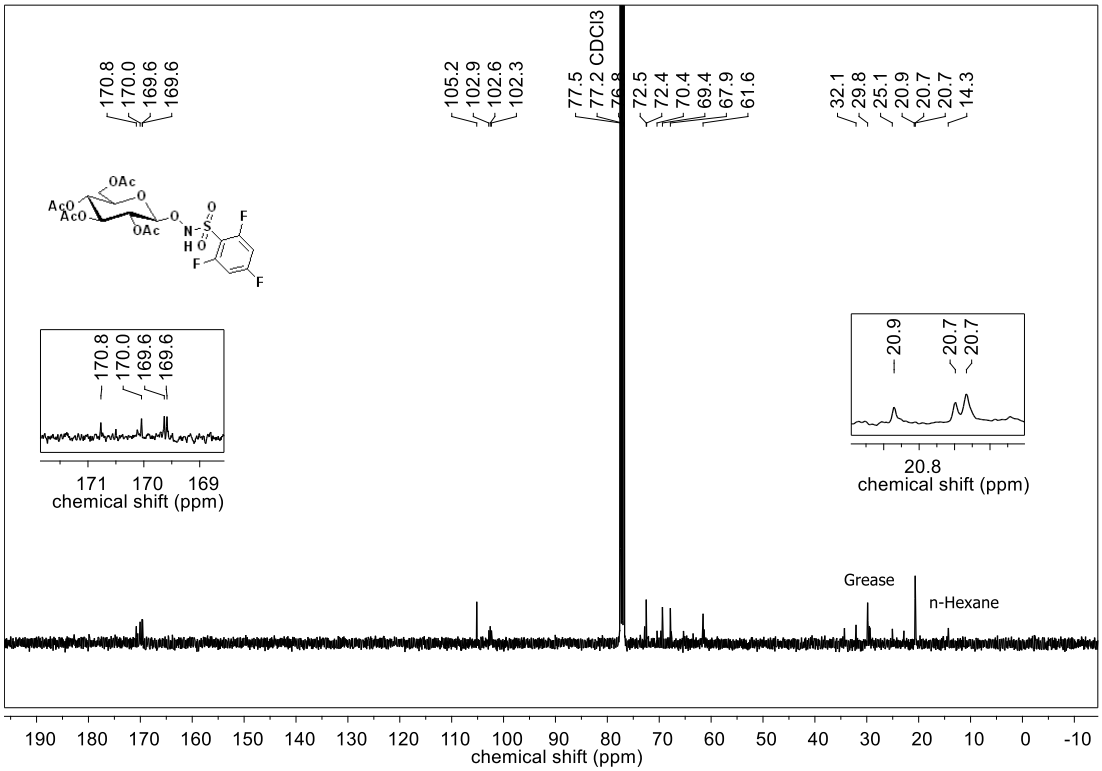

^{1}H NMR spectra for compound **13a**

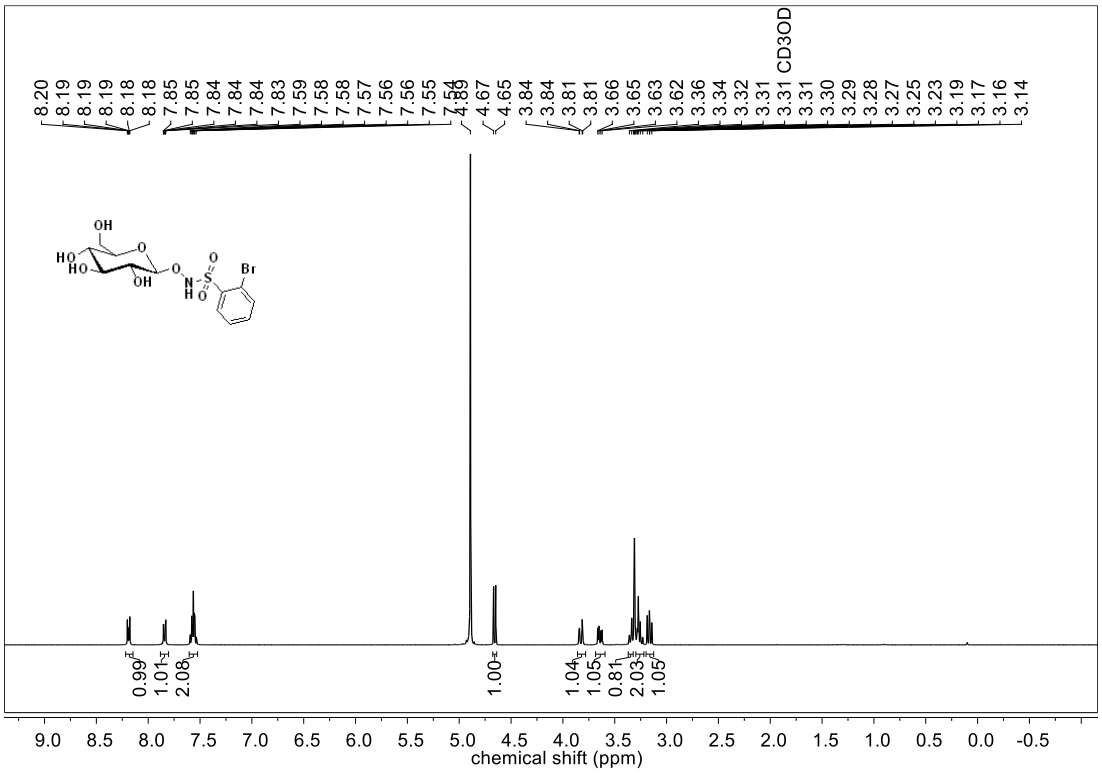

^{13}C NMR spectra for compound **13a**

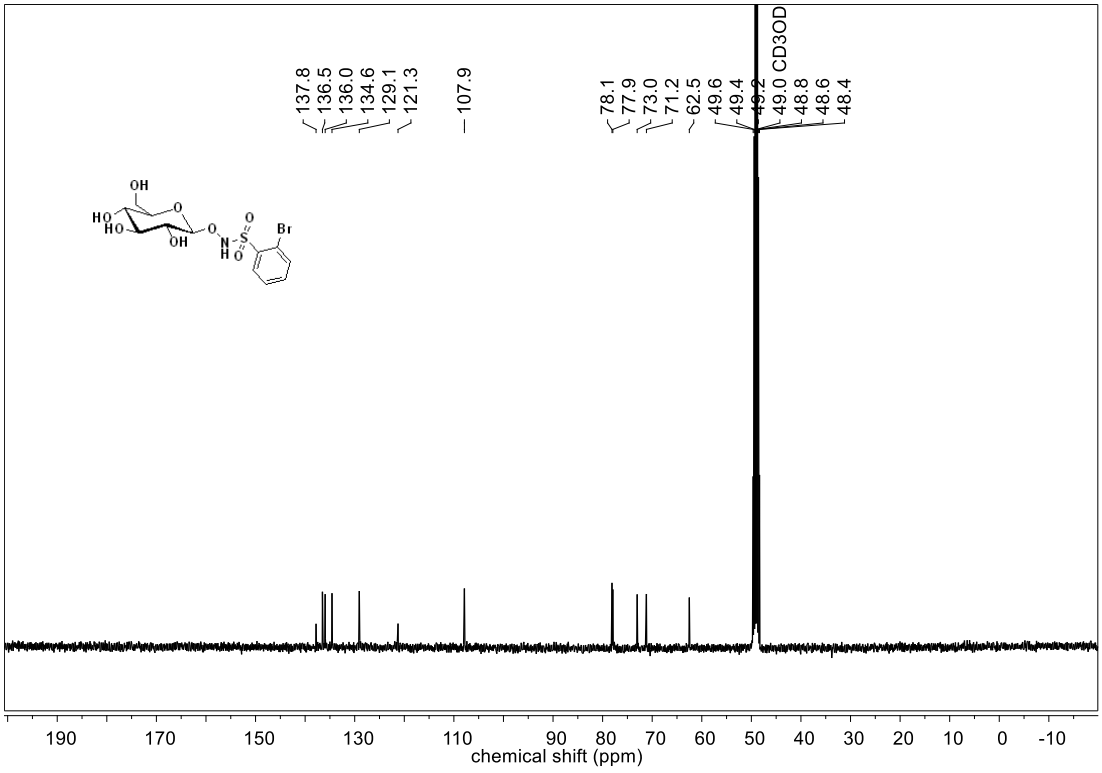

^{1}H NMR spectra for compound **13b**

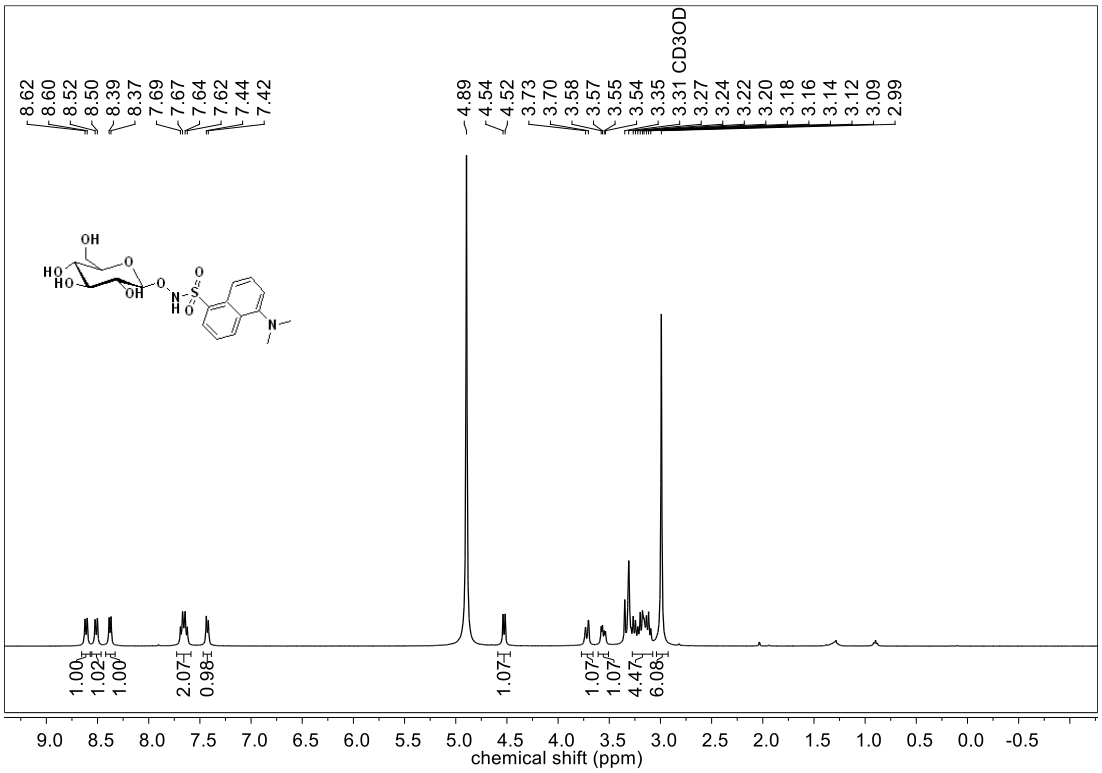

^{13}C NMR spectra for compound **13b**

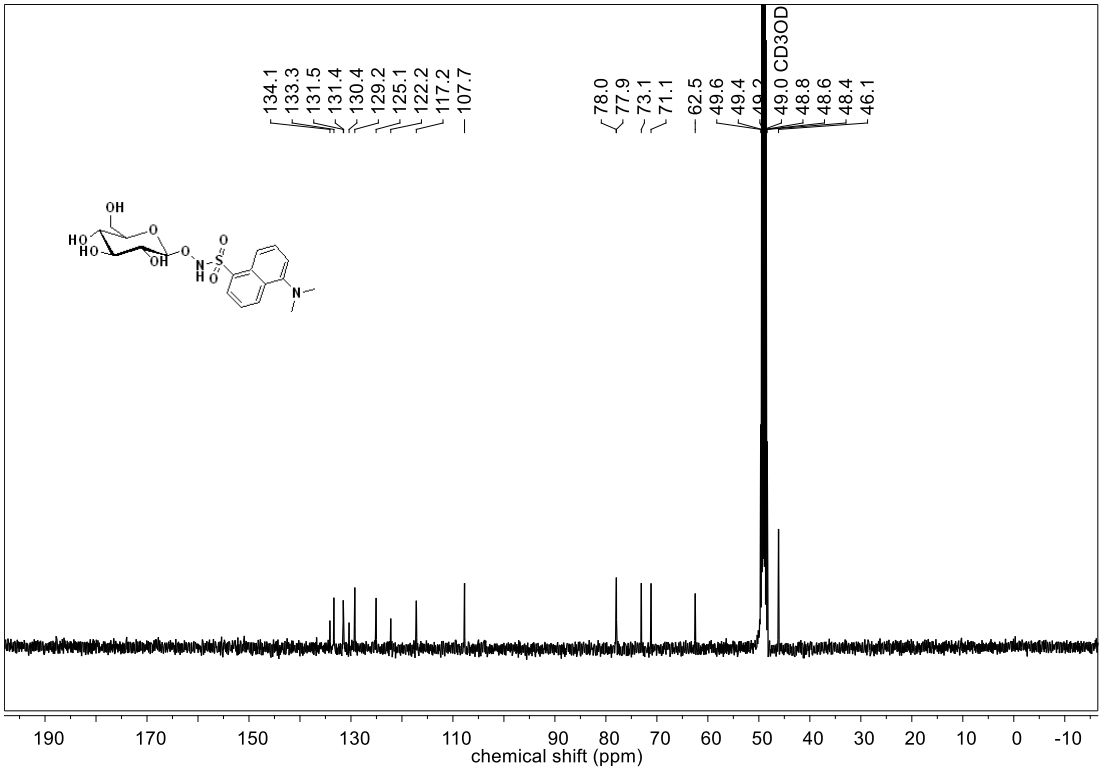

^{1}H NMR spectra for compound **13c**

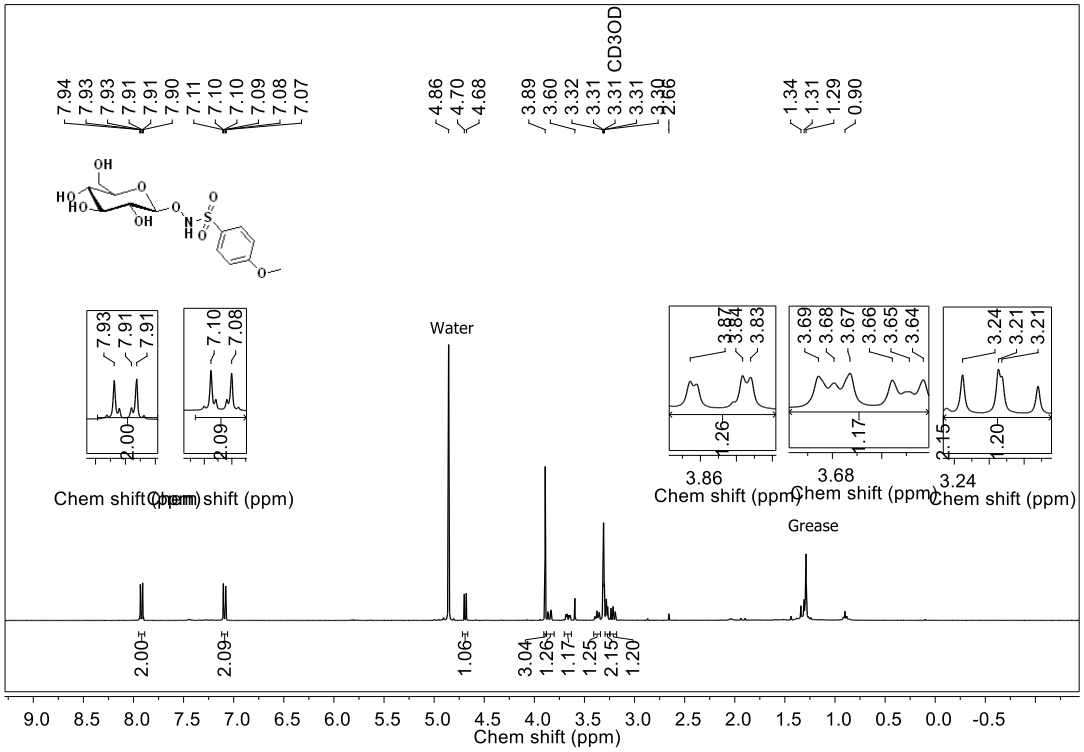

^{13}C NMR spectra for compound **13c**

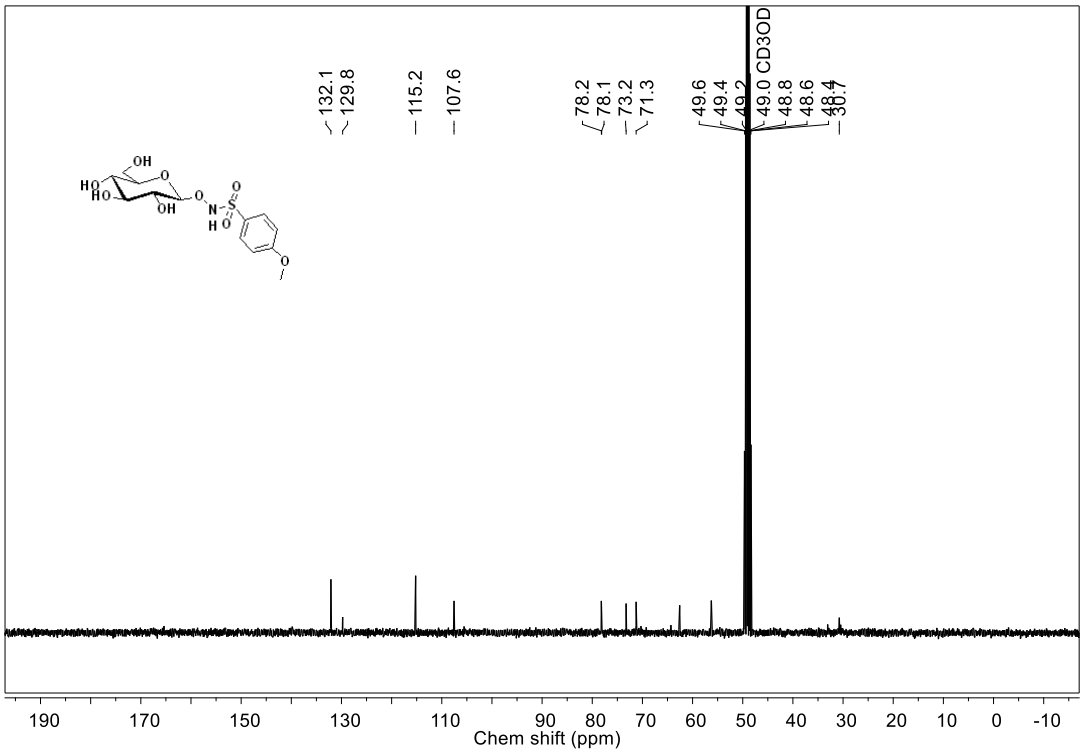

^{1}H NMR spectra for compound **13d**

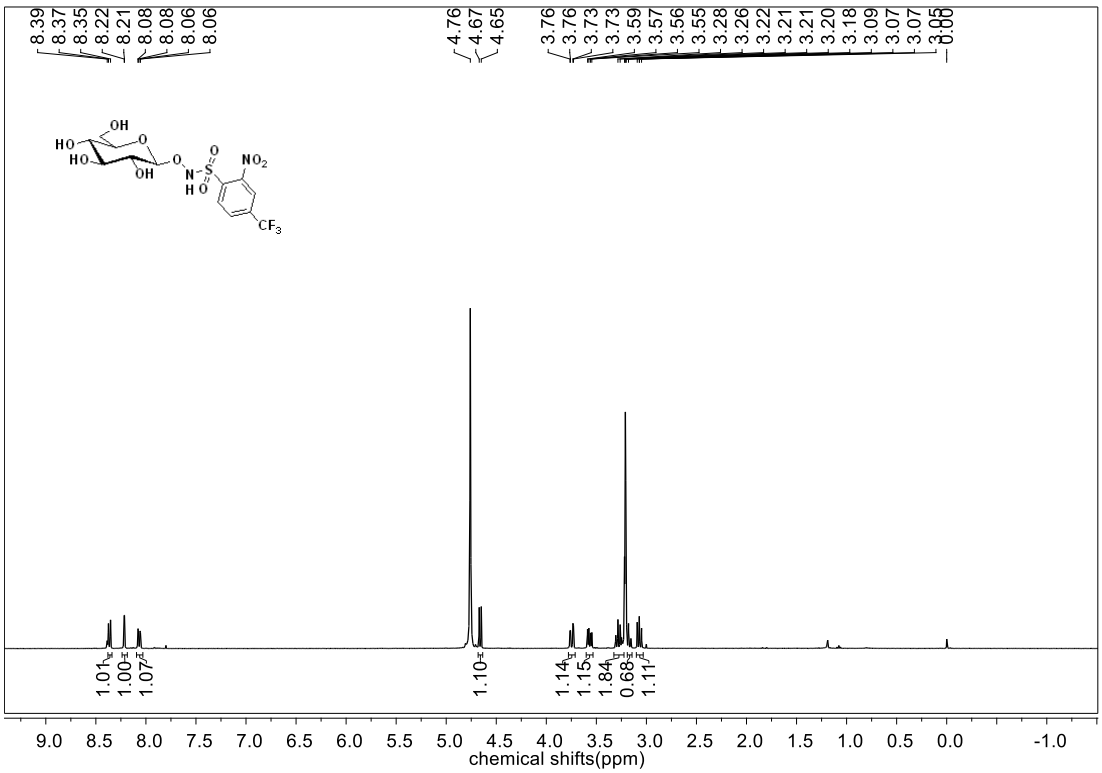

^{13}C NMR spectra for compound **13d**

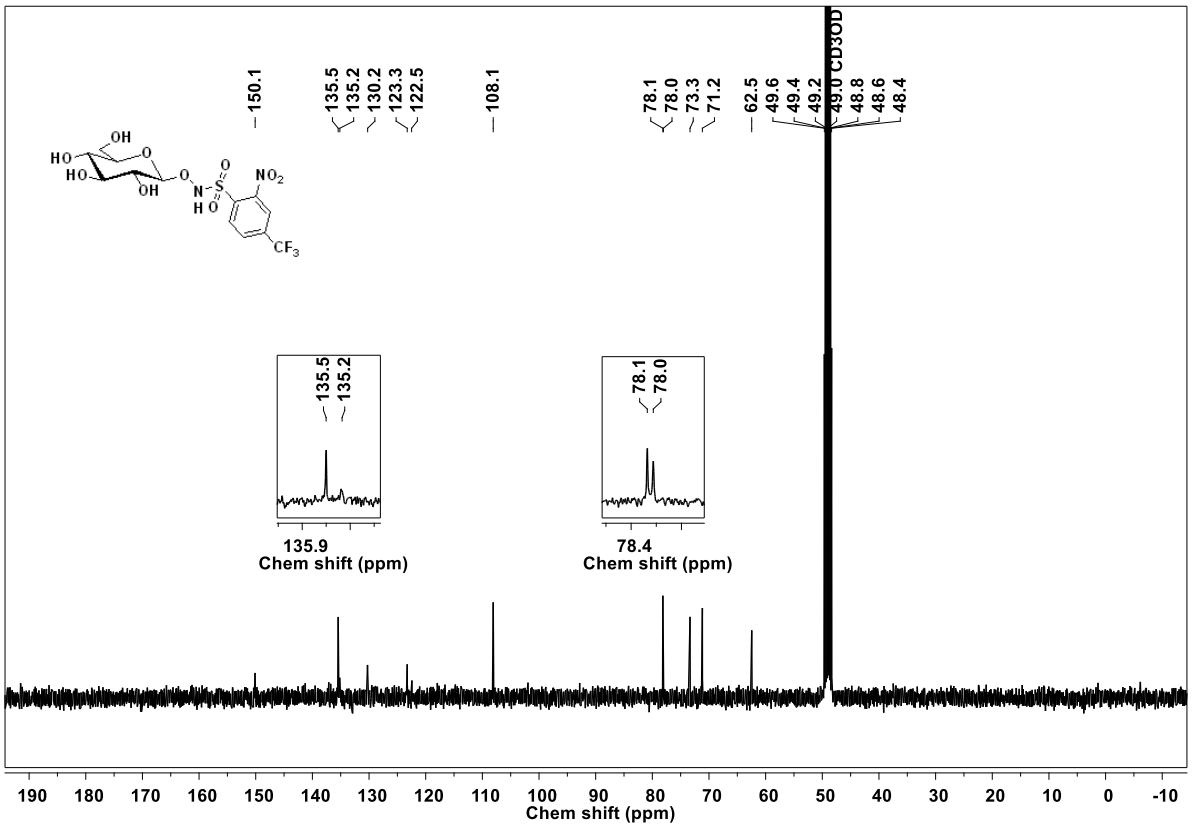

^{1}H NMR spectra for compound **13e**

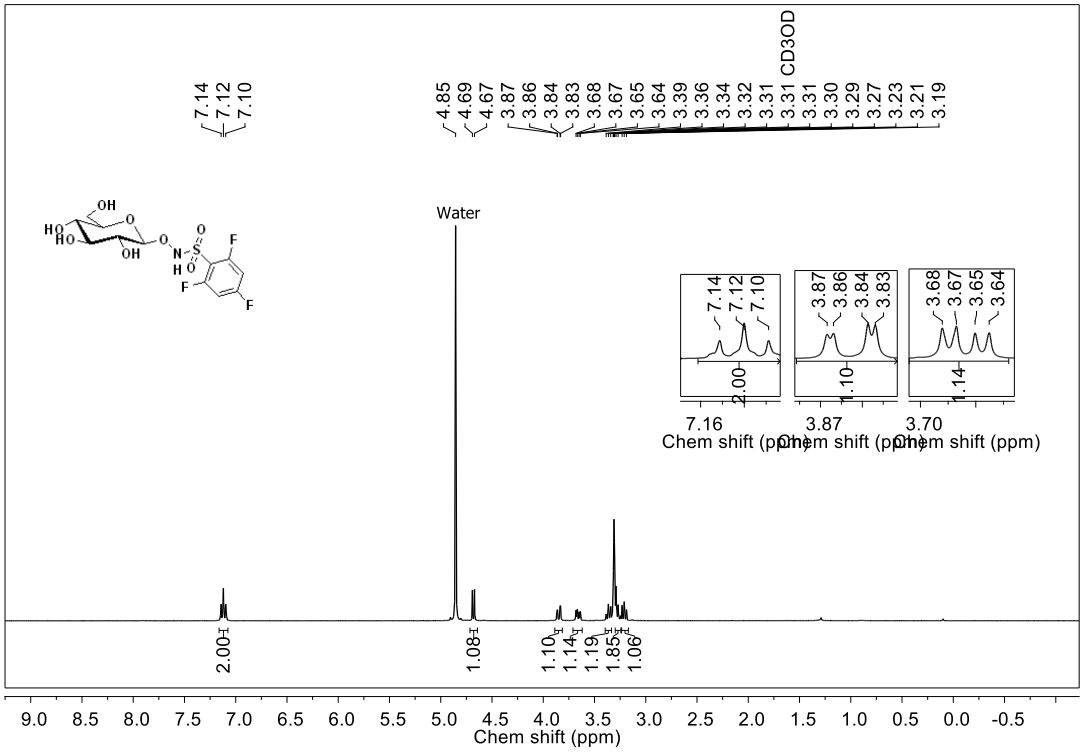

^{13}C NMR spectra for compound **13e**

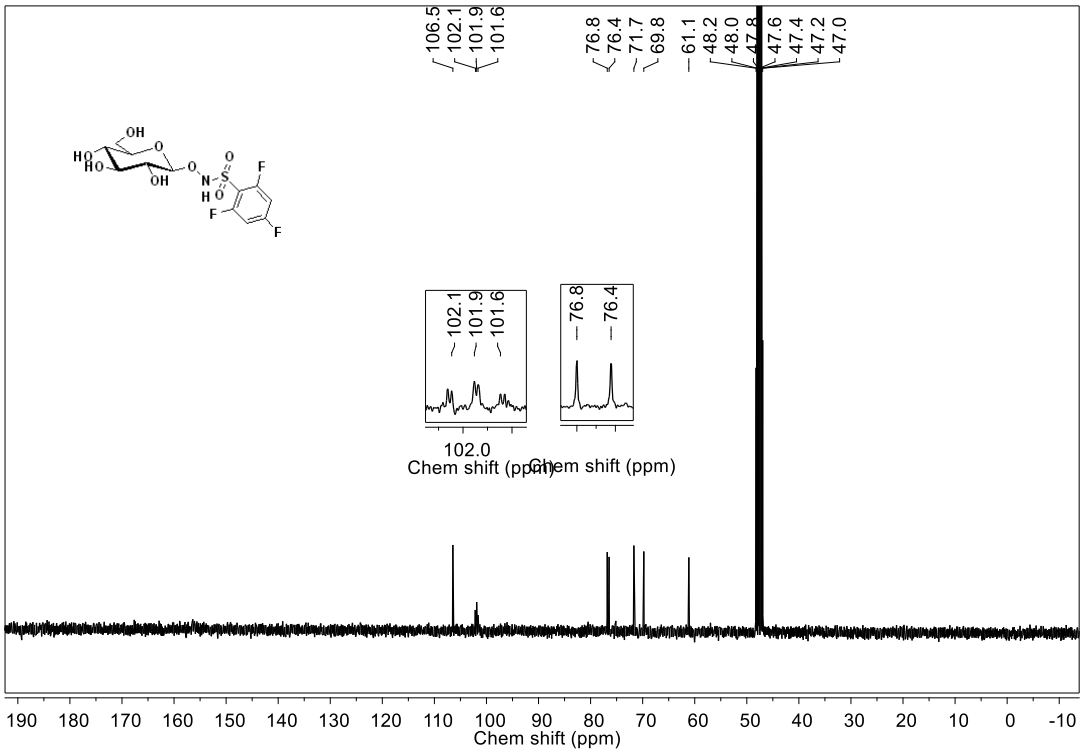

^{19}F NMR spectra for compound **13e**

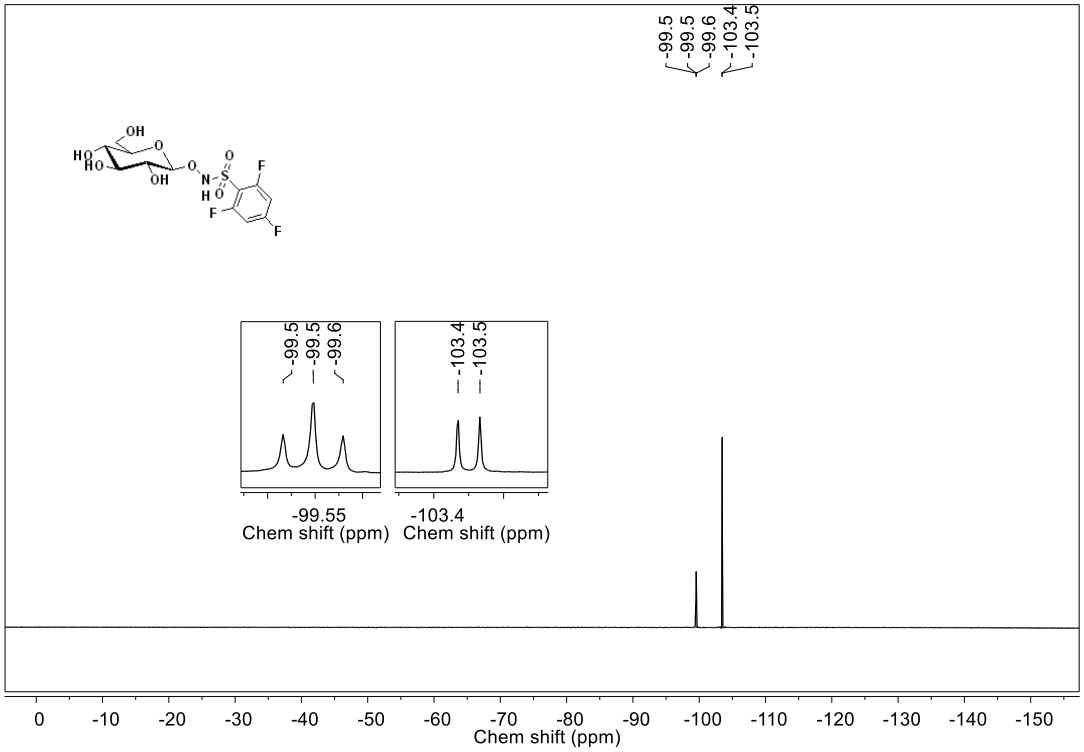

^{1}H NMR spectra for compound **14**

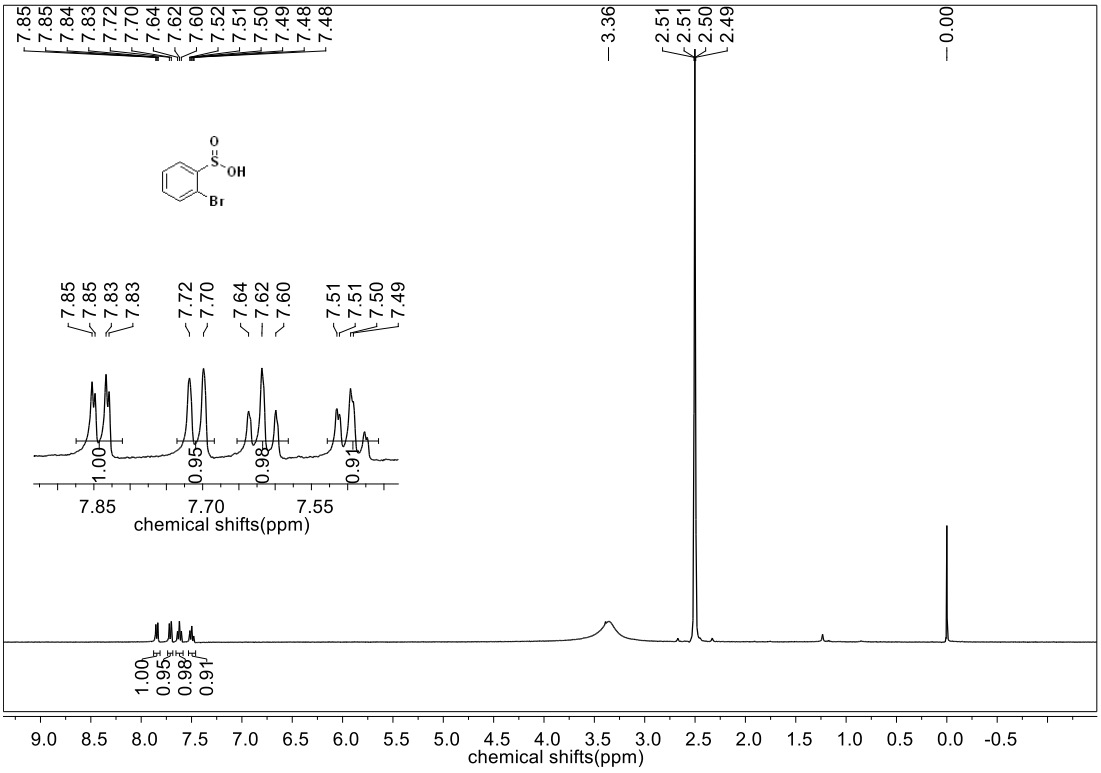

3.6. References

(1) Zhou, X.; Huang, Z.; Yang, H.; Jiang, Y.; Wei, W.; Li, Q.; Mo, Q.; Liu, J. β-Glucosidase Inhibition Sensitizes Breast Cancer to Chemotherapy. *Biomed. Pharmacother.* **2017**, *91*, 504–509.

(2) Zhang, Y.; Zhu, K.; Miao, X.; Hu, X.; Wang, T. Identification of β-Glucosidase 1 as a Biomarker and Its High Expression in Hepatocellular Carcinoma Is Associated with Resistance to Chemotherapy Drugs. *Biomarkers* **2016**, *21* (3), 249–256.

(3) Friend, D. R.; Chang, G. W. A Colon-Specific Drug-Delivery System Based on Drug Glycosides and the Glycosidases of Colonic Bacteria. *J. Med. Chem.* **1984**, *27* (3), 261–266.

(4) Tozer, T. N.; Rigod, J.; McLeod, A. D.; Gungon, R.; Hoag, M. K.; Friend, D. R. Colon-Specific Delivery of Dexamethasone from a Glucoside Prodrug in the Guinea Pig. *Pharm. Res.* **1991**, *8* (4), 445–454.

(5) Rubinstein, A. Approaches and Opportunities in Colon-Specific Drug Delivery. *Crit. Rev. Ther. Drug Carrier Syst.* **1995**, *12* (2–3), 101–149.

(6) Fernández, C.; Nieto, O.; Rivas, E.; Montenegro, G.; Fontenla, J. A.; Fernández-Mayoralas, A. Synthesis and Biological Studies of Glycosyl Dopamine Derivatives as Potential Antiparkinsonian Agents. *Carbohydr. Res.* **2000**, *327* (4), 353–365.

(7) Scott, L. E.; Telpoukhovskaia, M.; Rodríguez-Rodríguez, C.; Merkel, M.; Bowen, M. L.; Page, B. D. G.; Green, D. E.; Storr, T.; Thomas, F.; Allen, D. D.; Lockman, P. R.; Patrick, B. O.; Adam, M. J.; Orvig, C. N-Aryl-Substituted 3-(β-D-Glucopyranosyloxy)-2-Methyl-4(1H)-Pyridinones as Agents for Alzheimer's Therapy. *Chem. Sci.* **2011**, *2* (4), 642–648.

(8) Oliveri, V.; Giuffrida, M. L.; Vecchio, G.; Aiello, C.; Viale, M. Gluconjugates of 8-Hydroxyquinolines as Potential Anti-Cancer Prodrugs. *Dalt. Trans.* **2012**, *41* (15), 4530.

(9) Li, F.; Wu, G.; Zheng, H.; Wang, L.; Zhao, Z. Synthesis, Colon-Targeted Studies and Pharmacological Evaluation of an Anti-Ulcerative Colitis Drug 4-Aminosalicylic Acid-β-O-Glucoside. *Eur. J. Med. Chem.* **2016**, *108*, 486–494.

(10) Autar, R.; Khan, A. S.; Schad, M.; Hacker, J.; Liskamp, R. M. J.; Pieters, R. J. Adhesion

Inhibition of F1C-Fimbriated Escherichia Coli and Pseudomonas aeruginosa PAK and PAO by Multivalent Carbohydrate Ligands. *ChemBioChem* **2003**, *4* (12), 1317–1325.

(11) Zhou, Y.; Cink, R. B.; Dassanayake, R. S.; Seed, A. J.; Brasch, N. E.; Sampson, P. Rapid Photoactivated Generation of Nitroxyl (HNO) under Neutral PH Conditions. *Angew. Chemie Int. Ed.* **2016**, *55* (42), 13229–13232.

(12) Aizawa, K.; Nakagawa, H.; Matsuo, K.; Kawai, K.; Ieda, N.; Suzuki, T.; Miyata, N. Piloty's Acid Derivative with Improved Nitroxyl-Releasing Characteristics. *Bioorg. Med. Chem. Lett.*, **2013**, *23* (8).

(13) Kim, E.-J.; Kumar, R.; Sharma, A.; Yoon, B.; Kim, H. M.; Lee, H.; Hong, K. S.; Kim, J. S. In Vivo Imaging of β-Galactosidase Stimulated Activity in Hepatocellular Carcinoma Using Ligand-Targeted Fluorescent Probe. *Biomaterials* **2017**, *122*, 83–90.

(14) Mao, G. J.; Zhang, X. B.; Shi, X. L.; Liu, H. W.; Wu, Y. X.; Zhou, L. Y.; Tan, W.; Yu, R. Q. A Highly Sensitive and Reductant-Resistant Fluorescent Probe for Nitroxyl in Aqueous Solution and Serum. *Chem. Commun.* **2014**, *50* (43).

(15) Barrett, T.; Suresh, C.; Tolley, S.; Dodson, E.; Hughes, M. The Crystal Structure of a Cyanogenic β-Glucosidase from White Clover, a Family 1 Glycosyl Hydrolase. *Structure* **1995**, *3* (9), 951–960.

(16) Trott, O.; Olson, A. J. AutoDock Vina: Improving the Speed and Accuracy of Docking with a New Scoring Function, Efficient Optimization, and Multithreading. *J. Comput. Chem.* **2010**, *31* (2), 455–461.

(17) Laskowski, R. A.; Swindells, M. B. LigPlot+: Multiple Ligand-Protein Interaction Diagrams for Drug Discovery. *J. Chem. Inf. Model.* **2011**, *51* (10), 2778–2786.

Chapter 4: β-galactosidase triggered Nitroxyl (HNO) donors

4.1. Introduction

The development of β-glucosidase sensitive HNO donors is outlined in **Chapter 3**. This tool will be useful for the study of the role of HNO in cancer biology. Further, we were interested to study the role of HNO in aging (senescence cells). In an evolutionary biological system, aging is defined as a steady state loss in a particular fitness component of an organism caused by internal physiological deterioration.[1] Senescence shows all the typical signs of organismal aging such as cell growth arrest,[2] increased oxidative stress,[3] and inflammation.[4,5] Cellular senescence is a state of irreversible loss of proliferating capacity of cells, and it drives aging. Several biomarkers such as reactive oxygen species (ROS),[3] reactive nitrogen species (RNS), iNOS, senescence-associated secretory phenotypes,[4] β-galactosidase,[6,7] and HIF-1α[8] are overexpressed in senescent cells. Previous reports have shown that ROS can initiate and activate cellular senescence.[9,10]

Aging is not only limiting cellular functions but also increases the susceptibility to cardiovascular diseases,[11] cancer,[12] osteoarthritis,[13] osteoporosis,[14] type 2 diabetes,[15] and neurodegenerative disorders such as Alzheimer's and Parkinson's disease.[16,17] Hence, animal models show that reduction in oxidative stress and inflammation burden in senescent cells is a therapeutic approach to delaying the effects of aging.[18] As the level of β-galactosidase is associated with such pathological conditions, hence, several β-galactosidase sensitive fluorogenic molecules have been reported. Such molecules also help to measure the intracellular levels of the enzyme.[19] Also, β-galactosidase is widely used as a trigger for the delivery of prodrugs in cancer cells as well as in *E. coli*, a gram-negative bacterium (Figure 4.1).[20,21,22,23]

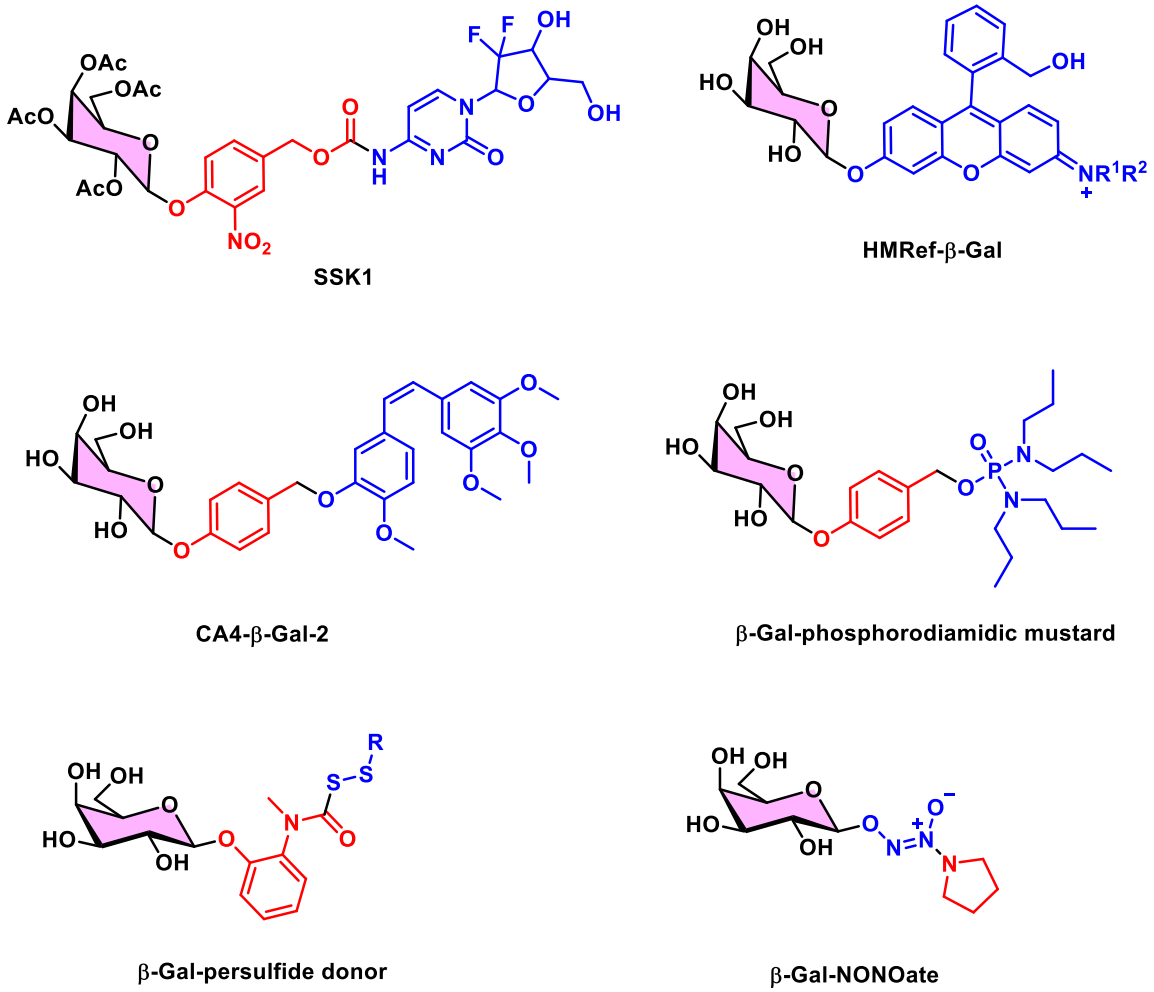

Figure 4.1. β-galactosidase sensitive prodrug strategies

Given that senescent cells have a higher level of β-galactosidase, ROS, HIF-1α and iNOS and HNO is known for quenching the ROS, inhibition of HIF-1α (involved in angiogenesis), inhibition of iNOS. Collectively, these characteristics of HNO make it an interesting candidate for reducing inflammation and oxidative stress in senescent cells.

Since β-galactosidase is overexpressed in senescent cells,[6,7] it makes a suitable trigger to develop a new HNO prodrug. β-galactosidase is known to cleave the glycosidic bond to release an aglycon. Also, ASGPR (Asialoglycoprotein receptor) is overexpressed on the cell wall of the senescent cells, it has a high affinity towards sugars, and it helps in the targeted delivery of HNO prodrug. Based on this, we designed a β-galactosidase activated HNO prodrug.

The design contained β-galactose moiety attached to an HNO donor (derivatives of Piloty's acid). Here, β-galactose moiety will act as a gate pass for the HNO prodrug to permeate senescent cells. Upon entry of the prodrug, senescence-associated β-galactosidase (SA β-Gal) is expected to cleave the glycosidic bond to release HNO (Figure 4.2).

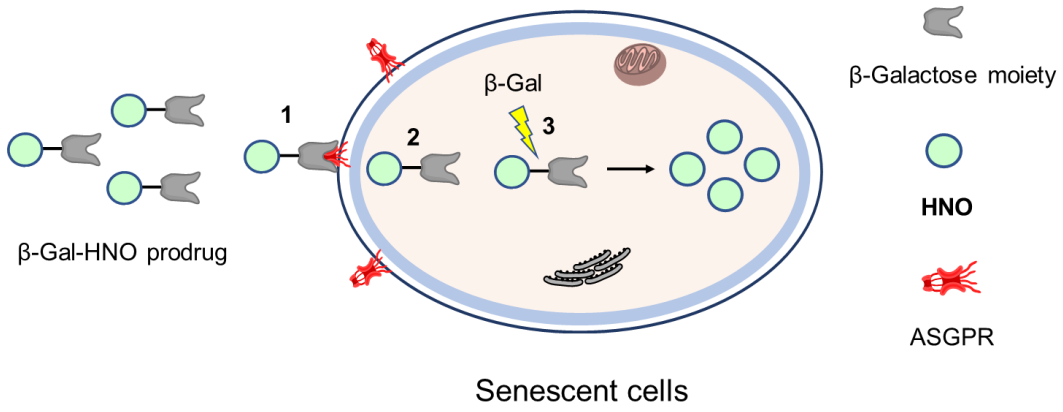

Figure 4.2. Design of β-galactosidase triggered nitroxyl (HNO) donor. (1) The interaction of HNO prodrug with ASGPR, (2) Entry into the senescent cells, and (3) β-galactosidase mediated cleavage of the glycosidic bond to release HNO.

The following mechanism was proposed for HNO generation from β-galactosidase activated nitroxyl (HNO) donors. It is well known that active site residues of the enzyme interact with the galactose moiety to cleave the anomeric C-O bond to release an active drug (Scheme 4.1).

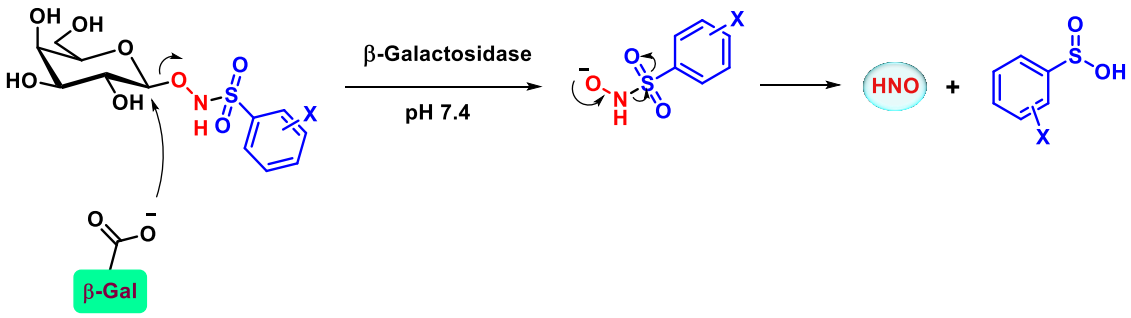

Scheme 4.1. Proposed mechanism of HNO generation upon activation by β-galactosidase

4.2. Result and discussion

4.2.1. Synthesis

Firstly, HNO prodrugs were synthesized to test the hypothesis. Synthesis was started with pentaacetate galactose, and the anomeric acetate group was converted into a bromo substituent using hydrobromic acid to afford compound **16**.[24] Next, the bromoside was coupled with *N*-hydroxyphthalimide under basic conditions to provide compound **17** which was later hydrolyzed using hydrazine hydrate to obtain **18**.[25] Further, *N*-sulfonation was performed in basic conditions to furnish compounds **19a** and **19b**.[26] which were later deacetylated to obtain **20a** and **20b** (Scheme 4.2 and table 4.1).[27]

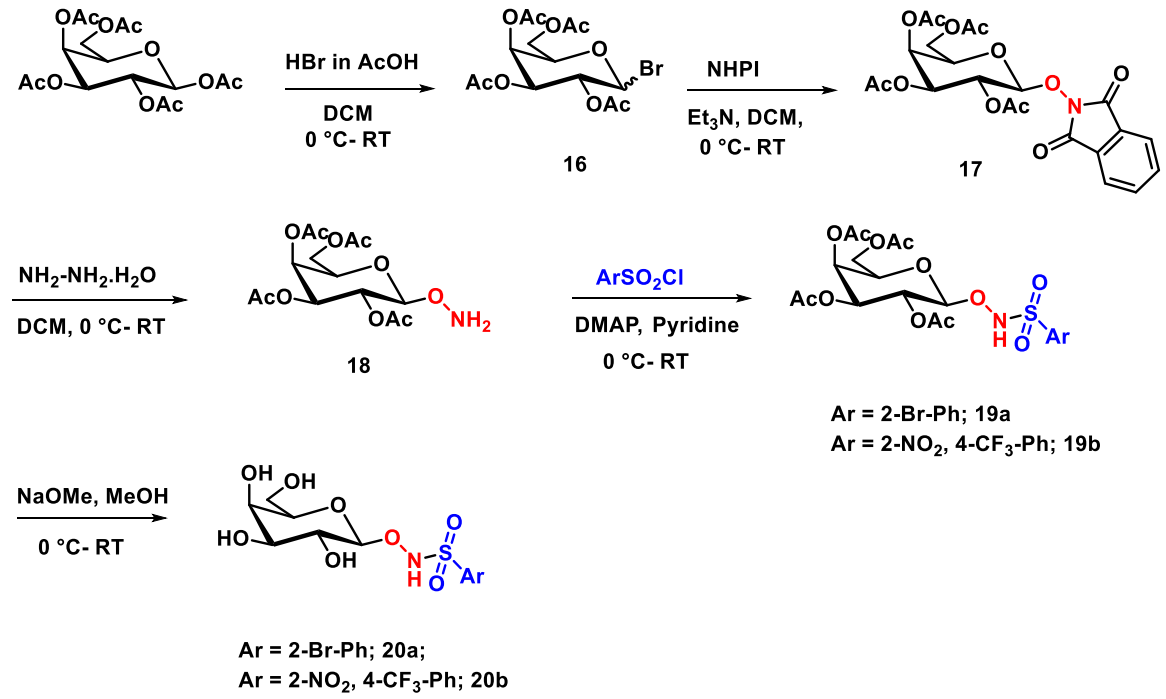

Scheme 4.2. Synthesis of compounds **20a** and **20b**

Table 4.1: Synthesis of compounds **19a-19b** and **20a-20b**

Entry	Product	Ar	Yield, %
1	**19a**	2-Br-Ph	63
2	**19b**	2- NO_2-4-CF_3-Ph	76
3	**20a**	2-Br-Ph	43
4	**20b**	2- NO_2-4-CF_3-Ph	41

Next, HNO probe **NAT** was synthesized using the following reported procedure. Here, tryptophan was acetylated using acetyl chloride in a basic condition to obtain **NAT** (Scheme 4.3).[28]

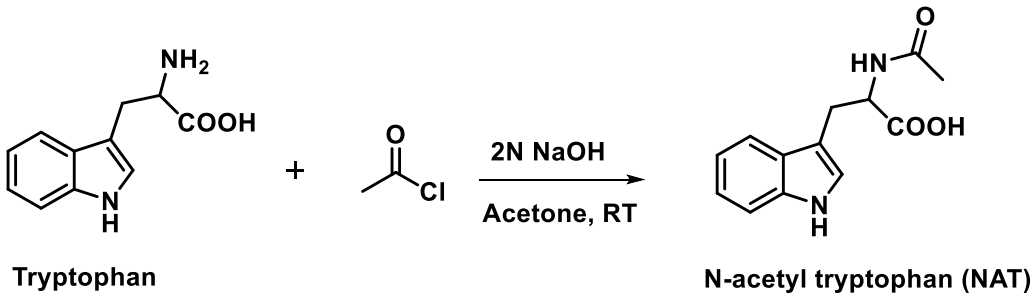

Scheme 4.3. Synthesis of compound **NAT**

4.2.2. HNO generation study

4.2.2.1. Detection of HNO generation using 5

To test the hypothesis of HNO generation from prodrug using **5**,[29] compounds **20a** and **20b** was co-incubated with the β-galactosidase from *E. coli* and **5** for 4 h. The time-dependent enhancement in fluorescence intensity from compounds **20a** and **20b** was recorded using an Ensight Multimode Plate Reader (excitation 370 nm; emission 460 nm) (Scheme 4.4 and figure 4.3). The fluorescence intensity corresponds to the amount of HNO release; compound **4** was used as a positive control; the dye used in this study refers to **5**.

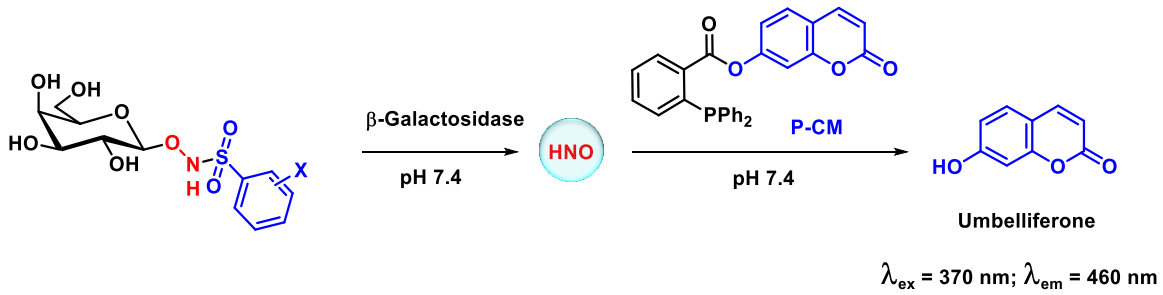

Scheme 4.4: Proposed mechanism for HNO generation and trapping HNO by **5**

In the absence of β-galactosidase, HNO release was not observed from compounds **20a** and **20b** in buffer. Whereas, compound **20a** showed a higher yield of HNO generation than compound **20b** in the presence of β-galactosidase (Figure 4.3). The rate constant (pseudo-first-order kinetics) for HNO release with **20a** was found to be 0.016 min^{-1} (R^2 = 0.9855).

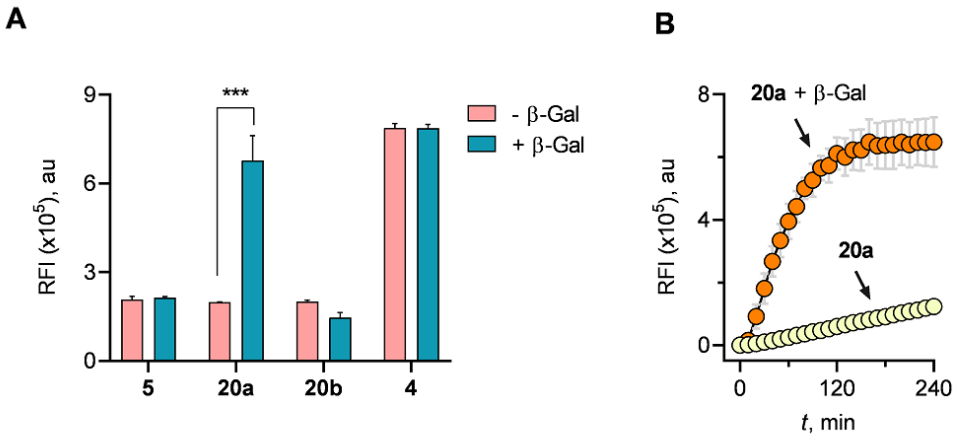

Figure 4.3. HNO Detection from compounds **20a** and **20b** in the presence β-galactosidase of using **5** in buffer.

4.2.2.2. Detection of N_2O by GC/MS analysis

HNO is known to react with itself, where one molecule of HNO acts as a nucleophile and another molecule acts as electrophile and dimerized to form hyponitrous acid which spontaneously decomposed to nitrous oxide and water (Scheme 4.5).[30]

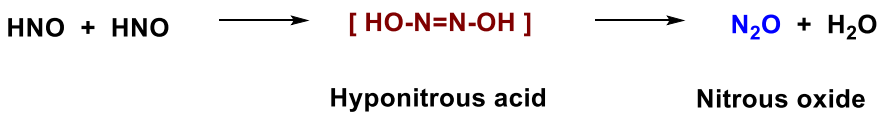

Scheme 4.5. The mechanism for dimerization of HNO

In this experiment, compound **4** was used as a positive control and N_2O formation with **4** was measured in buffer (pH 7.4) for 15 h using headspace GC analysis. The N_2O yield with **4** was 100% which was not affected by the β-galactosidase. Under similar conditions, the yield of N_2O from **20a** in the presence of β-galactosidase was 94% (Figure 4.4).

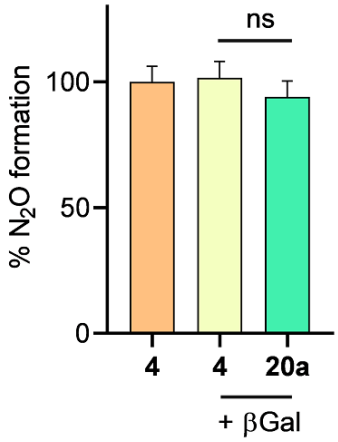

Figure 4.4. N_2O detection from **20a** by headspace GC analysis. The experiment was performed by Dr. Vinayak Khodade (Prof. J. Toscano's lab, John Hopkins University, Baltimore, MD).

4.2.2.3. Detection of HNO using *N*-acetyl tryptophan

Trapping of HNO using *N*-acetyl tryptophan is another method that has been previously used for the detection of HNO.[31] It is known that tryptophan derivatives (NAT) can react with HNO to form the *N*-hydroxylamine derivative of tryptophan, which can then undergo aerobic oxidation to produce the *N*-nitroso derivative of tryptophan (NAT-NO) in a buffer with a pH of 7.4. (Scheme 4.6). The formation of NAT-NO can be monitored at 335 nm.

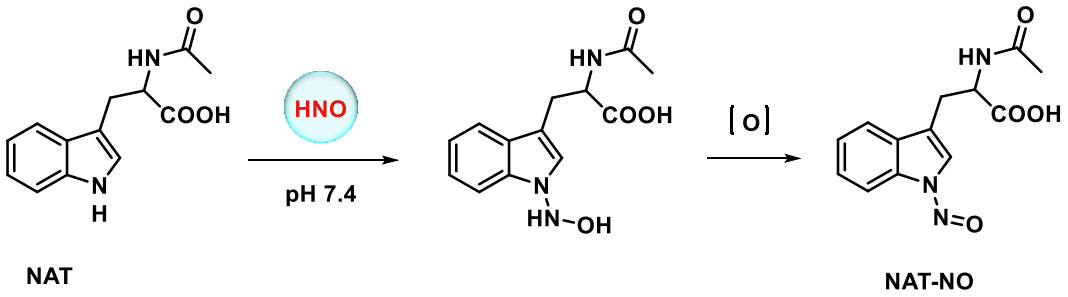

NAT NAT-NO

Scheme 4.6. The reaction of NAT with HNO to form NAT-NO

Firstly, to test this hypothesis, **4** and NAT were incubated in the absence and presence of β-galactosidase in buffer (pH 7.4) for 1 h. The time-dependent formation of NAT-NO was monitored at 335 nm. Similarly, the formation of NAT-NO was evaluated from compound **20a** and as expected, a comparable formation of NAT-NO was achieved (Figure 4.5).

In the control experiment, *N*-acetyl cysteine was used as an HNO quencher. *N*-acetyl cysteine was co-incubated with compounds **20a**, **4**, NAT, and the formation of NAT-NO was measured. As expected, the diminished yield of NAT-NO was observed (Figure 4.5).

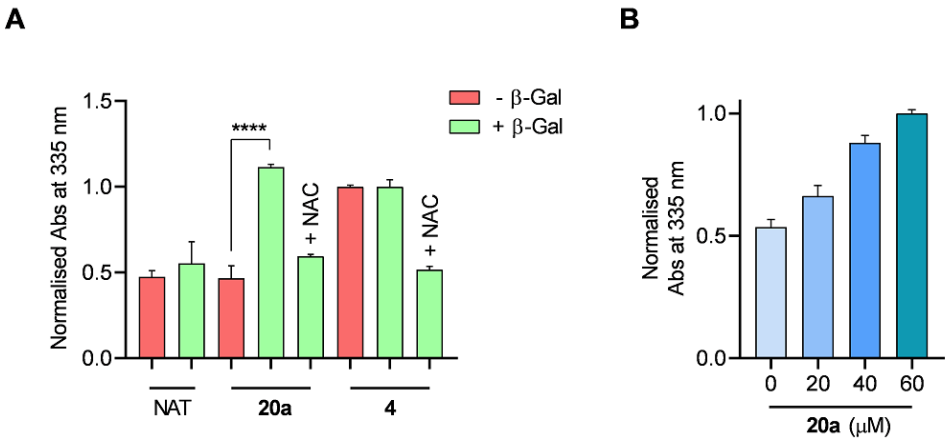

Figure 4.5. Detection of HNO from compound **20a** using *N*-acetyl tryptophan.

4.2.3. Detection of Nitric oxide (NO)

Next, Griess assay was performed to detect NO release from prodrug **20a** and **20b**.[32] **20a** and **20b** were incubated with β-galactosidase in buffer (pH 7.4) at 37 ˚C for 4 h and further incubated with Griess reagent for 25 min. The formation of the pink color azo product was observed and monitored at 540 nm. The improved selectivity for HNO over NO was achieved from compounds **20a** and **20b** compared to **4** (Figure 4.6).

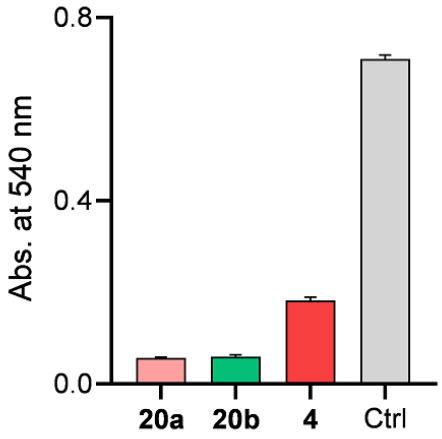

Figure 4.6. NO detection from **20a** using Griess assay.

4.2.4. HPLC study

4.2.4.1. Stability of compound 20a in buffer (pH 7.4)

In order to check the stability in the buffer, **20a** was incubated in the buffer (pH 7.4) at 37 ˚C for 48 h. As monitored by the HPLC, compound **20a** was stable in these conditions (Figure 4.7).

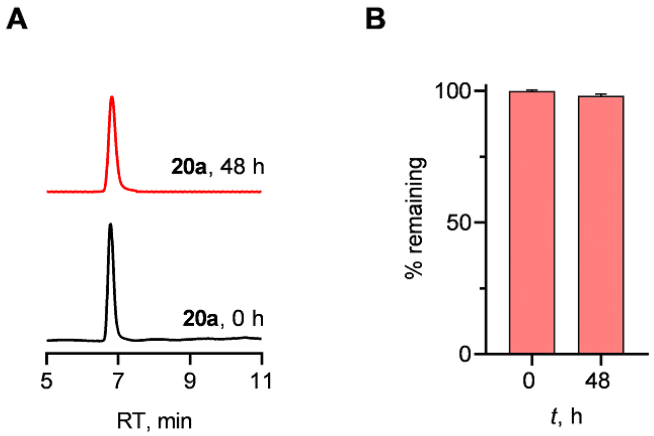

Figure 4.7. (A) HPLC traces of **20a** (RT = 6.9 min); (B) AUC for the stability of **20a** in buffer (pH 7.4).

4.2.4.2. Decomposition of 20a in the presence of β-galactosidase

In order to study the decomposition, compound **20a** was incubated with β-galactosidase (10 U/mL) in buffer (pH 7.4) at 37 ˚C. As monitored by HPLC, the gradual disappearance of compound **20a** (RT = 6.9 min) and the formation of compound **14** (RT = 8.9 min) were observed over 48 h (Figure 4.8) and rate constants for decomposition of **20a** as well as the formation of **14** were found to be 0.039 h^{-1} and 0.018 h^{-1}.

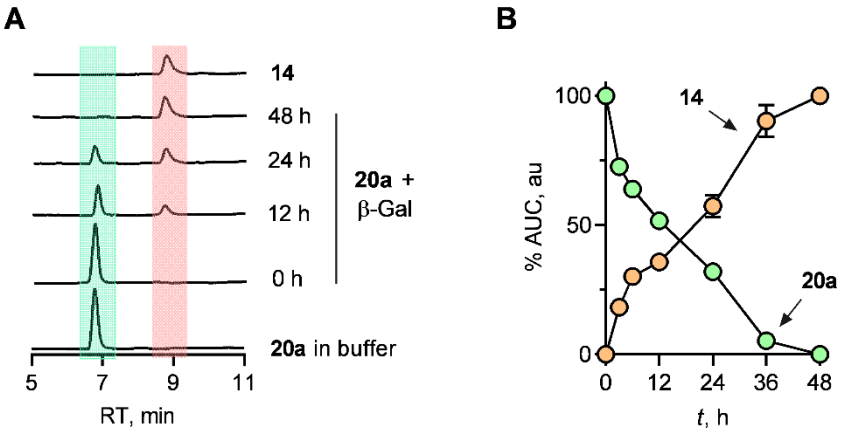

Figure 4.8. (A) HPLC traces of **20a** and **14**; (B) AUC for decomposition of **20a** (RT = 6.9 min) and formation of **14** (RT = 8.9 min) in the presence of β-galactosidase in buffer (pH 7.4).

4.2.4.3. Decomposition of 20b in the presence of β-galactosidase

To study the decomposition, compound **20b** was incubated with the β-galactosidase (10 U/mL) in buffer (pH 7.4) at 37 ˚C for 48 h. Surprisingly, compound **20b** (retention time (RT) = 12.2 min) was found to be stable under these conditions (Figure 4.9).

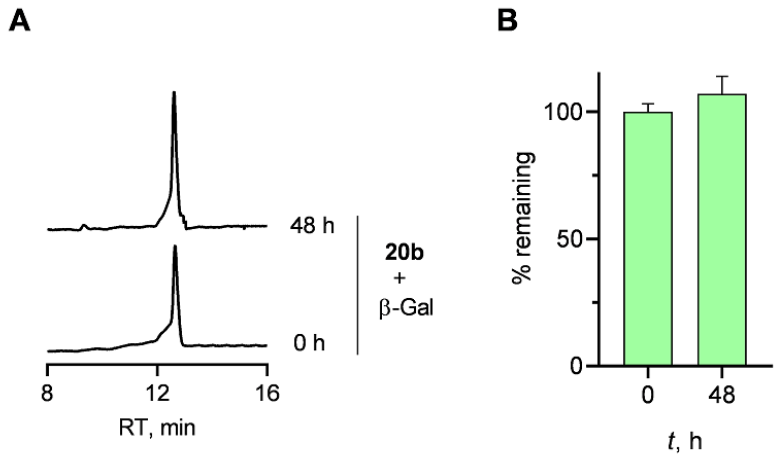

Figure 4.9. HPLC traces and AUC for decomposition of **20b** (RT = 12.2 min) in the presence of β-galactosidase in buffer (pH 7.4).

HPLC analysis revealed that compound **20a** was gradually cleaved and formed byproduct **14** in the presence of β-galactosidase in buffer whereas, compound **20b** was stable under these conditions.

4.2.5. Computational studies

Computational studies were carried out to understand the interaction of the compounds into the active site of the enzyme and explain the unusual behavior of structurally similar analogs, **20a** and **20b**.

The mechanism by which β-galactosidase cleaves the glycosidic bond has been described in detail by Matthews and coworkers.[33] The galactosyl moiety is observed to covalently bind to the nucleophilic Q537. E461 and Mg^{2+} are two potential acids, however, E461 is better positioned to directly help in the departure of an aglycon. It indicates that metal ion acts in a secondary role (Figure 4.10).

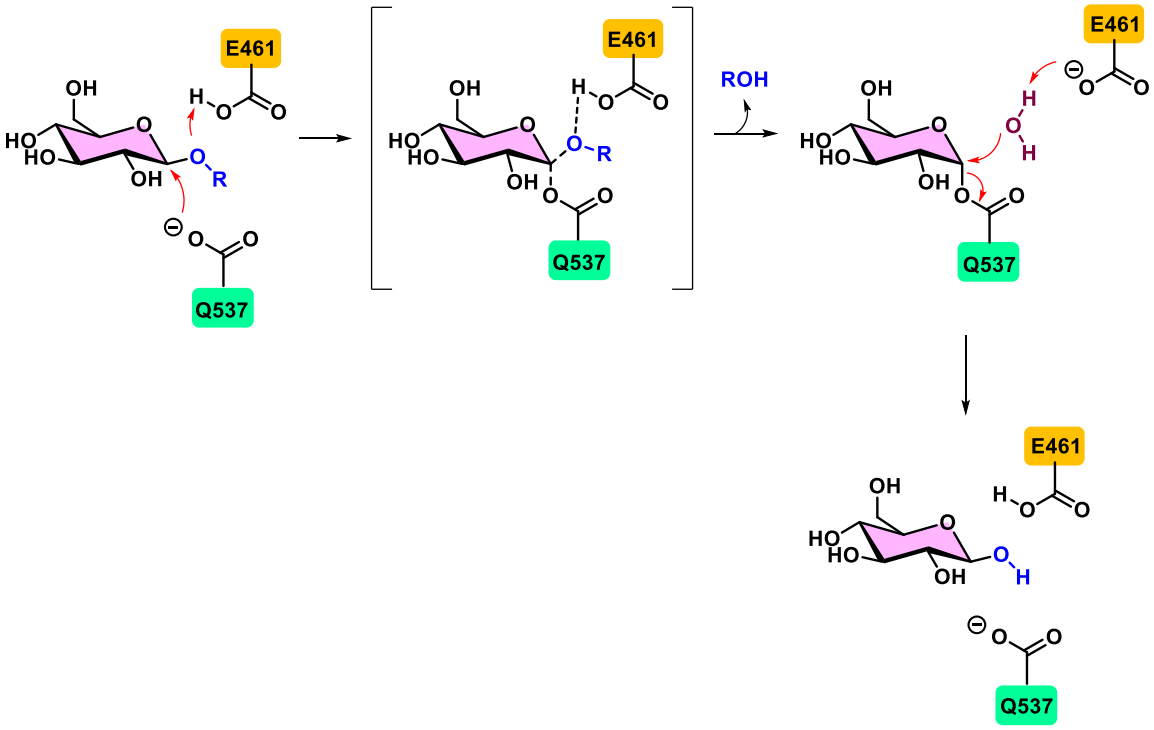

Figure 4.10: Plausible mechanism of hydrolysis of the glycosidic bond by β-galactosidase from *E. Coli.*

In silico molecular docking studies were carried out to examine the probability of hydrolysis of the allolactose and compounds **20a** and **20b** mediated by β-galactosidase (Figure 4.11). In this study, allolactose was used as a positive control to validate the docking simulations. The structures of compounds (**20a** and **20b**) were built with standard bond lengths and angles using ChemDraw and then energy minimized with Chem3D using the integrated MM2 energy minimization script. The X-ray crystal structure of β-galactosidase from *E. coli* (PDB ID: 1JYN; resolution = 1.80 Å) was retrieved from PDB and used for the docking studies. The protein and ligand PDBQT files were prepared using AutoDock Tools 1.5.6 (ADT) following the standard protocol.[34] The best-scored docking pose with the lowest binding energy (Table 4.2) was selected for analysis and figures were visualized using PyMOL (The PyMOL Molecular Graphics System, Version 2.0 Schrödinger, LLC) (Figure 4.12 and Figure 4.13). LigPLOT was used to depict the 2D interactions of ligands and proteins (Figure 4.12 and Figure 4.13).[35] These results were provided by T. Anand Kumar (Prof. Harinath Chakrapani Lab**,** IISER Pune).

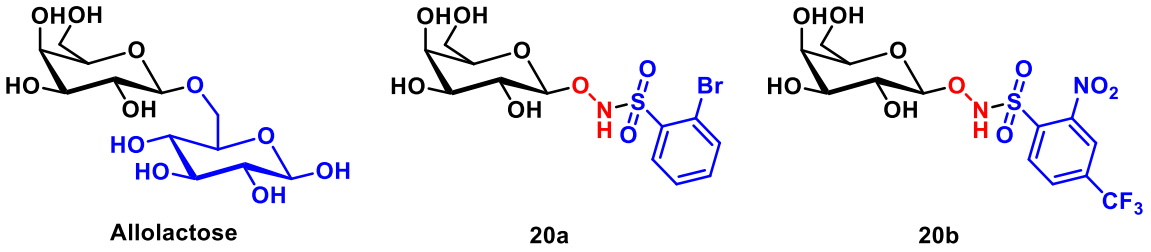

Figure 4.11: Structures of compounds used for docking analysis

Table 4.2: Comparative analysis of the docking results of prodrugs **20a** and **20b**

Entry	Ligand/ Prodrug	Affinity (kcal/mol)	Distance from O (RCOOH) of Q537 (Å)*
1	Allolactose	-7.7	4.4
2	**20a**	-8.1	3.7
3	**20b**	-8.0	10.4

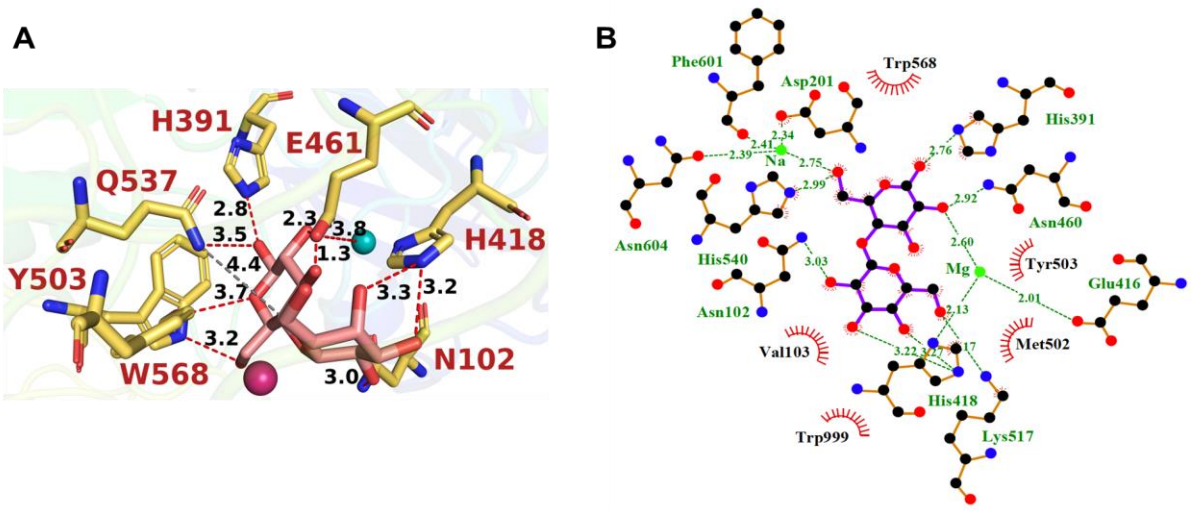

Figure 4.12. (A) Cartoon representation of docked compound allolactose into the active site of β-galactosidase from *E. coli* (PDB ID: 1JYN; resolution = 1.80 Å). The docked ligands were shown in the stick model and the active site residues are indicated by a 1-letter code. The hydrogen, hydrophobic and pi-pi interactions are drawn as blue, red and gray dotted lines, and the lengths are indicated. The figure was generated using PyMOL v 2.0. (B) LigPlot shows the 2D interactions of allolactose with β-galactosidase. The molecule is represented in a stick model. Active site residues are labeled by a 3-letter code and represented as a ball and stick model. The residues forming hydrophobic interactions are shown as red arcs while the hydrogen bonds are shown as blue dashed lines with indicated bond lengths.

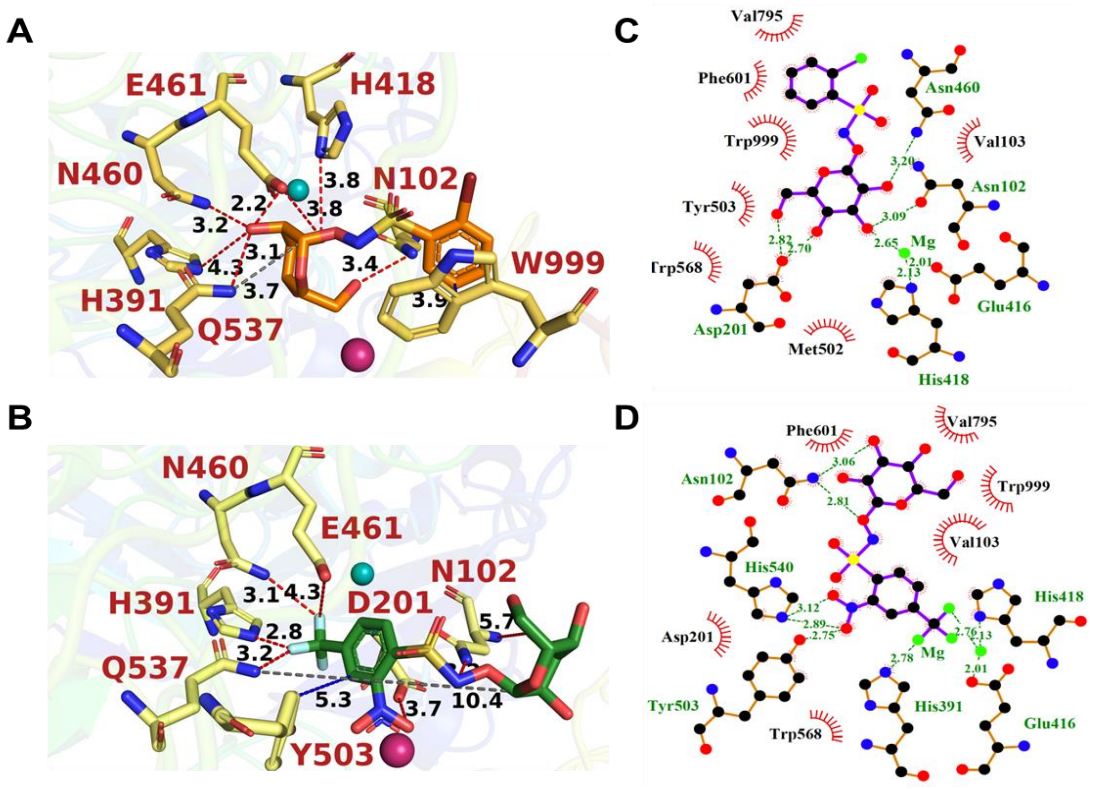

Figure 4.13. (A-B) Cartoon representation of docked compounds (A) **20a** and (B) **20b** into the active site of β-galactosidase from *E. coli* (PDB ID: 1JYN; resolution = 1.80 Å). The docked ligands were shown in the stick model and the active site residues are indicated by a 1-letter code. The hydrogen, hydrophobic and pi-pi interactions are drawn as blue, red and gray dotted lines, and the lengths are indicated. The figure was generated using PyMOL v 2.0. (C-D) LigPlot shows the 2D interactions of compounds (C) **20a** and (D) **20b** with β-galactosidase. The molecule is represented in a stick model. Active site residues are labeled by a 3-letter code and represented as a ball and stick model. The residues forming hydrophobic interactions are shown as red arcs while the hydrogen bonds are shown as blue dashed lines with indicated bond lengths.

As anticipated, positive control allolactose fitted into the active site (ΔG = -7.7 kcal/mol) and was found closer to catalytic active site residues (4.4 Å from Q537). The affinity and distance of allolactose with the active site of the enzyme enable favorable orientation and spacing for hydrolysis of the glycosidic bond. Similarly, compounds **20a** and **20b** were also fitted into the active site with varying docking scores ranging from -8.1 to -8.0 kcal/mol. It was noteworthy that the glycosidic moiety of **20a** was in proximity to the active site residues (3.3 Å from Q537) than **20b**. (Table 4.3, Figure 4.11 and Figure 4.12). Altogether, the docking studies revealed that

20a is a more suitable substrate of β-galactosidase than **20b**. This suggests that **20a** is more prone to hydrolysis by the β-galactosidase (Figure 4.13).

4.2.6. Polysulfide measurement by LC/MS analysis

HNO is known to react with hydrogen sulfide (H_2S) to enhance persulfide/polysulfide levels, or sulfane sulfur pool (cellular antioxidant reservoir).[36] It has been reported that H_2S is overexpressed in senescent cells.[37] Hence, it is important to study the cross-talk between HNO and H_2S. To study the formation of persulfide/polysulfide, compound **20a** was incubated with β-galactosidase in buffer for 15 min, followed by the addition of an electrophilic HPE-IAM probe to trap persulfide and further incubated for 15 min. The formation of HPE-AM adduct of sulfur species was monitored by LC/MS. Interestingly, the formation of H_2S_2, H_2S_3 and H_2S_4 was observed during the reaction of **20a** and H_2S in the presence of β-galactosidase in buffer (Scheme 4.7; Figure 4.14-4.19).

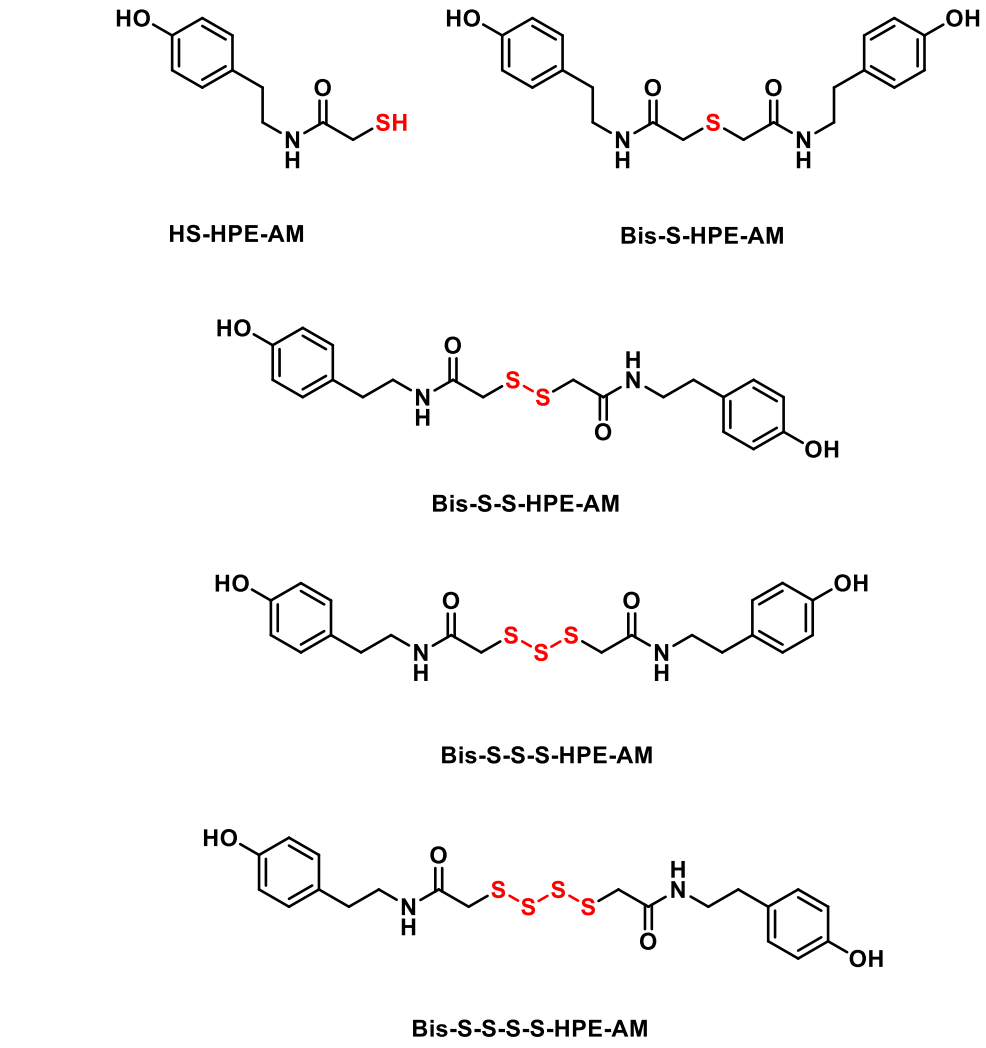

Scheme 4.7: Structures of sulfur species trapped by HPE-IAM probe

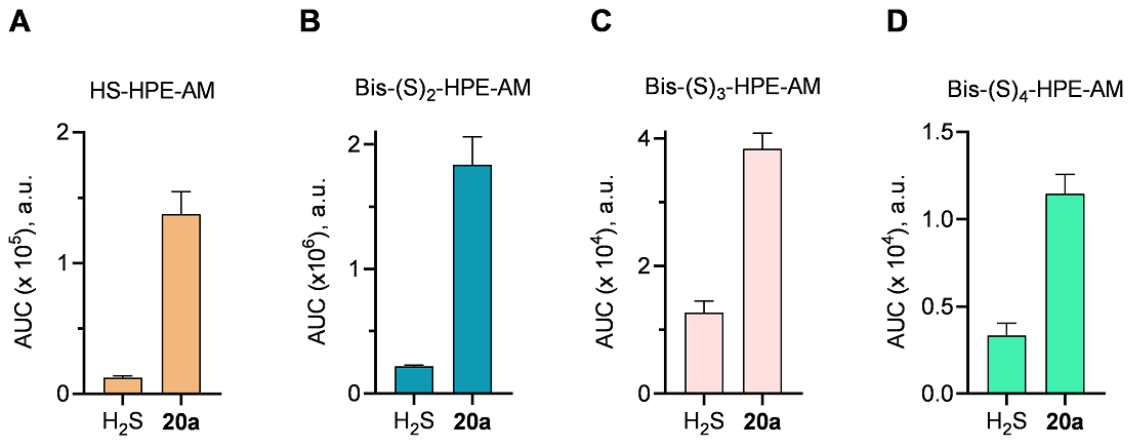

Figure 4.14: LC/MS study. Polysulfide formation was measured by detection of trapped HPE-IAM species from Na_2S and **20a** + Na_2S upon incubation with β-galactosidase in PBS

(pH 7.4) at 37 ˚C for 15 min. (A) Formation of HS-HPE-AM (Expected, m/z = 212.0740 [M + H]$^+$; observed, m/z = 212.0715); (B) Formation of Bis-SS-HPE-AM (expected, m/z = 421.1250 [M + H]$^+$; observed, m/z = 421.1151); (C) Formation of Bis-SSS-HPE-AM (expected, m/z = 453.0971 [M + H]$^+$; observed, m/z = 453.0865); (D) Formation of Bis-SSSS-HPE-AM (expected mass = 485.0692; observed mass = 485.0714).

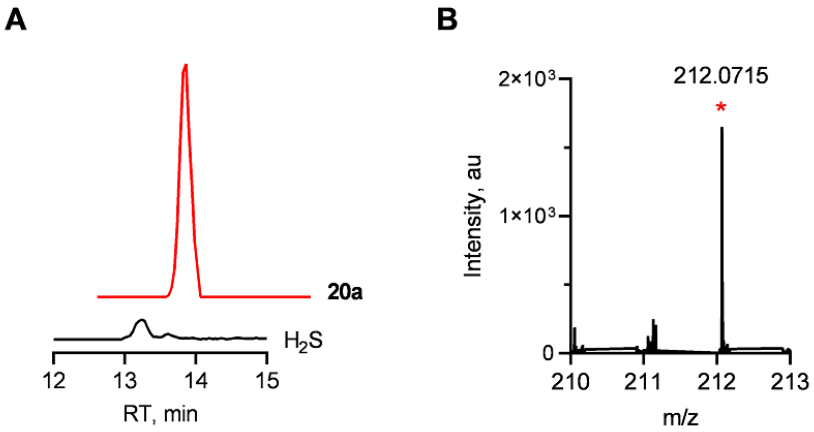

Figure 4.15: (A) Representative LC trace for HS-HPE-AM adduct from Na_2S and **20a** + Na_2S with HPE-IAM; (B) Mass spectra for HS-HPE-AM (expected, m/z = 212.0740 [M + H]$^+$; observed, m/z = 212.0715).

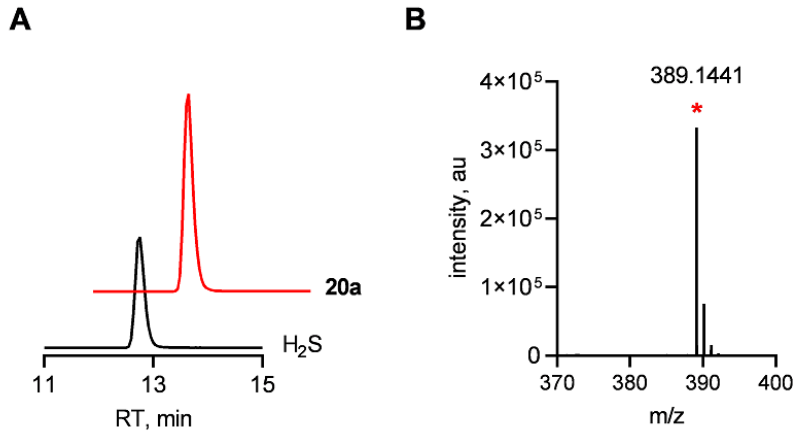

Figure 4.16: (A) Extracted ion chromatograms from an LC/MS analysis of Bis-S-HPE-AM formation from Na_2S, **20a** + Na_2S; (B) Mass spectra for Bis-S-HPE-AM (expected, m/z = 389.1530 [M + H]$^+$; observed, m/z = 389.1441).

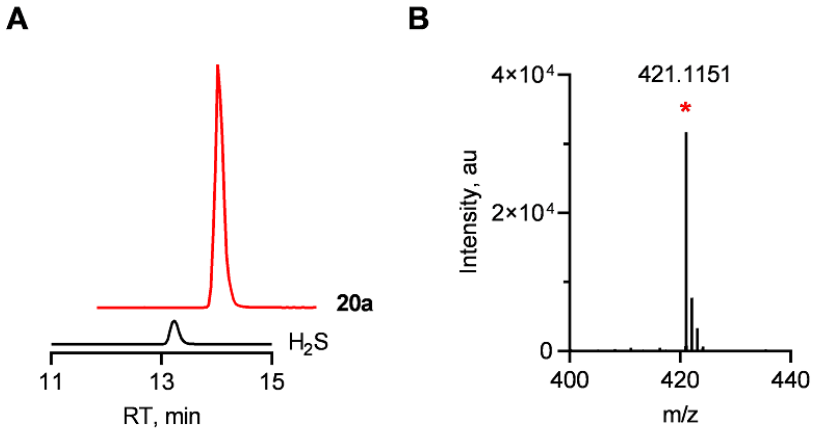

Figure 4.17: (A) Extracted ion chromatograms from an LC/MS analysis of Bis-SS-HPE-AM formation from Na_2S, **20a** + Na_2S; (B) Mass spectra for Bis-SS-HPE-AM (expected, m/z = 421.1250 $[M + H]^+$; observed, m/z = 421.1151).

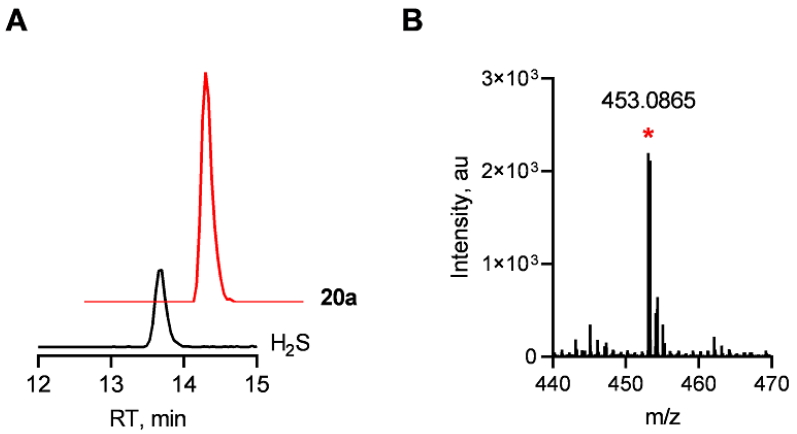

Figure 4.18: (A) Extracted ion chromatograms from an LC/MS analysis of Bis-SSS-HPE-AM formation from Na_2S, **20a** + Na_2S; (B) Mass spectra for Bis-SSS-HPE-AM (expected, m/z = 453.0971 $[M + H]^+$; observed, m/z = 453.0865).

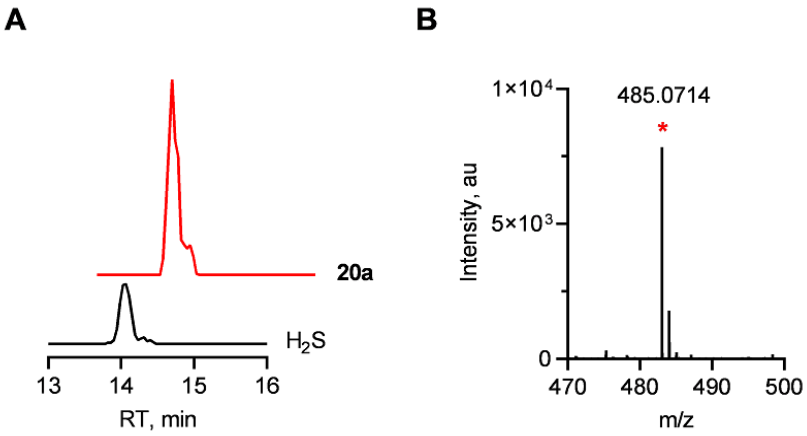

Figure 4.19: (A) Extracted ion chromatograms from an LC/MS analysis of Bis-SSSS-HPE-AM formation from Na_2S, **20a** + Na_2S; (B) Mass spectra for Bis-SSSS-HPE-AM (Expected, m/z = 485.0692 $[M + H]^+$; observed, m/z = 485.0714).

4.2.7. Cell viability assay

Next, an MTT assay was performed to check the cell viability. MCF-7 (Breast cancer cells) were treated with varying concentrations of **20a** and **20b** for 24 h. These compounds were well tolerated by the MCF-7 cells (Figure 4.20).

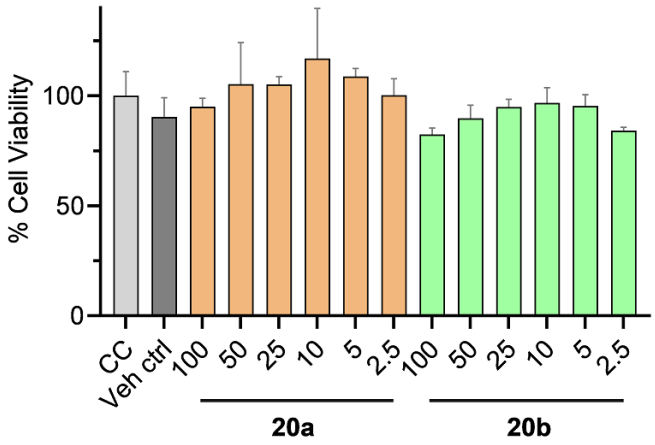

Figure 4.20: Cell viability assay carried out with varying concentrations of **20a** and **20b** on MCF-7 cells for 24 h. All data are presented as mean ± SD (n =3/group).

4.2.8. ROS quenching by compound 20a in senescent cells

Senescent cells always have large levels of ROS, which are crucial for cell viability. Hence, a selective delivery of ROS quenchers to mitigate ROS in senescent cells can be a therapeutic approach to treat senescent cells. Cells were treated with **4** (10 µM) and **20a** (50 µM) independently for 48 h and followed by incubation with an H_2DCFDA probe for 40 min and the fluorescence enhancement was recorded at excitation 492 nm and emission 525 nm. Cells were counted to express DCFDA fluorescence per cell. Compounds **4** and **20a** were able to reduce the ROS levels in senescent cells (Figure 4.21).

In another control experiment, cells were treated with compound **20a** and co-incubated with BCA (CSE inhibitor, 10 µM) or BCA alone for 48 h. The cells were then incubated with an H_2DCFDA probe for 40 min and an enhancement in fluorescence response was observed (Figure 4.21).

The results demonstrated that HNO induced an enhancement of the sulfane sulfur pool by reacting with intracellular H_2S, which resulted in ROS mitigation.

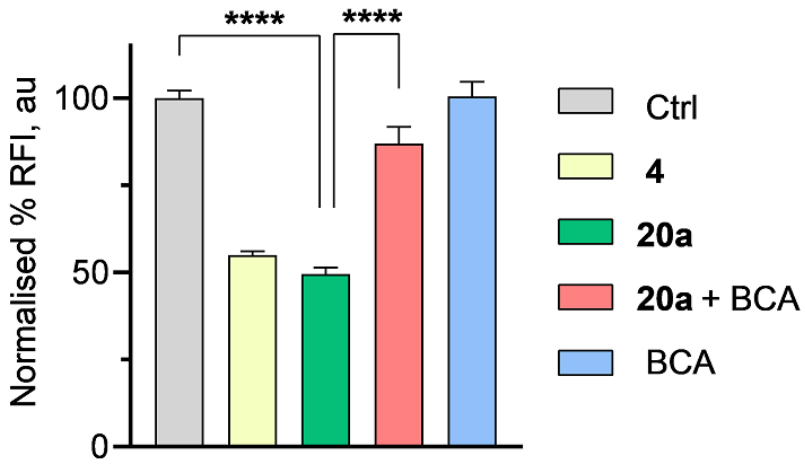

Figure 4.21: ROS quenching assay was conducted on senescent A459 cells with compounds **4**, **20a**, and BCA for 48 h; Ctrl refers to DMSO treated cells; **4** refers to 2-bromopiloty's acid; BCA refers to CSE inhibitor. An assay for ROS detection in senescent A549 cells was performed by Abraham Mathew (Dr. Deepak Saini lab, IISc, Bangalore).

4.3. Summary

To summarize, β-galactosidase activated HNO donors were designed and synthesized. The HNO generation was confirmed using three independent assays. In the first assay, HNO release was confirmed using **5**, and the quantitative yield of HNO generation from compound **20a** was observed. Surprisingly, HNO generation from compound **20b** was not observed. The generation of HNO was detected in the form of dimerized product N_2O in the second assay. Interestingly, a comparable yield of N_2O from compound **20a** was observed. In the third assay, HNO was trapped using *N*-acetyl tryptophan and the formation of NAT-NO was monitored. A similar profile for NAT-NO formation was observed from compounds **20a** and **4**. Next, nitric oxide (NO) generation from compounds was evaluated using the Griess assay and diminished NO release was observed compared to compound **4**. The decomposition profiles of the compounds were then investigated using HPLC. Here, compound **20a** gradually decomposes with a concomitant formation of **14** in the presence of β-galactosidase. However, compound **20b** was quite stable under these conditions. These results were complemented by docking studies, which again suggested that the orientation of the galactose moiety of compound **20a** is in proximity to the active site residues of the enzyme. Whereas, the galactose moiety of compound **20b** is oppositely oriented to the active site residues of enzyme.

Since HNO is known to enhance the sulfane sulfur pool by reacting with H_2S, we evaluated the persulfide formation from **20a** using an HPE-IAM probe and the formation of H_2S_2, H_2S_3 and H_2S_4 were observed. Next, cell viability assay was performed with compounds **20a** and **20b** to check the cytotoxicity in MCF-7 cells and compounds were well tolerated by cells. Finally, the mitigation of ROS by **20a** was studied in the senescent A549 cells. Interestingly, compound **20a** showed antioxidant properties by quenching the ROS in cells.

Collectively, these results demonstrated the utility of water-soluble β-galactosidase sensitive nitroxyl (HNO) donors in a controlled generation of HNO and its selective delivery to senescent cells.

4.4. Experimental protocols

4.4.1. Synthesis and characterization

Compound **16** was synthesized using the reported protocol and data were consistent with reported values.[24]

(2*R*,3*S*,4*S*,5*R*,6*S*)-2-(acetoxymethyl)-6-((1,3-dioxoisoindolin-2-yl)oxy)tetrahydro-2*H*-pyran-3,4,5-triyl triacetate (17):[25]

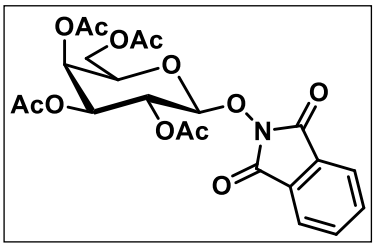

N-hydroxyphthalimide (7 g, 42.35 mmol, 3.5 eq.) and Et_3N (5 mL, 4 eq.) were dissolved in anhydrous DCM. To this solution, compound **16** (5 g, 12.1 mmol, 1 eq.) was added and the reaction mixture was stirred for 16 h at RT. Upon completion of the reaction (TLC analysis), the reaction mixture was quenched by adding water and extracted with dichloromethane. The combined organic extracts were dried over Na_2SO_4 and the filtrate was concentrated under reduced pressure and the product **17** was isolated as a light yellow solid (5.4 g, 90 %); ^1H NMR (400 MHz, $CDCl_3$): δ 7.88 – 7.86 (m, 2H), 7.70 – 7.78 (m, 2H), 5.48 (dd, *J* = 10.4, 8.2 Hz, 1H), 5.43 (dd, *J* = 0.9, 3.4 Hz, 1H), 5.12 (dd, *J* = 10.4, 3.4 Hz, 1H), 5.0 (d, *J* = 8.2 Hz, 1H), 4.26 – 4.15 (m, 2H), 3.95 – 3.92 (m, 1H), 2.22 (s, 3H), 2.20 (s, 3H), 2.02 (s, 3H), 1.99 (s, 3H). The analytical data are consistent with the previously reported values.

General procedure: Synthesis of (2R,3S,4S,5R,6S)-2-(acetoxymethyl)-6-(aminooxy)tetrahydro-2H-pyran-3,4,5-triyl triacetate (18):[25]

To a solution of compound **17** (1 eq.) in anhydrous DCM (5 mL), hydrazine monohydrate (1 eq.) was added dropwise at 0 ˚C. The reaction mixture was slowly warmed to room temperature and stirred for ~1 h. The white suspension was filtered off. The filtrate was washed with water and the aqueous layer was extracted with dichloromethane. The combined organic extracts were dried over Na_2SO_4, filtered and the filtrate was concentrated under reduced pressure to yield a crude product **18**, which was used for the next step without further purification.[25]

General procedure A: Synthesis of 19a and 19b:[26]

A mixture of compound **18** (1 eq.) and DMAP (1.2 eq.) in pyridine (5 mL) was independently added to aryl sulfonyl chloride derivatives (1.2 eq.) at 0 ˚C. The reaction mixture was warmed to RT and stirred for 2 - 3 h. Upon completion of the reaction (TLC analysis), the reaction

was quenched by adding 1 N HCl and extracted with EtOAC. The combined organic extracts were dried over Na_2SO_4, filtered and the filtrate was concentrated under reduced pressure to yield crude product **19a and 19b**, which was purified by silica column chromatography.

(2*R*,3*S*,4*S*,5*R*,6*S*)-2-(acetoxymethyl)-6-(((2-bromophenyl)sulfonamido)oxy) tetrahydro-2*H*-pyran-3,4,5-triyl triacetate (19a):

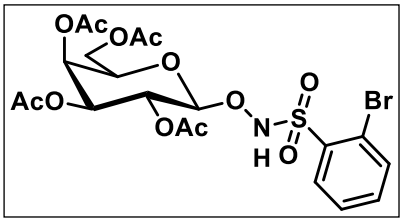

Starting with **18** (300 mg, 0.82 mmol), 2-bromobenzenesulfonyl chloride (210 mg, 0.82 mmol), DMAP (100 mg, 0.82 mmol) and the product **19a** was isolated as a pale yellow solid (300 mg, 63%); ^{1}H NMR (400 MHz, $CDCl_3$): δ 8.35 (s, 1H), 8.07 – 8.06 (m, 1H), 7.78 – 7.76 (m, 1H), 7.53 – 7.52 (m, 1H), 5.38 – 5.37 (m, 1H), 5.05 – 5.01 (m, 2H), 4.99 – 4.97 (m, 1H), 4.14 – 4.05 (m, 2H), 3.98 – 3.95 (m, 1H), 2.11 (s, 6H), 2.07 (s, 3H), 1.97 (s, 3H); ^{13}C NMR (100 MHz, $CDCl_3$): δ 170.4, 170.0, 169.9, 169.3, 135.4, 135.3, 135.2, 133.0, 127.8, 104.9, 71.7, 70.6, 69.9, 66.7, 61.1, 20.8, 20.7, 20.6, 20.5. HRMS (ESI): m/z for $C_{20}H_{23}BrNO_{12}S$ $[M+Na]^+$ calcd., 604.0100, found, 604.0096.

(2*R*,3*S*,4*S*,5*R*,6*S*)-2-(acetoxymethyl)-6-(((2-nitro-4-(trifluoromethyl)phenyl)sulfonamido)oxy) tetrahydro-2*H*-pyran-3,4,5-triyl triacetate (19b):

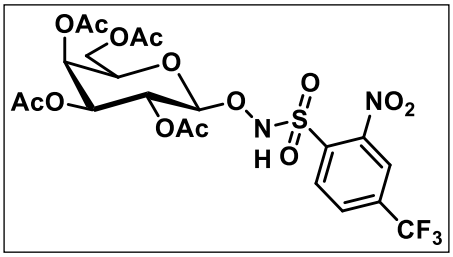

Starting with **18** (86 mg, 0.24 mmol), 2-nitro-4-(trifluoromethyl)benzenesulfonyl chloride (82 mg, 0.28 mmol), DMAP (30 mg, 0.28 mmol) and product **19b** was isolated as a pale yellow solid (110 mg, 76%); ^{1}H NMR (400 MHz, $CDCl_3$): δ 8.68 (br, 1H), 8.19 (d, *J* = 8.1 Hz, 1H), 8.14 (d, *J* = 1.4 Hz, 1H), 8.09 – 8.06 (M, 1H), 5.41 – 5.40 (m, 1H), 5.10 – 5.09 (m, 2H), 5.05 – 5.03 (m, 1H), 4.17 – 4.15 (m , 2h), 4.03 – 4.00 (m, 1H), 2.20 (s, 3H), 2.10 (s, 3H), 2.08 (s, 3H), 1.99 (s, 3H); ^{13}C NMR (100 MHz, $CDCl_3$): δ 170.5, 170.1, 170.0, 169.9, 148.7, 137.4, 137.1, 134.6, 133.3, 129.8, 123.0, 106.1, 71.3, 70.6, 67.2, 66.6, 61.2, 32.0, 29.8, 22.9, 21.1, 20.8, 20.6, 14.2; HRMS (ESI): m/z for $C_{21}H_{18}F_3N_2O_{14}S$ $[M+Na]^+$ calcd., 639.0814, found, 639.0811.

General procedure B: Synthesis of 20a and 20b:[27]

Compound **19** (1 eq.) was dissolved in methanol (5 mL) under a nitrogen atmosphere. Sodium methoxide (4 eq.) in methanol (2 mL) was added to the solution at 0 ˚C. The mixture was warmed at RT and stirred for ~3 h. Upon completion of the reaction (TLC analysis), cation-exchange resin (H^+) was added, filtered and washed with MeOH. The solvent was evaporated under reduced pressure. The crude product **20a** and **20b** was purified by prep-HPLC column chromatography (MeOH/H_2O) to give the desired compounds.

2-bromo-*N*-(((2*S*,3*R*,4*S*,5*R*,6*R*)-3,4,5-trihydro-6-(hydroxymethyl)tetrahydro-2*H*-pyran-2-yl)oxy)benzenesulfonamide (20a):

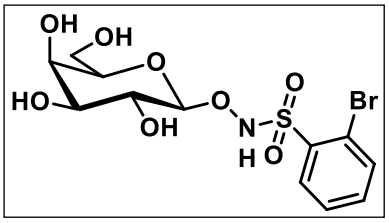

Starting with **19a** (300 mg, 0.51 mmol), sodium methoxide (111 mg, 2.05 mmol) and the product **20a** was isolated as a pale yellow solid (90 mg, 43%); ^{1}H NMR (400 MHz, CD_3OD): δ 8.20 – 8.17 (m, 1H), 7.85 – 7.83 (m, 1H), 7.59 – 7.53 (m, 2H), 4.63 (d, *J* = 7.7 Hz, 2H), 3.81 (s, 1H), 3.73 – 3.65 (m, 2H), 3.54 – 3.51 (m, 1H), 3.47 – 3.46 (m, 1H); ^{13}C NMR (100 MHz, CD_3OD): δ 135.9, 134.5, 133.9, 132.5, 127.0, 119.3, 106.6, 74.9, 72.9, 68.5, 68.0, 60.2; HRMS (ESI): m/z for $C_{12}H_{11}BrNO_6S$ $[M+H]^+$ calcd., 413.9853, found, 413.9876.

2-nitro-4-(trifluoromethyl)-*N*-(((2*S*,3*R*,4*S*,5*R*,6*R*)-3,4,5-trihydro-6-(hydroxymethyl)tetrahydro-2*H*-pyran-2-yl)oxy)benzenesulfonamide (20b):

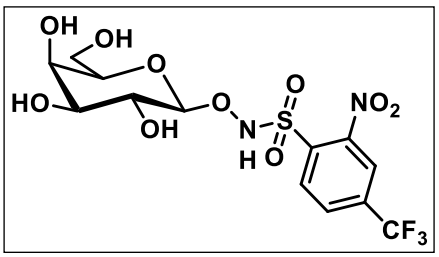

Starting with **19b** (100 mg, 0.16 mmol), sodium methoxide (36 mg, 0.65 mmol) and the product **20b** was isolated as a light yellow solid (30 mg, 41%); ^{1}H NMR (400 MHz, CD_3OD): δ 8.47 (d, *J* = 8.3 Hz, 1H), 8.32 (s, 1H), 8.17 (d, *J* = 8.3 Hz, 1H), 4.74 (d, *J* = 7.6 Hz,1H), 3.84 (d, *J* = 2.6 Hz, 1H), 3.75 – 3.67 (m, 2H), 3.59 – 3.56 (m, 1H), 3.52 – 3.44 (m, 2H); ^{13}C NMR (100 MHz, CD_3OD): δ 150.1, 135.5, 134.9, 130.3, 123.3, 122.4, 108.8, 79.5, 77.0, 75.0, 70.7, 70.0, 62.2; HRMS (ESI): m/z for $C_{13}H_{10}F_3N_2O_{10}S$ $[M+H]^+$ calcd., 471.0292, found, 471.0220.

Synthesis of *N*-acetyl tryptophan (NAT): Compound *N*-acetyl tryptophan was synthesized using a previously reported procedure and analytical data was consistent with reported values.[28]

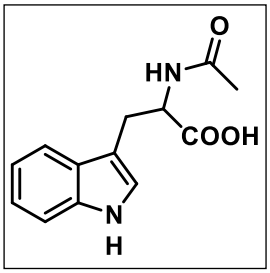

Tryptophan (200 mg, 1eq.) was dissolved in acetone and 2N NaOH (6 mL) was added, the reaction mixture was stirred for 10 min. Acetyl chloride (0.2 mL, 2 eq.) was added dropwise to the reaction mixture and stirred for a further 1 h at room temperature. Completion of the reaction was monitored by TLC. The reaction was quenched by adding 1N HCl and maintaining acidic pH. Evaporate the acetone and the aqueous layer were extracted with ethyl acetate (3 x 10 mL). The organic layer was washed with brine, dried over Na_2SO_4, filtered and the filtrate was concentrated under reduced pressure to yield the crude product which was purified by prep-HPLC to give NAT as a white solid (62 mg, 26%): ^{1}H NMR (400 MHz, CD_3COCD_3): δ 11.04 (s, 1H), 9.93 (s, 1H), 7.47 (d, *J* = 7.9 Hz, 1H), 7.23 (d, *J* = 8.0 Hz, 1H), 7.07 (s, 1H), 6.95 (t, *J* = 7.3 Hz, 1H), 6.88 (t, *J* = 7.5 Hz, 1H), 4.68 – 4.63 (m, 1H), 3.20 (dd, *J* = 14.7, 5.2 Hz, 1H), 3.06 (dd, *J* = 14.6, 8.6 Hz, 1H), 1.75 (s, 3H).

4.4.2. HNO detection by using 5

A stock solution of **5** (1 mM), **20a, 20b** and **4** (5 mM) in DMSO. β-galactosidase from *E. coli* (50 U/mL) stock solution in phosphate buffer saline (10 mM, pH 7.4) was prepared. The reaction mixture was prepared by adding 10 μM of **5** (2 μL, 1 mM), 50 μM of **20a, 20b** or **4** (2 μL, 5 mM) along with 10 U/mL of β-galactosidase (40 μL, 50 U/mL) from the stock solution and the volume was adjusted to 200 μL using phosphate buffer saline (10 mM, pH 7.4) in a 96-well plate and then incubated for 4 h at 37 ˚C. The fluorescence (excitation at 370 nm; emission at 460 nm) was measured using an Ensight Multimode Plate Reader (PerkinElmer) (Figure 4.3).

4.4.3. Analysis of Nitrous Oxide (N_2O) by Headspace Gas Chromatography

Stock solutions of **4** and **20a** (10 mM) were prepared in DMSO and used immediately after preparation. β-Galactosidase (100 U/mL) stock solutions were prepared in pH 7.4 PBS. In a 10 mL vial sealed with a rubber septum, 4.45 mL PBS (pH 7.4, 100 mM) containing DTPA as a metal chelator (100 μM) was purged with argon for 30 min. These vials were placed in a heated cell block, which was held at 37 ˚C. **20a** (100 μM) and β-galactosidase (10 U/ml) solution were added to each vial to obtain 5 mL total volume, and the resulting solutions were incubated for 15 h at 37 ˚C. A 100 μL gastight syringe with a sample lock was used for all

gas injections. Headspace gas samples (60 µL) were injected into an Agilent 8860 GC with a Restek column (ShinCarbon ST 80/100, 2m, 1/8" OD) to analyze for N_2O. These experiments were carried out in triplicate with three injections performed for each vial. The N_2O yield was averaged and reported relative to the standard **4** (2-bromo Piloty's acid) (Figure 4.4).

4.4.4. NAT-NO detection

A 1 mM stock solution of *N*-acetyl tryptophan (**NAT**), 5 mM stock solution of compound **20a** and **4**, *N* -acetyl-cysteine (NAC) in DMSO and β-galactosidase (10 U/mL from 100 U/mL) stock solution in PBS pH 7.4 were prepared. A reaction mixture of **NAT** (50 µM, 1 eq.) and compound **20a** or **4** (250 µM, 5 eq.) was prepared by mixing 3 µL of **NAT** and 3 µL of compound **20a** or **4** from the stock solutions and β-galactosidase (150 µL from 100 U/mL) in presence or absence of 3 µL of NAC (250 µM, 5 eq.) to phosphate buffer saline (pH 7.4, 10 mM) to make final volume 300 µL in a 96 well plate at 37 ºC for 1 h. Absorbance was measured at 335 nm on the Ensight Varioskan microtiter plate reader (Figure 4.5).

4.4.5. Nitric oxide (NO) detection by Griess assay

A 5 mM stock solution of compounds **20a, 20b** and **4** in DMSO were independently prepared. A typical reaction mixture consisted of compounds **20a, 20b**, **4** and $NaNO_2$ by mixing 2 µL from 5 mM stock solution and in the presence of β-galactosidase (20 µL from 100 U/mL stock solution in PBS pH 7.4) with phosphate buffer saline (pH 7.4, 10 mM) to make 200 µL final volume in a 96 well plate (with lid) and incubated for 4 h at 37 ºC. Then, 14 µL of Griess reagent was added to each well and incubated for 25 min at 37 ºC. Absorbance was measured at 540 nm on the Ensight Varioskan microtiter plate reader. The amount of NO released was estimated using a standard calibration curve generated with different concentrations of sodium nitrite ($NaNO_2$) solution (0 – 50 µM) using an Ensight Varioskan microtiter plate reader (Figure 4.6).

4.4.6. Decomposition study by HPLC

A stock solution of **20a** and **14** (10 mM) was prepared in DMSO and β-galactosidase (20 U/mL from 100 U/mL stock solution in PBS pH 7.4). The reaction mixture contained compound **20a** (5 µL, 10 mM), in the presence or absence of β-galactosidase in PBS pH 7.4 (Total volume = 1mL) and incubated at 37 ºC. The resulting mixture (100 µL) was taken out at predetermined time points and quenched by adding methanol (100 µL) subsequently

samples were subjected to high-performance liquid chromatography (HPLC Agilent Technologies 1260 Infinity). The mobile phase was water (0.1% TFA)/ Acetonitrile (0.1% TFA). The stationary phase was the C-18 reverse phase column (Phenomenex, 5 μm, 4.6 x 250 mm). A multistep gradient was used with the flow rate of 1 mL/min starting with 70:30 → 0 min, 70:30 to 60: 40 → 0 - 3 min, 60:40 to 50: 50 → 3 - 6 min, 50:50 to 40: 60 → 6 – 9 min, 40:60 to 30: 70 → 9 - 10 min, 30:70 to 50: 50 → 10 - 12 min, 50:50 to 60: 40 → 12 - 13 min, 60:40 to 70: 30 → 13 - 15 min, 70:30 to 70: 30 → 15 - 18 min. The retention time for **20a** was 6.9 min and for **7** was 8.9 min. The decomposition of **20a** and formation of **14** were monitored at 230 nm (Figure 4.7 and Figure 4.8).

The decomposition study of compound **20b** was performed using the aforementioned protocol. **20b** was incubated in the presence of the β-galactosidase in buffer for 24 h. Compound **20b** appeared at RT 12.2 min (Figure 4.9).

4.4.7. Polysulfide measurement using LC/MS

Stock solutions of **20a** (5 mM) and HPE-IAM (100 mM) were prepared in DMSO. A stock solution of Na_2S (20 mM) was prepared in DI water. A stock solution of β-galactosidase (10 U/mL from 50 U/mL stock solution in PBS pH 7.4). The reaction mixture was prepared by adding 50 μM of **20a** (5 μL, 10 mM) independently with 200 μM of Na_2S (10 μL, 20 mM) along with 10 U/mL of β-galactosidase (200 μL, 50 U/mL stock) and the volume was adjusted to 1 mL using phosphate buffer saline (10 mM, pH 7.4) in an eppendorf then incubated for 15 min at 37 ˚C on thermomixer (400 rpm). An aliquot (100 μL) was taken off the reaction mixture and then incubated with an HPE-IAM (2 μL, 100 mM) for a further 15 min. The reaction was quenched by adding 100 μL of acetonitrile. The samples were centrifuged at 10000g for 10 min at 37 ˚C, the supernatant was collected and assessed thereafter by LC/MS. All measurements were done using the following protocol: Acetonitrile (A) and 0.1% formic acid in water (B) were used as the mobile phase. A gradient was used with the flow rate of 0.3 mL/min starting with 100:0 → 0 min, 100:0 to 0:100 → 0 - 30 min. The MRM-HR mass spectrometry parameters for measuring compounds are m/z precursor ion mass ($M + H^+$) 215.0740 (HS-HPE-AM), 389.1530 (Bis-S-HPE-AM), 421.1250 (Bis-SS-HPE-AM), 453.0971 (Bis-SSS-HPE-AM) (Figure 4.14 – 4.19).

4.4.8. Cell viability Assay

Cytotoxicity of compounds **20a** and **20b** was studied in MCF-7 cells using the same protocol as outlined in Chapter 3 (Figure 4.20).

4.5. NMR spectra

^{1}H NMR spectra for compound **17**

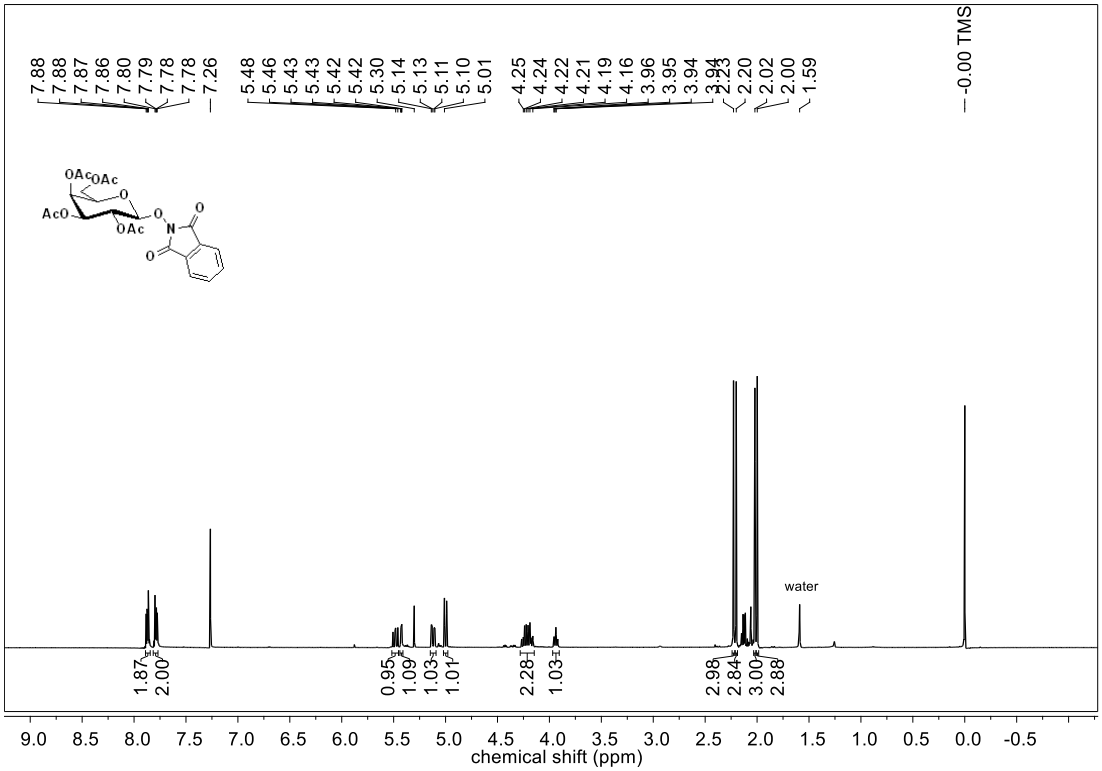

^{1}H NMR spectra for compound **19a**

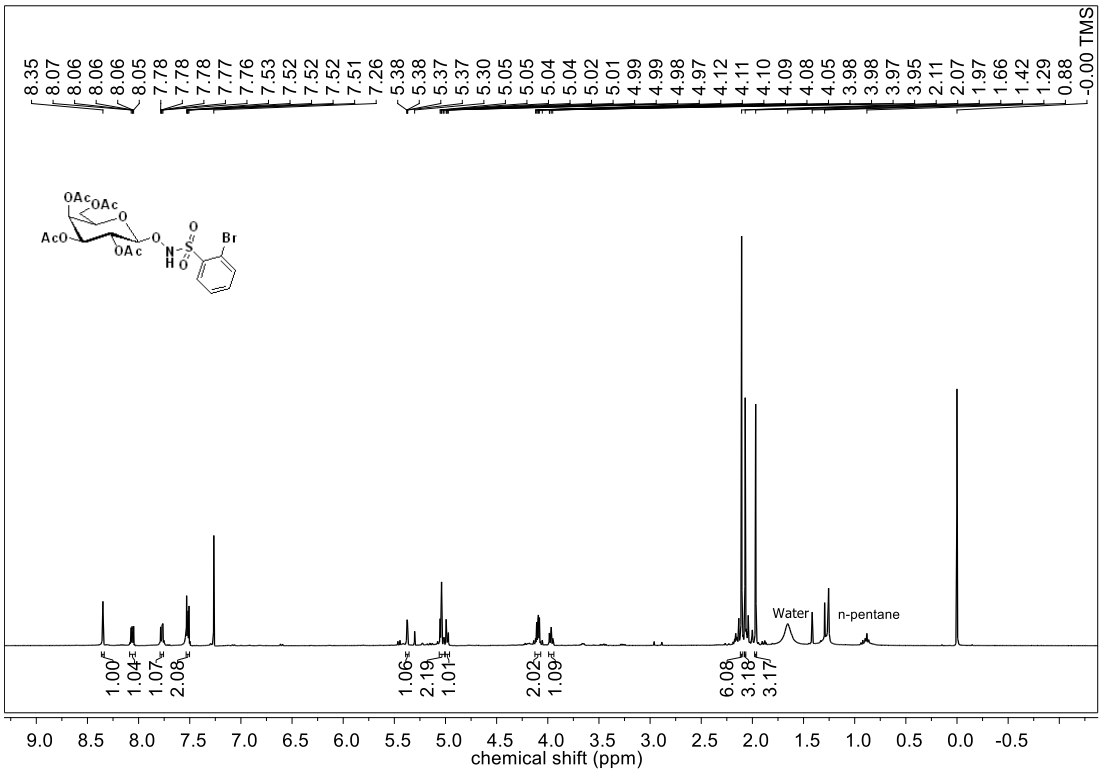

^{13}C NMR spectra for compound **19a**

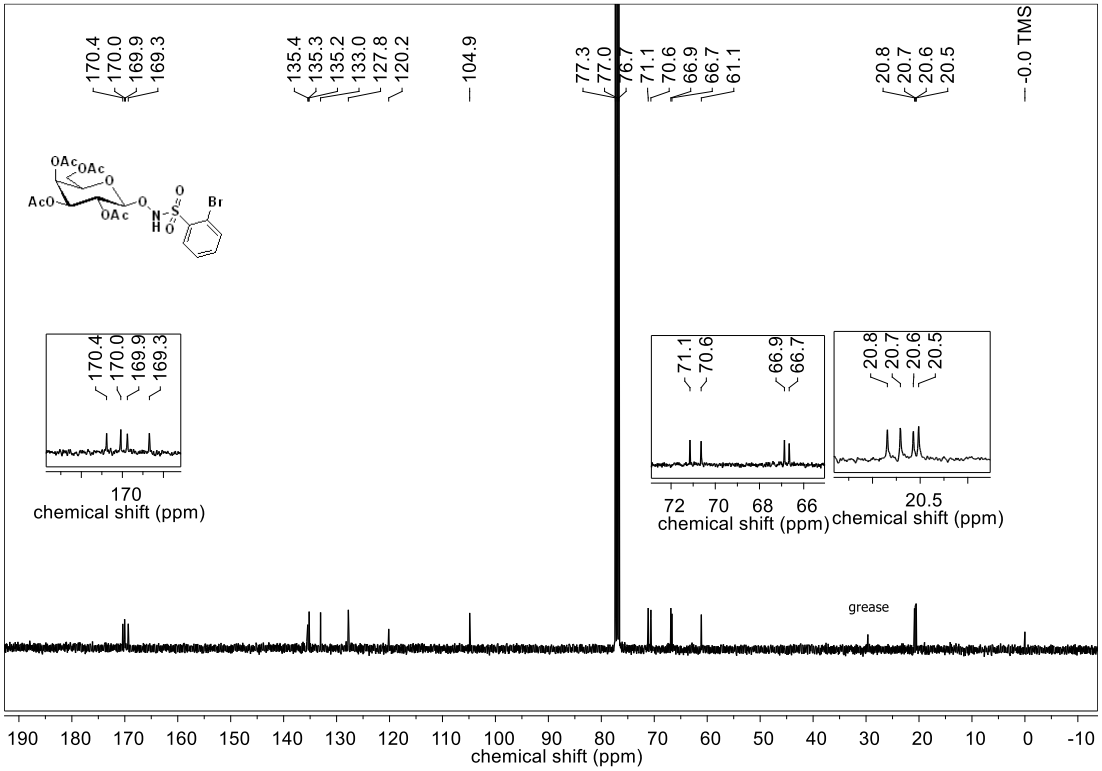

^{1}H NMR spectra for compound **19b**

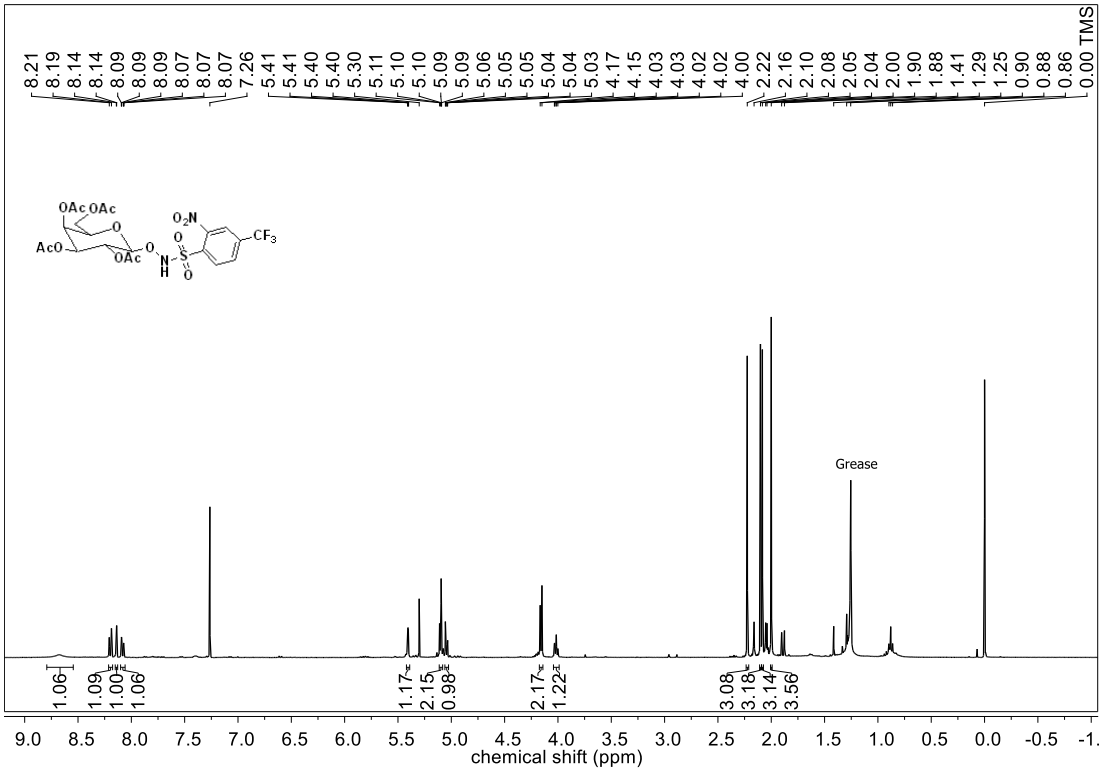

^{13}C NMR spectra for compound **19b**

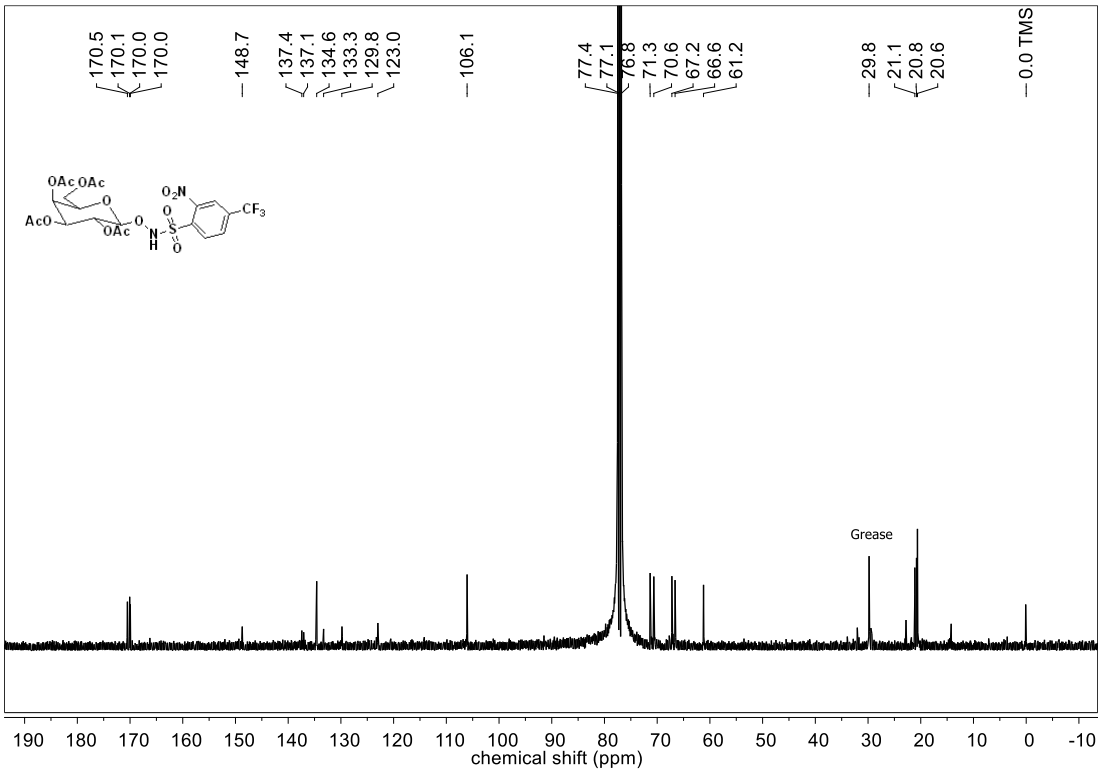

^{1}H NMR spectra for compound **20a**

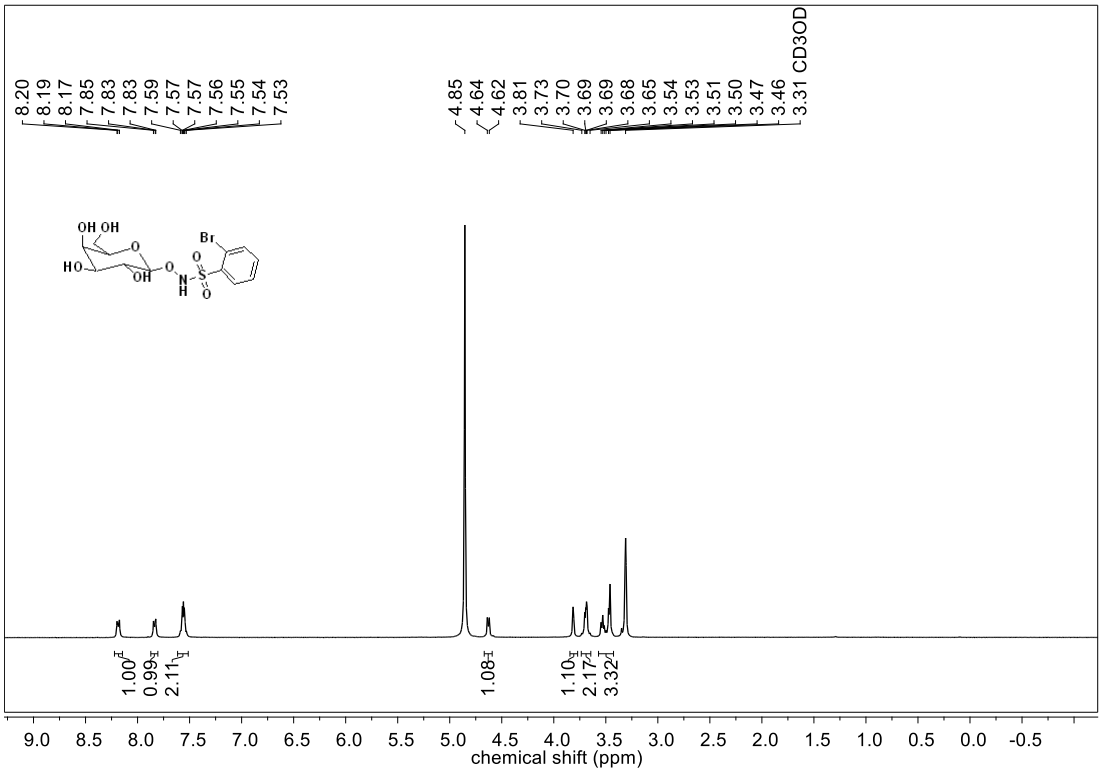

^{13}C NMR spectra for compound **20a**

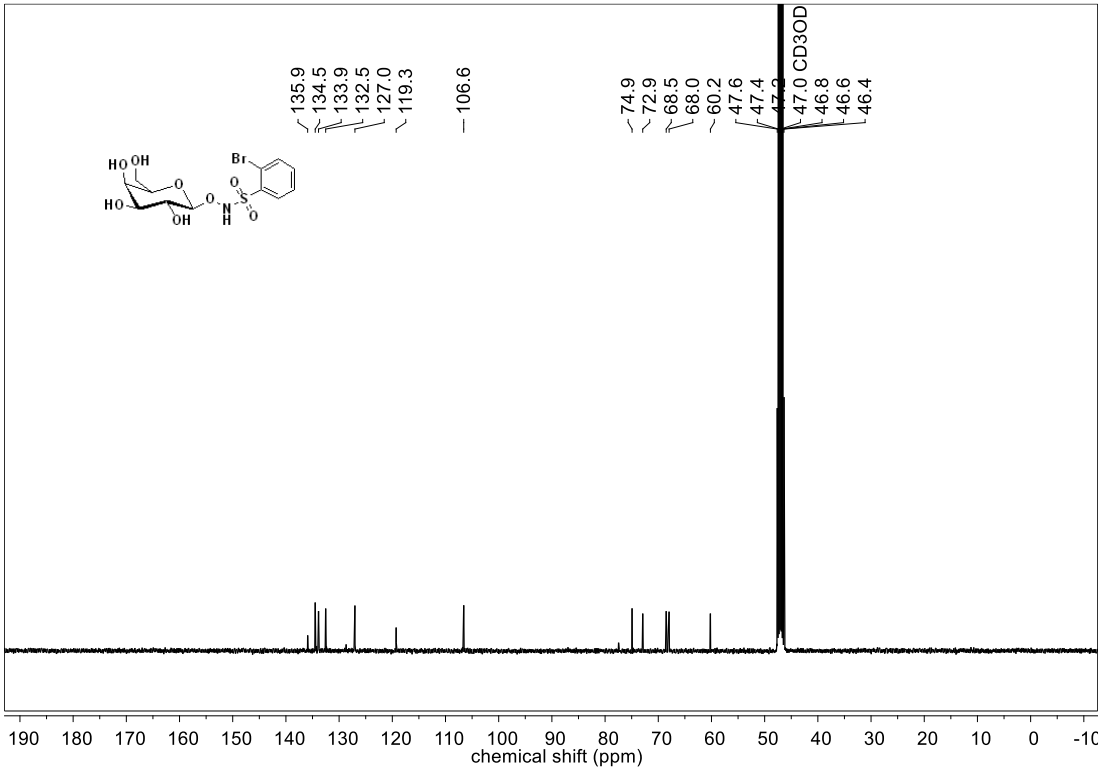

^{1}H NMR spectra for compound **20b**

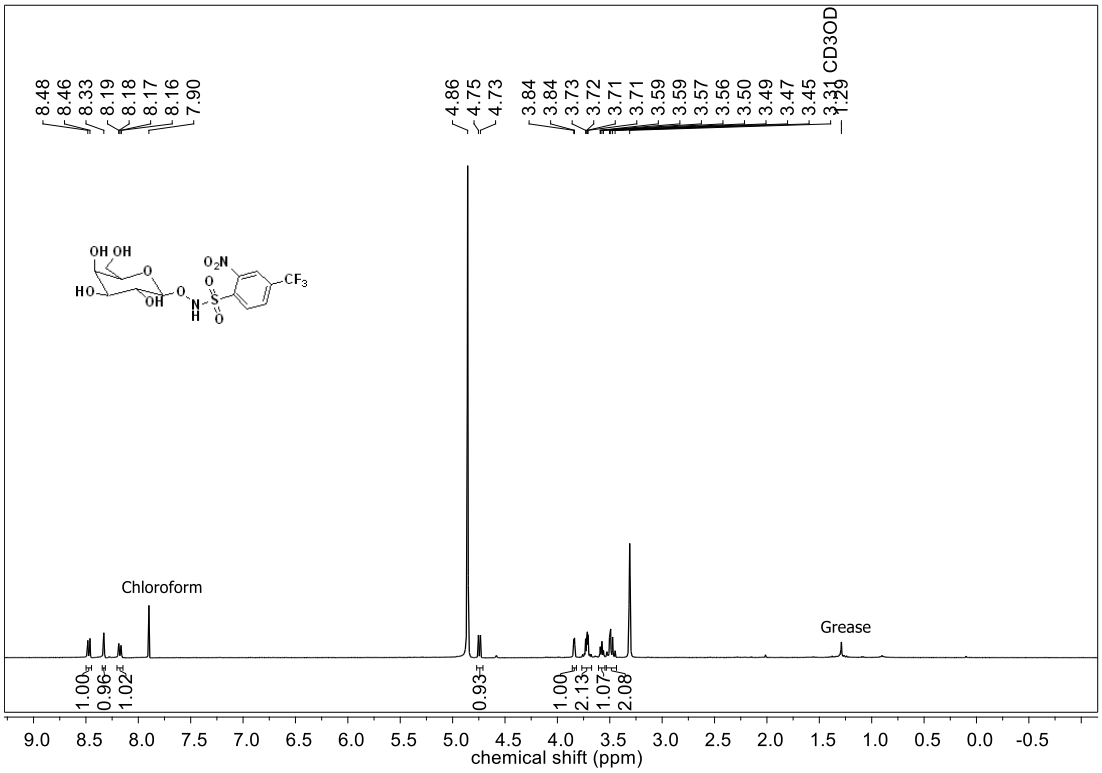

^{13}C NMR spectra for compound **20b**

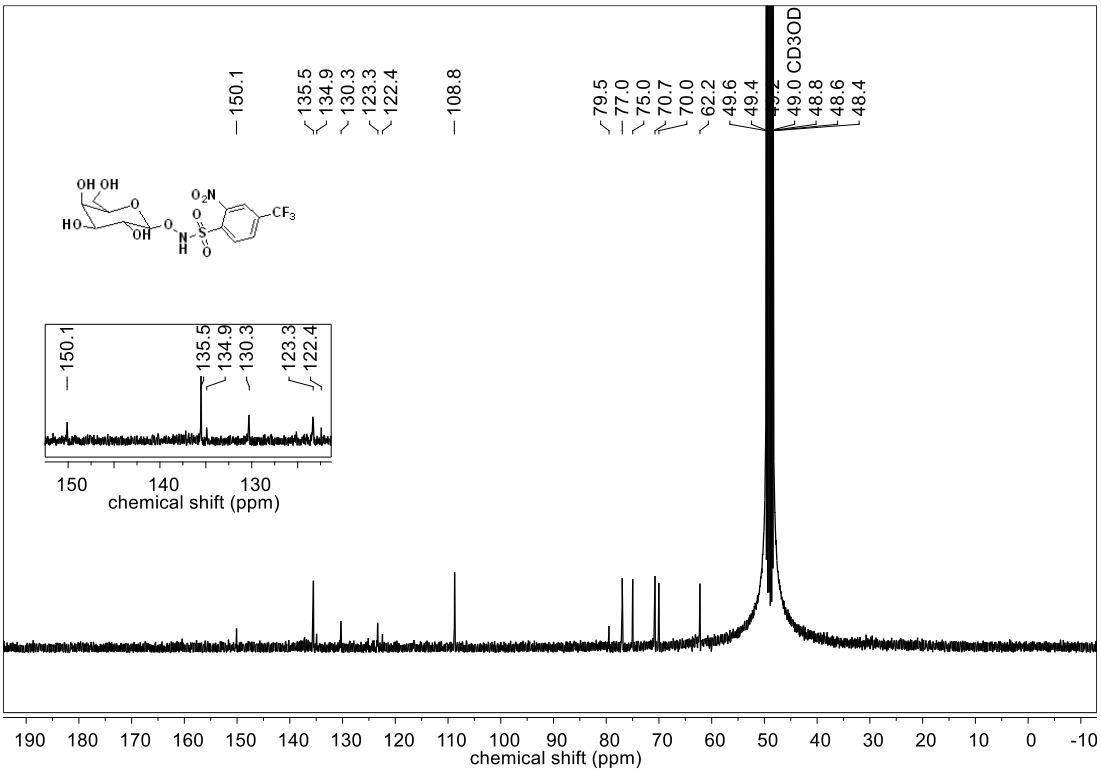

^{1}H NMR spectra for compound **NAT**

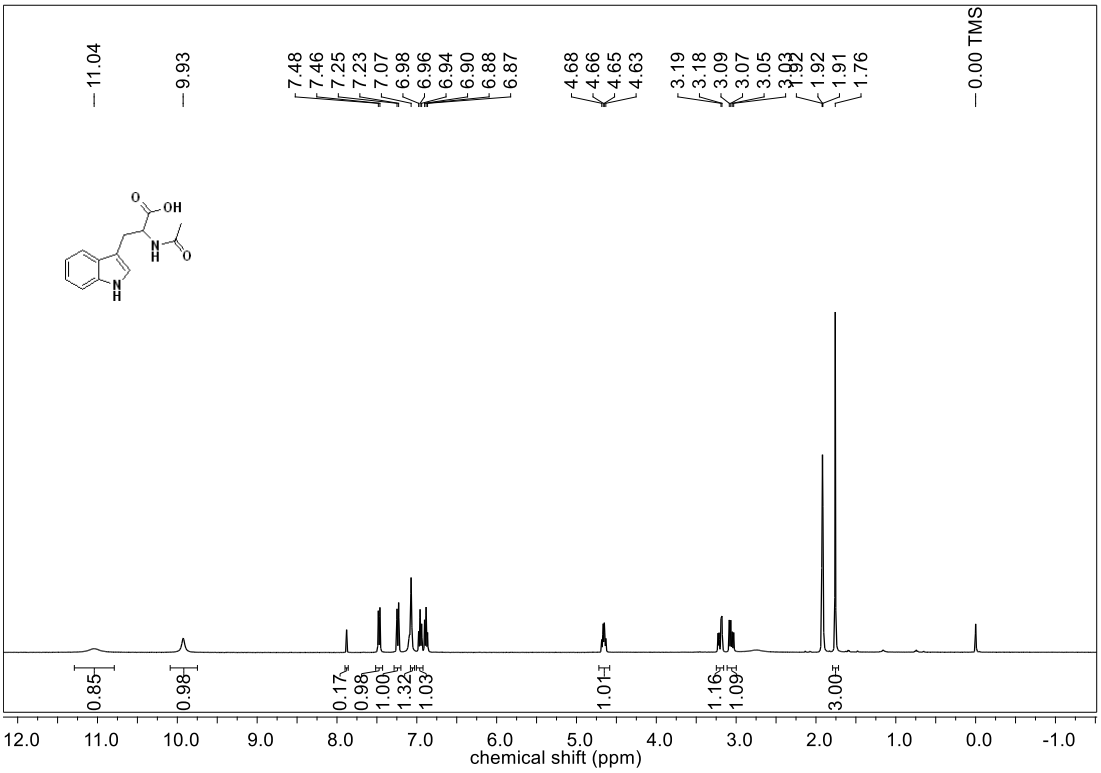

4.6. References

(1) Rose, M. R.; Flatt, T.; Graves, J. L.; Greer, L. F.; Martinez, D. E.; Matos, M.; Mueller, L. D.; Shmookler Reis, R. J.; Shahrestani, P. What Is Aging? *Front. Genet.* **2012**, *3*, 134.

(2) Di Leonardo, A.; Linke, S. P.; Clarkin, K.; Wahl, G. M. DNA Damage Triggers a Prolonged P53-Dependent G1 Arrest and Long-Term Induction of Cip1 in Normal Human Fibroblasts. *Genes Dev.* **1994**, *8* (21), 2540–2551.

(3) Adams, P. D. Healing and Hurting: Molecular Mechanisms, Functions, and Pathologies of Cellular Senescence. *Mol. Cell* **2009**, *36* (1), 2–14.

(4) Coppé, J.-P.; Desprez, P.-Y.; Krtolica, A.; Campisi, J. The Senescence-Associated Secretory Phenotype: The Dark Side of Tumor Suppression. *Annu. Rev. Pathol.* **2010**, *5*, 99–118.

(5) Davalos, A. R.; Coppe, J.-P.; Campisi, J.; Desprez, P.-Y. Senescent Cells as a Source of Inflammatory Factors for Tumor Progression. *Cancer Metastasis Rev.* **2010**, *29* (2), 273–283.

(6) Lee, B. Y.; Han, J. A.; Im, J. S.; Morrone, A.; Johung, K.; Goodwin, E. C.; Kleijer, W. J.; DiMaio, D.; Hwang, E. S. Senescence-Associated β-Galactosidase Is Lysosomal β-Galactosidase. *Aging Cell* **2006**, *5* (2), 187–195.

(7) Dimri, G. P.; Lee, X.; Basile, G.; Acosta, M.; Scott, G.; Roskelley, C.; Medrano, E. E.; Linskens, M.; Rubelj, I.; Pereira-Smith, O. A Biomarker That Identifies Senescent Human Cells in Culture and in Aging Skin in Vivo. *Proc. Natl. Acad. Sci. U. S. A.* **1995**, *92* (20), 9363–9367.

(8) Alique, M.; Sánchez-López, E.; Bodega, G.; Giannarelli, C.; Carracedo, J.; Ramírez, R. Hypoxia-Inducible Factor-1α: The Master Regulator of Endothelial Cell Senescence in Vascular Aging. *Cells* **2020**, *9* (1).

(9) Passos, J. F.; Von Zglinicki, T. Oxygen Free Radicals in Cell Senescence: Are They Signal Transducers? *Free Radic. Res.* **2006**, *40* (12), 1277–1283.

(10) Passos, J. F.; Nelson, G.; Wang, C.; Richter, T.; Simillion, C.; Proctor, C. J.; Miwa, S.;

Olijslagers, S.; Hallinan, J.; Wipat, A.; Saretzki, G.; Rudolph, K. L.; Kirkwood, T. B. L.; von Zglinicki, T. Feedback between P21 and Reactive Oxygen Production Is Necessary for Cell Senescence. *Mol. Syst. Biol.* **2010**, *6*, 347.

(11) Kuller, L. H.; Lopez, O. L.; Mackey, R. H.; Rosano, C.; Edmundowicz, D.; Becker, J. T.; Newman, A. B. Subclinical Cardiovascular Disease and Death, Dementia, and Coronary Heart Disease in Patients 80+ Years. *J. Am. Coll. Cardiol.* **2016**, *67* (9), 1013–1022.

(12) Zeng, S.; Shen, W. H.; Liu, L. Senescence and Cancer. *Cancer Transl. Med.* **2018**, *4* (3), 70–74.

(13) Jeon, O. H.; David, N.; Campisi, J.; Elisseeff, J. H. Senescent Cells and Osteoarthritis: A Painful Connection. *J. Clin. Invest.* **2018**, *128* (4), 1229–1237.

(14) Föger-Samwald, U.; Kerschan-Schindl, K.; Butylina, M.; Pietschmann, P. Age Related Osteoporosis: Targeting Cellular Senescence. *Int. J. Mol. Sci.* **2022**, *23* (5).

(15) Narasimhan, A.; Flores, R. R.; Robbins, P. D.; Niedernhofer, L. J. Role of Cellular Senescence in Type II Diabetes. *Endocrinology* **2021**, *162* (10).

(16) Liu, R.-M. Aging, Cellular Senescence, and Alzheimer's Disease. *Int. J. Mol. Sci.* **2022**, *23* (4).

(17) Vijg, J.; Campisi, J. Puzzles, Promises and a Cure for Ageing. *Nature* **2008**, *454* (7208), 1065–1071.

(18) Cai, Y.; Zhou, H.; Zhu, Y.; Sun, Q.; Ji, Y.; Xue, A.; Wang, Y.; Chen, W.; Yu, X.; Wang, L.; Chen, H.; Li, C.; Luo, T.; Deng, H. Elimination of Senescent Cells by β-Galactosidase-Targeted Prodrug Attenuates Inflammation and Restores Physical Function in Aged Mice. *Cell Res.* **2020**, *30* (7), 574–589.

(19) Asanuma, D.; Sakabe, M.; Kamiya, M.; Yamamoto, K.; Hiratake, J.; Ogawa, M.; Kosaka, N.; Choyke, P. L.; Nagano, T.; Kobayashi, H.; Urano, Y. Sensitive β-Galactosidase-Targeting Fluorescence Probe for Visualizing Small Peritoneal Metastatic Tumours in Vivo. *Nat. Commun.* **2015**, *6* (1), 6463.

(20) Doura, T.; Takahashi, K.; Ogra, Y.; Suzuki, N. Combretastatin A4-β-Galactosyl

Conjugates for Ovarian Cancer Prodrug Monotherapy. *ACS Med. Chem. Lett.* **2017**, *8* (2), 211–214.

(21) Adidala, R.; Devalapally, H.; Srivari, C.; Devarakonda R, K.; Raghuram Rao, A. An Improved Synthesis of Lysosomal Activated Mustard Prodrug for Tumor-Specific Activation and Its Cytotoxic Evaluation. *Drug Dev. Ind. Pharm.* **2012**, *38* (9), 1047–1053.

(22) Bora, P.; Sathian, M. B.; Chakrapani, H. Enhancing Cellular Sulfane Sulfur through β-Glycosidase-Activated Persulfide Donors: Mechanistic Insights and Oxidative Stress Mitigation. *Chem. Commun.* **2022**, *58* (18), 2987–2990.

(23) Chen, C.; Shi, Y.-Q.; Song, J.; Qi, Q.-S.; Gu, L.; Wang, P. G. Delivery of Nitric Oxide Released from Beta-Gal-NONOate Activation by Beta-Galactosidase and Its Activity against Escherichia Coli. *Biol. Pharm. Bull.* **2006**, *29* (6), 1239–1241.

(24) Autar, R.; Khan, A. S.; Schad, M.; Hacker, J.; Liskamp, R. M. J.; Pieters, R. J. Adhesion Inhibition of F1C-Fimbriated Escherichia Coli and Pseudomonas Aeruginosa PAK and PAO by Multivalent Carbohydrate Ligands. *ChemBioChem* **2003**, *4* (12), 1317–1325.

(25) Zhou, Y.; Cink, R. B.; Dassanayake, R. S.; Seed, A. J.; Brasch, N. E.; Sampson, P. Rapid Photoactivated Generation of Nitroxyl (HNO) under Neutral PH Conditions. *Angew. Chemie Int. Ed.* **2016**, *55* (42), 13229–13232.

(26) Aizawa, K.; Nakagawa, H.; Matsuo, K.; Kawai, K.; Ieda, N.; Suzuki, T.; Miyata, N. Piloty's Acid Derivative with Improved Nitroxyl-Releasing Characteristics. *Bioorg. Med. Chem. Lett.* **2013**, *23* (8), 2340–2343.

(27) Kim, E.-J.; Kumar, R.; Sharma, A.; Yoon, B.; Kim, H. M.; Lee, H.; Hong, K. S.; Kim, J. S. In Vivo Imaging of β-Galactosidase Stimulated Activity in Hepatocellular Carcinoma Using Ligand-Targeted Fluorescent Probe. *Biomaterials* **2017**, *122*, 83–90.

(28) Lan, J.-S.; Xie, S.-S.; Li, S.-Y.; Pan, L.-F.; Wang, X.-B.; Kong, L.-Y. Design, Synthesis and Evaluation of Novel Tacrine-(β-Carboline) Hybrids as Multifunctional Agents for the Treatment of Alzheimer's Disease. *Bioorg. Med. Chem.* **2014**, *22* (21), 6089–6104.

(29) Mao, G. J.; Zhang, X. B.; Shi, X. L.; Liu, H. W.; Wu, Y. X.; Zhou, L. Y.; Tan, W.; Yu, R. Q. A Highly Sensitive and Reductant-Resistant Fluorescent Probe for Nitroxyl in Aqueous Solution and Serum. *Chem. Commun.* **2014**, *50* (43), 5790-5792.

(30) Shafirovich, V.; Lymar, S. V. Nitroxyl and Its Anion in Aqueous Solutions: Spin States, Protic Equilibria, and Reactivities toward Oxygen and Nitric Oxide. *Proc. Natl. Acad. Sci.* **2002**, *99* (11), 7340–7345.

(31) Keceli, G.; Moore, C. D.; Toscano, J. P. Comparison of HNO Reactivity with Tryptophan and Cysteine in Small Peptides. *Bioorg. Med. Chem. Lett.* **2014**, *24* (16), 3710–3713.

(32) Griess, P. Bemerkungen Zu Der Abhandlung Der HH. Weselsky Und Benedikt ‚Ueber Einige Azoverbindungen". *Berichte der Dtsch. Chem. Gesellschaft* **1879**, *12* (1), 426–428.

(33) Juers, D. H.; Heightman, T. D.; Vasella, A.; McCarter, J. D.; Mackenzie, L.; Withers, S. G.; Matthews, B. W. A Structural View of the Action of Escherichia Coli (LacZ) Beta-Galactosidase. *Biochemistry* **2001**, *40* (49), 14781–14794.

(34) Trott, O.; Olson, A. J. AutoDock Vina: Improving the Speed and Accuracy of Docking with a New Scoring Function, Efficient Optimization, and Multithreading. *J. Comput. Chem.* **2010**, *31* (2), 455–461.

(35) Laskowski, R. A.; Swindells, M. B. LigPlot+: Multiple Ligand-Protein Interaction Diagrams for Drug Discovery. *J. Chem. Inf. Model.* **2011**, *51* (10), 2778–2786.

(36) Zarenkiewicz, J.; Khodade, V. S.; Toscano, J. P. Reaction of Nitroxyl (HNO) with Hydrogen Sulfide and Hydropersulfides. *J. Org. Chem.* **2021**, *86* (1), 868–877.

(37) Gupta, K.; Mathew, A. B.; Chakrapani, H.; Saini, D. K. H2S Contributed from CSE during Cellular Senescence Suppresses Inflammation and Nitrosative Stress. *Biochim. Biophys. acta. Mol. cell Res.* **2023**, *1870* (2), 119388.

Synopsis

Synthesis and Evaluation of Enzyme-Activated Nitroxyl (HNO) Generators

Chapter 1. Introduction

Nitroxyl/nitroxyl anion (HNO/NO^-), also known as azanone, nitrosyl hydride, hydrogen oxonitrate and hydridooxidonitrogen. It is a redox sibling, a 1-electron-reduced and protonated form of nitric oxide.[1] Nitroxyl was first reported by Angeli *et al* in 1896.[2] It is a short-lived species that rapidly dimerizes with a second-order rate constant ($k = 8 \times 10^6\ M^{-1}\ s^{-1}$) to give hyponitrous acid in an aqueous solution. Hyponitrous acid forms nitrous oxide (N_2O) and water upon decomposition (Eq. 1)[3] (Scheme 1).

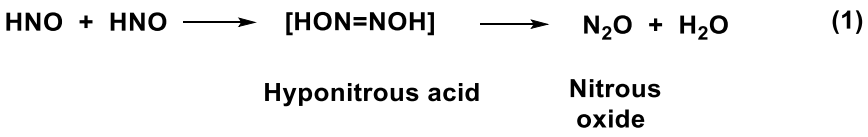

Scheme 1. The mechanism for the dimerization of HNO to form N_2O

Interestingly, HNO is believed to be endogenously synthesized by various biosynthetic pathways like its sibling, NO. Several plausible biosynthetic pathways for the endogenous generation of HNO has been proposed; (1) Oxidation of *L*-arginine by NOS in the absence of tetrahydrobiopterin (BH_4) cofactor;[4] (2) Interconversion between NO and HNO facilitated by superoxide dismutase;[5] (3) Reduction of NO to HNO by cytochrome *c*;[6] (4) Oxidation of hydroxylamine by heme protein;[7] (5) Reduction of nitrite by hydrogen sulphide (H_2S) in the presence of heme protein;[8] (6) the reaction of thionitrous acid (HSNO) with hydrogen sulfide (H_2S)[9] and (7) the reaction between NO and H_2S[10] (Figure 1).

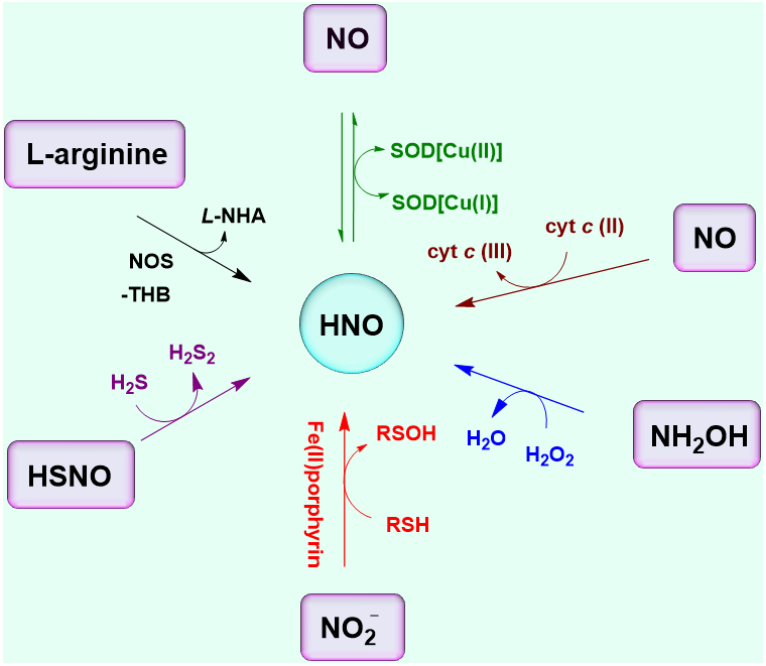

Figure 1. Biosynthesis of HNO generation. **NOS**: Nitric Oxide Synthase; **BH_4**: Tetrahydrobiopterin; ***L*-NHA**: *N*-hydroxy-*L*-arginine; **SOD**: Superoxide Dismutase

Owing to the thiophilic nature of HNO, it majorly targets the thiols and thiol-containing proteins. Recently, the reaction of HNO with H_2S and persulfides have studied by Toscano's research group. Upon reaction between HNO and H_2S formed persulfides and elemental sulfur while reaction with persulfides, generation of polysulfides were reported.[11] Similarly, thiols react with HNO to form sulfinamide or disulfide depending on the thiol concentration (Scheme 2).[12]

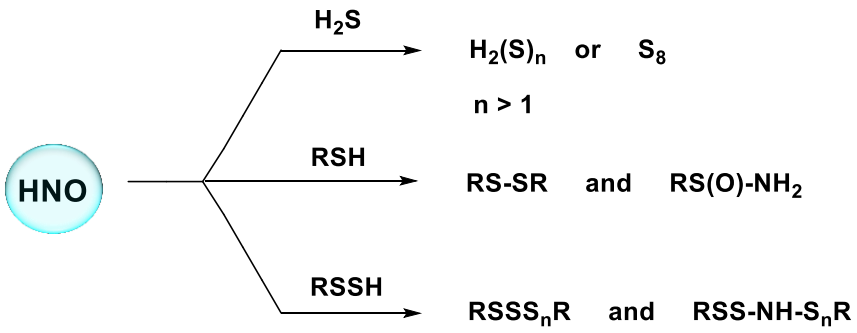

Scheme 2. The reaction of HNO with sulfur species

HNO has a unique and potentially important effects on the heart including vasorelaxation and enhanced cardiac contractility. Paolocci and coworkers reported that HNO has not only a positive inotropic (myocardial contractility) but also positive lusitropic (myocardial relaxation) effect on the heart. These effects were independent of β-adrenoceptor signaling, a potentially novel mechanism for modulating heart function.[13] Further, several research groups particularly, Several research groups showed that HNO can increase myocyte Ca^{2+} cycling by activation of the SARCA2A (sarcoplasmic Ca^{2+} reuptake pump) via interacting with the phospholamban (SARCA2A regulating protein) and activation of ryanodine receptor-2 (RyR2). These characteristics have led to the current pharmaceutical development of HNO donors as heart failure therapies (Figure 3).[14,15,16,17]

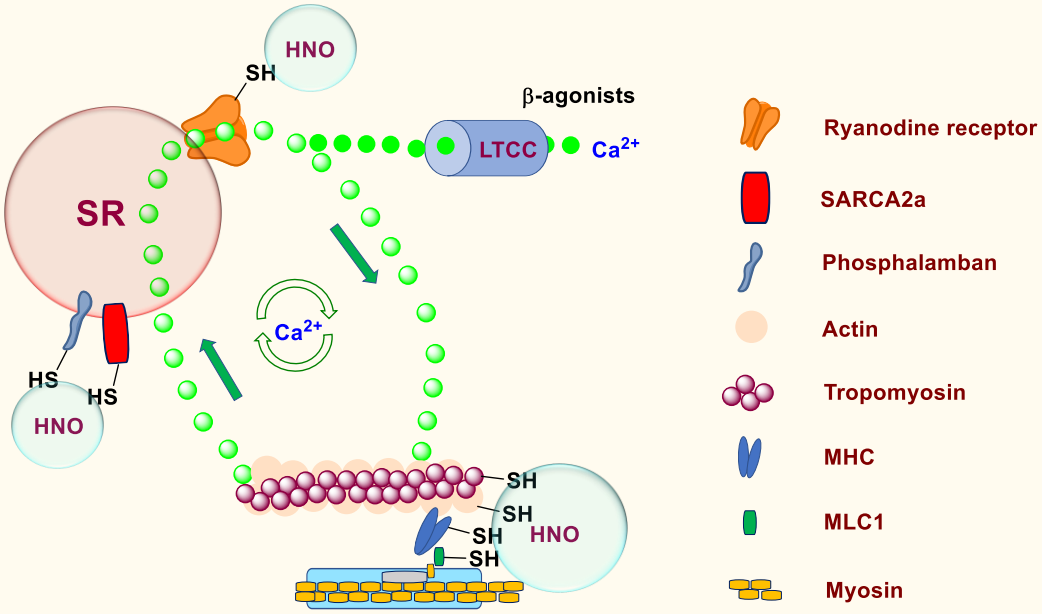

Figure 3: HNO in the cardiovascular system.

The most commonly used strategies to generate HNO at physiological conditions involves (i) -OH deprotonation; (ii) cleavage of PG by a specific stimulus and (iii) nucleophilic attack on acyl nitroso moiety. In the first case, -OH deprotonation takes place at physiological pH 7.4 and undergoes further decomposition to release HNO. Next, the stimulus was used for the cleavage of the protecting group to generate HNO. Finally, the formation of acyl nitroso intermediate takes place, which on nucleophilic attack or hydrolysis to release nitroxyl anion

(NO^-). In the second and third strategies, different stimuli such as light, thiol, heat, and enzymes were used to generate HNO (Scheme 3).

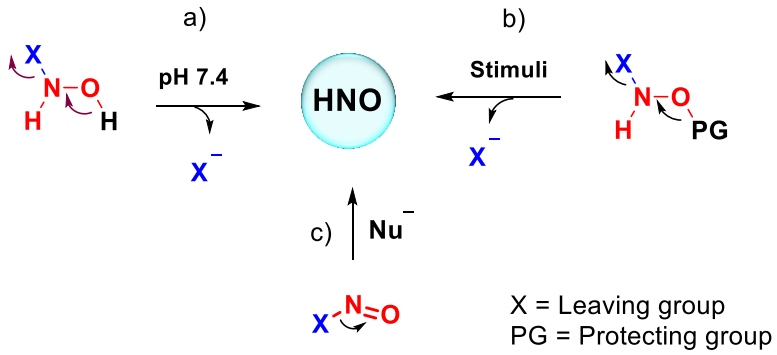

Scheme 3: General strategy for the HNO generation

The reported approaches to generating HNO have some limitations. Reported HNO donors generate HNO in an uncontrolled manner (burst HNO release) leading to the dimerization of HNO.[2,18] These donors have no selectivity in the delivery of HNO. To overcome these limitations, UV light-triggered HNO donors have been developed.[19,20] However, UV light can enhance the oxidative stress in the cellular system and affect the function of vital cellular biomolecules. Since low tissue penetration of UV light, *in vivo* studies become more challenging. Hence, UV light-triggered HNO donors are unsuitable for study of the HNO biology and pharmacology. Next, thiol activated HNO donor was reported and HNO is thiophilic in nature, the effective concentration of HNO will be less and the donor is not selective.[21] Retro Diels-Alder reaction-based HNO donor needs quite heating conditions to generate HNO, making it unsuitable in cellular studies.[22,23] Recently, an esterase triggered donors were developed, however, the issues with these donors are low HNO yield and concurrent generation of NO.[24,25] To achieve the selective delivery of HNO, β-galactosidase sensitive IPA/NO-based HNO donors are reported.[26] Given that, IPA/NO gives concomitant release of HNO/NO, the studies become more complicated.

For the detection of HNO, several types of probes are reported such as phosphine, thiol, and Cu(II) based probes.[27,28,29,30,31] However, these probes consume HNO during the time of detection. Also, phosphine-based probes are sensitive to cellular conditions. Reported probes do not have selectivity between HNO and NO, unsuitable to use in physiological conditions.

Hence, to overcome these limitations of existing prodrug strategies and HNO probes, the development of versatile HNO donors along with the concurrent release of fluorescent reporters is in urgent need.

We aim to design and develop a new HNO donor with the following characteristics: (i) the donor should be triggerable and the trigger should be selective; (ii) HNO release should be in a controlled manner to minimize dimerization; (iii) Fluorescence reporter should be turn ON and stable for the extended period; (iv) Fluorophore should not consume HNO during the detection (Figure 4).

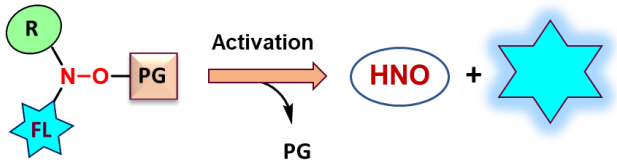

Figure 4: Design of the real-time monitoring of HNO

In order to achieve the aforementioned goals, in **Chapter 2**, we develop the HNO donor along with the fluorescence reporter. Upon activation by esterase, it generates HNO and fluorescence signals without the consumption of HNO during its detection. In addition, we synthesized a focused small library of compounds to achieve the tunable HNO release. Here, we used esterase as a trigger which is present ubiquitously in all types of cells. It offers a broad scope to study HNO biology and pharmacology in nearly all cell lines. Since, cancer cells produce a higher level of β-glucosidase enzyme, in **Chapter 3**, we designed β-Glu-HNO donors. These donors can generate HNO in a controlled manner upon activation by β-glucosidase. Further, to make specific delivery of HNO in aging (senescent cells), in **Chapter 4**, we developed β-galactosidase sensitive HNO donors. The presence of the ASGP receptors on the aged cells allowed the specific delivery of the donor. The β-Gal-HNO donor can generate HNO in a steady state and can mitigate the ROS level in the senescent cells.

Altogether, the studies described in this thesis address the several awaited problems associated with the existing HNO donors such as real-time monitoring of HNO in cells, triggerable and tunable HNO release, site-specific delivery of HNO, low concurrent generation of NO, benign byproducts. These tools will play an important role in exploring HNO biology and pharmacology, which is yet to be completely understood.

Chapter 2: Esterase-triggered Nitroxyl (HNO) Donors with a Fluorescence Reporter

We designed an HNO prodrug based on *N*,*N*,*O*-protected hydroxylamine. The oxygen of hydroxylamine was protected with cylcopropylcarboxylic ester, and on the nitrogen, a leaving group and Boc/H substituent was placed. Esterase is expected to cleave the ester linkage and further decomposition leads to HNO release (Scheme 4).

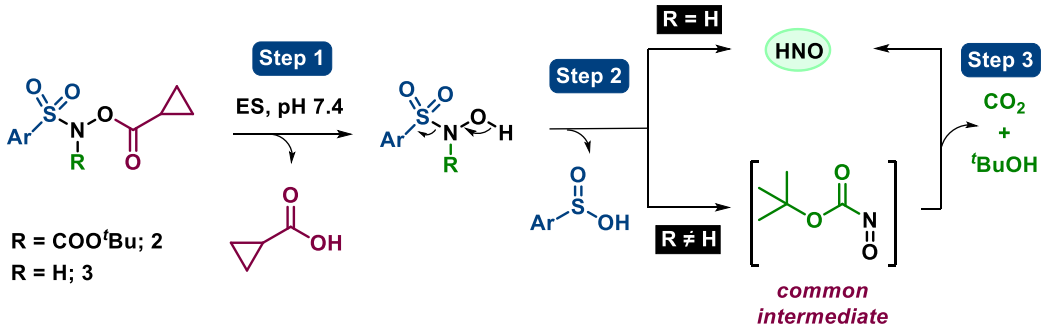

Scheme 4. Proposed mechanism of HNO generation upon activation by esterase

We synthesized the focused small library of compounds **2a-2g** and **3a-3g** to study the tunable HNO generation (Scheme 5). Next, compounds from series **2** and **3** were incubated independently with **5** and esterase from the porcine liver (0.5 U/mL) in phosphate buffer saline (pH 7.4), fluorescence enhancement was recorded using an Ensight Multimode Plate Reader (excitation 370 nm; emission 460 nm) (Table 1).

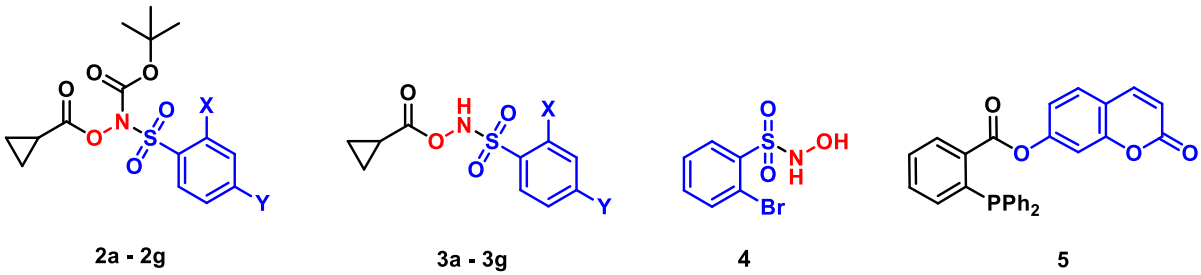

Scheme 5: Structures of compounds **2a-2g** and **3a-3g**

Table 1: Compounds **2a-2g** and **3a-3g** with the % HNO yields

Entry	X	Y	Compd No.	% HNO
1	H	H	**2a**	98
2	Br	H	**2b**	89
3	H	Br	**2c**	98
4	CF_3	H	**2d**	100
5	Br	CF_3	**2e**	89
6	NO_2	H	**2f**	70
7	H	NO_2	**2g**	75
8	H	H	**3a**	27
9	Br	H	**3b**	92
10	H	Br	**3c**	77
11	CF_3	H	**3d**	98
12	Br	CF_3	**3e**	100
13	NO_2	H	**3f**	76
14	H	NO_2	**3g**	17

During the HNO detection, the cleavage of **5** was observed upon incubation with esterase, which can limit the use of the HNO probe.

Further, to overcome the limitation associated with the probe, we designed dansyl based HNO donor (Figure 5 and Scheme 6).

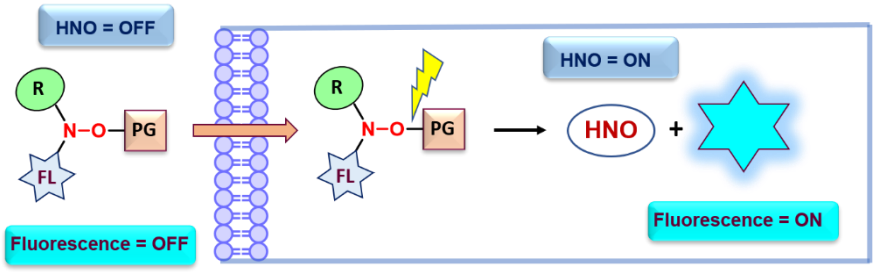

Figure 5. Design of stimuli-responsive concomitant release of nitroxyl (HNO) and fluorescence reporter by the HNO donor.

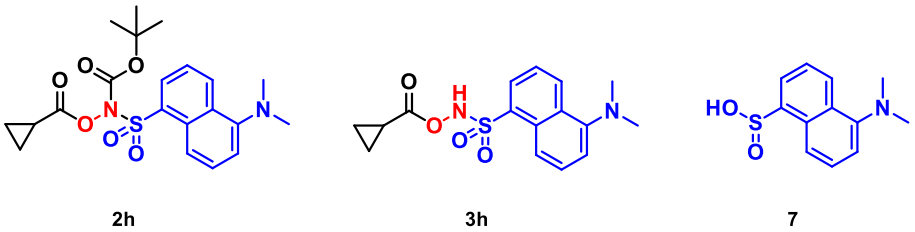

Scheme 6: Structures of compounds **2h**, **3h** and **7**

Upon incubation with esterase, the donor showed concomitant release of HNO and fluorescent reporter (Table 2). The incorporation of latent fluorophore in the donor eliminates the need for a secondary assay for monitoring HNO (Figure 6).

Table 2: Compounds **2h** and **3h** with the % yields of HNO and **7**

Entry	Compd No.	% HNO	% **7**
1	**2a**	74	95
2	**2b**	30	98

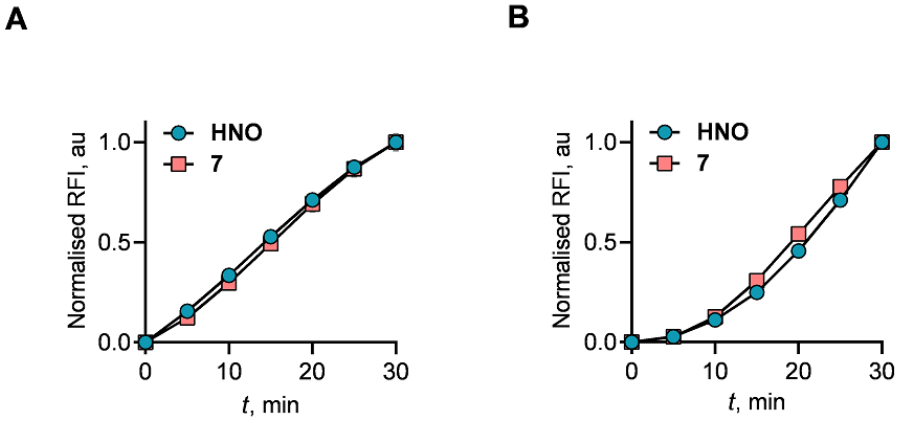

Figure 6. Time-dependent release of HNO and **7**: (A) Compounds **2h** (50 µM); (B) **3h** (50 µM) were incubated in the presence of esterase (0.5 U/mL) in buffer (pH 7.4) at 37 ˚C. Fluorescence enhancement was monitored over 30 min.

Since, persulfides/polysulfides are the reservoirs of antioxidants, known to mitigate ROS levels. Hence, it is important to study the cross-talk between HNO and H_2S to generate the persulfides/polysulfides (Figure 7).

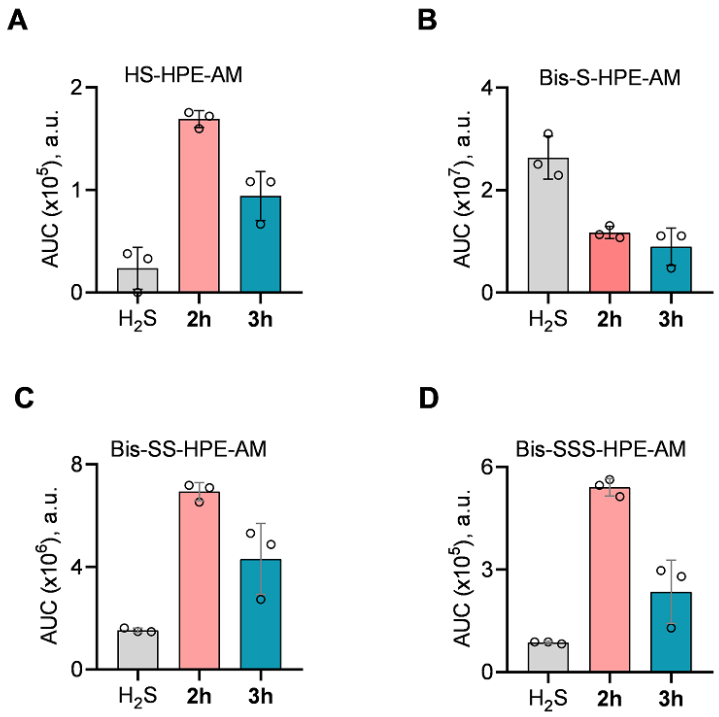

Figure 7: LC/MS study. Polysulfide formation was measured by detection of trapped HPE-IAM species from Na_2S, **2h** and **3h** upon incubation with esterase in PBS (pH 7.4) at 37 ˚C for 15 min; (A) Formation of HS-HPE-AM; (B) Formation of Bis-S-HPE-AM; (C) Formation of Bis-SS-HPE-AM; (D) Formation of Bis-SSS-HPE-AM.

Next, we aimed to monitor the release of HNO and **7** in a cellular system. The following compounds were used for cellular imaging (Scheme 7).

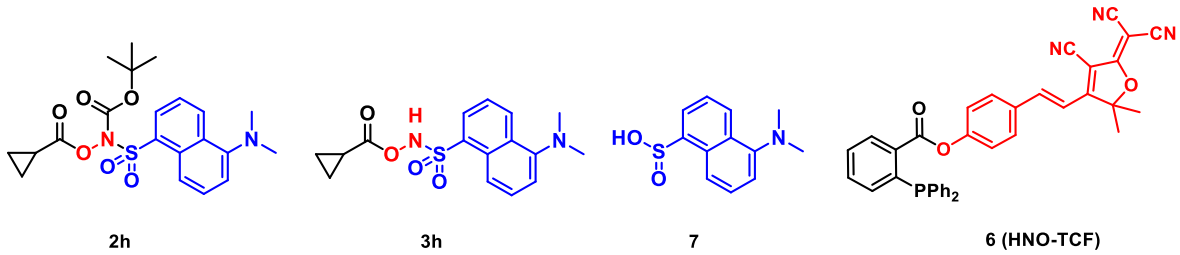

Scheme 7: Structures of compounds **2h**, **3h**, **4** and **6** used for the cellular imaging

Cells were incubated with compounds **2h, 3h** and **4** independently with and without the HNO probe **6** (HNO-TCF dye) for 2h and cells were imaged on the Carl Zeiss LSM710 laser scanning confocal microscope with anisotropy (Figure 8).

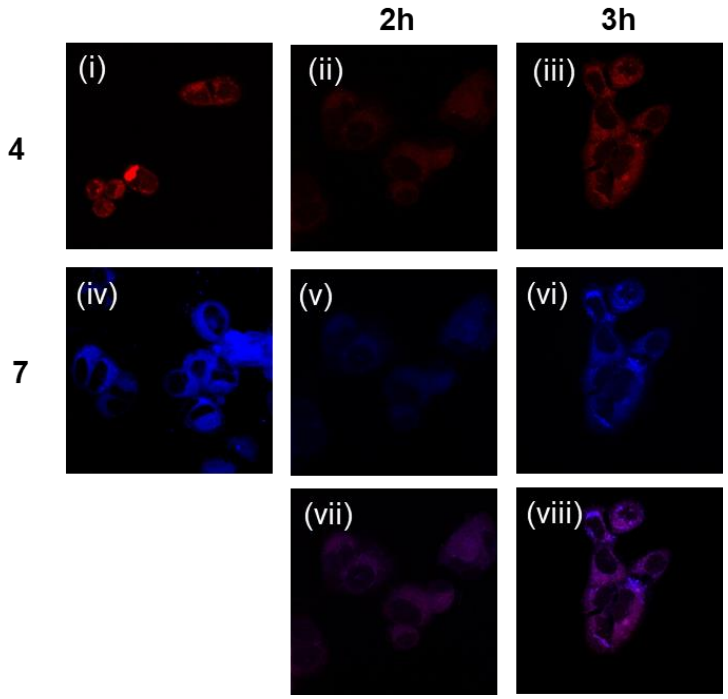

Figure 8: Confocal microscopy images of HNO and **7** in breast cancer cells (MCF-7). **HNO detection:** MCF-7 cells were pre-incubated with HNO-TCF dye **6 (**20 μM) for 30 min followed by treatment of (i) **4** (2-bromo-Piloty's acid); (ii) **2h** (iii) **3h** (200 μM) independently for 2 h. The cells were imaged on Carl Zeiss LSM710 laser scanning confocal microscope with anisotropy. The cells were imaged in the RED channel (Alexa fluor 568 for HNO detection). (iv) **7** (200 μM); (v) **2h** (vi) **3h**. The cells were imaged in the DAPI channel (Detection of **7**). (vii) Merged image of (ii and v); (viii) Merged image of (iii and vi).

As expected, compounds **2a-2g** and **3a-3g** show the tunable generation of HNO. Next, compounds **2h** and **3h** showed a concurrent generation of HNO along with fluorescence reporter. In addition, compounds **2h** and **3h** can generate persulfide/polysulfide by reacting with the H_2S. Further, we successfully imaged the release of HNO and **7** in a cellular system.

Chapter 3: β-glucosidase activated Nitroxyl (HNO) donors

Designing a tool for specific HNO delivery is desirable to overcome the limitations associated with the esterase-based strategy. To achieve this goal, glucoside was chosen as protecting group for hydroxylamine. Glucose with free hydroxyl groups that are expected to enhance aqueous solubility. The expression and activity of β-glucosidase enzymes were significantly upregulated in breast cancer tissues and hepatocellular carcinoma (HCC) cell lines.[32,33]

Design and development of β-glucosidase sensitive HNO prodrug was considered. Since glucose transporters were overexpressed in cancer cells.

It is expected that a nucleophilic attack of β-glucosidase takes place on the anomeric carbon of glucoside resulting in the cleavage of the glucosidic bond to release an anionic intermediate. Further, the intermediate undergoes subsequent decomposition in pH 7.4 to release HNO and aryl sulfinic acid (Scheme 8).

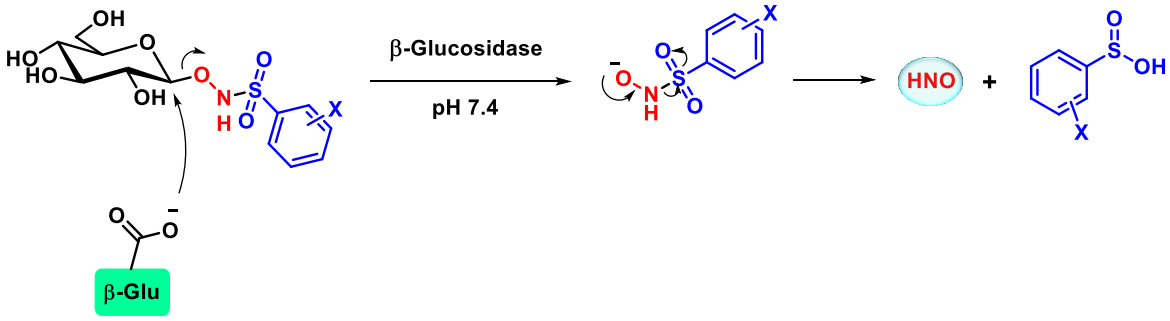

Scheme 8. Design and proposed mechanism of HNO generation upon activation by β-glucosidase

With this design, we synthesized the five derivatives by appending the different groups on the aromatic ring (Table 3).

Table 3: Compounds **13a-3e** with the % HNO yields

Entry	Product	Ar	% HNO
1	**13a**	2-Br-Ph	95
2	**13b**	Dansyl	0
3	**13c**	4-OMe-Ph	0
4	**13d**	2- NO_2-4- CF_3-Ph	0
5	**13e**	2,4,6-trifluoro-Ph	0

To test the HNO generation from prodrug, a fluorescence-based experiment was performed using β-glucosidase from almonds and **5**.[27] Compounds **13a-13e** are expected to the cleaved

by β-glucosidase to release HNO, which can be trapped by **5** to release fluorescent umbelliferone (excitation = 370 nm; emission = 460 nm). Compound **13a** was shown the comparable release of HNO with positive control **4** (2-bromo-Piloty's acid, known HNO generator). While HNO generation from compounds **13b**-**13e** was not detected (Figure 9).

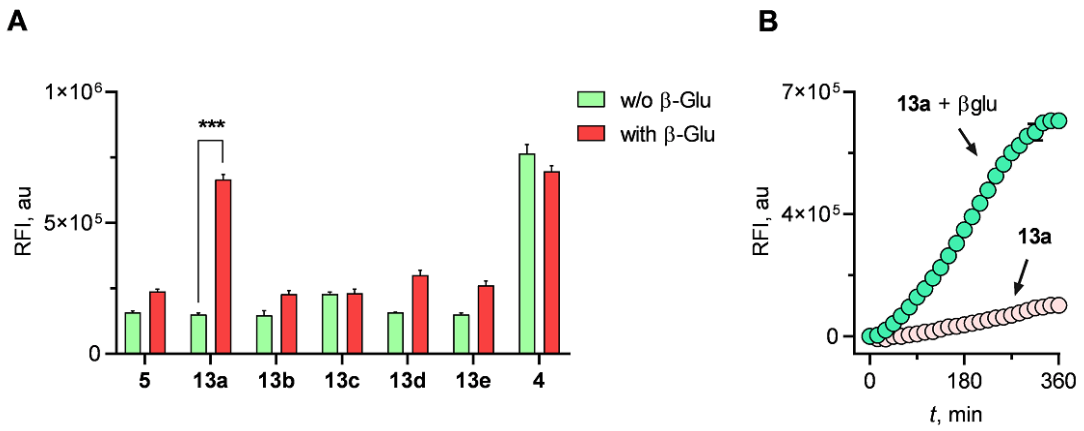

Figure 9: Detection of HNO using **5.** (A) Compounds **13a-13e** were incubated with **5** and in the presence and absence of the β-glucosidase in buffer (pH 7.4) at 37 ˚C for 6 h; (B) Time-dependent release of HNO from compound **13a** in the absence and presence of β-glucosidase in buffer (pH 7.4) at 37 ˚C for 6 h. Dye refers to **5**; **4** refers to 2-bromo-piloty's acid (λ_{ex} = 370 nm; λ_{em} = 460 nm).

Further, a decomposition study was carried out using HPLC. Compound **13a** was incubated with the β-glucosidase (10 U/mL) in buffer and the decomposition of the compound was monitored over 36 h. As expected, the decomposition of compound **13a** with concomitant formation of **14** was observed only in the presence of β-glucosidase (Figure 10).

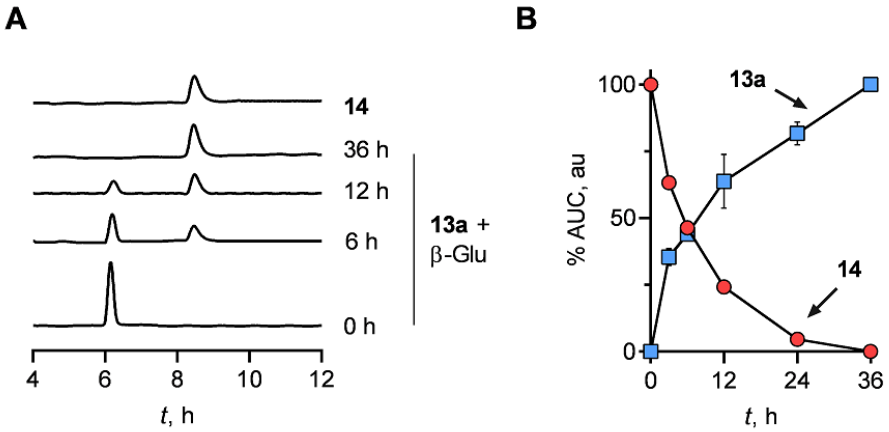

Figure 10: HPLC traces and AUC for decomposition of **13a** (RT = 6.1 min) and formation of **14** (RT = 8.4 min) in the presence of β-glucosidase in buffer (pH 7.4).

Further, we performed the docking analysis with compounds **13a-13e** to study the interaction of compounds with the active site residues of β-glucosidase. The docking studies revealed that **13a** binds well to the β-glucosidase over other derivatives. The residues involved in catalysis were also appropriately aligned (**13a-13e**). Together, these model data suggest the importance of binding of the substrate to the active site and also permit to the sensitivity of the active site to minor modification in the substrate. Further, the cytotoxicity of compounds **13a – 13e** was checked and the compounds were found to be non-toxic.

Chapter 4: β-galactosidase triggered Nitroxyl (HNO) donors

We expanded our goal to design and synthesize water-soluble HNO donors which are selective to the senescent cells (Figure 11). Given that senescent cells have a higher level of ROS, HIF-1α, iNOS and β-galactosidase. As HNO is known for ROS quenching, inhibition of HIF-1α and iNOS. Collectively, these characteristics of HNO make it an interesting candidate for reducing inflammation and oxidative stress in senescent cells. Since β-galactosidase is overexpressed in senescent cells,[34,35] it makes a suitable trigger to develop a new HNO prodrug. Also, ASGPR (Asialoglycoprotein receptor) is overexpressed on the cell wall of the senescent cells, it has a high affinity towards sugars, and it helps in the targeted delivery of HNO prodrug. Based on this, we designed a β-galactosidase activated HNO prodrug.

The design contained β-galactose moiety attached to an HNO donor (derivatives of Piloty's acid). Here, β-galactose moiety will act as a gate pass for the HNO prodrug to permeate senescent cells. Upon entry of the prodrug, senescence-associated β-galactosidase (SA β-Gal) is expected to cleave the glycosidic bond to release HNO.

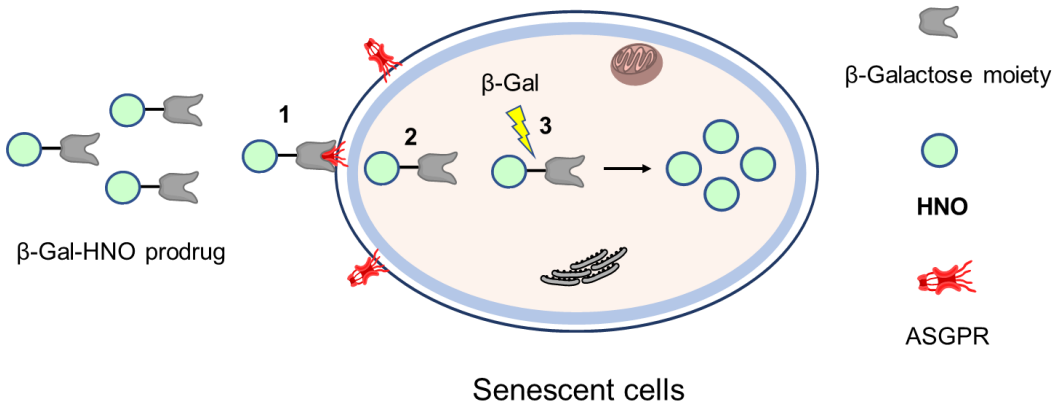

Figure 11. Design of β-galactosidase triggered nitroxyl (HNO) donor. (1) The interaction of HNO prodrug with ASGPR, (2) Entry into the senescent cells, and (3) β-galactosidase mediated cleavage of the glycosidic bond to release HNO.

The following mechanism was proposed for HNO generation from β-galactosidase activated nitroxyl (HNO) donors. It is well known that active site residues of the enzyme interact with the galactose moiety to cleave the anomeric C-O bond to release an active drug (Scheme 9).

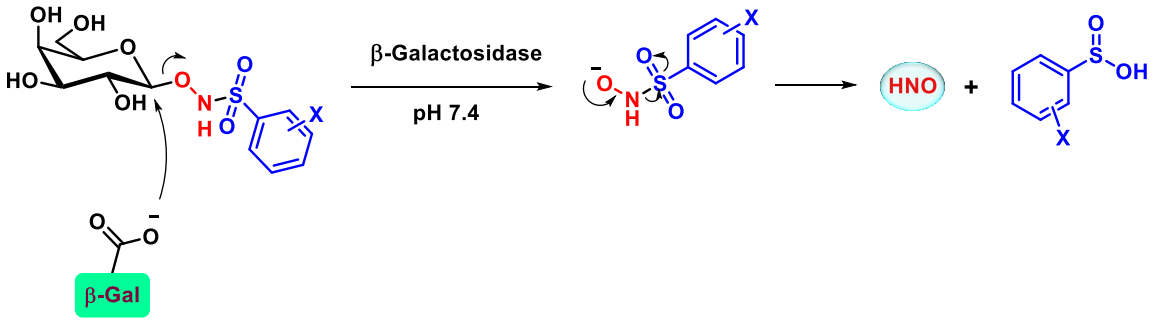

Scheme 9. Proposed mechanism of HNO generation upon activation by β-galactosidase

To test the hypothesis of HNO generation from prodrug using **5**,[27] compounds **20a** and **20b** was co-incubated with the β-galactosidase from *E. coli* and **5** for 4 h. The time-dependent

enhancement in fluorescence intensity from compounds **20a** and **20b** was recorded using an Ensight Multimode Plate Reader (excitation 370 nm; emission 460 nm).

Upon incubation with β-galactosidase, compound **20a** showed a higher yield of HNO than compound **20b** (Figure 12).

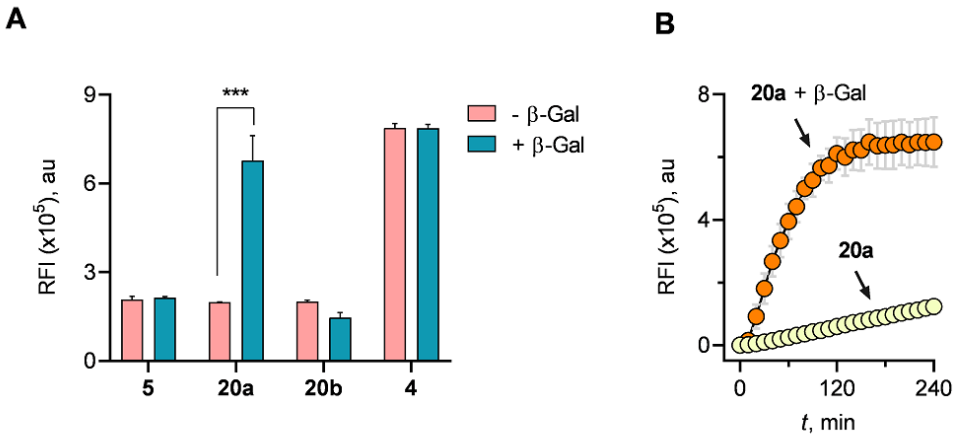

Figure 12. HNO Detection using **5**

HNO is known to react with itself, where one molecule of HNO acts as a nucleophile and another molecule acts as electrophile and dimerized to form hyponitrous acid which spontaneously decomposed to nitrous oxide and water (Scheme 4.5).[3]

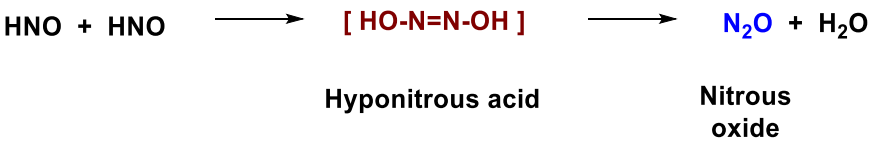

Scheme 10. Dimerization of HNO

In this experiment, compound **4** was used as a positive control and N_2O formation with **4** was measured in buffer (pH 7.4) for 15 h using headspace GC analysis. The N_2O yield with **4** was 100% which was not affected by the β-galactosidase. Under similar conditions, the yield of N_2O from **20a** in the presence of β-galactosidase was 94% (Figure 13).

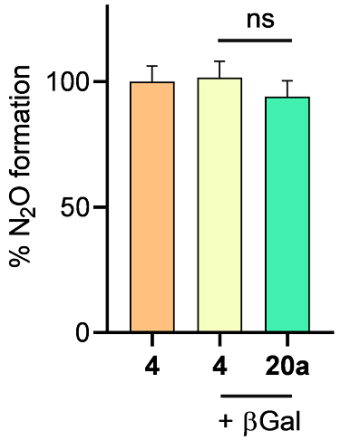

Figure 4.4. N_2O detection from **20a** by headspace GC analysis. The experiment was performed by Dr. Vinayak Khodade (Prof. J. Toscano's lab, John Hopkins University, Baltimore, MD).

Next, to study the decomposition, compound **20a** was incubated with β-galactosidase (10 U/mL) in buffer (pH 7.4) at 37 ˚C. As monitored by HPLC, the gradual disappearance of compound **20a** (RT = 6.9 min) and the formation of compound **14** (RT = 8.9 min) were observed over 48 h (Figure 14).

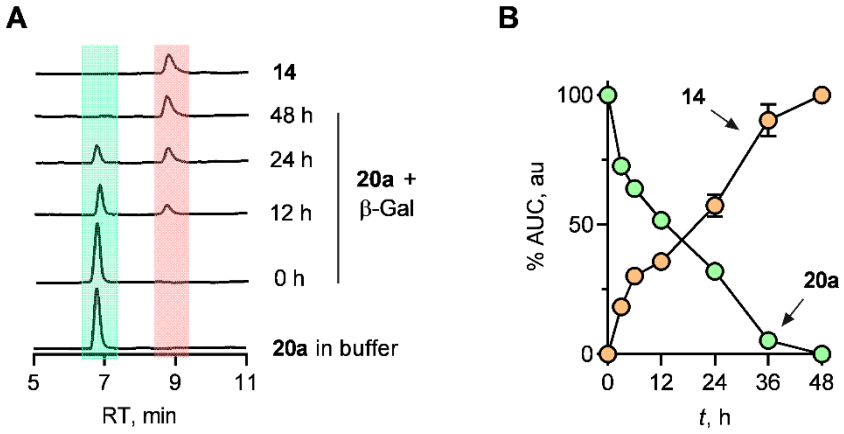

Figure 14. (A) HPLC traces of **20a** and **14**; (B) AUC for decomposition of **20a** (RT = 6.9 min) and formation of **14** (RT = 8.9 min) in the presence of β-galactosidase in buffer (pH 7.4).

Similarly, the decomposition of **20b** in the presence of β-galactosidase was monitored by HPLC and decomposition of **20b** was not observed over an extended period. Also, these results were confirmed by docking studies. The docking studies revealed that **20a** is a more suitable substrate of β-galactosidase over **20b**.

It has been reported that H_2S is overexpressed in senescent cells.[36] Hence, it is important to study the cross-talk between HNO and H_2S. To study the formation of persulfide/polysulfide, compound **20a** was incubated with β-galactosidase in buffer for 15 min, followed by the addition of an electrophilic HPE-IAM probe to trap persulfide and further incubated for 15 min. The formation of HPE-AM adduct of sulfur species was monitored by LC/MS. Interestingly, the formation of H_2S_2, H_2S_3 and H_2S_4 was observed from during the reaction of **20a** and H_2S in the presence of β-galactosidase in buffer (Figure 15).

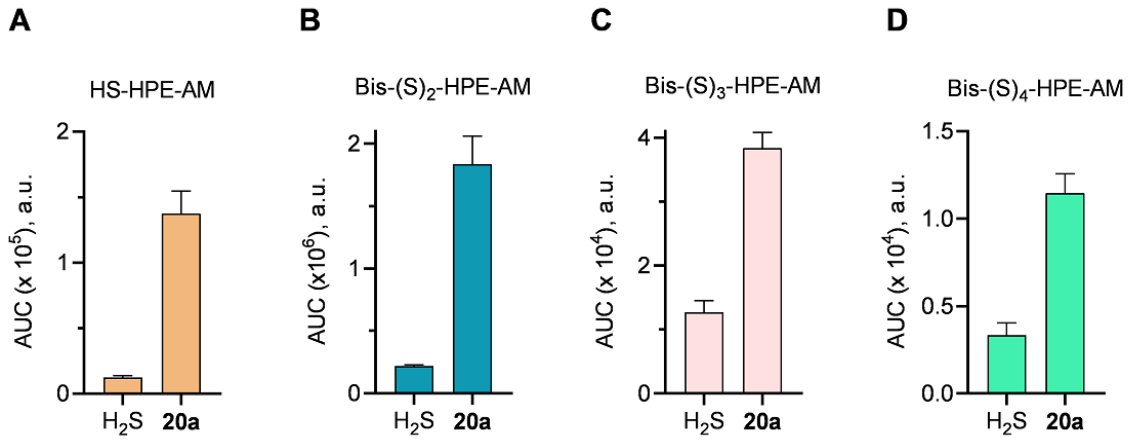

Figure 15: LC/MS study. Polysulfide formation was measured by detection of trapped HPE-IAM species from Na_2S and **20a** + Na_2S upon incubation with β-galactosidase in PBS (pH 7.4) at 37 ˚C for 15 min. (A) Formation of HS-HPE-AM; (B) Formation of Bis-SS-HPE-AM; (C) Formation of Bis-SSS-HPE-AM; (D) Formation of Bis-SSSS-HPE-AM.

Senescent cells are known to have large levels of ROS. Hence, selective delivery of ROS quenchers in senescent cells can be a therapeutic approach to treat senescent cells. Next, our objective was to study the consequences of cross-talk between HNO and H_2S in senescent cells. Senescent cells were treated with **4** and **20a** independently for 48 h and followed by incubation with an H_2DCFDA probe for 40 min and the fluorescence enhancement was recorded at excitation 492 nm and emission 525 nm. Cells were counted to express DCFDA fluorescence per cell. Interestingly, reductions in the ROS levels were observed upon treatment of compounds **4** and **20a** in senescent cells (Figure 16). In another control experiment, cells were treated with compound **20a** and co-incubated with BCA (CSE inhibitor, 10 µM) or BCA alone for 48 h. The cells were then incubated with an H_2DCFDA probe for 40 min and an enhancement in fluorescence response was observed (Figure 16). The

results demonstrated that HNO induced an enhancement of the sulfane sulfur pool by reacting with intracellular H_2S, eventually resulting in ROS mitigation.

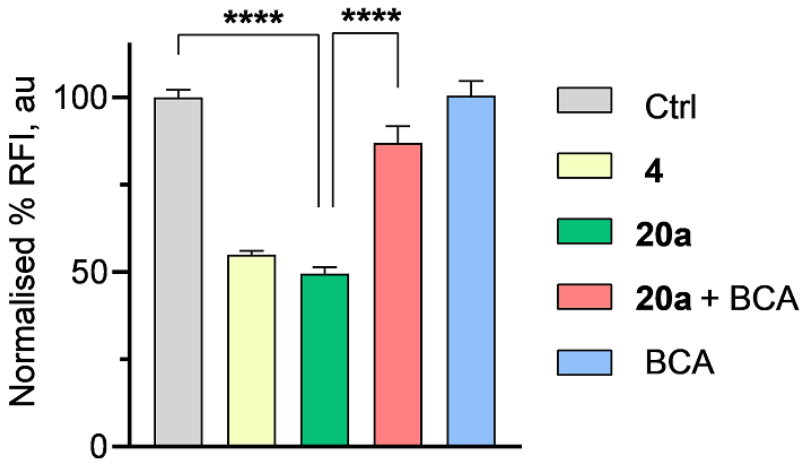

Figure 16: ROS quenching assay was conducted on senescent A459 cells with compounds **4**, **20a**, and BCA for 48 h; Ctrl refers to DMSO treated cells; **4** refers to 2-bromopiloty's acid; BCA refers to CSE inhibitor. An assay for ROS detection in senescent A549 cells was performed by Abraham Mathew (Dr. Deepak Saini lab, IISc, Bangalore).

In summary, a series of stimuli-responsive HNO donors have been developed, which may help to solve a few problems which were associated with the reported donors. Here, we developed triggerable and tunable HNO generation along with the fluorescence reporter, which will avoid the use of external HNO probes for HNO detection. Further, we developed water-soluble donors with controlled HNO generation and selective delivery in cancer and senescent cells. These donors exhibited an important role in ROS quenching in senescent cells.

References

(1) Lymar, S. V; Shafirovich, V.; Poskrebyshev, G. A. One-Electron Reduction of Aqueous Nitric Oxide: A Mechanistic Revision. *Inorg. Chem.* **2005**, *44* (15), 5212–5221.

(2) A. Angeli, sopra la nitroidrossilammina, *Gazz. Chim. Ital*., 1896, 26, 17

(3) Shafirovich, V.; Lymar, S. V. Nitroxyl and Its Anion in Aqueous Solutions: Spin States, Protic Equilibria, and Reactivities toward Oxygen and Nitric Oxide. *Proc. Natl. Acad. Sci.* **2002**, *99* (11), 7340–7345.

(4) Adak, S.; Wang, Q.; Stuehr, D. J. Arginine Conversion to Nitroxide by Tetrahydrobiopterin-Free Neuronal Nitric-Oxide Synthase. Implications for Mechanism. *J. Biol. Chem.* **2000**, *275* (43), 33554–33561.

(5) Murphy, M. E.; Sies, H. Reversible Conversion of Nitroxyl Anion to Nitric Oxide by Superoxide Dismutase. *Proc. Natl. Acad. Sci. U. S. A.* **1991**, *88* (23), 10860–10864.

(6) Sharpe, M. A.; Cooper, C. E. Reactions of Nitric Oxide with Mitochondrial Cytochrome c: A Novel Mechanism for the Formation of Nitroxyl Anion and Peroxynitrite. *Biochem. J.* **1998**, *332 (Pt 1* (Pt 1), 9–19.

(7) Choe, C.; Lewerenz, J.; Fischer, G.; Uliasz, T. F.; Espey, M. G.; Hummel, F. C.; King, S. B.; Schwedhelm, E.; Böger, R. H.; Gerloff, C.; Hewett, S. J.; Magnus, T.; Donzelli, S. Nitroxyl Exacerbates Ischemic Cerebral Injury and Oxidative Neurotoxicity. *J. Neurochem.* **2009**, *110* (6), 1766–1773.

(8) Miljkovic, J. L.; Kenkel, I.; Ivanović-Burmazović, I.; Filipovic, M. R. Generation of HNO and HSNO from Nitrite by Heme-Iron-Catalyzed Metabolism with H 2 S. *Angew. Chemie Int. Ed.* **2013**, *52* (46), 12061–12064.

(9) Filipovic, M. R.; Miljkovic, J. L.; Nauser, T.; Royzen, M.; Klos, K.; Shubina, T.; Koppenol, W. H.; Lippard, S. J.; Ivanović-Burmazović, I. Chemical Characterization of the Smallest S -Nitrosothiol, HSNO; Cellular Cross-Talk of H 2 S and S -Nitrosothiols. *J. Am. Chem. Soc.* **2012**, *134* (29), 12016–12027.

(10) Eberhardt, M.; Dux, M.; Namer, B.; Miljkovic, J.; Cordasic, N.; Will, C.; Kichko, T. I.; de la Roche, J.; Fischer, M.; Suárez, S. A.; Bikiel, D.; Dorsch, K.; Leffler, A.; Babes, A.; Lampert, A.; Lennerz, J. K.; Jacobi, J.; Martí, M. A.; Doctorovich, F.; Högestätt,

E. D.; Zygmunt, P. M.; Ivanovic-Burmazovic, I.; Messlinger, K.; Reeh, P.; Filipovic, M. R. H2S and NO Cooperatively Regulate Vascular Tone by Activating a Neuroendocrine HNO–TRPA1–CGRP Signalling Pathway. *Nat. Commun.* **2014**, *5* (1), 4381.

(11) Zarenkiewicz, J.; Khodade, V. S.; Toscano, J. P. Reaction of Nitroxyl (HNO) with Hydrogen Sulfide and Hydropersulfides. *J. Org. Chem.* **2021**, *86* (1), 868–877.

(12) Doyle, M. P.; Mahapatro, S. N.; Broene, R. D.; Guy, J. K. Oxidation and Reduction of Hemoproteins by Trioxodinitrate(II). The Role of Nitrosyl Hydride and Nitrite. *J. Am. Chem. Soc.* **1988**, *110* (2), 593–599.

(13) Paolocci, N.; Saavedra, W. F.; Miranda, K. M.; Martignani, C.; Isoda, T.; Hare, J. M.; Espey, M. G.; Fukuto, J. M.; Feelisch, M.; Wink, D. A.; Kass, D. A. Nitroxyl Anion Exerts Redox-Sensitive Positive Cardiac Inotropy in Vivo by Calcitonin Gene-Related Peptide Signaling. *Proc. Natl. Acad. Sci. U. S. A.* **2001**, *98* (18), 10463–10468.

(14) Cheong, E.; Tumbev, V.; Abramson, J.; Salama, G.; Stoyanovsky, D. A. Nitroxyl Triggers Ca2+ Release from Skeletal and Cardiac Sarcoplasmic Reticulum by Oxidizing Ryanodine Receptors. *Cell Calcium* **2005**, *37* (1), 87–96.

(15) Tocchetti, C. G.; Wang, W.; Froehlich, J. P.; Huke, S.; Aon, M. A.; Wilson, G. M.; Di Benedetto, G.; O'Rourke, B.; Gao, W. D.; Wink, D. A.; Toscano, J. P.; Zaccolo, M.; Bers, D. M.; Valdivia, H. H.; Cheng, H.; Kass, D. A.; Paolocci, N. Nitroxyl Improves Cellular Heart Function by Directly Enhancing Cardiac Sarcoplasmic Reticulum Ca 2+ Cycling. *Circ. Res.* **2007**, *100* (1), 96–104.

(16) Froehlich, J. P.; Mahaney, J. E.; Keceli, G.; Pavlos, C. M.; Goldstein, R.; Redwood, A. J.; Sumbilla, C.; Lee, D. I.; Tocchetti, C. G.; Kass, D. A.; Paolocci, N.; Toscano, J. P. Phospholamban Thiols Play a Central Role in Activation of the Cardiac Muscle Sarcoplasmic Reticulum Calcium Pump by Nitroxyl. *Biochemistry* **2008**, *47* (50), 13150–13152.

(17) Sivakumaran, V.; Stanley, B. A.; Tocchetti, C. G.; Ballin, J. D.; Caceres, V.; Zhou, L.; Keceli, G.; Rainer, P. P.; Lee, D. I.; Huke, S.; Ziolo, M. T.; Kranias, E. G.; Toscano, J. P.; Wilson, G. M.; O'Rourke, B.; Kass, D. A.; Mahaney, J. E.; Paolocci, N. HNO Enhances SERCA2a Activity and Cardiomyocyte Function by Promoting Redox-Dependent Phospholamban Oligomerization. *Antioxid. Redox Signal.* **2013**, *19* (11),

1185–1197.

(18) Aizawa, K.; Nakagawa, H.; Matsuo, K.; Kawai, K.; Ieda, N.; Suzuki, T.; Miyata, N. Piloty's Acid Derivative with Improved Nitroxyl-Releasing Characteristics. *Bioorg. Med. Chem. Lett.* **2013**, *23* (8), 2340–2343.

(19) Zhou, Y.; Cink, R. B.; Dassanayake, R. S.; Seed, A. J.; Brasch, N. E.; Sampson, P. Rapid Photoactivated Generation of Nitroxyl (HNO) under Neutral PH Conditions. *Angew. Chemie Int. Ed.* **2016**, *55* (42), 13229–13232.

(20) Zhou, Y.; Cink, R. B.; Seed, A. J.; Simpson, M. C.; Sampson, P.; Brasch, N. E. Stoichiometric Nitroxyl Photorelease Using the (6-Hydroxy-2-Naphthalenyl)Methyl Phototrigger. *Org. Lett.* **2019**, *21* (4), 1054–1057.

(21) Silva Sousa, E. H.; Ridnour, L. A.; Gouveia, F. S.; Silva da Silva, C. D.; Wink, D. A.; de França Lopes, L. G.; Sadler, P. J. Thiol-Activated HNO Release from a Ruthenium Antiangiogenesis Complex and HIF-1α Inhibition for Cancer Therapy. *ACS Chem. Biol.* **2016**, *11* (7), 2057–2065.

(22) Zeng, B.-B.; Huang, J.; Wright, M. W.; King, S. B. Nitroxyl (HNO) Release from New Functionalized N-Hydroxyurea-Derived Acyl Nitroso-9,10-Dimethylanthracene Cycloadducts. *Bioorg. Med. Chem. Lett.* **2004**, *14* (22), 5565–5568.

(23) Adachi, Y.; Nakagawa, H.; Matsuo, K.; Suzuki, T.; Miyata, N. Photoactivatable HNO-Releasing Compounds Using the Retro-Diels–Alder Reaction. *Chem. Commun.* **2008**, No. 41, 5149.

(24) Lee, M. J. C.; Shoeman, D. W.; Goon, D. J. W.; Nagasawa, H. T. N-Hydroxybenzenecarboximidic Acid Derivatives: A New Class of Nitroxyl-Generating Prodrugs. *Nitric Oxide* **2001**, *5* (3), 278–287.

(25) Andrei, D.; Salmon, D. J.; Donzelli, S.; Wahab, A.; Klose, J. R.; Citro, M. L.; Saavedra, J. E.; Wink, D. A.; Miranda, K. M.; Keefer, L. K. Dual Mechanisms of HNO Generation by a Nitroxyl Prodrug of the Diazeniumdiolate (NONOate) Class. *J. Am. Chem. Soc.* **2010**, *132* (46), 16526–16532.

(26) Holland, R. J.; Paulisch, R.; Cao, Z.; Keefer, L. K.; Saavedra, J. E.; Donzelli, S. Enzymatic Generation of the NO/HNO-Releasing IPA/NO Anion at Controlled Rates in Physiological Media Using β-Galactosidase. *Nitric Oxide* **2013**, *35*, 131–136.

(27) Mao, G. J.; Zhang, X. B.; Shi, X. L.; Liu, H. W.; Wu, Y. X.; Zhou, L. Y.; Tan, W.; Yu, R. Q. A Highly Sensitive and Reductant-Resistant Fluorescent Probe for Nitroxyl in Aqueous Solution and Serum. *Chem. Commun.* **2014**, *50* (43).

(28) Jin, X.; Sun, X.; Di, X.; Zhang, X.; Huang, H.; Liu, J.; Ji, P.; Zhu, H. Novel Fluorescent ESIPT Probe Based on Flavone for Nitroxyl in Aqueous Solution and Serum. *Sensors Actuators B Chem.* **2016**, *224*, 209–216.

(29) Zhu, X.; Xiong, M.; Liu, H.; Mao, G.; Zhou, L.; Zhang, J.; Hu, X.; Zhang, X.-B.; Tan, W. A FRET-Based Ratiometric Two-Photon Fluorescent Probe for Dual-Channel Imaging of Nitroxyl in Living Cells and Tissues. *Chem. Commun.* **2016**, *52* (4), 733–736.

(30) Zhang, H.; Liu, R.; Tan, Y.; Xie, W. H.; Lei, H.; Cheung, H.-Y.; Sun, H. A FRET-Based Ratiometric Fluorescent Probe for Nitroxyl Detection in Living Cells. *ACS Appl. Mater. Interfaces* **2015**, *7* (9), 5438–5443.

(31) Ren, M.; Deng, B.; Zhou, K.; Wang, J.-Y.; Kong, X.; Lin, W. A Targetable Fluorescent Probe for Imaging Exogenous and Intracellularly Formed Nitroxyl in Mitochondria in Living Cells. *J. Mater. Chem. B* **2017**, *5* (10), 1954–1961.

(32) Zhou, X.; Huang, Z.; Yang, H.; Jiang, Y.; Wei, W.; Li, Q.; Mo, Q.; Liu, J. β-Glucosidase Inhibition Sensitizes Breast Cancer to Chemotherapy. *Biomed. Pharmacother.* **2017**, *91*, 504–509.

(33) Zhang, Y.; Zhu, K.; Miao, X.; Hu, X.; Wang, T. Identification of β-Glucosidase 1 as a Biomarker and Its High Expression in Hepatocellular Carcinoma Is Associated with Resistance to Chemotherapy Drugs. *Biomarkers* **2016**, *21* (3), 249–256.

(34) Lee, B. Y.; Han, J. A.; Im, J. S.; Morrone, A.; Johung, K.; Goodwin, E. C.; Kleijer, W. J.; DiMaio, D.; Hwang, E. S. Senescence-Associated β-Galactosidase Is Lysosomal β-Galactosidase. *Aging Cell* **2006**, *5* (2), 187–195.

(35) Dimri, G. P.; Lee, X.; Basile, G.; Acosta, M.; Scott, G.; Roskelley, C.; Medrano, E. E.; Linskens, M.; Rubelj, I.; Pereira-Smith, O. A Biomarker That Identifies Senescent Human Cells in Culture and in Aging Skin in Vivo. *Proc. Natl. Acad. Sci. U. S. A.* **1995**, *92* (20), 9363–9367.

(36) Gupta, K.; Mathew, A. B.; Chakrapani, H.; Saini, D. K. H2S Contributed from CSE

during Cellular Senescence Suppresses Inflammation and Nitrosative Stress. *Biochim. Biophys. acta. Mol. cell Res.* **2023**, *1870* (2), 119388.

List of Figures

Figure 1.1	Biosynthetic pathway for NO production	1
Figure 1.2	Biosynthesis of HNO generation. **NOS**: Nitric Oxide Synthase; **BH_4**: Tetrahydrobiopterin; ***L*-NHA**: *N*-hydroxy-*L*-arginine; **SOD**: Superoxide Dismutase	3
Figure 1.3	Role of HNO in the cardiovascular system	9
Figure 1.4	Proposed mechanism for the effect of HNO on the sGC activity	10
Figure 1.5	Role of HNO in the cancer therapy	11
Figure 1.6	Structures of HNO donors	12
Figure 1.7	Light-activated HNO donors, $L^1 = PMe_3$; L^2 = Glutamate	13
Figure 1.8	Thiol and thermally activated HNO donors	15
Figure 1.9	Enzymatically activated HNO donors	16
Figure 1.10	Staudinger ligation reaction of phosphine with the HNO	17
Figure 1.11	Phosphine-based HNO probes	19
Figure 1.12	The schematic diagram for the HNO detection by the Cu(II) based probes	21
Figure 1.13	Cu(II) based probes for the HNO detection	21
Figure 1.14	Design of the real-time monitoring of HNO	24
Figure 2.1	Design of stimuli-responsive nitroxyl (HNO) donor	35
Figure 2.2	Enhancement in fluorescence signal corresponding to the generation of HNO from compounds **2a-2g** (50 µM) and **3a-3g** (50 µM) in the presence of **5** and esterase (0.5 U/mL) in PBS (10 mM, pH 7.4) at 37 ˚C for 30 minutes. **5** refers to PCM probe; **4** refers to 2-bromopiloty's acid; (λ_{ex} = 370 nm; λ_{em} = 460 nm).	40
Figure 2.3	Time-dependent HNO generation from compounds **(a) 2a-2c, (b) 2d-2g, (c) 3a-3c** and (d) **2d-2g** (50 µM) using **5** were incubated in the presence of esterase (0.5 U/mL) in PBS (10 mM, pH 7.4) at 37 ˚C and fluorescence enhancement was monitored over 30 min. (λ_{ex} = 370 nm; λ_{em} = 460 nm).	41
Figure 2.4	Design of stimuli-responsive concomitant release of nitroxyl (HNO) and fluorescence reporter by the HNO donor. The incorporation of latent fluorophore in the donor eliminates the need for a secondary assay for monitoring HNO.	42

Figure 2.5	The UV absorption spectrum of **7** (100 µM) was measured in buffer (pH 7.4).	43
Figure 2.6	The fluorescence spectrum of **7** was measured in buffer (pH 7.4) (λ_{ex} = 308 nm; λ_{em} = 320 - 700 nm).	44
Figure 2.7	Fluorescence stability of **7** (50 µM) was measured in buffer (pH 7.4) upon excitation at 308 nm.	45
Figure 2.8	Fluorescence stability of **7** (50 µM) was measured in buffer (pH 7.4) for 12 h. (λ_{ex} = 308 nm; λ_{em} = 497 nm).	45
Figure 2.9	Time-resolved (lifetime) PL studies of **7** (10 µM) were measured by TCSPC (Time-Correlated Single Photon Counting) in PBS pH 7.4 for 200 ns. The data were fitted by second exponential and the τ_{avg} was observed at 13.82 ns. CHISQ is a chi-square, used to compare observed results with expected results.	47
Figure 2.10	(A) Monitoring of fluorescence signals (λ_{ex} = 370 nm; λ_{em} = 460 nm) corresponding to HNO generation using **5** from compounds **2h** and **3h** (50 µM) were incubated in the absence and presence of esterase (0.5 U/mL) in buffer (pH 7.4) at 37 ˚C for 30 min. **5** refers to PCM probe; **4** refers to 2-bromopiloty's acid; + PMSF refers to esterase inhibitor; (B) Time course of HNO generation from compounds **2h** and **3h** (50 µM) over 30 min.	48
Figure 2.11	Concentration-dependent release of compound **7**: (A) Compounds **2h** and **3h** (50 µM) were incubated in the presence of esterase (0.5 U/mL) in buffer (pH 7.4) at 37 ˚C for 2 hours. **7** refers to dansylsulfinic acid; + PMSF refers to esterase inhibitor; (λ_{ex} = 308 nm; λ_{em} = 497 nm).	49
Figure 2.12	(A) Time-dependent release of **7** from **2h** in buffer; (B) Time-dependent release of **7** from **3h** in buffer.	50
Figure 2.13	Time-dependent release of HNO and **7**: (A) Compounds **2h** (50 µM); (B) **3h** (50 µM) were incubated in the presence of esterase (0.5 U/mL) in buffer (pH 7.4) at 37 ˚C. Fluorescence enhancement was monitored over 30 min.	51
Figure 2.14	Calibration curve for varying concentrations of $NaNO_2$	52

Figure 2.15	Griess assay for NO detection. Compounds **2a-2h** and **3a-3h** were incubated with esterase in buffer (pH 7.4) at 37 ˚C for 30 min and NO release was at 540 nm. Ctrl refers to the $NaNO_2$ and the data was normalized with $NaNO_2$ (50 µM).	54
Figure 2.16	LC/MS study. (A) Decomposition of **2h** upon incubation with esterase (0.5 U/mL) as monitored by LC/MS. (B) Extracted ion chromatograms from an LC/MS analysis of **2h** (C) Mass spectra for compound **2h** (expected, m/z = 435.1582 $[M + H]^+$; observed, m/z = 435.1584).	54
Figure 2.17	LC/MS study. (A) Formation of intermediate **I** (or **II**) during the decomposition of **2h** upon incubation with esterase (0.5 U/mL) as monitored by LC/MS. (B) Extracted ion chromatograms from an LC/MS analysis of intermediate **I** (or **II**) (C) mass spectra for intermediate **I** (or **II**) (expected, m/z = 367.1329 $[M + H]^+$; observed, m/z = 367.1322).	55
Figure 2.18	LC/MS study. (A) Formation of **3h** during the decomposition of **2h** upon incubation with esterase (0.5 U/mL) as monitored by LC/MS. (B) Extracted ion chromatograms from an LC/MS analysis of intermediate **3h**; (C) Mass spectra for **3h** (expected, m/z = 335.1060 $[M + H]^+$; observed, m/z = 335.1058).	55
Figure 2.19	LC/MS study. (A) Formation of **8** during the decomposition of **2h** upon incubation with esterase (0.5 U/mL) as monitored by LC/MS. (B) Extracted ion chromatograms from an LC/MS analysis of **8**; (C) Mass spectra for **8** (expected, m/z = 267.0798 $[M + H]^+$; observed, m/z = 267.0805).	56
Figure 2.20	LC/MS study. (A) Formation of **7** during the decomposition of **2h** upon incubation with esterase (0.5 U/mL) as monitored by LC/MS; (B) Extracted ion chromatograms from an LC/MS analysis of **7**; (C) Mass spectra for **7** (expected, m/z = 236.0739 $[M + H]^+$; observed, m/z = 236.0742).	56
Figure 2.21	LC/MS study. Stability of compound **3h** in buffer (pH 7.4) for 0 and 5 h.	57

Figure 2.22	Extracted ion chromatograms from an LC/MS analysis of decomposition of **3h** upon incubation with esterase (0.5 U/mL) in PBS (pH 7.4). The time points considered were 0 min, 60 min, 120 min and 240 min.	57
Figure 2.23	**LC/MS study.** (A) Decomposition of **3h** and formation of **7** upon incubation with esterase (0.5 U/mL) in PBS (pH 7.4) at 37 ˚C as monitored by LC/MS. **3h** (expected, m/z = 335.1060 $[M + H]^+$; observed, m/z = 335.1058), **7** (expected, m/z = 236.0739 $[M + H]^+$; observed, m/z = 236.0742). (B) Formation of **8** during the decomposition of **3h** upon incubation with esterase (0.5 U/mL) as monitored by LC/MS. **8** (expected, m/z = 267.0798 $[M + H]^+$; observed, m/z = 267.0805). All data are presented as mean $\pm$ SD (n = 3 per group).	58
Figure 2.24	LC/MS study. Polysulfide formation was measured by detection of trapped HPE-IAM species from Na_2S, **2h** and **3h** upon incubation with esterase in PBS (pH 7.4) for at 37 ˚C for 15 min; (A) Formation of HS-HPE-AM (expected, m/z = 212.0740 $[M + H]^+$; observed, m/z = 212.0719); (B) Formation of Bis-S-HPE-AM (expected, m/z = 389.1530 $[M + H]^+$; observed, m/z = 389.1489); (C) Formation of Bis-SS-HPE-AM (expected, m/z = 421.1205 $[M + H]^+$; observed, m/z = 421.1214); (D) Formation of Bis-SSS-HPE-AM (expected, m/z = 453.0971 $[M + H]^+$; observed, m/z = 453.0923).	62
Figure 2.25	(A) Representative LC trace; (B) Mass spectra for the HS-HPE-AM adduct from Na_2S with HPE-IAM (expected, m/z = 212.0740 $[M + H]^+$; observed, m/z = 212.0719).	63
Figure 2.26	(A) Extracted ion chromatograms from an LC/MS analysis of Bis-S-HPE-AM formation from Na_2S, **2h** and **3h**; (B) Mass spectra for Bis-S-HPE-AM (expected, m/z = 389.1530 $[M + H]^+$; observed, m/z = 389.1489).	63
Figure 2.27	(A) Extracted ion chromatograms from an LC/MS analysis of Bis-SS-HPE-AM formation from Na_2S, **2h** and **3h**; (B) Mass	64

	spectra for Bis-SS-HPE-AM (expected, m/z = 421.1250 [M + H]$^+$; observed, m/z = 421.1205).	
Figure 2.28	(A) Extracted ion chromatograms from an LC/MS analysis of Bis-SSS-HPE-AM formation from Na_2S, **2h** and **3h**; (B) Mass spectra for Bis-SSS-HPE-AM (expected, m/z = 453.0971 [M + H]$^+$; observed, m/z = 453.0927).	64
Figure 2.29	A comparison of sulfur species measured by detection of trapped HPE-AM species from H_2S with **4** and structures of polysulfide adduct with HPE-IAM. HS-HPE-AM (expected, m/z = 212.0740 [M + H]$^+$; observed, m/z = 212.0720); Bis-S-HPE-AM (expected, m/z = 389.1530 [M + H]$^+$; observed, m/z = 389.1489); Bis-SS-HPE-AM (expected, m/z = 421.1250 [M + H]$^+$; observed, m/z = 421.1203): Bis-SSS-HPE-AM (expected, m/z = 453.0971 [M + H]$^+$; observed, m/z = 453.0923).	65
Figure 2.30	Compounds **2h, 3h** and **7** were incubated in A549 cell lysate (1 mg/mL) in the presence and absence of PMSF (esterase inhibitor) for 3 h; cell ctrl refers to untreated cell lysate; + PMSF refers to cell lysate were preincubated with PMSF for 30 min. Fluorescence measurement (λ_{ex} = 308 nm; λ_{em} = 497 nm) was carried out by varying concentrations of **2h** and **3h; 7** refers to dansylsulfinic acid.	66
Figure 2.31	Cell viability assay was carried out with varying concentrations of compounds **2h**, **3h** and **7** on MCF-7 cells for 24 h. All data are presented as mean ± SD (n =3/group).	67
Figure 2.32	Cell viability assay was carried out with varying concentrations of compounds **2h**, **3h** and **7** on MEF cells for 24 h. All data are presented as mean ± SD (n =3/group).	67
Figure 2.33	Cell viability assay was carried out with varying concentrations of compounds **2h**, **3h** and **7** on A549 cells for 24 h. All data are presented as mean ± SD (n =3/group).	68
Figure 2.34	Confocal microscopy images of HNO and **7** in breast cancer cells (MCF-7). **HNO detection:** MCF-7 cells were pre-incubated with HNO-TCF dye **6 (**20 μM) for 30 min followed by treatment of (i)	69

	4; (ii) **2h** (iii) **3h** (200 μM) independently for 2 h. The cells were imaged on Carl Zeiss LSM710 laser scanning confocal microscope with anisotropy. The cells were imaged in the RED channel (Alexa fluor 568 for HNO detection). (iv) **7** (200 μM); (v) **2h** (vi) **3h**. The cells were imaged in the DAPI channel (Detection of **7**). (vii) Merged image of (ii and v); (viii) Merged image of (iii and vi).	
Figure 2.35	Bright-field images for (i) **4**; (ii) **2h**; (iii) **3h** and (iv) **7** were imaged on Carl Zeiss LSM710 laser scanning confocal microscope with anisotropy.	70
Figure 3.1	β-glucosidase activated prodrugs	107
Figure 3.2	Design of β-glucosidase stimulated nitroxyl (HNO) donor	107
Figure 3.3	Detection of HNO using PCM **5.** (A) Compounds **13a-13e** were incubated with PCM **5** and in the presence and absence of the β-glucosidase in buffer (pH 7.4) at 37 ˚C for 6 h. Dye refers to PCM **5**; **4** refers to 2-bromo-piloty's acid (λ_{ex} = 370 nm; λ_{em} = 460 nm).	111
Figure 3.4	NO detection by Griess assay	111
Figure 3.5	Stability of prodrug **13a** in buffer. (A) HPLC trace of stability of **13a** (RT = 6.1 min; (B) Area under the curve corresponding to **13a** (absorbance 230 nm).	112
Figure 3.6	HPLC traces and AUC for decomposition of **13a** (RT = 6.1 min) and formation of **14** (RT = 8.4 min) in the presence of β-glucosidase in buffer (pH 7.4).	112
Figure 3.7	Sequence alignment of β-glucosidase from white clover leaf (Uniprot no. P26205) and almonds (Uniprot no. H9ZGD8). Computational studies were performed by T. Anand Kumar (Prof. Harinath Chakrapani Lab**,** IISER Pune).	113
Figure 3.8	The ligand binding pocket of β-glucosidase (PDB: 1CBG from white clover [*Trifolium repens*]) was predicted using the CASTp web server with a cartoon representation of the protein and probe radius 1.4 Å. The pocket was shown as surface colored as warm pink. (B) Zoom view of the active site of pocket 1 containing catalytic residues of β-glucosidase.	114

Figure 3.9	Structures of compounds **15** and **13a-13e** used for docking analysis	116
Figure 3.10	Cartoon representation of docked compounds (A) **15**; (B) **13a**; (C) **13b**; (D) **13c**; (E) **13d**; (F) **13e** into the active site of cyanogenic β-glucosidase from white clover (Trifolium repens L.; PDB = 1CBG). The docked ligands were shown in the stick model and the active site residues are indicated by a 1-letter code. The hydrogen, hydrophobic and pi-pi interactions are drawn as blue, red and gray dotted lines, and the lengths are indicated. The figures were generated using PyMOL v 2.0.	117
Figure 3.11	LigPlot shows the 2D interactions of compounds (A) **15**; (B) **13a**; (C) **13b**; (D) **13c**; (E) **13d**; (F) **13e** with β-glucosidase. The molecule is represented in a stick model. Active site residues are labeled by a 3-letter code and represented as a ball and stick model. The residues forming hydrophobic interactions are shown as red arcs while the hydrogen bonds are shown as blue dashed lines with indicated bond lengths (Table 3.4).	118
Figure 3.12	Cell viability assay was carried out with varying concentrations of compound **13a-13c** on MCF-7 cells for 24 h. All data are presented as mean ± SD (n =3/group).	119
Figure 3.14	Cell viability assay was carried out with varying concentrations of compound **13d-13e** on MCF-7 cells for 24 h. All data are presented as mean ± SD (n =3/group).	119
Figure 4.1	β-galactosidase sensitive prodrug strategies	144
Figure 4.2	Design of β-galactosidase triggered Nitroxyl (HNO) donor. (1) The interaction of HNO prodrug with ASGPR, (2) Entry into the senescent cells, and (3) β-galactosidase mediated cleavage of the glycosidic bond to release HNO.	145
Figure 4.3	HNO Detection from compounds **20a-20b** in the presence β-galactosidase of using PCM **5** in buffer.	148
Figure 4.4	N_2O detection from **20a** by GC/MS analysis. N_2O detection by GC/MS analysis was performed by Dr. Vinayak Khodade (Prof. J. Toscano's lab, John Hopkins University, Baltimore, MD).	149

Figure 4.5	Detection of HNO from compound **20a** using *N*-acetyl tryptophan.	150
Figure 4.6	NO detection from **20a** using Griess assay.	151
Figure 4.7	(A) HPLC traces of **20a** (RT = 6.9 min); (B) AUC for the stability of **20a** in buffer (pH 7.4).	151
Figure 4.8	(A) HPLC traces of **20a** and **14**; (B) AUC for decomposition of **20a** (RT = 6.9 min) and formation of **14** (RT = 8.9 min) in the presence of β-galactosidase in buffer (pH 7.4).	152
Figure 4.9	HPLC traces and AUC for decomposition of **20b** (RT = 12.2 min) in the presence of β-galactosidase in buffer (pH 7.4).	153
Figure 4.10	A plausible mechanism of hydrolysis of the glycosidic bond by β-galactosidase from *E. Coli*.	154
Figure 4.12	(A) Cartoon representation of docked compound allolactose into the active site of β-galactosidase from *E. coli* (PDB ID: 1JYN; resolution = 1.80 Å). The docked ligands were shown in the stick model and the active site residues are indicated by a 1-letter code. The hydrogen, hydrophobic and pi-pi interactions are drawn as blue, red and gray dotted lines, and the lengths are indicated. The figure was generated using PyMOL v 2.0. (B) LigPlot shows the 2D interactions of allolactose with β-galactosidase. The molecule is represented in a stick model.	155
Figure 4.13	(A-B) Cartoon representation of docked compounds (A) **20a** and (B) **20b** into the active site of β-galactosidase from *E. coli* (PDB ID: 1JYN; resolution = 1.80 Å). The docked ligands were shown in the stick model and the active site residues are indicated by a 1-letter code. The hydrogen, hydrophobic and pi-pi interactions are drawn as blue, red and gray dotted lines, and the lengths are indicated. The figure was generated using PyMOL v 2.0. (C-D) LigPlot shows the 2D interactions of compounds (C) **20a** and (D) **20b** with β-galactosidase. The molecule is represented in a stick model. Active site residues are labeled by a 3-letter code and represented as a ball and stick model. The residues forming hydrophobic interactions are shown as red arcs while the	156

	hydrogen bonds are shown as blue dashed lines with indicated bond lengths.	
Figure 4.14	LC/MS study. Polysulfide formation was measured by detection of trapped HPE-IAM species from Na_2S and **20a** + Na_2S upon incubation with β-galactosidase in PBS (pH 7.4) at 37 ˚C for 15 min. (A) Formation of HS-HPE-AM (Expected, m/z = 212.0740 $[M + H]^+$; observed, m/z = 212.0715); (B) Formation of Bis-SS-HPE-AM (expected, m/z = 421.1250 $[M + H]^+$; observed, m/z = 421.1151); (C) Formation of Bis-SSS-HPE-AM (expected, m/z = 453.0971 $[M + H]^+$; observed, m/z = 453.0865); (D) Formation of Bis-SSSS-HPE-AM (expected mass = 485.0692; observed mass = 485.0714).	158
Figure 4.15	(A) Representative LC trace for HS-HPE-AM adduct from Na_2S and **20a** + Na_2S with HPE-IAM; (B) Mass spectra for HS-HPE-AM (expected, m/z = 212.0740 $[M + H]^+$; observed, m/z = 212.0715).	159
Figure 4.16	(A) Extracted ion chromatograms from an LC/MS analysis of Bis-S-HPE-AM formation from Na_2S, **20a +** Na_2S; (B) Mass spectra for Bis-S-HPE-AM (expected, m/z = 389.1530 $[M + H]^+$; observed, m/z = 389.1441).	159
Figure 4.17	(A) Extracted ion chromatograms from an LC/MS analysis of Bis-SS-HPE-AM formation from Na_2S, **20a +** Na_2S; (B) Mass spectra for Bis-SS-HPE-AM (expected, m/z = 421.1250 $[M + H]^+$; observed, m/z = 421.1151).	160
Figure 4.18	(A) Extracted ion chromatograms from an LC/MS analysis of Bis-SSS-HPE-AM formation from Na_2S, **20a +** Na_2S; (B) Mass spectra for Bis-SSS-HPE-AM (expected, m/z = 453.0971 $[M + H]^+$; observed, m/z = 453.0865).	160
Figure 4.19	(A) Extracted ion chromatograms from an LC/MS analysis of Bis-SSSS-HPE-AM formation from Na_2S, **20a +** Na_2S; (B) Mass spectra for Bis-SSSS-HPE-AM (Expected, m/z = 485.0692 $[M + H]^+$; observed, m/z = 485.0714).	161

Figure 4.20	Cell viability assay was carried out with varying concentrations of compound **20a – 20b** on MCF-7 cells for 24 h. All data are presented as mean ± SD (n =3/group).	161
Figure 4.21	ROS quenching assay was conducted on senescent A459 cells with compounds **4**, **20a**, and BCA for 48 h; Ctrl refers to DMSO treated cells; **4** refers to 2-bromopiloty's acid; BCA refers to CSE inhibitor. An assay for ROS detection in senescent A549 cells was performed by Abraham Mathew (Dr. Deepak Saini lab, IISc, Bangalore).	162

List of Schemes

Scheme 1.1	The mechanism for the dimerization of HNO to form N_2O	2
Scheme 1.2	The reaction of HNO with the hydrogen sulfide and persulfides	3
Scheme 1.3	The reaction of HNO with thiols	4
Scheme 1.4	The reaction of HNO with the myoglobin	5
Scheme 1.5	The reaction of HNO with the aquacobalmin	6
Scheme 1.6	The reaction of HNO with the superoxide dismutase	6
Scheme 1.7	The reaction of HNO with the oxygen	7
Scheme 1.8	The Reactions of HNO and NO^- with the NO	7
Scheme 1.9	Mechanism of generation of HNO from cyanamide and inactivation of aldehyde dehydrogenase by HNO	8
Scheme 1.10	A general strategy for the HNO generation	12
Scheme 1.11	Decomposition of Angeli's salt and proposed mechanism of HNO generation	12
Scheme 1.12	Proposed mechanism of the HNO detection by phosphine probe	18
Scheme 1.13	Proposed mechanism for the HNO detection by thiol-based HNO probe	20
Scheme 1.14	Mechanism of HNO detection by TEMPO-9-AC	20
Scheme 1.15	Mechanism of HNO detection by the Cu(II) complex	21
Scheme 2.1	Proposed mechanism of HNO generation	36
Scheme 2.2	Synthesis of compound **1**	36
Scheme 2.3	Synthesis of compound **2**	37
Scheme 2.4	Synthesis of compound **3**	37
Scheme 2.5	Synthesis of 2-bromopiloty's acid	38
Scheme 2.6	Synthesis of **5** and **6**	39
Scheme 2.7	Mechanism of HNO trapping by **5** to release highly fluorescent product umbelliferone	39
Scheme 2.8	Synthesis of **2h** and **3h**	43
Scheme 2.9	Synthesis of **7**	43
Scheme 2.10	Proposed mechanism of generation of HNO and fluorescent reporter **7**	47
Scheme 2.11	The reaction of nitrite (NO_2^-) with Griess reagents forms an azo dye	52

Scheme 2.12	Proposed mechanism for NO release from Piloty's acid	53
Scheme 2.13	Proposed mechanism of generation of HNO and **7**	59
Scheme 2.14	LC/MS study. (A) Proposed mechanism of HNO reaction with H_2S; (B) Proposed mechanism of polysulfides formation; Ar refers to 4-hydroxyphenyl	60
Scheme 2.15	Structures of sulfur species trapped by HPE-IAM probe	61
Scheme 2.16	Proposed mechanism for HNO detection by **6** and release of TCF-OH	68
Scheme 3.1	Proposed mechanism of HNO generation upon activation by β-glucosidase	108
Scheme 3.2	Synthesis of compound **12**	108
Scheme 3.3	Synthesis of compound **13**	109
Scheme 3.4	Synthesis of compound **14**	110
Scheme 3.5	Proposed mechanism for HNO trapping by **5** and release of fluorescent umbelliferone	110
Scheme 3.6	A plausible mechanism of hydrolysis of the glucosidic bond by β-glucosidase	115
Scheme 4.1	Proposed mechanism of HNO generation upon activation by β-galactosidase	145
Scheme 4.2	Synthesis of compound **20**	146
Scheme 4.3	Synthesis of compound **NAT**	147
Scheme 4.4	Proposed mechanism for HNO generation and trapping HNO by **5**	148
Scheme 4.5	The mechanism for dimerization of HNO	149
Scheme 4.6	The reaction of NAT with HNO to form NAT-NO	150
Scheme 4.7	Structures of sulfur species trapped by HPE-IAM probe	158

List of Tables

Table 1.1	The rate constant of HNO with biomolecules	5
Table 2.1	Synthesis of Boc-protected compounds **2a-2g** from **1**	37
Table 2.2	Synthesis of compounds **3a-3g** from **2**	38
Table 2.3	Fluorescence lifetime of known fluorophores	46
Table 2.4	The fluorescence lifetime of **7**	47
Table 3.1	Synthesis of compounds **12a-12e**	109
Table 3.2	Synthesis of compounds **13a-13e** from **12**	109
Table 3.3	Comparative analysis of the docking results of prodrugs **13a-13e**	116
Table 4.1	Synthesis of compounds **19a-19b** and **20a-20b**	147
Table 4.2	Comparative analysis of the docking results of prodrugs **20a** and **20b**	155

List of publications

1. **Sawase, L. R.,** Jishnu C. V., Manna, S., Chakrapani, H. A modular scaffold for triggerable and tunable nitroxyl (HNO) generation with a fluorescence receptor, *Chem. Commun*., **2023,** 59, 3415-3418.

ChemComm

COMMUNICATION

View Article Online
View Journal | View Issue

Cite this: *Chem. Commun.*, 2023, **59**, 3415

Received 13th November 2022,
Accepted 17th February 2023

DOI: 10.1039/d2cc06134a

rsc.li/chemcomm

A modular scaffold for triggerable and tunable nitroxyl (HNO) generation with a fluorescence reporter†

Laxman R. Sawase, Jishnu C. V., Suman Manna and Harinath Chakrapani *

Nitroxyl (HNO) is a short-lived mediator of cell signalling and can enhance the sulfane sulfur pool, a cellular antioxidant reservoir, by reacting with hydrogen sulfide (H_2S). Here, we report esterase-activated HNO-generators that are suitable for tunable HNO release and the design of these donors allows for real-time monitoring of HNO release. These tools will help gain a better understanding of the cross-talk among short-lived gaseous signalling molecules that have emerged as major players in health and disease.

Gaseous species derived from nitrogen, sulfur, and even carbon (carbon monoxide) have in the past several decades become central to the understanding of redox cellular biology and the cross-talk among these biologically active gaseous species has become the focus of much attention.[1,2] Nitroxyl (HNO), which is a short-lived species, has been considered as an intermediate in nitrogen metabolism in cells. HNO activates soluble guanylate cyclase (sGC), a key enzyme involved in vascular smooth muscle relaxation.[3,4] Compounds that dissociate to produce HNO have shown promise in cardiovascular[5,6] and anti-cancer applications.[7,8] Recently, hydrogen sulfide (H_2S) has emerged as a major player in redox homeostasis and the cross-talk between H_2S and HNO has important implications in antioxidant response. For example, HNO can react with H_2S to produce persulfide and polysulfide, which together constitute the sulfane sulfur pool.[9] Together, the sulfane sulfur pool is implicated in numerous cellular stress responses, including protective effects against reactive oxygen species (ROS) and inflammation.[10,11] Hence, platforms for reliable generation of HNO are essential for a better understanding of the chemical biology of this short-lived species.

Protected hydroxylamines were considered as HNO donors (Fig. 1A). Activation of these donors is performed to expose the hydroxyl group of the hydroxylamine, which results in HNO generation, in either two or three steps (Fig. 1A). When an *N,O*-protected hydroxylamine (R = H; **1**, Fig. 1B) is used, the intermediate **3** can collapse to generate HNO, with the sulfinate leaving group determining the rate of HNO generation. When *N,N,O*-protected hydroxylamines (R ≠ H; **2**, Fig. 1B) are used, the product of cleavage is **3**, which does not directly produce HNO, but an additional step through the production of a common intermediate is required. The rate of collapse of the common intermediate would determine the rate of HNO generation. Else, if this collapse is rapid, the preceding steps would likely determine the rates of HNO generation. Together, by varying the protective groups, leaving groups, and intermediates, this modular scaffold can be used to tune the rate of HNO generation.

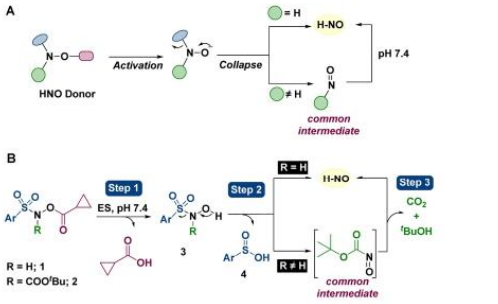

Fig. 1 (A) A modular scaffold for HNO generation: Activation of the donor followed by collapse produces either HNO or the active HNO generating species, which dissociates to produce HNO. (B) Derivatives **1** or **2** can be cleaved by esterase to produce intermediate **3**, which can either directly produce HNO and an arylsulfinic acid **4** or lose a sulfinic acid to generate a nitroso-intermediate that collapses to produce HNO. If the sulfinic acid is fluorescent and the corresponding donor is weakly fluorescent, this design allows for a fluorescence reporter for HNO release.

Department of Chemistry, Indian Institute of Science Education and Research Pune, Pune 411 008, Maharashtra, India. E-mail: harinath@iiserpune.ac.in

† Electronic supplementary information (ESI) available. See DOI: https://doi.org/10.1039/d2cc06134a

Certain *N*,*N*,*O*-protected hydroxylamines have been previously reported by Toscano and coworkers but these compounds spontaneously hydrolysed in buffer to generate HNO.[12] Hence, the *t*-butyl ester was the choice of *N*-protective group since the carbamate that is formed is less likely to be spontaneously hydrolysed in pH 7.4. The cyclopropylcarboxyl group, which is hydrolysed by esterases, was used as an *O*-protective group. HNO donors activated by light[13,14] or an enzyme[15,16] or chemically[17] are known but there are limited structural features that allow for triggerable as well as tunable release of HNO. Furthermore, given the complications associated with the detection of HNO, the incorporation of a fluorescent reporter for HNO production would be useful. Here, we designed and developed a modular scaffold that can generate HNO, and we incorporated a latent fluorophore, which upon release produces a fluorophore, hence reporting the generation of HNO.

Among the esterase-cleavable functional groups, cyclopropyl carboxylic acid-based esters are preferred due to their extended stability in pH 7.4 buffer.[18,19] The *N*-Boc hydroxylamine (HO-NH-Boc) was reacted with cyclopropyl carbonyl chloride to afford **5** (Scheme 1).[20] Reaction of **5** with phenyl sulfonyl chloride gave **2a** (Ar = Ph) (Scheme 1).[12]

The deprotection of the Boc-group was carried out with trifluoroacetic acid (TFA) and **1a** was isolated in 56% yield (Table 1, entry 1).[12]

The two derivatives **1a** and **2a** were independently treated with esterase in pH 7.4 buffer and HNO generation was monitored using the reported coumarin-based fluorescent probe, **PCM** (**6**).[21] In the absence of esterase, neither compound produced significant amounts of HNO (Fig. 2A and B). In the presence of esterase, the time course of HNO generation from **1a** during 30 min was significantly different from the time course of HNO generation from **2a** and the yield of HNO from **2a** was higher when compared with **1a** (Fig. 2A and B and see ESI,† Fig. S1). The diminished yield of HNO from **1a** is consistent with a previous report where the yield of HNO from *N*-hydroxy-benzenesulfonamide was low at pH 7.4 and increasing the pH led to an increase in HNO yield.[22,23]

Next, in order to understand if the release of HNO depended on the nature of the leaving group, a series of analogues were prepared (Table 1, entries 2–7). When tested, all analogues **2b–2g** produced HNO at comparable levels (Fig. 2C). Among the derivatives **1b–1g**, except for the 4-nitrophenyl derivative, all compounds tested produced HNO (Fig. 2C and see ESI,† Fig. S2). The lack of HNO production from **1g** is consistent with previous reports where the yield of HNO from *N*-hydroxy-4-nitrobenzenesulfonamide was diminished at pH 7.4.[6]

Having established that these compounds can be triggered by esterase to generate HNO, we next proceeded to prepare the dansyl derivatives **1h** and **2h** (Fig. 3A, for synthesis see ESI,† Scheme S1). The product formed during HNO release is dansic acid **4h**, whose fluorescence properties such as Stokes shift (189 nm, Fig. S3, ESI†), pH stability (Fig. S4, ESI†), extended lifetime (τ_{avg} = 13.82 ns, Fig. S5, ESI†), and quantum yield (83%) make it an excellent candidate for reporting fluorescence in cells.[24] The derivatives **1h** and **2h** are expected to be cleaved by esterase to produce HNO as well as a dansic acid-based fluorescence reporter **4h** (Fig. 3A and see ESI† Fig. S6 and S7). Esterase-catalyzed HNO release from compounds **1h** and **2h** was monitored and an increase in HNO levels was observed during 30 min (Fig. 3B). Pre-treatment with PMSF (phenylmethanesulfonyl fluoride), an inhibitor of esterase,[25] showed a significant decrease in HNO yield. Notably, HNO generated by **3b**, a positive control, was not affected by esterase or by the presence of PMSF (Fig. 3B). The yield of HNO from **2h** was significantly higher when compared with **1h** (Fig. 3B).

Next, the fluorescence attributable to the formation of **4h** was studied during esterase-catalysed cleavage of **1h**. Compounds **1h** and **2h** were themselves weakly fluorescent (excitation, 308 nm and emission, 497 nm; see ESI,† Fig. S7A). In the presence of esterase, in

Table 1 Synthesis of *N*,*O*-protected hydroxylamines (**1**) from *N*,*N*,*O*-protected hydroxylamines (**2**)

2 1

Entry	X	Y	Compd No	Compd No	Yield, %
1	H	H	**2a**	**1a**	56
2	Br	H	**2b**	**1b**	53
3	H	Br	**2c**	**1c**	92
4	CF_3	H	**2d**	**1d**	41
5	Br	CF_3	**2e**	**1e**	40
6	NO_2	H	**2f**	**1f**	95
7	H	NO_2	**2g**	**1g**	65

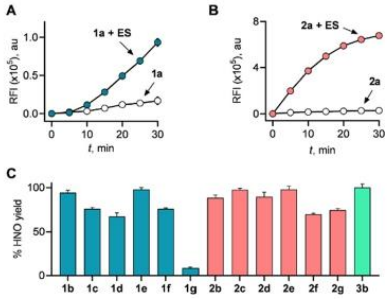

Fig. 2 HNO detection using PCM dye **6**. Compounds were incubated with and w/o esterase (0.5 U mL^{-1}) in PBS (pH 7.4) at 37 °C for 30 min and fluorescence was measured (excitation 370 nm and emission at 460 nm); (A) compound **1a**; (B) compounds **2a**; (C) compounds **1b–1g** and **2b–2g**, **3b**. **3b** refers to 2-bromopiloty's acid, a known HNO generator and yield of HNO from this compound was assigned as 100%.

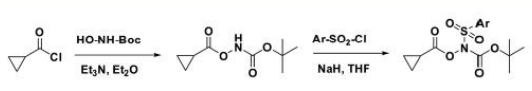

5 2

Scheme 1 Synthesis of **2**. Ar refers to mono or di-substituted phenyl groups.

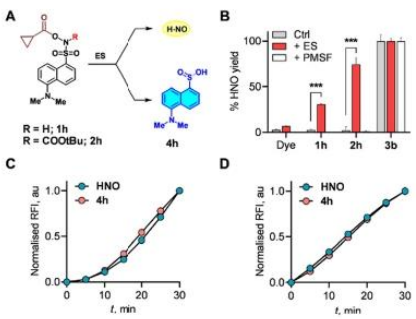

Fig. 3 (A) Design of HNO donors with a fluorescence reporter. Compound **1h** or **2h** is expected to be cleaved by esterase to produce HNO and **4h**; (B) HNO release from compounds **1h** and **2h** upon incubation with PCM dye **6** in the presence and absence of esterase (0.5 U mL^{-1}) with and without esterase inhibitor (**PMSF**) in PBS (pH 7.4) at 37 °C for 30 min; dye refers to PCM **6** alone (see ESI† for structure); **+ ES** refers to the compounds incubated with esterase; **+ PMSF** (phenylmethanesulfonyl fluoride) refers to pre-treatment of **ES** with **PMSF** followed by compound treatment; **3b** is 2-bromopiloty's acid, a known HNO generator and the yield of HNO from this compound was assigned as 100%; ***$P < 0.001$; **4h** was weakly fluorescent (370 nm excitation, 460 nm emission) and does not contribute to HNO's signal in this assay (see ESI,† Fig. S6B). (C) Time course of release of HNO and **4h** during incubation of **1h** with esterase in PBS (pH 7.4) at 37 °C. The rate constant for **4h** release was found to be 1.77 h^{-1} (see ESI,† Fig. S7C). (D) Time course of release of HNO and **4h** during incubation of **2h** with esterase in PBS (pH 7.4) at 37 °C. All data are presented as mean ± SD (n = 3 per group). The rate constant for **4h** release was found to be 1.06 h^{-1} (see ESI,† Fig. S7D).

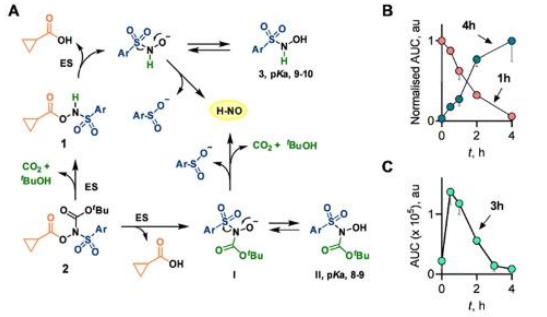

Fig. 4 LC/MS study. (A) Proposed mechanism for the decomposition of derivatives **1** and **2** to release HNO; Ar refers to dansyl. (B) Decomposition of **1h** and formation of **4h** upon incubation with esterase (0.5 U mL^{-1}) in PBS (pH 7.4) at 37 °C as monitored by LC/MS. **1h** (expected, m/z = 335.1060 $[M + H]^+$; observed, m/z = 335.1058), **4h** (expected, m/z = 236.0739 $[M + H]^+$; observed, m/z = 236.0742). (C) Formation of **3h** during the decomposition of **1h** upon incubation with esterase (0.5 U mL^{-1}) as monitored by LC/MS. **3h** (expected, m/z = 267.0798 $[M + H]^+$; observed, m/z = 267.0805). All data are presented as mean ± SD (n = 3 per group). pk_a values were calculated by using Chemaxon software.

the first 30 min, in the case of **1h**, we find a nearly concomitant release of HNO as well as **4h** (Fig. 3C) in a dose-dependent manner (see ESI,† Fig. S7B). A similar profile was observed in the case of **2h** (Fig. 3D). Together, these data indicate that we have developed an HNO donor with a fluorescence reporter.

An important feature of HNO donors is the selectivity towards the generation of HNO *versus* nitric oxide (NO), which have distinct activity in cells.[8] Compound **3b**, for example, generates a significant amount of NO (detected as nitrite using the Griess assay: see ESI,† Fig. S8) in aerobic conditions. The donors **1h** and **2h** produced significantly lower amounts of NO when compared with **3b** (see ESI,† Fig. S8).

Based on the above results, a mechanism for HNO release from this scaffold was considered (Fig. 4A). Compounds belonging to series **1** were cleaved by esterase to produce the anionic intermediate, which equilibrates with **3**. LC/MS analysis of **1h** in pH 7.4 shows the stability in buffer over 300 mins (see ESI,† Fig. S9), the reaction mixture of **1h** and esterase revealed complete consumption of **1h** (Fig. 4B and see ESI,† Fig. S10 and S11A) and the formation of the intermediate **3h** (Fig. 4C and see ESI,† Fig. S11B). The concentration of **3h** builds up over time and then disappears, to produce dansyl sulfinic acid **4h** (Fig. 4b and see ESI,† Fig. S11C) and HNO (see ESI,† Fig. S6A). During 30 min, the yield of HNO from **1h** is somewhat lower when compared with most other derivatives tested. Two factors determine the yield of HNO: firstly, the strength and polarization of the S–N bond, and secondly, the leaving group ability of **4h**. The calculated pK_a of the corresponding sulfinic acid is 0.9 (see ESI,† Table S1)[26] and is likely a good leaving group and hence, the HNO yield depends on the bond strength and polarization of the S–N bond. The diminished yield of HNO from **1h** in 30 min could be due to the slow rate of cleavage by esterase (nearly 4 h to complete consumption, Fig. 4B) as well as the electron-donating dimethylamino group that leads to a decrease in the acidity of the hydroxamic acid (see ESI,† Table S2) and perhaps, steric effects of the neighboring aromatic ring.

Among the HNO donors belonging to series **2**, esterase cleavage produces intermediate **I** (Fig. 4A). Loss of sulfinate gives the common intermediate (Fig. 1B), which collapses to produce CO_2, *t*BuOH and HNO. TLC analysis of **2h** in the presence of ES in pH 7.4 buffer revealed complete disappearance with **1h** being formed as a minor product suggesting the lability of the *t*-Boc group under these conditions (see ESI,† Fig. S12). LC/MS analysis of **2h** + ES revealed the disappearance of this compound (see ESI,† Fig. S13) and the formation of the intermediate **I** (see ESI,† Fig. S14), as well as the gradual formation of **4h** (see ESI,† Fig. S15C). However, due to the conditions used for LC/MS analysis (formic acid in the eluant), we also observed the loss of the *t*-Boc group and the formation of **1h** (Fig. S15A, ESI†) complicating further mechanistic analysis from this assay. However, the nearly concomitant release of HNO and **4h** in the absence of formic acid (Fig. 3D) suggests that **2h** can be used as a tool for HNO generation with a fluorescence reporter. The yield of HNO from **2h** was significantly higher than the yield of HNO from **1h**. The presence of an electron-withdrawing *t*-Boc group is likely to polarize intermediate **I** and facilitate the departure of the sulfinate group (the estimated pK_a of **II** is 8–9, see ESI,† Table S2). This observation supports a sulfinate leaving group-independent mechanism for HNO generation, which is consistent

with the formation of a neutral common intermediate (Fig. 1B) that undergoes hydrolysis to produce HNO; this hydrolysis can be accelerated by esterase. The close correlation between HNO and **4h** suggests that, under the reaction conditions, the hydrolysis of the common intermediate is fast ($t_{\frac{1}{2}} < 5$ min).

Since HNO is known to react with H_2S to produce persulfide and polysulfide (Scheme S6A),[18] the ability of donors **1h** and **2h** to produce persulfide and polysulfide in the presence of H_2S was investigated using an established **HPE-IAM** electrophile trapping method using LC/MS detection (see ESI,† Scheme S6B).[27] Here, **HPE-IAM** reacts with HS^- to produce **HS-HPE-AM** (m/z 212.0723), which can further react with another mole of **HPE-IAM** to produce **Bis-S-HPE-AM** (m/z = 389.1489) (see ESI,† Scheme S6B). If persulfide or polysulfide is produced, the adducts **Bis (S)$_n$HPE-AM** where $n \geq 2$ are expected to be formed. The reaction mixture containing **1h** or **2h** was treated with Na_2S and esterase followed by the addition of **HPE-IAM**. Separately, Na_2S was treated with **HPE-IAM**; this mixture served as a control. LC/MS analysis showed the formation of **HS-HPE-AM** and **Bis-S-HPE-AM** in all the aforementioned reaction mixtures (see ESI,† Fig. S16, S17 and S18). Reaction mixtures containing **1h** or **2h** produced higher levels of **Bis-SS-HPE-AM** and **Bis-SSS-HPE-AM**, which is consistent with HNO's ability to produce persulfide with a higher yield of the latter species in the mixture containing **2h** as compared with **1h**, perhaps due to higher HNO yield from **2h** (see ESI,† Fig. S16C and S19). The increased formation of **Bis-SSS-HPE-AM** with **2h** when compared with **1h** is consistent with **2h**'s higher yield of HNO in 30 min when compared with **1h** (see ESI,† Fig. S16D and S20). When the HNO donor **3b** was used, a similar yield of **Bis-SS-HPE-AM** to **1h** and **2h** was seen but a significantly higher yield of **Bis-SSS-HPE-AM** was seen, suggesting that the rate of HNO production played an important role in polysulfide generation from H_2S (Fig. S21 and S22, ESI†). Hence, HNO donors can be used to enhance the sulfane sulfur pool in the presence of H_2S.

Lastly, we studied the ability of the newly developed donors to permeate cells to generate HNO as well as a fluorescence signal. Imaging data in MCF-7 breast cancer cells showed the formation of HNO by using the HNO-TCF probe (RED channel, Alexa fluor 568, see ESI,† Fig. S23) as well as a fluorescence signal attributable to the formation of **4h** (DAPI channel, see ESI,† Fig. S23, bright field images, see ESI,† Fig. S24). The formation of **4h** was also confirmed through incubation of cell lysates with **1h** or **2h** (see ESI,† Fig. S25). Both compounds were found to be well tolerated up to 25 μM in MCF-7 cells but higher cytotoxicity in MEF and A549 cells was observed (see ESI,† Fig. S26–S28).

In summary, we report a new series of cell-permeable HNO donors that can be cleaved enzymatically to produce HNO along with a fluorophore. These probes, with a well characterized mechanism of HNO generation, enhance polysulfide levels in the presence of H_2S, and can be used to study the biology of sulfur-nitrogen species cross-talk.

Financial support was from the Science and Engineering Research Board (CRG/2019/002900), the Department of Biotechnology (HC, BH/HRD/NBM-NWB/39/2020-21) and IISER Pune. DST Fund for Improvement of S&T Infrastructure (SR/FST/LSII-043/2016) to the IISER Pune Biology Department for setting up the Biological Mass Spectrometry Facility. The manuscript was written with inputs from all authors. LRS, JCV and SM carried out all experiments.

Conflicts of interest

There are no conflicts to declare.

Notes and references

1 J. P. Marcolongo, M. F. Venâncio, W. R. Rocha, F. Doctorovich and J. A. Olabe, *Inorg. Chem.*, 2019, **58**, 14981–14997.
2 J. C. Pieretti, C. V. C. Junho, M. S. Carneiro-Ramos and A. B. Seabra, *Pharmacol. Res.*, 2020, **161**, 105121.
3 J. C. Wanstall, T. K. Jeffery, A. Gambino, F. Lovren and C. R. Triggle, *Br. J. Pharmacol.*, 2001, **134**, 463–472.
4 M. Tare, R. S. R. Kalidindi, K. J. Bubb, H. C. Parkington, W.-M. Boon, X. Li, C. G. Sobey, G. R. Drummond, R. H. Ritchie and B. K. Kemp-Harper, *Naunyn. Schmiedebergs. Arch. Pharmacol*, 2017, **390**, 397–408.
5 E. Cheong, V. Tumbev, J. Abramson, G. Salama and D. A. Stoyanovsky, *Cell Calcium*, 2005, **37**, 87–96.
6 W. D. Gao, C. I. Murray, Y. Tian, X. Zhong, J. F. DuMond, X. Shen, B. A. Stanley, D. B. Foster, D. A. Wink, S. B. King, J. E. Van Eyk and N. Paolocci, *Circ. Res.*, 2012, **111**, 1002–1011.
7 A. J. Norris, M. R. Sartippour, M. Lu, T. Park, J. Y. Rao, M. I. Jackson, J. M. Fukuto and M. N. Brooks, *Int. J. Cancer*, 2008, **122**, 1905–1910.
8 E. H. Silva Sousa, L. A. Ridnour, F. S. Gouveia, C. D. Silva da Silva, D. A. Wink, L. G. de França Lopes and P. J. Sadler, *ACS Chem. Biol.*, 2016, **11**, 2057–2065.
9 J. Zarenkiewicz, V. S. Khodade and J. P. Toscano, *J. Org. Chem.*, 2021, **86**, 868–877.
10 T. Ida, T. Sawa, H. Ihara, Y. Tsuchiya, Y. Watanabe, Y. Kumagai, M. Suematsu, H. Motohashi, S. Fujii, T. Matsunaga, M. Yamamoto, K. Ono, N. O. Devarie-Baez, M. Xian, J. M. Fukuto and T. Akaike, *Proc. Natl. Acad. Sci. U.S.A.*, 2014, **111**, 7606–7611.
11 K. G. Fosnacht, M. M. Cerda, E. J. Mullen, H. C. Pigg and M. D. Pluth, *ACS Chem. Biol.*, 2022, **17**, 331–339.
12 A. D. Sutton, M. Williamson, H. Weismiller and J. P. Toscano, *Org. Lett.*, 2012, **14**, 472–475.
13 Y. Zhou, R. B. Cink, R. S. Dassanayake, A. J. Seed, N. E. Brasch and P. Sampson, *Angew. Chem., Int. Ed.*, 2016, **55**, 13229–13232.
14 M. Kawaguchi, T. Tani, R. Hombu, N. Ieda and H. Nakagawa, *Chem. Commun.*, 2018, **54**, 10371–10374.
15 R. J. Holland, R. Paulisch, Z. Cao, L. K. Keefer, J. E. Saavedra and S. Donzelli, *Nitric oxide Biol. Chem.*, 2013, **35**, 131–136.
16 G. Bharadwaj, P. G. Z. Benini, D. Basudhar, C. N. Ramos-Colon, G. M. Johnson, M. M. Larriva, L. K. Keefer, D. Andrei and K. M. Miranda, *Nitric oxide*, 2014, **42**, 70–78.
17 Y. Long, Z. Xia, A. M. Rice and S. B. King, *Molecules*, 2022, **27**, 5305.
18 Y. Zheng, B. Yu, K. Ji, Z. Pan, V. Chittavong and B. Wang, *Angew. Chem., Int. Ed.*, 2016, **55**, 4514–4518.
19 K. A. Pardeshi, G. Ravikumar and H. Chakrapani, *Org. Lett.*, 2018, **20**, 4–7.
20 J. T. M. Correia, G. Piva da Silva, E. André and M. W. Paixão, *Adv. Synth. Catal.*, 2019, **361**, 5558–5564.
21 G. J. Mao, X. B. Zhang, X. L. Shi, H. W. Liu, Y. X. Wu, L. Y. Zhou, W. Tan and R. Q. Yu, *Chem. Commun.*, 2014, **50**, 5790–5792.
22 M. N. Hughes and R. Cammack, *Methods Enzymol.*, 1999, **301**, 279–287.
23 K. Aizawa, H. Nakagawa, K. Matsuo, K. Kawai, N. Ieda, T. Suzuki and N. Miyata, *Bioorg. Med. Chem. Lett.*, 2013, **23**, 2313–2317.
24 Q. Guo, Y. Wu, L. Zhang, Y. Qin, J. Bao, Y. Feng, Y. Liu and Y. Zhou, *Sens. Actuators, B*, 2022, **369**, 132309.
25 P. C. Smith, A. F. McDonagh and L. Z. Benet, *J. Pharmacol. Exp. Ther.*, 1990, **252**, 218–224.
26 Marvin 5.4.0.1, **https://www.chemaxon.com**.
27 T. Akaike, T. Ida, F.-Y. Wei, M. Nishida, Y. Kumagai, M. M. Alam, H. Ihara, T. Sawa, T. Matsunaga, S. Kasamatsu, A. Nishimura, M. Morita, K. Tomizawa, A. Nishimura, S. Watanabe, K. Inaba, H. Shima, N. Tanuma, M. Jung, S. Fujii, Y. Watanabe, M. Ohmuraya, P. Nagy, M. Feelisch, J. M. Fukuto and H. Motohashi, *Nat. Commun.*, 2017, **8**, 1177.

